Global-in-Time Domain Decomposition Methods for Flow and Transport Problems in Fractured Porous Media

by

Toan Huynh

A dissertation submitted to the Graduate Faculty of
Auburn University
in partial fulfillment of the
requirements for the Degree of
Doctor of Philosophy

Auburn, Alabama
August 3rd, 2024

Keywords: domain decomposition, flow and transport in fractured porous media, reduced fracture model, time-dependent Steklov-Poincaré operator, optimized Schwarz waveform relaxation, operator splitting, mixed-hybrid finite elements, local timestepping, mixed formulations

Approved by

Thi-Thao-Phuong Hoang, Chair, Associate Professor of Mathematics and Statistics
Yanzhao Cao, Professor of Mathematics and Statistics
Hans Werner Van Wyk, Associate Professor of Mathematics and Statistics
Junshan Lin, Associate Professor of Mathematics and Statistics
Xing Fang, Professor of Civil and Environmental Engineering, University Reader

Abstract

This thesis contributes to the development of numerical methods for the reduced fracture models of flow and transport problems in porous media containing fractures. In particular, our goal is to construct numerical algorithms that enable different time steps on the fracture and on the surrounding area by utilizing global-in-time domain decomposition (DD) methods. In this work, we focus on two types of methods: the first one is based on time-dependent Steklov-Poincaré operator, while the second one employs the optimized Schwarz waveform relaxation (OSWR) approach with Ventcel-Robin transmission conditions. Each method is formulated in a mixed formulation which is suitable for handling problems arising in the modeling of flow and transport in porous media.

We first consider the compressible fluid flow in a fractured porous medium in which the fracture represents a fast pathway (i.e., with high permeability) and is modeled as a hypersurface embedded in the porous medium. Three different global-in-time DD methods are derived using the pressure continuity equation and the tangential PDEs in the fracture-interface as transmission conditions. Each method leads to a space-time interface problem which is solved iteratively and globally in time. Efficient preconditioners are designed to accelerate the convergence of the iterative methods while preserving the accuracy in time with nonconforming grids. Numerical results for two-dimensional problems with different types of fractures and with different number of subdomains are presented to show the improved performance of the proposed methods.

We then focus on constructing efficient numerical methods for the reduced fracture model of the advection diffusion equation. We develop three global-in-time DD methods coupled with operator splitting to treat the advection and the diffusion with different numerical schemes and with different time steps. For each method, separate transmission conditions are formulated for the advection and the diffusion and are combined together to write the discrete space-time interface system. Numerical results for two-dimensional problems with various Péclet numbers and different types of fracture are presented to illustrate and compare the convergence and accuracy in time of the proposed methods with local time-stepping.

We finally reconsider the reduced fracture model of the advection-diffusion equation and aim to tackle the case when the advection is strongly dominated. Three upwind methods are constructed in the content of mixed hybrid finite elements. The first method is a monolithic scheme obtained by fully discretizing the reduced model directly. To incorporate local time-stepping technique, two global-in-time DD methods are derived by decoupling the monolithic solver and imposing appropriate transmission conditions. Several numerical results in two dimensions are presented to verify the optimal order of convergence of the monolithic solver and to illustrate the performance of the two decoupled schemes with local time-stepping on problems of high Péclet numbers.

Acknowledgments

First of all, I would like to express my deepest gratitude to my advisors, Dr. Thi-Thao-Phuong Hoang and Dr. Yanzhao Cao for their support and guidance over the last five years. Having an opportunity to work with you all provided me valuable experience and helped me grow up as an independent researcher. During my PhD, it was comfortable and fruitful to discuss with you as you were always patient to my mistakes and questions and your advice helped me progress a lot. I always enjoyed the conservation with you at the beginning of each meeting which made me less nervous and felt more confident. Thank you Dr. Phuong Hoang for your help and advice that made the first day of my PhD life became less difficult. I will not forget all discussions we had which were not just about work but also about life and many other things. Your advice and knowledge during these meetings always encouraged me whenever I felt down and disappointed in my research. I will be always grateful to your suggestion about the ”dual version” which leads to the discovery of our new method. Thank you Dr. Yanzhao for always be there to patiently answer all my questions not just about research but also about those that arose during my PhD journey. I have learned so many things from you, most importantly, your wisdom, thoroughness, calmness and your thoughtfulness for others.

I'm also very thankful to Dr. Junshan Lin for your acceptance to be a committee member. Your advice during the semester when I was your GTA provided me a lot of experience for my teaching assignment in the following years. I'm grateful to you for granting me permission to use the university's supercomputer which made my research more easier.

I would like to express my gratefulness to Dr. Hans Van Wyk for accepting to be a committee member. I will always remember our 8-hours trip together to the conference in Virginia in which we had a lot of interesting discussions. Your earnestness and positive energy had encouraged me a lot to believe more in myself.

I am very grateful to Prof. Xing Fang for kindly accepting to be the reviewer of this thesis. I highly appreciate your evaluation and comments on my work.

My next expression of gratitude is directed to my colleagues at Department of Mathematics and Statistics. I'm obliged to you all, Chinedu Eleh, Hewan Shemtaga, Cao Kha Doan,

Ridvan Ozdemir, Ian Ruau, Ogonnaya Michael Romanus for your kindness towards me. Your support and friendship have greatly enhanced my experience at Auburn University, making it much more enjoyable. I'm additionally thankful to you Chinedu for for our morning conversations. These discussions provided me with a tremendous amount of energy to start each day.

Finally, I am deeply grateful to my family for their unwavering support and endless love. Their constant presence and encouragement have been my cornerstone throughout this journey. I could not have gone this far without them always by my side, providing both the strength and solace needed to persevere.

Table of Contents

List of Tables

List of Figures

Chapter 1

Introduction

Motivation

Fluid flow and transport problems in porous media are very interesting subjects and have many application in various fields such as subsurface hydrology, geophysics, and reservoir geomechanics. Therefore, it is important to have fast and accurate numerical simulations for such problems. However, such tasks are often challenging due to the domain of calculation being a combination of many sub-regions with different processes, which leads to the presence of multiple spatial and temporal scales and drastically different physical properties. In particular, this is the case for a domain where there exist fractures and faults. A fracture can represent either a fast pathway or a geological barrier, depending on whether its permeability is much higher or much lower than the surrounding rock matrix. Thus, the time scales in the fractures and in the rock matrix may vary significantly. Additionally, the width of the fractures is much smaller than the size of the domain of calculation and any reasonable parameter of spatial discretization. To accurately represent the fractures, one must refine the grids locally around the fractures, which is known to be computationally costly. One effective way to deal with this situation is to transform the original problem into a new one, namely reduced fracture model or mixed-dimensional model, in which the fractures are treated as lower dimensional interfaces embedded in the rock matrix. The new model then consists of $d-$ dimensional problems in the subdomains coupled with $(d-1)$-dimensional problems on the fractures, where the interaction between the fractures and the surrounding rock matrix is taken into account. To deal with the involvement of different time scales in the numerical simulation, we employ global-in-time DD methods for the reduced fracture model in which different time scales can be imposed in the fracture and in the subdomains.

In this work, we mainly focus on the numerical solutions for the reduced fracture models of the diffusion equation and the linear advection-diffusion equation. The fracture is also assumed to have larger permeability than the surrounding porous media, which results in faster physical

processes in the fracture compared to those in the surrounding rock matrix. Therefore, it is more efficient to have smaller time step sizes in the fracture and larger ones in the subdomains. The aim of this thesis is to derive and analyze global-in-time DD methods for these two types of models before moving on to more complicated problems.

Main objective of the thesis: Global-in-time DD methods for reduced fracture models

Reduced fracture model was first introduce in [4, 5] to treat a single-phase Darcy's law equation in fractured porous media in which the fractures are assumed to have much higher permeability compared to that of surrounding medium so that the fractures act as hydraulic conductors, providing easy pathways for fluid flow. In this case, the pressure was assumed to be continuous across the fractures. However the flux was not supposed to be continuous as the fluid could flow into and out of as well as along the fractures. Later on in [88], the authors generalized the earlier model so that it can handle both large and small permeability in the fracture. For this model it is no longer assumed that the pressure is continuous across the fracture. Existence, uniqueness, and error estimates of the proposed model were also derived. In [9], these reduced fracture models were extended to the case when the fractures are fully immersed inside the domain of calculation. Rigorous analysis of the extended model was also establish in the framework of discrete dual finite volume. In [19, 8, 15, 107, 13], the reduced fracture models were further generalized to treat the case with intersecting fractures in which extra steps were needed to deal with the intersections between fractures. A posteriori error estimates for these models were studied in [92, 60]. When the flow in the fracture has sufficiently high flow rate, models that assumed Darcy's law in the fracture do not give correct experimental results anymore [40, 39]. To handle the case with significantly rapid flow in the fracture, new models were introduced in which nonlinear law is assumed to govern the fracture flow, such as Forchheimer [40, 39, 3], Brinkman [79], and Reynolds lubrication equations [51, 50, 53]. In additional to the work mentioned above, there are other approaches to derive the reduced

fracture models, which can be found in, for example, [45, 93, 83]. The setting of reduced fracture models leads naturally to domain decomposition methods as the fractures decompose the domain into non-overlapping subregions, and the PDEs that govern the flow in the fractures directly serve or can be manipulated to give transmission conditions for the DD methods. DD method was first introduced to formulate the reduced model in [4] and have been widely used in later work [88, 3, 19, 2, 38, 67, 39].

Global-in-time DD methods [68, 66, 67, 65, 64, 70, 72, 71, 59, 56] provide a powerful tool to perform parallel simulations of time-dependent physical phenomena with different time steps across the domain. Unlike classical DD approach [101, 99] where the model problem is first discretized in time by an implicit scheme, then at each time step the iteration is performed and involves the solution of stationary problems in the subdomains. As a consequence, a single time step is required for the classical approach, while for global-in-time DD, local time discretizations can be enforced in different regions of the domain.

There are basically two types of global-in-time DD methods:

1) The first class of methods is called Schur-type method, which is a global-in-time substructuring method and uses a Steklov-Poincaré type operator. Steklov-Poincaré operators are interface operators that enforce physical transmission conditions on the interfaces between subdomains. They were introduced for stationary problems [1, 101, 112, 16] to analyze domain decomposition algorithms for both homogeneous and heterogeneous problems, and were later improved by the uses of Neumann-Neumann preconditioner [20, 106, 98], which is a local preconditioner defined by solving Neumann boundary problems in the subdomains. Steklov-Poincaré operators were extended to parabolic problems in [35, 52] in which the authors imposed uniform time steps and performed the iterations at each time step. Later on, time-dependent extensions of these operators were derived and analyzed for parabolic problems in [78, 84, 48, 47].

2) The second type of methods is named Schwarz-type methods, which is based on the Optimized Schwarz Waveform Relaxation (OSWR) approach. The OSWR algorithm is an iterative method that employs more general transmission operators, such as Robin or

Ventcel, to exchange space-time boundary data across the interface between the subdomains. These operators contain some free parameters which play the role of preconditioners and can be optimized to improve the methods' convergence rates. Regarding stationary problems, Robin and Ventcel transmission conditions for the alternating Schwarz method were proposed in [95] and the optimized conditions were introduced [73, 74]. The OSWR method was introduced for parabolic and hyperbolic problems in [43] and was extended to advection-reaction-diffusion problems with constant coefficients in [87]. Later on, several work was devoted to deriving the optimized Robin or Ventcel parameters in different cases [14, 17, 18, 57, 44, 42, 56, 58].

Both classes of global-in-time DD methods were developed and analyzed for the diffusion equation [68] and the linear advection-diffusion equation [66, 64] for the case without fractures in which an artificial interface and additional equations on that interface are introduced to write the transmission conditions. In particular, the global-in-time primal Schur (GTP-Schur) method with its preconditioners and the global-in-time optimized Schwarz (GTO-Schwarz) method were proposed in [68, 66, 64]. For each method, an interface problem on the space-time interfaces between subdomains is derived and is solved iteratively over the whole time interval.

For both methods, mixed methods such as mixed finite elements and mixed hybrid finite elements were used to discretized the problems in space. The interest of mixed methods lies in the fact that they are locally mass conservative and simultaneously provide accurate approximations of a scalar and a flux unknown. Moreover, the flux approximations are continuous across inter-element boundaries. Mixed finite element methods are numerical methods first introduced by engineers in the mid 1960's for problems in solid mechanics [109, 62, 63]. Their mathematical analysis and convergence properties were provided by F. Brezzi [21], T. Oden and N. Reddy [97, 104], G. Ciarlet and A. Raviart [29], and C. Johnson [77]. Examples of successful approximation spaces associated with the methods are Raviart–Thomas elements [103] or Brezzi–Douglas–Marini elements [22] on 2D triangular and quadrilateral mesh and those of Nédélec [96], and Brezzi–Douglas-Duran–Fortin elements [25] on 3D tetrahedral or hexahedral grids. The linear system obtained from the mixed finite element methods often indefinite,

thus iterative solvers with standard preconditioners cannot be applied. One way to overcome this difficulty is to hybridize the system by introducing another variable representing the traces of the pressure at the element edges [23] to obtain a symmetric, positive definite system. This approach is named mixed hybrid finite elements. For a development from a mathematical point of view for both methods, see [23, 105]. The mixed formulation which incorporates two types of variables is highly compatible with the application of domain decomposition [54, 89], especially since one has available both Dirichlet and Neumann data on the boundary.

Regarding the linear advection-diffusion equations, global-in-time DD methods were coupled with operator splitting [10, 69, 90, 91, 108, 111] to derive local time stepping for such equations, with the aim of using different space-time discretizations for the advection and the diffusion. It has been shown that treating the advection explicitly can significantly reduce the numerical diffusion [28]. However, it was observed numerically in [66] that GTP-Schur did not perform well when advection was dominant; particularly, the convergence speed of GTP-Schur with the (generalized) Neumann-Neumann preconditioner could be even slower than using no preconditioner. Therefore, in [64], the authors coupled global-in-time DD methods with upwind-mixed hybrid finite elements [102, 26] to derive fully implicit local time stepping methods to tackle the case when the advection is strongly dominant. The upwind-mixed hybrid finite element scheme for the transport problem (with no fractures) was first introduced in [102] and analyzed in [26]. Unlike the standard upwind-mixed schemes [33, 34] where the flux variable only represents the diffusive flux, the upwind-mixed hybrid scheme employs a mixed hybrid finite element method for spatial discretization in which the flux variable approximates the total flux consisting of both advective and diffusive fluxes. To define the upwind weights for the scheme, the Lagrange multipliers arising in the hybrid formulation are utilized to give an approximation for the advective flux. A similar idea was also employed in [110] for the discretization with Raviart–Thomas elements of lowest order and in [27] with Brezzi–Douglas–Marini elements of lowest order. Optimal first-order convergence in both spatial and temporal errors for the upwind-mixed scheme was proved in [26]. It was shown in [102,

26] that the upwind-mixed hybrid scheme is fully mass conservative and provides the same accuracy as the upwind-mixed method [33], while being more robust and less costly for problems with high Péclet numbers.

The main objective of this thesis is to study global-in-time DD methods for flow and transport problems in porous media containing a fracture. A reduced fracture model is formulated for each problem where the fracture serves as a physical interface which decomposes the rock matrix into non-overlapping subdomains. In this thesis, we focus on two types of equations: diffusion equation and advection-diffusion equation.

1) Regarding the reduced fracture model of the diffusion equation, GTP-Schur and GTO-Schwarz were introduced for such model in [67] which based on the physical transmission conditions consist of the pressure continuity equation and the tangential PDEs in the fracture. The space-time interface problem for GTP-Schur is formulated directly from the physical transmission conditions using the time-dependent Dirichlet-to-Neumann operator. Two preconditioners were considered in [67]: the local preconditioner and the time-dependent Neumann-Neumann preconditioner. The former is adapted from [7] (for second-order elliptic PDEs) and the latter is an extension of the balancing domain decomposition (BDD) preconditioner [30, 85, 86] to time-dependent problems. The GTO-Schwarz method uses the so-called Ventcel-to-Robin transmission conditions which are obtained by taking the linear combinations of the pressure continuity equation and the PDEs in the fracture. In the context of reduced fracture models, these methods have two drawbacks. Firstly, the preconditioners for GTP-Schur are not effective: numerical results in [67] show that the convergence of GTP-Schur with either local or Neumann-Neumann preconditioner is much slower than that of GTO-Schwarz. Secondly, while GTO-Schwarz converges remarkably fast, it does not preserve the accuracy in time in the fracture with nonconforming time grids. In particular, using a smaller time step in the fracture than in the surrounding rock matrix does not improve the errors in the fracture, compared to using the same time step in the whole domain. This is also the case for GTP-Schur with the Neumann-Neumann preconditioner. Therefore, in this thesis, we aim to construct a new method that can overcome these difficulties. In particular, our goal is to

derive an algorithm that converges as fast as GTO-Schwarz without the need of preconditioners while still preserves the accuracy in time on the fracture when nonconforming time grids are imposed on the fracture and on the subdomains. We also aim to formulate a new preconditioner for GTP-Schur which can achieve better performance compared to the existing preconditioners.

2) We then consider the reduced fracture model of the linear advection-diffusion equation and aim to construct local time stepping method for such problem using global-in-time DD methods. In this thesis, we propose and study two approaches. In the first approach, global-in-time DD methods are coupled with operator splitting to derive numerical methods that allow nonconforming time grids for the advection and for the diffusion as well as on the fracture and on the subdomains. For the second approach, numerical algorithms are developed by combining global-in-time DD methods with upwind-mixed hybrid finite elements to treat the case where the advection is strongly dominated. Moreover, as there is a rich literature on the numerical methods for the reduced fracture model of the flow problems and their convergence analysis with or without providing the order of convergence [3, 8, 9, 19, 32, 41, 45, 88, 83, 94, 93], there has been little work that explores these aspects for the transport problems [6, 55]. Therefore, we also aim to perform rigorous analysis for the proposed methods in the context of mixed hybrid finite elements.

For each proposed method, the reduced fracture model is transformed into an interface problem on the space-time interface between subdomains. In such problem, different time discretizations can be imposed on the fracture and on the rock matrix via the use of an L^2-projection in time developed in [49, 46] to exchange information on the space-time interfaces. The discrete counterpart of the interface problem is then solved numerically using iterative methods such as GMRES or Jacobi iteration. Numerical experiments are carried out for different test cases with different types of fracture as well as different number of subdomains to investigate and compare the performance of the proposed methods and to analyze the accuracy in time obtained from each method with the nonconforming time grids.

Contents of the thesis

This thesis consists of three main parts:

1. Regarding the reduced fracture model of the diffusion equation, we have developed two new global-in-time DD methods, namely global-in-time dual Schur (GTD-Schur) and global-in-time fracture-based Schur (GTF-Schur), which resolve the drawbacks of the existing global-in-time DD methods. The first method is a dual version of GTP Schur, while the second one is formulated by combining the best features of GTP-Schur and GTD-Schur. The corresponding semi-discrete in time interface problem with nonconforming grids is presented for each method. We also construct a new preconditioner, namely Ventcel-Ventcel (V-V) preconditioner, for the GTP-Schur method which further accelerates its performance and makes it comparable to the GTO-Schwarz method. Numerical experiments in 2D for both non-immersed and partially immersed fractures with two or more subdomains are presented to verify and compare the performance of the proposed methods with different time steps in the fracture and in the rock matrix.

   The work is this section is the main object of the publication [70].

2. For the local time-stepping methods with operator splitting, we have extended the best methods developed for the diffusion problem, that is, GTF-Schur and GTO-Schwarz, for the reduced fracture model of the transport problems. The new algorithms are formulated by combining the transmission conditions considered for the diffusion part with newly constructed transmission conditions for the advection part. This approach results in a fully discrete interface system for each method which consists of one equation for the advection and one equation for the diffusion. We study the performance of each method by carrying out numerical experiments with various Péclet numbers and different types of fracture to verify and compare the performance of the proposed methods with nonconforming time grids in the fracture and in the rock matrix.

   The main contents of this section have also been published in the paper [72].

3. For the global-in-time DD methods constructed based on the mixed hybrid finite element approach, we have developed three fully implicit methods for the reduced fracture model of the advection-diffusion equation which can handle well the case of advection dominated. The first method is a monolithic upwind-mixed hybrid finite element method which is derived by discretizing the reduced fracture model directly and utilizing the Lagrange multipliers arising from the hybridization process. To enable nonconforming time grids on the fracture and on the subdomains, two decoupled global-in-time DD methods, namely GTP-Schur and GTO-Schwarz, are formulated from the monolithic scheme, which do not require separated treatment for the advection and the diffusion equations. Rigorous convergence analyses also presented for the monolithic scheme as well as for GTO-Schwarz. We present numerical experiments to confirm the theoretical result for the monolithic method and show numerical results in 2D with various Péclet numbers to verify and compare the performance of the two proposed DD methods, especially when the value of the Péclet number is high.

   The content of the work presented in this section can also be found in the publication [71].

The rest of the thesis is organized as follows: we present in Chapter 2 the two new global-in-time DD methods as well as the new preconditioner for GTP-Schur for the reduced fracture model of diffusion problems. Numerical results are also shown to compare the performance of the proposed methods with GTP-Schur and GTO-Schwarz. The subject of Chapter 3 is to constructed local time stepping methods for the reduced fractured model of linear transport problems in the context of operator splitting. We derive in Chapter 4 new global-in-time DD algorithms for reduced fracture model of advection-diffusion equations by incorporating mixed hybrid finite element methods. The proposed methods in this chapter are analyzed theoretically and numerically.

Major contribution of the thesis

The main contributions of this thesis include three aspects. Firstly, we construct a noble global-in-time DD method that resolve the remaining drawbacks of the existing global-in-time DD

methods. The main difficulty lied in the reformulation of the transmission conditions so that the obtained iterative algorithm converges fast without any preconditioner as well as can reserve the accuracy in time with nonconforming time grids. Secondly, we propose local time stepping methods for the reduced fracture model of linear transport problem by coupling global-in-time DD methods with operator splitting and mixed hybrid finite elements. The main difficulty was to formulate appropriate transmission conditions so that we still obtain the fast convergence and accuracy-preserving properties as in the case without the advection. Lastly, we establish optimal order convergence for the monolithic solver as well as the convergence of GTO-Schwarz for the reduced fracture model of linear transport problems in the context of mixed hybrid finite elements. The main difficulty of proving the optimal error estimate lied in the terms representing the traces on the fracture of the normal fluxes from the subdomains which will cause sub-optimal order convergence in space if they are not handled appropriately.

Chapter 2

Global-in-time DD methods for the reduced fracture model of diffusion equation

Contents

This chapter consists of three main parts. In the first part, we present the time-dependent diffusion problem written in mixed formulation and introduce its reduced fracture model. The well-posedness result for the reduced problem as well as the transmission conditions for the global-in-time DD methods are also stated. In the second part, we recall the formulation of the nonoverlapping global-in-time primal Schur (GTP-Schur) method and develop a new preconditioner, namely Ventcel-Ventcel preconditioner, for the method. Two new global-in-time DD

methods are also derived; the first method is the dual version of GTP-Schur, namely global-in-time dual (GTD-Schur), while the second one is constructed by combining the ideas of GTP-Schur and GTD-Schur, which is called global-in-time fracture-based Schur (GTF-Schur). The semi-discrete problems for all proposed methods in time using different time grids in the subdomains are also formulated. In the third part, numerical results with different types of fracture and with different numbers of subdomains are presented to illustrate and compare the performance of the proposed methods with GTO-Schwarz.

2.1. A reduced fracture model

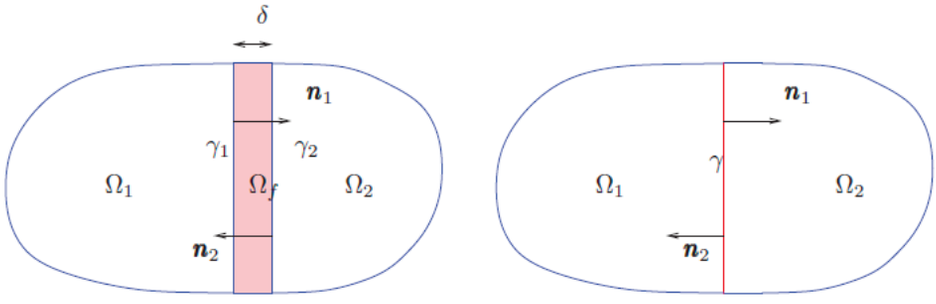

Figure 2.1: The domain Ω with the fracture Ω_f (left) and the fracture-interface γ (right).

Let Ω be a bounded domain in $\mathbb{R}^d$ $(d = 2, 3)$ with Lipschitz boundary $\partial\Omega$, and $T > 0$ be some fixed time. Consider the flow problem of a single phase, compressible fluid written in mixed form as follows:

$$\begin{aligned} \phi\partial_t p + \operatorname{div} \boldsymbol{u} &= q && \text{in } \Omega \times (0,T), \\ \boldsymbol{u} &= -\boldsymbol{K}\nabla p && \text{in } \Omega \times (0,T), \\ p &= 0 && \text{on } \partial\Omega \times (0,T), \\ p(\cdot,0) &= p_0 && \text{in } \Omega, \end{aligned} \tag{2.1}$$

where p is the pressure, $\boldsymbol{u}$ the velocity, q the source term, ϕ the storage coefficient, and $\boldsymbol{K}$ a symmetric, time-independent, hydraulic, conductivity tensor. Suppose that the fracture Ω_f is a subdomain of Ω, whose thickness is δ, that separates Ω into two connected subdomains: $\Omega \backslash \overline{\Omega}_f = \Omega_1 \cup \Omega_2$, and $\Omega_1 \cap \Omega_2 = \emptyset$ as depicted in Figure 2.1. For simplicity, we assume further that Ω_f can be expressed as

$$\Omega_f = \left\{ \boldsymbol{x} \in \Omega : \boldsymbol{x} = \boldsymbol{x}_\gamma + s\boldsymbol{n} \text{ where } \boldsymbol{x}_\gamma \in \gamma \text{ and } s \in \left(-\frac{\delta}{2}, \frac{\delta}{2}\right) \right\},$$

where γ is the intersection between a line $(d = 2)$ or a plane $(d = 3)$ with Ω.

We denote by γ_i the part of the boundary of Ω_i shared with the boundary of the fracture Ω_f: $\gamma_i = (\partial\Omega_i \cap \partial\Omega_f) \cap \Omega$, for $i = 1, 2$. Let $\boldsymbol{n}_i$ be the unit, outward pointing, normal vector field on $\partial\Omega_i$, where $\boldsymbol{n} = \boldsymbol{n}_1 = -\boldsymbol{n}_2$. For $i = 1,\ 2,\ f$, and for any scalar, vector, or tensor valued function g defined on Ω, we denote by g_i the restriction of g to Ω_i. The original problem (2.1) can be rewritten as the following transmission problem:

$$\begin{aligned}
\phi_i \partial_t p_i + \text{div}\, \boldsymbol{u}_i &= q_i && \text{in } \Omega_i \times (0,T), && i = 1,2,f,\\
\boldsymbol{u}_i &= -\boldsymbol{K}_i \nabla p_i && \text{in } \Omega_i \times (0,T), && i = 1,2,f,\\
p_i &= 0 && \text{on } (\partial\Omega_i \cap \partial\Omega) \times (0,T), && i = 1,2,f,\\
p_i &= p_f && \text{on } \gamma_i \times (0,T), && i = 1,2,\\
\boldsymbol{u}_i \cdot \boldsymbol{n}_i &= \boldsymbol{u}_f \cdot \boldsymbol{n}_i && \text{on } \gamma_i \times (0,T), && i = 1,2,\\
p_i(\cdot,0) &= p_{0,i} && \text{in } \Omega_i, && i = 1,2,f.
\end{aligned} \tag{2.2}$$

The reduced fracture model that we consider in this paper was first proposed in [4, 5] under the assumption that the fracture has larger permeability than that in the rock matrix. The model is obtained by averaging across the transversal cross sections of the d-dimensional fracture Ω_f. We use the notation ∇_τ and div_τ for the tangential gradient and tangential divergence, respectively. We write ϕ_γ and $\boldsymbol{K}_\gamma$ for $\delta\phi_f$ and $\boldsymbol{K}_{f,\tau}$, respectively, where $\boldsymbol{K}_{f,\tau}$ is the tangential component of $\boldsymbol{K}_f$. The reduced model consists of equations in the subdomains,

$$\begin{aligned}
\phi_i \partial_t p_i + \text{div}\, \boldsymbol{u}_i &= q_i && \text{in } \Omega_i \times (0,T),\\
\boldsymbol{u}_i &= -\boldsymbol{K}_i \nabla p_i && \text{in } \Omega_i \times (0,T),\\
p_i &= 0 && \text{on } (\partial\Omega_i \cap \partial\Omega) \times (0,T),\\
p_i &= p_\gamma && \text{on } \gamma \times (0,T),\\
p_i(\cdot,0) &= p_{0,i} && \text{in } \Omega_i,
\end{aligned} \tag{2.3}$$

for $i = 1, 2$, and equations in the fracture,

$$\begin{aligned}
\phi_\gamma \partial_t p_\gamma + \text{div}_\tau \boldsymbol{u}_\gamma &= q_\gamma + \sum_{i=1}^{2} (\boldsymbol{u}_i \cdot \boldsymbol{n}_i)_{|\gamma} && \text{in } \gamma \times (0,T),\\
\boldsymbol{u}_\gamma &= -\boldsymbol{K}_\gamma \delta \nabla_\tau p_\gamma && \text{in } \gamma \times (0,T),\\
p_\gamma &= 0 && \text{on } \partial\gamma \times (0,T),\\
p_\gamma(\cdot,0) &= p_{0,\gamma} && \text{in } \gamma.
\end{aligned} \tag{2.4}$$

To write the weak formulation of (2.3)-(2.4), we use the convention that if V is a space of functions, then $\boldsymbol{V}$ is a space of vector functions having each component in V. For arbitrary

domain $\mathcal{O}$, we denote by $(\cdot,\cdot)_{\mathcal{O}}$ the inner product in $L^2(\mathcal{O})$ or $\boldsymbol{L^2}(\mathcal{O})$. We next define the following Hilbert spaces:

$$\begin{aligned} M &= \left\{v=(v_1,v_2,v_\gamma)\in L^2(\Omega_1)\times L^2(\Omega_2)\times L^2(\gamma)\right\},\\ \Sigma &= \Big\{\boldsymbol{v}=(\boldsymbol{v}_1,\boldsymbol{v}_2,\boldsymbol{v}_\gamma)\in \boldsymbol{L}^2(\Omega_1)\times\boldsymbol{L}^2(\Omega_2)\times\boldsymbol{L}^2(\gamma):\ \text{div}\,\boldsymbol{v}_i\in L^2(\Omega_i),\ i=1,2,\\ &\qquad \text{and } \text{div}_\tau\,\boldsymbol{v}_\gamma-\sum_{i=1}^{2}\boldsymbol{v}_i\cdot\boldsymbol{n}_{i|\gamma}\in L^2(\gamma)\Big\}. \end{aligned} \tag{2.5}$$

We define the bilinear forms $a(\cdot,\cdot)$, $b(\cdot,\cdot)$ and $c(\cdot,\cdot)$ on $\Sigma\times\Sigma$, $\Sigma\times M$, and $M\times M$, respectively, and the linear form L_q on M by

$$a(\boldsymbol{u},\boldsymbol{v})=\sum_{i=1}^{2}\left(\boldsymbol{K}_i^{-1}\boldsymbol{u}_i,\boldsymbol{v}_i\right)_{\Omega_i}+\left(\left(\boldsymbol{K}_\gamma\delta\right)^{-1}\boldsymbol{u}_\gamma,\boldsymbol{v}_\gamma\right)_\gamma,\ b(\boldsymbol{u},\mu)=\sum_{i=1}^{2}\left(\text{div}\,\boldsymbol{u}_i,\mu_i\right)_{\Omega_i}+\left(\text{div}_\tau\,\boldsymbol{u}_\gamma-\sum_{i=1}^{2}\boldsymbol{u}_i\cdot\boldsymbol{n}_{i|\gamma},\mu_\gamma\right)_\gamma,$$
$$c_\phi(\eta,\mu)=\sum_{i=1}^{2}\left(\phi_i\eta_i,\mu_i\right)_{\Omega_i}+\left(\phi_\gamma\eta_\gamma,\mu_\gamma\right)_\gamma,\quad L_q(\mu)=\sum_{i=1}^{2}(q_i,\mu_i)_{\Omega_i}+(q_\gamma,\mu_\gamma)_\gamma.$$

The weak form of (2.3)-(2.4) can be written as follows:

Find $p\in H^1(0,T;M)$ and $\boldsymbol{u}\in L^2(0,T;\Sigma)$ such that

$$\begin{aligned} a(\boldsymbol{u},\boldsymbol{v})-b(\boldsymbol{v},p) &= 0 \qquad \forall\boldsymbol{v}\in\Sigma,\\ c_\phi(\partial_t p,\mu)+b(\boldsymbol{u},\mu) &= L_q(\mu) \quad \forall\mu\in M, \end{aligned} \tag{2.6}$$

together with the initial conditions:

$$p_i(\cdot,0)=p_{0,i},\ \text{in }\Omega_i,\ i=1,2,\quad \text{and}\quad p_\gamma(\cdot,0)=p_{0,\gamma},\ \text{in }\gamma. \tag{2.7}$$

The well-posedness of problem (2.6)-(2.7) is given by the following theorem. The reader is referred to [67, Theorem 2.1] for the details of the proof.

Theorem 2.1. *[67] Assume that the storage coefficient ϕ_i, $i=1,2,\gamma$ is bounded above and below by positive constants, and that there exist positive constants $\boldsymbol{K}_-$ and $\boldsymbol{K}_+$ such that*

(i) $\zeta^T\boldsymbol{K}_i^{-1}(x)\zeta\geq\boldsymbol{K}_-|\zeta|^2$, *and* $|\boldsymbol{K}_i(x)\zeta|\leq\boldsymbol{K}_+|\zeta|$, *for a.e.* $x\in\Omega_i$ *and* $\forall\zeta\in\mathbb{R}^d$, $i=1,2$,

(ii) $\eta^T\left(\boldsymbol{K}_\gamma(s)\delta\right)^{-1}\eta\geq\boldsymbol{K}_-|\eta|^2$ *and* $|\left(\boldsymbol{K}_\gamma(s)\delta\right)^{-1}\eta|\leq\boldsymbol{K}_+|\eta|$, *for a.e.* $s\in\gamma$ *and* $\forall\eta\in\mathbb{R}^{d-1}$.

Given q in $L^2(0,T;M)$ and $p_0=(p_{0,1},\ p_{0,2},\ p_{0,\gamma})$ in H^1_*, where

$$H^1_*:=\Big\{\mu=(\mu_1,\mu_2,\mu_\gamma)\in H^1(\Omega_1)\times H^1(\Omega_2)\times H^1_0(\gamma):\ \mu_i=0\ \text{on}\ \partial\Omega_i\cap\partial\Omega,\ \text{and}\ \mu_i-\mu_\gamma=0\ \text{on}\ \gamma,\ i=1,2\Big\}.$$

Then problem (2.6)-(2.7) *has a unique solution* $(p, \boldsymbol{u}) \in H^1(0,T;M) \times L^2(0,T;\Sigma)$.

We shall use global-in-time DD to find a numerical solution of problem (2.6)-(2.7) with different time steps in the fracture and the surrounding medium. The DD formulation can be obtained by treating the fracture as an (physical) interface between subdomains with the following transmission conditions:

$$p_i = p_\gamma, \qquad \text{on } \gamma \times (0,T), \tag{2.8}$$

$$\begin{aligned} \phi_\gamma \partial_t p_\gamma + \text{div}_\tau \boldsymbol{u}_\gamma &= q_\gamma + \sum_{i=1}^{2} (\boldsymbol{u}_i \cdot \boldsymbol{n}_i)_{|\gamma} && \text{in } \gamma \times (0,T), \\ \boldsymbol{u}_\gamma &= -\boldsymbol{K}_\gamma \delta \nabla_\tau p_\gamma && \text{in } \gamma \times (0,T), \\ p_\gamma &= 0 && \text{on } \partial\gamma \times (0,T), \\ p_\gamma(\cdot,0) &= p_{0,\gamma} && \text{in } \gamma. \end{aligned} \tag{2.9}$$

In the next sections, three global-in-time DD methods are derived based on these physical transmission conditions. For each method, a space-time interface problem is formulated and solved iteratively.

2.2. Global-in-time primal Schur (GTP-Schur) method

The idea of GTP-Schur is to impose (2.8) as Dirichlet boundary conditions for the subdomain problems:

$$p_i = \lambda, \quad \text{on } \gamma \times (0,T),\ i = 1,2, \tag{2.10}$$

where λ represents the fracture pressure p_γ. Then a space-time interface problem is formed by enforcing the remaining transmission condition (2.9). To derive the formulation of GTP-Schur, we define the Dirichlet-to-Neumann operators $\mathcal{S}_i^{\text{DtN}},\ i = 1,2$:

$$\begin{aligned} \mathcal{S}_i^{\text{DtN}} : H^1(0,T;H_{00}^{\frac{1}{2}}(\gamma)) \times L^2(0,T;L^2(\Omega_i)) \times H^1_{*,\gamma}(\Omega_i) &\longrightarrow L^2\left(0,T;(H_{00}^{\frac{1}{2}}(\gamma))'\right), \\ (\lambda, q_i, p_{0,i}) &\longmapsto \boldsymbol{u}_i \cdot \boldsymbol{n}_{i|\gamma}, \end{aligned}$$

where $H^1_{*,\gamma}(\Omega_i) := \{\mu \in H^1(\Omega_i) : \mu = 0 \text{ on } (\partial\Omega_i \cap \partial\Omega)\}$ and $(p_i, \boldsymbol{u}_i)$ is the solution of the problem

$$
\begin{aligned}
\phi_i \partial_t p_i + \operatorname{div} \boldsymbol{u}_i &= q_i && \text{in } \Omega_i \times (0,T), \\
\boldsymbol{u}_i &= -\boldsymbol{K}_i \nabla p_i && \text{in } \Omega_i \times (0,T), \\
p_i &= 0 && \text{on } (\partial\Omega_i \cap \partial\Omega) \times (0,T), \\
p_i &= \lambda && \text{on } \gamma \times (0,T), \\
p_i(\cdot,0) &= p_{0,i} && \text{in } \Omega_i.
\end{aligned} \tag{2.11}
$$

The space-time interface problem with unknown λ reads as:

$$
\begin{aligned}
\phi_\gamma \partial_t \lambda + \operatorname{div}_\tau \boldsymbol{u}_\gamma &= q_\gamma + \sum_{i=1}^{2} \mathcal{S}_i^{\mathrm{DtN}}(\lambda, q_i, p_{0,i}) && \text{in } \gamma \times (0,T), \\
\boldsymbol{u}_\gamma &= -\boldsymbol{K}_\gamma \delta \nabla_\tau \lambda && \text{in } \gamma \times (0,T), \\
\lambda &= 0 && \text{on } \partial\gamma \times (0,T), \\
\lambda(\cdot,0) &= p_{0,\gamma} && \text{in } \gamma,
\end{aligned} \tag{2.12}
$$

or equivalently,

$$
\begin{aligned}
\phi_\gamma \partial_t \lambda + \operatorname{div}_\tau \boldsymbol{u}_\gamma - \sum_{i=1}^{2} \mathcal{S}_i^{\mathrm{DtN}}(\lambda, 0, 0) &= q_\gamma \quad + \sum_{i=1}^{2} \mathcal{S}_i^{\mathrm{DtN}}(0, q_i, p_{0,i}), \text{ in } \gamma \times (0,T), \\
\boldsymbol{u}_\gamma &= -\boldsymbol{K}_\gamma \delta \nabla_\tau \lambda && \text{in } \gamma \times (0,T), \\
\lambda &= 0 && \text{on } \partial\gamma \times (0,T), \\
\lambda(\cdot,0) &= p_{0,\gamma} && \text{in } \gamma,
\end{aligned} \tag{2.13}
$$

or in compact form (space-time),

$$
\mathcal{S}_{\mathcal{P}}(\lambda) = \chi_{\mathcal{P}}. \tag{2.14}
$$

Note that from the second equation of (2.13), $\boldsymbol{u}_\gamma$ is a function in λ, hence, the right-hand side operator of (2.14) is actually an operator in only one variable λ.

The space-time problem (2.14) is solved iteratively using, e.g., GMRES. The resulting algorithm is matrix-free as the discrete counterpart of $\mathcal{S}_{\mathcal{P}}$ is not computed explicitly. At each GMRES iteration, $\mathcal{S}_{\mathcal{P}}(\lambda)$ is obtained by first solving the subdomain problems (2.11) over the whole time interval, then using the tangential PDEs (2.13) in the fracture-interface. The convergence of the iterative algorithm is known to be significantly slow, thus finding a suitable preconditioner is necessary to accelerate the iteration. Two preconditioners were introduced in [67]. The local preconditioner, $\boldsymbol{P}_{\mathrm{loc}}^{-1}$, is computed by finding the discrete counterpart of the operator $\left(\operatorname{div}_\tau \left(\boldsymbol{K}_\gamma \delta \nabla_\tau\right)\right)^{-1}$. This preconditioner was proposed first in [7] for stationary problems using the fact that the second order operator $\left(\operatorname{div}_\tau \left(\boldsymbol{K}_\gamma \delta \nabla_\tau\right)\right)$ is the dominant term in the

interface problem. The second preconditioner is the (time-dependent) Neumann-Neumann preconditioner, $\boldsymbol{P}_{\mathrm{NN}}^{-1}$, obtained by computing the (pseudo-)inverse of the Dirichlet-to-Neumann operators. Such a preconditioner involves the solution of the subdomain problems with Neumann boundary conditions on the fracture-interface. For the case with no fracture, the Neumann-Neumann preconditioner has been shown to be effective [68]. However, for the considered reduced fracture model, it has been shown numerically in [67] that the convergence speed of the iterative algorithm combined with these preconditioners is still slow and not efficient, especially the local preconditioner. From the derivation of these preconditioners, it can be seen that they do not provide good approximations of the inverse of the space-time operator on the left-hand side of the first equation in (2.13). Based on this observation, we derive a new preconditioner, namely the Ventcel-Ventcel preconditioner, in the following.

Ventcel-Ventcel preconditioner

As λ represents the fracture pressure p_γ and by the definition of $\mathcal{S}_i^{\mathrm{DtN}}$, the left-hand side of the first equation in (2.13) can be rewritten as

$$\phi_\gamma \partial_t \lambda + \mathrm{div}_\tau\, \boldsymbol{u}_\gamma - \sum_{i=1}^{2} \mathcal{S}_i^{\mathrm{DtN}}\left(p_\gamma, 0, 0\right) = \phi_\gamma \partial_t p_\gamma + \mathrm{div}_\tau\, \boldsymbol{u}_\gamma - \sum_{i=1}^{2} \boldsymbol{u}_i \cdot \boldsymbol{n}_{i|\gamma}. \tag{2.15}$$

The right-hand side of this equation resembles Ventcel boundary conditions [67]. Thus, the preconditioned system for (2.13) should be computed by solving the subdomain problems with such Ventcel boundary conditions (2.15) (instead of with Neumann conditions as used for the Neumann-Neumann preconditioner). To formulate local problems with Ventcel conditions, we introduce the Lagrange multipliers $p_{i,\gamma},\ i = 1, 2$, with $p_{i,\gamma}$ representing the trace on the interface γ of the pressure p_i in the subdomain Ω_i. It follows from the continuity of the pressure across the interface that

$$p_{1,\gamma} = p_{2,\gamma} = p_\gamma, \text{ in } \gamma \times (0, T). \tag{2.16}$$

We write the Darcy equation associated with each $p_{i,\gamma}$ in the fracture as

$$\boldsymbol{u}_{\gamma,i} := -\boldsymbol{K}_\gamma \delta \nabla_\tau p_{i,\gamma}, \quad \text{in } \gamma \times (0, T),\ i = 1, 2. \tag{2.17}$$

Note that $\boldsymbol{u}_{\gamma,i},\ i=1,2$ represents the tangential velocity in the fracture associated with the pressure $p_{i,\gamma}$, and $\boldsymbol{u}_{\gamma,1}=\boldsymbol{u}_{\gamma,2}=\boldsymbol{u}_{\gamma},\quad$ in $\gamma\times(0,T)$ according to (2.16) and (2.17). With such notation, the subdomain problem with Ventcel boundary condition reads as:

$$\begin{aligned}
\phi_i\partial_t p_i+\operatorname{div}\boldsymbol{u}_i &= 0 && \text{in } \Omega_i\times(0,T),\\
\boldsymbol{u}_i &= -\boldsymbol{K}_i\nabla p_i && \text{in } \Omega_i\times(0,T),\\
p_i &= 0 && \text{on } (\partial\Omega_i\cap\partial\Omega)\times(0,T),\\
\phi_\gamma\partial_t p_{i,\gamma}+\operatorname{div}_\tau\boldsymbol{u}_{\gamma,i}-\boldsymbol{u}_i\cdot\boldsymbol{n}_{i|\gamma} &= \theta && \text{on } \gamma\times(0,T),\\
\boldsymbol{u}_{\gamma,i} &= -\boldsymbol{K}_i\delta\nabla_\tau p_{i,\gamma} && \text{on } \gamma\times(0,T),\\
p_{i,\gamma} &= 0 && \text{on } \partial\gamma\times(0,T),\\
p_i(\cdot,0) &= 0 && \text{in } \Omega_i,
\end{aligned} \tag{2.18}$$

for $i=1,2$, where θ is the given Ventcel data. It can be shown that problem (2.18) has a unique weak solution; interested readers are referred to [67, Theorem 4.1] for more details of the proof. Next, we define the following Ventcel-to-Dirichlet operator $\mathcal{S}_i^{\text{VtD}},\ i=1,2$:

$$\begin{aligned}
\mathcal{S}_i^{\text{VtD}}: L^2\left(0,T;L^2\left(\gamma\right)\right) &\longrightarrow H^1\left(0,T;L^2\left(\gamma\right)\right),\\
\theta &\longrightarrow p_{i,\gamma},
\end{aligned}$$

where $(p_i,\ \boldsymbol{u}_i,\ p_{i,\gamma},\ \boldsymbol{u}_{\gamma,i})$, $i=1,2$, is the solution of the subdomain problem (2.18). Then the Ventcel-Ventcel preconditioner P_{VV}^{-1} for problem (2.14) is given by

$$\boldsymbol{P}_{\text{VV}}^{-1}:=\sigma_1\mathcal{S}_1^{\text{VtD}}+\sigma_2\mathcal{S}_2^{\text{VtD}},$$

where $\sigma_i:\gamma\times(0,T)\to[0,1]$ is such that $\sigma_1+\sigma_2=1$. The preconditioned system for (2.14) with the Ventcel-Ventcel preconditioner is defined as:

$$\boldsymbol{P}_{\text{VV}}^{-1}\left(\mathcal{S}_{\mathcal{P}}(\lambda)\right)=P_{\text{VV}}^{-1}(\chi_{\mathcal{P}}),\ \text{ in } \gamma\times(0,T). \tag{2.19}$$

We summarize the GTP-Schur method with the Ventcel-Ventcel preconditioner in Algorithm 1. Note that the operator $\boldsymbol{P}_{\text{VV}}^{-1}$ can be replaced by $\boldsymbol{P}_{\text{NN}}^{-1}$ (i.e., the Neumann-Neumann preconditioner) or by the identity operator (i.e., no preconditioner). We will compare numerical performance of these algorithms and verify the improvement by the Ventcel-Ventcel preconditioner in Section 2.6.

Algorithm 1 GTP-Schur method with Ventcel-Ventcel preconditioner

Input: initial guess $\lambda^{(0)}$, stopping tolerance $0 < \epsilon \ll 1$, maximum number of iterations $N_{\max}$.
Output: space-time fracture pressure λ.

1: Compute $\chi_{\mathcal{P}} = q_\gamma + \sum_{i=1}^{2} \mathcal{S}_i^{\mathrm{DtN}}(0, q_i, p_{0,i})$.
2: Evaluate $\mathcal{S}_{\mathcal{P}}(\lambda^{(0)}) = \phi_\gamma \partial_t \lambda^{(0)} - \mathrm{div}_\tau \boldsymbol{K}_\gamma \delta \nabla_\tau \lambda^{(0)} - \sum_{i=1}^{2} \mathcal{S}_i^{\mathrm{DtN}}(\lambda^{(0)}, 0, 0)$.
3: Set $r_0 := \chi_{\mathcal{P}} - \mathcal{S}_{\mathcal{P}}(\lambda^{(0)})$.
4: Calculate $\boldsymbol{P}_{\mathrm{VV}}^{-1}(r_0) = \sigma_1 \mathcal{S}_1^{\mathrm{VtD}}(r_0) + \sigma_2 \mathcal{S}_2^{\mathrm{VtD}}(r_0)$.
5: Set $\tilde{r}_0 := \boldsymbol{P}_{\mathrm{VV}}^{-1}(r_0)$ and $q_0 := \tilde{r}_0$.
6: **for** $k = 1, \cdot, N_{\max}$ **do**: ▷ Start GMRES iterations.
7: Generate $\lambda^{(k)}$ as the solution to the least square problem:

$$\min_{\mu \in R_k} \|\boldsymbol{P}_{\mathrm{VV}}^{-1}(\chi_{\mathcal{P}} - \mathcal{S}_{\mathcal{P}}(\mu))\|_{L^2},$$

where $R_k := \lambda^{(0)} + \mathrm{span}(q_0, q_1, \cdots, q_{k-1})$.
8: Set $\tilde{r}_k := \boldsymbol{P}_{\mathrm{VV}}^{-1}\left(\chi_{\mathcal{P}} - \mathcal{S}_{\mathcal{P}}(\lambda^{(k)})\right)$.
9: **if** $\|\tilde{r}_k\|/\|\tilde{r}_0\| \leq \epsilon$ **then**
10: stop the iteration, return $\lambda = \lambda^{(k)}$.
11: **end if**
12: Compute $q_k := \boldsymbol{P}_{\mathrm{VV}}^{-1}(\mathcal{S}_{\mathcal{P}}(q_{k-1}))$ as in Steps 2 and 4.
13: **end for**

Remark 2.2. *By definition,* $q_0 = \tilde{r}_0$*, and for* $k = 1, \ldots, N_{max}$,

$$q_k = \boldsymbol{P}_{VV}^{-1}\mathcal{S}_{\mathcal{P}}(q_{k-1}) = \boldsymbol{P}_{VV}^{-1}\mathcal{S}_{\mathcal{P}}\left((\boldsymbol{P}_{VV}^{-1}\mathcal{S}_{\mathcal{P}})^{k-1}(q_0)\right) = (\boldsymbol{P}_{VV}^{-1}\mathcal{S}_{\mathcal{P}})^{k}(q_0).$$

Thus, the space R_k *in Step* 8 *is the Krylov subspace corresponding to* $\boldsymbol{P}_{VV}^{-1}\mathcal{S}_{\mathcal{P}}$*:*

$$R_k = \lambda^{(0)} + \mathit{span}\left(\tilde{r}_0, (\boldsymbol{P}_{VV}^{-1}\mathcal{S}_{\mathcal{P}})(\tilde{r}_0), \cdots, (\boldsymbol{P}_{VV}^{-1}\mathcal{S}_{\mathcal{P}})^{k-1}(\tilde{r}_0)\right).$$

2.3. Global-in-time dual Schur (GTD-Schur) method

The dual Schur method is obtained by imposing Neumann boundary conditions for the subdomain problems, instead of Dirichlet conditions as in the primal Schur approach. Due to the presence of a high permeability fracture in the medium, the normal flux may not be continuous across the fracture-interface. Thus, we introduce two variables

$$\varphi_i := \boldsymbol{u}_i \cdot \boldsymbol{n}_{i|\gamma},\ i = 1, 2,$$

representing the normal flux from each subdomain along the fracture. To formulate the interface problem for GTD-Schur with two unknowns φ_1 and φ_2, we define the Neumann-to-Dirichlet operator:

$$\begin{array}{rcl} \mathcal{S}_i^{\text{NtD}} : L^2\left(0,T;L^2(\gamma)\right) \times L^2\left(0,T;L^2(\Omega_i)\right) \times H^1_{*,\gamma}(\Omega_i) & \longrightarrow & H^1\left(0,T;L^2(\gamma)\right), \\ (\varphi_i, q_i, p_{0,i}) & \longmapsto & (p_i)_{|\gamma}, \end{array}$$

where $(p_i, \boldsymbol{u}_i)\,,\ i = 1, 2$ is the solution to the subdomain problem with Neumann conditions:

$$\begin{array}{rcll} \phi_i \partial_t p_i + \text{div}\, \boldsymbol{u}_i & = & q_i & \text{in } \Omega_i \times (0,T), \\ \boldsymbol{u}_i & = & -\boldsymbol{K}_i \nabla p_i & \text{in } \Omega_i \times (0,T), \\ p_i & = & 0 & \text{on } (\partial\Omega_i \cap \partial\Omega) \times (0,T), \\ \boldsymbol{u}_i \cdot \boldsymbol{n}_i & = & \varphi_i & \text{on } \gamma \times (0,T), \\ p_i(\cdot, 0) & = & p_{0,i} & \text{in } \Omega_i. \end{array} \tag{2.20}$$

Next we denote by S_γ the local operator on the fracture:

$$\begin{array}{rcl} \mathcal{S}_\gamma : \left(L^2\left(0,T;L^2(\gamma)\right)\right)^2 \times L^2\left(0,T;L^2(\gamma)\right) \times H^1_0(\gamma) & \longrightarrow & H^1\left(0,T;L^2(\gamma)\right), \\ (\varphi_1, \varphi_2, q_\gamma, p_{0,\gamma}) & \longmapsto & p_\gamma, \end{array}$$

where $(p_\gamma, \boldsymbol{u}_\gamma)$ is the solution to the $(d-1)$-dimensional fracture problem:

$$\begin{array}{rcll} \phi_\gamma \partial_t p_\gamma + \text{div}_\tau \boldsymbol{u}_\gamma & = & q_\gamma + \displaystyle\sum_{i=1}^{2} \varphi_i & \text{in } \gamma \times (0,T), \\ \boldsymbol{u}_\gamma & = & -\boldsymbol{K}_\gamma \delta \nabla_\tau p_\gamma & \text{in } \gamma \times (0,T), \\ p_\gamma & = & 0 & \text{on } \partial\gamma \times (0,T), \\ p_\gamma(\cdot, 0) & = & p_{0,\gamma} & \text{in } \gamma. \end{array} \tag{2.21}$$

The space-time interface problem is obtained by enforcing the continuity of the pressure across the fracture and is given by

$$\begin{array}{rcl} \mathcal{S}_\gamma(\varphi_1, \varphi_2, q_\gamma, p_{0,\gamma}) & = & \mathcal{S}_1^{\text{NtD}}(\varphi_1, q_1, p_{0,1}),\ \text{in } \gamma \times (0,T), \\ \mathcal{S}_\gamma(\varphi_1, \varphi_2, q_\gamma, p_{0,\gamma}) & = & \mathcal{S}_2^{\text{NtD}}(\varphi_2, q_2, p_{0,2}),\ \text{in } \gamma \times (0,T), \end{array} \tag{2.22}$$

or in compact form,

$$\mathcal{S}_\mathcal{D} \begin{pmatrix} \varphi_1 \\ \varphi_2 \end{pmatrix} = \chi_\mathcal{D}, \quad \text{in } \gamma \times (0,T), \tag{2.23}$$

where

$$\mathcal{S}_{\mathcal{D}}\begin{pmatrix}\varphi_1\\ \varphi_2\end{pmatrix} = \begin{pmatrix} \mathcal{S}_\gamma(\varphi_1,\varphi_2,0,0) - \mathcal{S}_1^{\text{NtD}}(\varphi_1,0,0) \\ \mathcal{S}_\gamma(\varphi_1,\varphi_2,0,0) - \mathcal{S}_2^{\text{NtD}}(\varphi_2,0,0) \end{pmatrix}, \tag{2.24}$$

and

$$\chi_{\mathcal{D}} = \begin{pmatrix} \mathcal{S}_1^{\text{NtD}}(0,q_1,p_{0,1}) - \mathcal{S}_\gamma(0,0,q_\gamma,p_{0,\gamma}) \\ \mathcal{S}_2^{\text{NtD}}(0,q_2,p_{0,2}) - \mathcal{S}_\gamma(0,0,q_\gamma,p_{0,\gamma}) \end{pmatrix}. \tag{2.25}$$

The interface problem (2.23) is solved iteratively, and we propose the following Dirichlet-Dirichlet preconditioner, $\boldsymbol{P}_{\text{DD}}^{-1}$, to enhance its convergence (cf. Section 2.6):

$$\boldsymbol{P}_{\text{DD}}^{-1}\left(\mathcal{S}_{\mathcal{D}}\begin{pmatrix}\varphi_1\\ \varphi_2\end{pmatrix}\right) = \boldsymbol{P}_{\text{DD}}^{-1}\left(\chi_{\mathcal{D}}\right), \quad \text{in } \gamma\times(0,T), \tag{2.26}$$

where

$$\boldsymbol{P}_{\text{DD}}^{-1}\begin{pmatrix}\lambda_1\\ \lambda_2\end{pmatrix} = \begin{pmatrix}\widetilde{\mathcal{S}}_1^{\text{DtN}}\left(\lambda_1\right)\\ \widetilde{\mathcal{S}}_2^{\text{DtN}}\left(\lambda_2\right)\end{pmatrix}, \tag{2.27}$$

and $\widetilde{\mathcal{S}}_i^{\text{DtN}},\ i=1,2$ is a Dirichlet-to-Neumann operator defined as

$$\widetilde{\mathcal{S}}_i^{\text{DtN}}(\lambda_i) := \mathcal{S}_i^{\text{DtN}}\left(\lambda_i,0,0\right) = \boldsymbol{u}_i\cdot\boldsymbol{n}_{i|\gamma}. \tag{2.28}$$

The GTD-Schur method with the Dirichlet-Dirichlet preconditioner is outlined in Algorithm 2. The case without preconditioner follows the same steps with $\boldsymbol{P}_{\text{DD}}^{-1}$ being replaced by the identity operator.

2.4. Global-in-time fracture-based Schur (GTF-Schur) method

The primal and dual Schur methods generally require suitable preconditioners to achieve satisfactory convergence speed. Though the number of iterations is reduced with preconditioning, additional subdomain problems need to be solved. It would be desirable to develop a DD method that converges fast without any preconditioners. By combining the ideas of GTP-Schur and GTD-Schur, we derive the GTF-Schur method whose space-time interface operator is close to the identity operator, thus, making the new interface problem better-conditioned. Instead of having two interface unknowns as in the GTD- Schur method, only one term $\varphi := \sum_{i=1}^{2}\boldsymbol{u}_i\cdot\boldsymbol{n}_{i|\gamma}$ representing the jump of the normal flux across the fracture will be introduced. The fracture pressure p_γ is then recovered by solving the fracture problem (2.13) provided the new unknown.

Algorithm 2 GTD-Schur method with Dirichlet-Dirichlet preconditioner

Input: initial guess $(\varphi_1^{(0)}, \varphi_2^{(0)})$, stopping tolerance $0 < \epsilon \ll 1$, maximum number of iterations $N_{\max}$.

Output: pair of space-time fracture normal fluxes (φ_1, φ_2).

1: Compute $\chi_{\mathcal{D}} = \begin{pmatrix} \mathcal{S}_1^{\text{NtD}}(0, q_1, p_{0,1}) - \mathcal{S}_\gamma(0, 0, q_\gamma, p_{0,\gamma}) \\ \mathcal{S}_2^{\text{NtD}}(0, q_2, p_{0,2}) - \mathcal{S}_\gamma(0, 0, q_\gamma, p_{0,\gamma}) \end{pmatrix}$.

2: Evaluate $\mathcal{S}_{\mathcal{D}}(\varphi_1^{(0)}, \varphi_2^{(0)}) = \begin{pmatrix} \mathcal{S}_\gamma(\varphi_1^{(0)}, \varphi_2^{(0)}, 0, 0) - \mathcal{S}_1^{\text{NtD}}(\varphi_1^{(0)}, 0, 0) \\ \mathcal{S}_\gamma(\varphi_1^{(0)}, \varphi_2^{(0)}, 0, 0) - \mathcal{S}_2^{\text{NtD}}(\varphi_2^{(0)}, 0, 0) \end{pmatrix}$.

3: Set $r_0 = (r_{0,1}, r_{0,2}) := \chi_{\mathcal{D}} - \mathcal{S}_{\mathcal{D}}(\varphi_1^{(0)}, \varphi_2^{(0)})$.

4: Compute $\boldsymbol{P}_{\text{DD}}^{-1}(r_0) = \begin{pmatrix} \widetilde{\mathcal{S}}_1^{\text{DtN}}(r_{0,1}) \\ \widetilde{\mathcal{S}}_2^{\text{DtN}}(r_{0,2}) \end{pmatrix}$.

5: Set $\tilde{r}_0 = \boldsymbol{P}_{\text{DD}}^{-1}(r_0)$ and $q_0 = \tilde{r}_0$.

6: **for** $k = 1, \cdots, N_{\max}$ **do**: ▷ Start GMRES iterations.

7: Generate $(\varphi_1^{(k)}, \varphi_2^{(k)})$ as the solution to the least square problem:

$$\min_{(\psi_1, \psi_2) \in R_k} \|\boldsymbol{P}_{\text{DD}}^{-1}(\chi_{\mathcal{D}} - \mathcal{S}_{\mathcal{D}}(\psi_1, \psi_2))\|_{L^2},$$

where $R_k := (\varphi_1^{(0)}, \varphi_2^{(0)}) + \text{span}(q_0, q_1, \cdots, q_{k-1})$.

8: Set $\tilde{r}_k = \boldsymbol{P}_{\text{DD}}^{-1}\left(\chi_{\mathcal{D}} - \mathcal{S}_{\mathcal{D}}(\varphi_1^{(k)}, \varphi_2^{(k)})\right)$.

9: **if** $\|\tilde{r}_k\|/\|\tilde{r}_0\| \leq \epsilon$ **then**

10: stop the iteration, return $(\varphi_1, \varphi_2) = (\varphi_1^{(k)}, \varphi_2^{(k)})$.

11: **end if**

12: Compute $q_k = \boldsymbol{P}_{\text{DD}}^{-1}(\mathcal{S}_{\mathcal{D}}(q_{k-1}))$ as in Steps 2 and 4.

13: **end for**

Toward this end, we define the solution operator

$$\begin{array}{rcl} \widehat{\mathcal{S}}_\gamma : L^2(0,T;L^2(\gamma)) \times L^2(0,T;L^2(\gamma)) \times H_0^1(\gamma) & \longrightarrow & H^1(0,T;L^2(\gamma)), \\ (\varphi, q_\gamma, p_{0,\gamma}) & \longmapsto & p_\gamma, \end{array}$$

where $(p_\gamma, \boldsymbol{u}_\gamma)$ is the solution to the flow problem on the fracture:

$$\begin{array}{rcll} \phi_\gamma \partial_t p_\gamma + \text{div}_\tau \boldsymbol{u}_\gamma & = & q_\gamma + \varphi & \text{in } \gamma \times (0,T), \\ \boldsymbol{u}_\gamma & = & -\boldsymbol{K}_\gamma \delta \nabla_\tau p_\gamma & \text{in } \gamma \times (0,T), \\ p_\gamma & = & 0 & \text{on } \partial\gamma \times (0,T), \\ p_\gamma(\cdot, 0) & = & p_{0,\gamma} & \text{in } \gamma. \end{array} \tag{2.29}$$

Using $p_\gamma = \widehat{\mathcal{S}}_\gamma(\varphi, q_\gamma, p_{0,\gamma})$ as Dirichlet boundary data on the fracture-interface,

$$p_i = p_\gamma, \quad \text{on } \gamma \times (0,T),$$

we solve the subdomain problem (2.11) to obtain $(p_i, \boldsymbol{u}_i)$, from which the normal flux is computed:

$$\mathcal{S}_i^{\text{DtN}}(\widehat{\mathcal{S}}_\gamma(\varphi, q_\gamma, p_{0,\gamma}), q_i, p_{0,i}) = \boldsymbol{u}_i \cdot \boldsymbol{n}_{i|\gamma},\ i = 1, 2,$$

where $\mathcal{S}_i^{\text{DtN}}$ is the same Dirichlet-to-Neumann operator as in GTP-Schur. Finally, the interface problem for GTF-Schur is obtained by matching φ with the total normal fluxes:

$$\varphi \quad = \quad \sum_{i=1}^{2} \mathcal{S}_i^{\text{DtN}}(\widehat{\mathcal{S}}_\gamma(\varphi, q_\gamma, p_{0,\gamma}), q_i, p_{0,i}),\ \text{in } \gamma \times (0, T), \tag{2.30}$$

or in compact form,

$$\mathcal{S}_{\mathcal{F}}(\varphi) \quad = \quad \chi_{\mathcal{F}}, \quad \text{in } \gamma \times (0, T), \tag{2.31}$$

where

$$\mathcal{S}_{\mathcal{F}}(\varphi) = \sum_{i=1}^{2} \mathcal{S}_i^{\text{DtN}}(\widehat{\mathcal{S}}_\gamma(\varphi, 0, 0), 0, 0),\ \chi_{\mathcal{F}} = \sum_{i=1}^{2} \mathcal{S}_i^{\text{DtN}}(\widehat{\mathcal{S}}_\gamma(0, q_\gamma, p_{0,\gamma}), q_i, p_{0,i}).$$

Again, we solve the interface problem (2.31) iteratively using GMRES (without any preconditioner) as summarized in Algorithm 3. Numerical performance of GTF-Schur will be discussed and compared with GTP-Schur and GTD-Schur in Section 2.6.

Remark 2.3. *One can straightforwardly extend all Schur-type methods and GTO-Schwarz method to the three-dimensional case where the rock matrix is decomposed into strips (each strip being a subdomain) by non-intersecting fractures. Regarding the case of intersecting fractures, one needs to pay attention to the intersection lines and points between fractures. In particular, the Schur-type methods can be generalized by following the technique developed in [7, 8] for the Steklov–Poincaré method applying to stationary problems. For the GTO-Schwarz method, the situation is more complicated as the local Ventcel problems are less obviously solvable due to the presence of corners at the intersection of two or more fractures. Special techniques such as the interface cement equilibrated mortar method (NICEM) method introduced in [76, 75] could be used for handling such a case.*

Algorithm 3 GTF-Schur method

Input: initial guess $\varphi^{(0)}$, stopping tolerance $0 < \epsilon \ll 1$, maximum number of iterations $N_{\max}$.
Output: space-time total normal flux φ.

1: Compute $\chi_{\mathcal{F}} = \sum_{i=1}^{2} \mathcal{S}_i^{\text{DtN}}(\widehat{\mathcal{S}}_\gamma(0, q_\gamma, p_{0,\gamma}), q_i, p_{0,i})$.
2: Evaluate $\mathcal{S}_{\mathcal{F}}(\varphi^{(0)}) = \sum_{i=1}^{2} \mathcal{S}_i^{\text{DtN}}(\widehat{\mathcal{S}}_\gamma(\varphi^{(0)}, 0, 0), 0, 0)$.
3: Set $r_0 = \chi_{\mathcal{F}} - \mathcal{S}_{\mathcal{F}}(\varphi^{(0)})$.
4: **for** $k = 1, \cdots, N_{\max}$ **do**: ▷ Start GMRES iterations.
5: Generate $\varphi^{(k)}$ as a solution to the least square problem:

$$\min_{\psi \in R_k} \|\chi_{\mathcal{F}} - \mathcal{S}_{\mathcal{F}}(\psi)\|_{L^2},$$

where $R_k := \varphi^{(0)} + \text{span}(r_0, \mathcal{S}_{\mathcal{F}}(r_0), \cdots, \mathcal{S}_{\mathcal{F}}^{k-1}(r_0))$.
6: Set $r_k = \chi_{\mathcal{F}} - \mathcal{S}_{\mathcal{F}}(\varphi^{(k)})$.
7: **if** $\|r_k\|/\|r_0\| \leq \epsilon$ **then**
8: stop the iteration, return $\varphi = \varphi^{(k)}$.
9: **end if**
10: Compute $\mathcal{S}_{\mathcal{F}}^k(r_0) = \mathcal{S}_{\mathcal{F}}\left(\mathcal{S}_{\mathcal{F}}^{k-1}(r_0)\right)$ as in Step 2.
11: **end for**

2.5. Nonconforming discretization in time

All three DD methods presented in previous sections are globally in time, i.e., the subdomain problems are solved over the whole time interval at each iteration and space-time information is exchanged on the fracture-interface. Thus, it is possible to use different time steps in the fracture and in the rock matrix. In this section, we derive the semi-discrete interface problem for the proposed DD methods with nonconforming time grids.

Let $\mathcal{T}_1, \mathcal{T}_2$, and $\mathcal{T}_\gamma$ be three different partitions of the time interval $(0, T]$ into subintervals $J_m^i = \left(t_{m-1}^i, t_m^i\right]$ for $m = 1, \cdots, M_i$, and $i = 1, 2, \gamma$ (see Figure 2.2). For simplicity, we consider uniform partitions and denote by $\Delta t_i,\ i = 1, 2, \gamma$, the corresponding time steps such that $\Delta t_\gamma \ll \Delta t_i,\ i = 1, 2$ (note that the fracture is assumed to have much larger permeability than the surrounding domain). We use the backward Euler method to discretize the problem in time. The same idea can be generalized to higher order methods [58].

We denote by $P_0\left(\mathcal{T}_i,\ L^2(\gamma)\right)$ the space of functions which are piecewise constant in time on grid $\mathcal{T}_i$ with values in $L^2(\gamma)$:

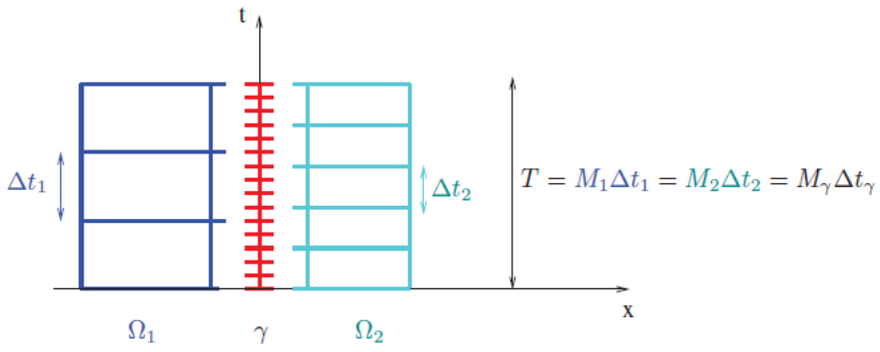

Figure 2.2: Nonconforming time grids in the rock matrix and in the fracture.

$$P_0\left(\mathcal{T}_i,\ L^2(\gamma)\right) = \left\{\psi : (0,T) \to L^2(\gamma), \psi \text{ is constant on } J,\ \forall J \in \mathcal{T}_i\right\}.$$

In order to exchange data on the space-time interface between different time grids $\mathcal{T}_i$ and $\mathcal{T}_j$ (for i, j in $\{1, 2, \gamma\}$), we use the L^2 projection Π_{ji} from $P_0\left(\mathcal{T}_i,\ L^2(\gamma)\right)$ to $P_0\left(\mathcal{T}_j,\ L^2(\gamma)\right)$: for $\psi \in P_0\left(\mathcal{T}_i,\ L^2(\gamma)\right)$, $\Pi_{ji}\psi_{|J_m^j}$ is the average value of ψ on J_m^j, for $m = 1, \cdots, M_j$.

2.5.1. GTP-Schur method

The unknown λ in (2.12) is piecewise constant in time on grid $\mathcal{T}_\gamma$ as it represents the pressure on the fracture. In order to obtain Dirichlet boundary data for the subdomain problem (2.11), we project λ into $P_0\left(\mathcal{T}_i,\ L^2(\gamma)\right)$: $p_i = \Pi_{i\gamma}(\lambda)$ on, $i = 1, 2$. The semidiscrete counterpart of the interface problem (2.12) is obtained by weakly enforcing the fracture problem over each time subinterval of $\mathcal{T}_\gamma$ as follows:

$$\begin{aligned} \phi_\gamma\left(\lambda^{m+1} - \lambda^m\right) + \int_{t_\gamma^m}^{t_\gamma^{m+1}} \mathrm{div}_\tau\, \boldsymbol{u}_\gamma^{m+1} &= \int_{t_\gamma^m}^{t_\gamma^{m+1}} \left(\sum_{i=1}^{2} \Pi_{\gamma i}\left(\mathcal{S}_i^{\mathrm{DtN}}\left(\Pi_{i\gamma}(\lambda), q_i, p_{0,i}\right)\right)\right), \\ \boldsymbol{u}_\gamma^{m+1} &= -\boldsymbol{K}_\gamma \delta \nabla_\tau \lambda^{m+1}, \end{aligned} \tag{2.32}$$

in γ, for $m = 0, \cdots, M_\gamma - 1$. Problem (2.32) is completed with the initial and boundary conditions: $\lambda^0 = p_{0,\gamma}$, in γ and $\lambda^{m+1} = 0$, on $\partial\gamma$, for $m = 0, \cdots, M_\gamma - 1$.

To compute the semi-discrete Ventcel-Ventcel preconditioner, which is still denoted by P_{VV}^{-1}, we first project the data $\theta \in P_0\left(\mathcal{T}_\gamma, L^2(\gamma)\right)$ onto the subdomain grid $\mathcal{T}_i$, $i = 1, 2$ to solve the subdomain problem with Ventcel conditions (2.18). Then P_{VV}^{-1} is obtained by projecting the trace of the subdomain pressure on the fracture-interface from $\mathcal{T}_i$ onto $\mathcal{T}_\gamma$:

$$P_{\mathrm{VV}}^{-1}(\theta) := \sum_{i=1}^{2} \sigma_i \Pi_{\gamma i} \left(\mathcal{S}_i^{\mathrm{VtD}} \left(\Pi_{i\gamma}(\theta) \right) \right). \tag{2.33}$$

2.5.2. GTD-Schur method

The two interface unknowns φ_1 and φ_2 are piecewise constant in time on the fine grid $\mathcal{T}_\gamma$: $\varphi_i \in P_0\left(\mathcal{T}_\gamma, L^2(\gamma)\right)$ for $i = 1, 2$. In order to obtain Neumann boundary data for the subdomain problem (2.20), we project φ_i into $P_0\left(\mathcal{T}_i,\ L^2(\gamma)\right)$: $\boldsymbol{u}_i \cdot \boldsymbol{n}_i = \Pi_{i\gamma}(\varphi_i)$ on, $i = 1, 2$. The semidiscrete counterpart of the interface problem (2.22) is defined on $\mathcal{T}_\gamma$ as follows:

$$\begin{aligned} \textstyle\int_{t_\gamma^m}^{t_\gamma^{m+1}} \mathcal{S}_\gamma(\varphi_1, \varphi_2, q_\gamma, p_{0,\gamma}) &= \textstyle\int_{t_\gamma^m}^{t_\gamma^{m+1}} \Pi_{\gamma 1} \left(\mathcal{S}_1^{\mathrm{NtD}} \left(\Pi_{1\gamma}(\varphi_1), q_1, p_{0,1} \right) \right), \\ \textstyle\int_{t_\gamma^m}^{t_\gamma^{m+1}} \mathcal{S}_\gamma(\varphi_1, \varphi_2, q_\gamma, p_{0,\gamma}) &= \textstyle\int_{t_\gamma^m}^{t_\gamma^{m+1}} \Pi_{\gamma 2} \left(\mathcal{S}_2^{\mathrm{NtD}} \left(\Pi_{2\gamma}(\varphi_2), q_2, p_{0,2} \right) \right), \end{aligned} \tag{2.34}$$

in γ, for $m = 0, \cdots, M_\gamma - 1$.

The semidiscrete Dirichlet-Dirichlet preconditioner $\boldsymbol{P}_{DD}^{-1}$ is computed by

$$\boldsymbol{P}_{DD}^{-1} \begin{pmatrix} \lambda_1 \\ \lambda_2 \end{pmatrix} = \begin{pmatrix} \Pi_{\gamma 1} \left(\widetilde{\mathcal{S}}_1^{\mathrm{DtN}} \left(\Pi_{1\gamma}(\lambda_1) \right) \right) \\ \Pi_{\gamma 2} \left(\widetilde{\mathcal{S}}_2^{\mathrm{DtN}} \left(\Pi_{2\gamma}(\lambda_2) \right) \right) \end{pmatrix}, \tag{2.35}$$

in which we first solve the subdomain problems with Dirichlet data projected from the $\mathcal{T}_\gamma$ onto $\mathcal{T}_i,\ i = 1, 2$, then extract the normal flux along the fracture and project backward from $\mathcal{T}_i$ onto $\mathcal{T}_\gamma$.

2.5.3. GTF-Schur method

The interface unknown φ in this case represents the total normal flux, and again, it is piecewise constant in time on $\mathcal{T}_\gamma$: $\varphi \in P_0\left(\mathcal{T}_\gamma, L^2(\gamma)\right)$. Solving the fracture problem (2.29) with φ, we obtain $p_\gamma = \widehat{\mathcal{S}}_\gamma(\varphi, q_\gamma, p_{0,\gamma}) \in P_0\left(\mathcal{T}_\gamma, L^2(\gamma)\right)$. As for GTP-Schur, the fracture pressure p_γ is projected to $\mathcal{T}_i$, for $i = 1, 2$, to give Dirichlet data for solving the subdomain problems. The semidiscrete counterpart of (2.30) is then defined on $\mathcal{T}_\gamma$ as follows:

$$\varphi^m - \sum_{i=1}^{2} \Pi_{\gamma i} \left(\mathcal{S}_i^{\mathrm{DtN}} \left(\Pi_{i\gamma} \left(\widehat{\mathcal{S}}_\gamma(\varphi, 0, 0) \right), 0, 0 \right) \right)_{|_{J_m^\gamma}} = \sum_{i=1}^{2} \Pi_{\gamma i} \left(\mathcal{S}_i^{\mathrm{DtN}} \left(0, q_\gamma, p_{0,\gamma}, q_i, p_{0,i} \right) \right)_{|_{J_m^\gamma}}, \tag{2.36}$$

on γ, for $m = 0, \cdots, M_\gamma - 1$.

2.6. Numerical results

We study and compare the convergence and accuracy in time of four global-in-time DD methods: GTP-Schur with Neumann-Neumann (N-N) or Ventcel-Ventcel (V-V) preconditioner, GTD-Schur with Dirichlet-Dirichlet (D-D) preconditioner, GTF-Schur, and GTO-Schwarz. We refer to [67] for the detailed derivation and formulation of the GTO-Schwarz method and optimized parameters. Briefly, the analysis is performed on a two half-space decomposition $\Omega_1 = \mathbb{R}^- \times \mathbb{R}, \Omega_2 = \mathbb{R}^+ \times \mathbb{R}$. The primal formulation of the two-subdomain problem with Ventcel-Robin transmission conditions is first recast into an ordinary differential equation (ODE) using a Fourier transform in time and in the y direction. The ODE is then solved to compute the convergence factor of the iterative algorithm. Finally, the optimized parameters are obtained by minimizing the convergence factor over low and high frequencies, which leads us to solving a min-max problem.

Three test cases are considered: Test case 1.1 and Test case 1.2 with a non-immersed fracture (i.e., the fracture cuts through the rock matrix), and Test case 1.3 with a partially immersed fracture. For Test case 1.1 and Test case 1.3, we assume that the two subdomains have the same permeability $\boldsymbol{K}_i = \mathsf{k}_i I$, for $i = 1, 2, f$, where $\mathsf{k}_1 = \mathsf{k}_2 = 1$ and $\mathsf{k}_f = 10^3$. For Test case 1.2, the original two subdomains are further divided into smaller strips with differerent permeability, more details will be given in Subsection 2.5.2. For spatial discretization, we consider mixed finite elements with the lowest order Raviart–Thomas space on a uniform, conforming triangular mesh of size h. We remark that the focus of this work is local time stepping; non-conforming spatial meshes will be the topic of our future work. The interface problem for each method is solved iteratively using GMRES with a random initial guess; the iteration is stopped when the residual error is less than 10^{-6} (Test case 1.1) or 10^{-8} (Test cases 1.2 and 1.3). All computed errors are relative space-time errors in the space $L^2(0, T; L^2(\mathcal{O}))$-norm, where $\mathcal{O}$ is either Ω_1, Ω_2, or γ. To compare the convergence of the corresponding iterative algorithms (with or without preconditioners), we count the number of subdomain solves instead of the number of iterations. Note that one iteration of GTP-Schur or GTD-Schur with a preconditioner costs

twice as much as one iteration of the respective method with no preconditioner (in terms of the number of subdomain solves).

2.6.1. Test case 1.1: non-immersed fracture with two subdomains

The domain of calculation $\Omega = (0, 2) \times (0, 1)$ is divided into two equally sized subdomains by a fracture of width $\delta = 0.001$ parallel to the y-axis (see Figure 2.3). For the boundary conditions, we impose $p = 1$ at the bottom and $p = 0$ at the top of the fracture. On the external boundaries of the subdomains, a no-flow boundary condition is imposed except on the lower fifth (length 0.2) of both lateral sides where a Dirichlet condition is imposed: $p = 1$ on the right and $p = 0$ on the left. We show in Figure 2.4 the snapshot of the reference solution at $T = 0.5$.

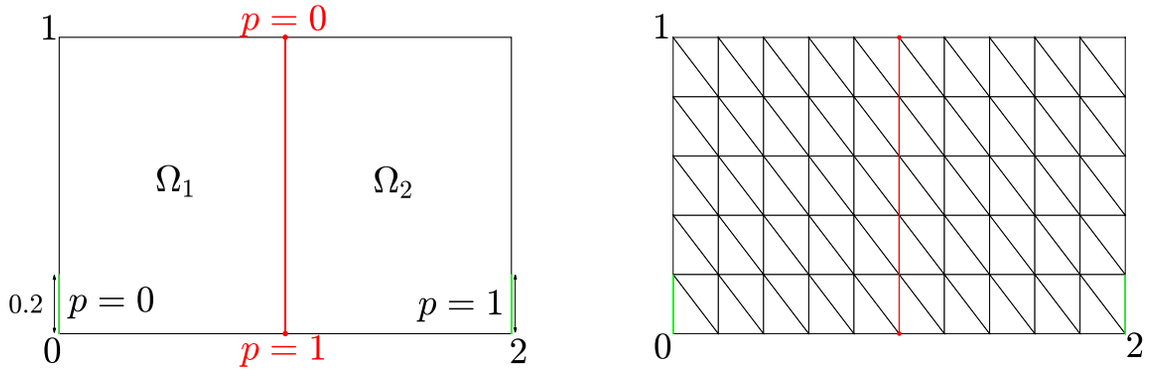

Figure 2.3: [Test case 1.1] (Left) Geometry and boundary conditions of the test case. (Right) Example of an uniform triangular mesh for spatial discretization.

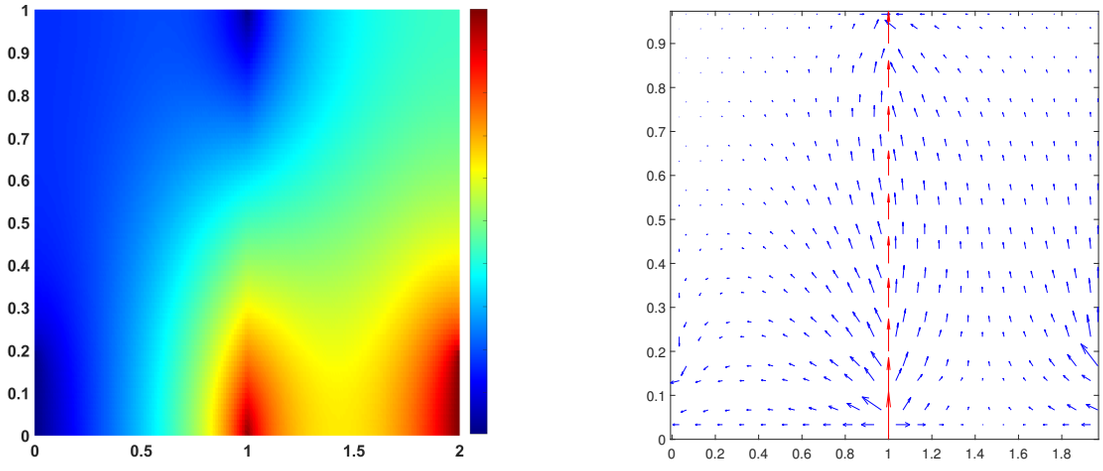

Figure 2.4: [Test case 1.1] Pressure field (left) and velocity field (right) at the final time $T = 0.5$.

We first consider the *conforming* time step case to verify the errors and compare the convergence of the four global-in-time DD algorithms. We fix the final time $T = 0.5$, the spatial mesh $h = 1/50$, and vary the time step sizes $\Delta t_i = \Delta t$ for $i = 1, 2, \gamma$. The errors are computed

using a reference solution on a fine time step $\Delta t_{\text{ref}} = T/2000$. Table 2.1 shows the L^2 errors for the pressure and velocity computed once GMRES converges. Note that all methods produce nearly the same approximate solutions since the same time step is imposed in the fracture and in the subdomains. From this table, first order convergence in time is observed for both pressure and velocity.

	Errors for pressure			Errors for velocity		
Δt	Ω_1	Ω_2	γ	Ω_1	Ω_2	γ
T/4	6.76e-02	6.82e-02	3.29e-02	4.96e-02	9.24e-02	5.47e-02
T/8	3.55e-02 [0.92]	3.57e-02 [0.93]	1.59e-02 [1.05]	2.56e-02 [0.95]	4.87e-02 [0.92]	2.64e-02 [1.05]
T/16	1.81e-02 [0.97]	1.81e-02 [0.98]	7.73e-03 [1.04]	1.30e-02 [0.97]	2.49e-02 [0.96]	1.28e-02 [1.04]
T/32	9.06e-03 [0.99]	9.07e-03 [0.99]	3.76e-03 [1.03]	6.52e-03 [0.99]	1.24e-02 [1.00]	6.24e-03 [1.03]

Table 2.1: [Test case 1.1] Relative L^2-errors of the pressure and velocity with *conforming* time steps. The corresponding convergence rates are shown in square brackets.

In Table 2.2, we report the number of subdomain solves needed to obtain such errors. In particular, we stop GMRES when the relative residual is smaller than 10^{-6}. For GTP-Schur, we see that without preconditioner, the convergence is extremely slow and deteriorates as the time step decreases. With V-V preconditioner, the number of iterations is significantly reduced and independent of the time step size. For GTD-Schur, even without a preconditioner, the performance is much better than that of GTP-Schur, and applying D-D preconditioner results in a comparable result as GTP-Schur with V-V preconditioner. Importantly, GTF-Schur works remarkably well with no preconditioner needed, and in terms of computational cost (or subdomain solves), it is the only Schur type method that can compete with GTO-Schwarz.

Next we investigate the case with *nonconforming* time grids. We only consider GTP-Schur with V-V preconditioner, GTD-Schur with D-D preconditioner, GTF-Schur and GTO-Schwarz since they give fastest convergence. The diffusion coefficients in the subdomains are the same and smaller than that in the fracture, thus we impose the same large time step in the subdomains and a smaller one in the fracture: $\Delta t_1 = \Delta t_2 = 4\Delta t_\gamma$. We show the relative errors of the pressure and velocity in Table 2.3 and 2.4, respectively. We see that these methods still

	Δt	T/4	T/8	T/16	T/32
GTP-Schur	with no precond.	191	282	331	407
	with N-N precond.	78	92	102	140
	with V-V precond.	10	12	12	12
GTD-Schur	with no precond.	33	34	33	33
	with D-D precond.	16	16	16	16
GTF-Schur		8	8	8	8
GTO-Schwarz		6	6	6	6

Table 2.2: [Test case 1.1] Numbers of subdomain solves when *conforming* time steps are used; the tolerance for GMRES is set to be 10^{-6}.

preserve the first order of convergence in time when we have nonconforming discretization in time. However, due to the nonconforming time projections, the errors are different between the following two groups:

- Group 1: GTP-Schur with V-V preconditioner, and GTO-Schwarz,
- Group 2: GTD-Schur with D-D preconditioner, and GTF-Schur.

		GTP-Schur with V-V precond. GTO-Schwarz			GTD-Schur with D-D precond. GTF-Schur		
Δt_i	Δt_γ	Ω_1	Ω_2	γ	Ω_1	Ω_2	γ
T/4	T/16	6.76e-02	6.82e-02	3.29e-02	6.34e-02	6.62e-02	1.29e-02
T/8	T/32	3.55e-02 [0.92]	3.57e-02 [0.93]	1.59e-02 [1.05]	3.27e-02 [0.95]	3.43e-02 [0.95]	6.25e-03 [1.04]
T/16	T/64	1.81e-02 [0.97]	1.81e-02 [0.98]	7.73e-03 [1.04]	1.65e-02 [0.98]	1.73e-02 [0.99]	3.01e-03 [1.05]
T/32	T/128	9.06e-03 [0.99]	9.07e-03 [0.99]	3.76e-03 [1.03]	8.22e-03 [1.00]	8.64e-03 [1.00]	1.42e-03 [1.08]

Table 2.3: [Test case 1.1] Relative L^2-errors of the *pressure* with nonconforming time grids. The corresponding convergence rates are shown in square brackets.

It can be observed by comparing with Table 2.1 that the errors in the fracture for both pressure and velocity obtained from Group 1 follow the coarse time grid in the subdomains. This behavior was observed numerically in [67] for the GTO-Schwarz method. It is due to the fact that for GTO-Schwarz and GTP-Schur with V-V preconditioner, the fracture problem is treated as the Ventcel boundary condition for the subdomain problems. Consequently, the approximate fracture pressure follows the coarse time grid in the subdomains. However, for the methods in Group 2, it can be seen that the errors in the fracture are smaller and are closer to that of the

		GT-Schur with V-V precond. GTO-Schwarz			GTD-Schur with D-D precond. GTF-Schur		
Δt_i	Δt_γ	Ω_1	Ω_2	γ	Ω_1	Ω_2	γ
T/4	T/16	4.96e-02	9.24e-02	5.47e-02	4.73e-02	9.38e-02	2.21e-02
T/8	T/32	2.56e-02 [0.95]	4.87e-02 [0.92]	2.64e-02 [1.05]	2.41e-02 [0.97]	4.87e-02 [0.95]	1.06e-02 [1.06]
T/16	T/64	1.30e-02 [0.97]	2.49e-02 [0.96]	1.28e-02 [1.04]	1.21e-02 [0.99]	2.47e-02 [0.98]	5.09e-03 [1.05]
T/32	T/128	6.52e-03 [0.99]	1.24e-02 [1.00]	6.24e-03 [1.03]	6.05e-03 [1.00]	1.23e-02 [1.00]	2.41e-03 [1.08]

Table 2.4: [Test case 1.1] Relative L^2-errors of the *velocity* with nonconforming time grids. The corresponding convergence rates are shown in square brackets.

$\Delta t_1 = \Delta t_2$	T/4	T/8	T/16	T/32
Δt_γ	T/16	T/32	T/64	T/128
GTP-Schur with V-V precond.	12	12	12	14
GTD-Schur with D-D precond.	16	16	16	16
GTF-Schur	8	8	8	8
GTO-Schwarz	6	6	6	6

Table 2.5: [Test case 1.1] Numbers of subdomain solves when *nonconforming* time steps are used; the tolerance for GMRES is set to be 10^{-6}.

fine time grid. This is because we separate the fracture problem and the subdomain problems, and the fracture problem is actually solved on the fine time grid.

We now analyze the convergence of the four algorithms. Table 2.5 shows the number of subdomain solves for each method to reach the relative residual smaller than 10^{-6}. We can see that the obtained numbers are almost the same as those in Table 2.2 and are not affected by the small time steps in the fracture. Hence, these methods are suitable for using nonconforming discretization in time. From the accuracy and convergence of the four methods in this test case, it appears that GTF-Schur is the most effective method which converges fast and preserves the accuracy in time in the fracture with smaller time steps.

2.6.2. Test case 1.2: non-immersed fracture with four subdomains and variable permeability

We consider in this subsection the case with multiple strip subdomains and variable permeability. In particular, four subdomains are formed by introducing two artificial interfaces $\gamma_{a,1}$

and $\gamma_{a,2}$ besides the fracture-interface as depicted in Figure 2.5. Each subdomain has a specific value of permeability. We assume that $\boldsymbol{K}_i = \mathsf{k}_i I, i = 1,2,3,4$ where $\mathsf{k}_1 = \mathsf{k}_4 = 1e-01$ and $\mathsf{k}_2 = \mathsf{k}_3 = 1$. The time step size on each new subdomain is denoted by $\Delta t_i, i = 1,2,3,4$, respectively. We fix the mesh size $h = 1/80$ and the final time $T = 1$. The boundary conditions and the permeability of the fracture are assumed to be the same as in Test case 1.1.

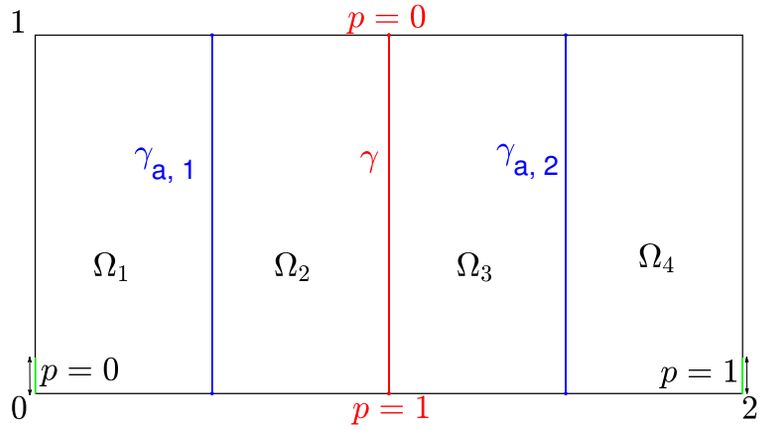

Figure 2.5: [Test case 1.2] Geometry and boundary conditions. The blue vertical lines are the artificial interfaces.

To apply global-in-time DD methods for this test case, additional transmission conditions, representing the continuity of the pressure and normal flux, are imposed on each artificial interface $\gamma_{a,i},\ i = 1,2$:

$$\begin{aligned} p_{i,1} &= p_{i,2}, \\ \boldsymbol{u}_{i,1} \cdot \boldsymbol{n}_{i,1} + \boldsymbol{u}_{i,2} \cdot \boldsymbol{n}_{i,2} &= 0, \end{aligned} \qquad \text{on } \gamma_{a,i} \times (0,T),\ i = 1,2. \tag{2.37}$$

Global-in-time DD methods for parabolic equations in a domain without fractures have been well studied in [68], and thus details of their formulations are not presented here. For the fracture-interface γ, we reuse the transmission conditions associated with the reduced fracture model (cf. Equations (2.8)-(2.9)). The interface problem for each global-in-time DD method then consists of the equations on the interface-fracture (as derived in the previous sections for the non-immersed fracture case) and the ones on the artificial interfaces as studied in [68]. For the latter, we will also use preconditioners to enhance the convergence of the iterative algorithms. In particular, for GTP-Schur and GTF-Schur, a time-dependent Neumann-Neumann preconditioner [68] is applied on each artificial interface, while for GTD-Schur, a time-dependent Dirichlet-Dirichlet preconditioner is performed. By combining all the preconditioners on the fracture-interface and on all artificial interfaces, we obtain the following

methods: preconditioned GTP-Schur, preconditioned GTD-Schur, and preconditioned GTF-Schur method. For GTO-Schwarz, the equations on the artificial interfaces represent the Robin transmission conditions with optimized parameters; more details can be found in [68].

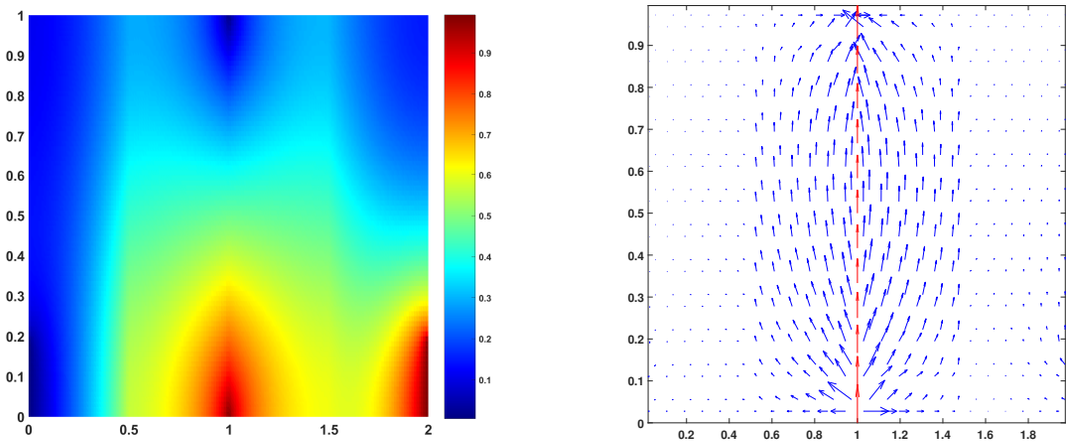

Figure 2.6: [Test case 1.2] Pressure field (left) and velocity field (right) at the final time $T = 1$.

$\Delta t_1 = \Delta t_4$	T/2	T/4	T/8	T/16
$\Delta t_2 = \Delta t_3$	T/4	T/8	T/16	T/32
Δt_γ	T/8	T/16	T/32	T/64
Precond. GTP-Schur	42	50	58	64
Precond. GTD-Schur	52	72	80	90
Precond. GTF-Schur	22	22	22	22
GTO-Schwarz	25	26	26	28

Table 2.6: [Test case 1.2] Numbers of subdomain solves when *nonconforming* time steps are used; the tolerance for GMRES is set to be 10^{-8}.

We first show in Figure 2.6 the snapshots of the pressure field and velocity field at the final time $T = 1$. As the regions near the lateral boundaries have smaller permeability compared to the ones near the fracture, the magnitude of the corresponding vector field is smaller there than near the fracture. We report next in Table 2.6 the number of subdomain solves obtained from each method. Preconditioned GTD-Schur is the slowest method among the three Schur-type methods, while preconditioned GTF-Schur is the fastest. Preconditioned GTF-Schur is also the only Schur-type method that is comparable to GTO-Schwarz in terms of convergence speed. Moreover, preconditioned GTF-Schur as well as GTO-Schwarz are the only methods that are mostly independent of the size of the time grid. From Tables 2.5 and 2.6, we deduce that preconditioned GTF-Schur is the most efficient Schur-type method for the case of strong heterogeneity as it still preserves its fast convergence while for the other two methods, the

increasing in the number of subdomain solves is significant. We remark that our main focus for this test case is the convergence speed of the proposed methods when multiple subdomains with variable permeability are used. Results regarding the accuracy in time are similar to what we observe in Test case 1.1 (as well as in the next test case), thus are omitted here.

2.6.3. Test case 3: partially immersed fracture

We consider a test case adapted from [9] where only one tip of the fracture is attached to the external boundary, while the other tip is submerged inside the rock matrix as depicted in Figure 2.7 (left). A no-flow boundary condition is considered at the tip which is immersed inside the domain, while $p = 1$ is imposed at the other tip. Analysis of the steady-state flow problem with an immersed fracture can be found in [9] and the references therein. For the external boundary, the pressure is prescribed on the upper fifth (length 0.2) of both lateral sides, $p = 1$ on the right and $p = 0$ on the left, and a no-flow condition is imposed on the rest of the boundary. Note that we use the same physical parameters as in Test case 1.1.

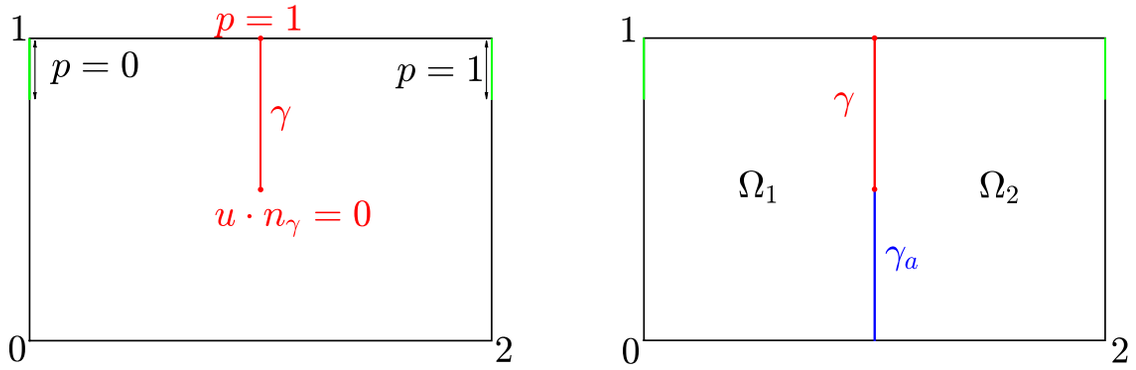

Figure 2.7: [Test case 1.3] (Left) Geometry and boundary conditions with immersed fracture γ. (Right) An artificial interface γ_a is introduced to decompose the domain into two disjoint subdomains.

To apply global-in-time DD methods for this test case, we first introduce an artificial interface γ_a so that, together with the partially immersed fracture γ, they form a single fracture Γ separating the original domain into two disjoint subdomains (cf. Figure 2.7 (right)). Next, suitable transmission conditions will be imposed on this new interface Γ. On the fracture-interface γ, we make use of the Equations (2.8)-(2.9)) representing the transmission conditions for the reduced fracture model. Note that due to the presence of the immersed tip, we use a no-flow boundary condition at that tip, instead of a Dirichlet condition as in Test case 1.1.

On the artificial interface γ_a, we impose the same standard DD transmission conditions (cf. Equations (2.37)) as in Test case 1.2. The interface system on $\Gamma \times (0,T)$ for each method is then a combination of the equations on both $\gamma \times (0,T)$ and $\gamma_a \times (0,T)$. Similar to Test case 1.2, preconditioning is needed for the interface problem on $\gamma_a \times (0,T)$ to improve the convergence speed of all Schur-type methods. In particular, we reuse the Neumann-Neumann preconditioner for GTP-Schur and GTF-Schur, and apply the Dirichlet-Dirichlet preconditioner for GTD-Schur as what has been done in Test case 1.2. As a result, we obtain the following methods: preconditioned GTP-Schur , preconditioned GTD-Schur and preconditioned GTF-Schur. These methods will be tested and compared with the performance of GTO-Schwarz. Note that the transmission conditions for GTO-Schwarz on the artificial interface $\gamma_a \times (0,T)$ are still Robin conditions with optimized parameters as in Test case 1.2.

We first show the snapshots of pressure and velocity fields at the final time $T = 1$ in Figure 2.8. The length of each arrow is proportional to the magnitude of the velocity and the red arrows represent the flow in the fracture. The length of the red arrows decreases as the flow travels toward the immersed tip since a no-flow boundary condition is imposed there. As $\mathsf{k}_f \gg \mathsf{k}_i,\ i = 1,2$, the velocity in the fracture has larger magnitude than the one in the rock matrix.

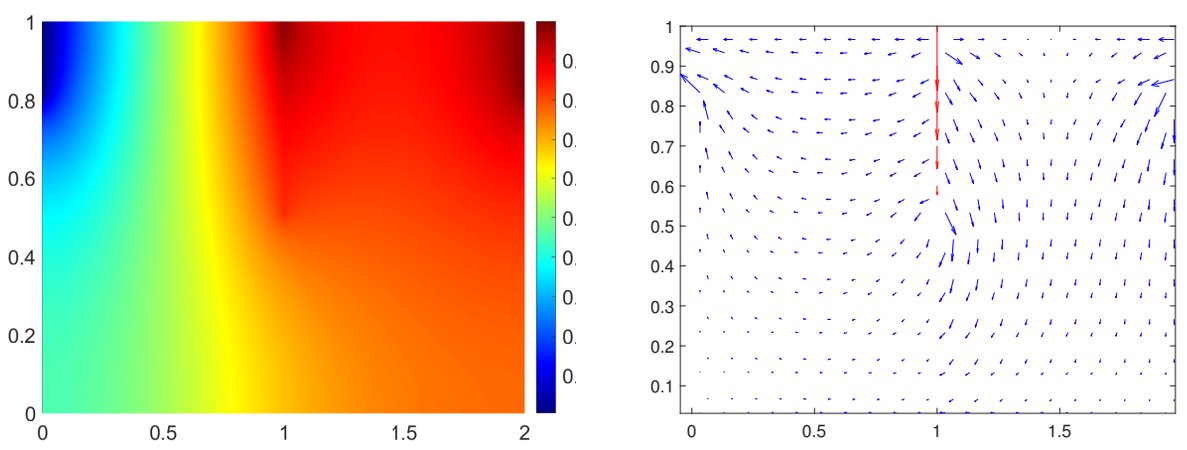

Figure 2.8: [Test case 1.3] Pressure field (left) and velocity field (right) at the final time $T = 1$.

Next, we present the numerical results for these methods when *conforming* time grids are used. We fix the spatial mesh $h = 1/100$ and vary the time step sizes $\Delta t_i = \Delta t$ for $i = 1, 2, \gamma$. The reference solution used in computing the errors are found on a fine time grid $\Delta t_{\text{ref}} = T/2000$ where $T = 1$. Table 2.7 shows the relative L^2-errors computed from all

methods for pressure and velocity. Similar to the non-immersed fracture case, we only have one table showing the errors for each term since the approximate solutions obtained from all method are nearly the same. It can be observed that we still have first-order convergence in time for both pressure and velocity, even in the immersed fracture case which is more complicated.

We report in Table 2.8 the number of subdomain solves needed to reach the errors obtained in Table 2.7. It can be seen that among the proposed methods, the preconditioned GTD-Schur has the slowest convergence speed. Unlike Test case 1.1, the preconditioner GTP-Schur is the fastest method compared to the other Schur-type methods, even faster than GTO-Schwarz. The convergence speed of preconditioned GTF-Schur is acceptable and is comparable to that of GTO-Schwarz.

	Errors for pressure			Errors for velocity		
Δt	Ω_1	Ω_2	γ	Ω_1	Ω_2	γ
T/4	7.85e-02	6.67e-02	2.55e-02	8.52e-02	2.88e-01	1.97e-01
T/8	4.15e-02 [0.92]	3.43e-02 [0.96]	1.27e-02 [1.00]	4.54e-02 [0.91]	1.49e-01 [0.95]	9.83e-02 [1.00]
T/16	2.12e-02 [0.97]	1.73e-02 [0.99]	6.36e-03 [0.99]	2.34e-02 [0.96]	7.55e-02 [0.98]	4.93e-02 [0.99]
T/32	1.07e-02 [0.99]	8.65e-03 [1.00]	3.17e-03 [1.00]	1.18e-02 [0.99]	3.77e-02 [1.00]	2.46e-02 [1.00]

Table 2.7: [Test case 1.3] Relative L^2-errors of the pressure and velocity with *conforming* time steps. The corresponding convergence rates are shown in square brackets.

Methods \ Δt	T/4	T/8	T/16	T/32
Preconditioned GTP-Schur	16	16	16	18
Preconditioned GTD-Schur	42	50	62	66
Preconditioned GTF-Schur	18	20	22	24
GTO-Schwarz	23	23	24	24

Table 2.8: [Test case 1.3] Numbers of subdomain solves when *conforming* time steps are used; the tolerance for GMRES is set to be 10^{-8}.

We next investigate the numerical performance of these methods with *nonconforming* time grids. For the preconditioned GTP-Schur and preconditioned GTD-Schur methods, numerical results suggest that the initial guess for GMRES needs to be rescaled to obtain accurate numerical solutions. Such a rescaling is done in our numerical experiments by using the Hegedüs formula (cf. [82, Chapter 5, Subsection 5.8.3]). The relative errors for pressure and velocity

		Preconditioned GTP-Schur GTO-Schwarz			Preconditioned GTD-Schur Preconditioned GTF-Schur		
Δt	Δt_γ	Ω_1	Ω_2	γ	Ω_1	Ω_2	γ
T/4	T/16	7.85e-02	6.67e-02	2.55e-02	7.61e-02	6.51e-02	1.50e-02
T/8	T/32	4.15e-02 [0.92]	3.43e-02 [0.96]	1.27e-02 [1.00]	3.98e-02 [0.93]	3.33e-02 [0.97]	7.32e-03 [1.03]
T/16	T/64	2.12e-02 [0.97]	1.73e-02 [0.99]	6.36e-03 [0.99]	2.04e-02 [0.96]	1.67e-02 [0.99]	3.58e-03 [1.03]
T/32	T/128	1.07e-02 [0.99]	8.65e-03 [1.00]	3.17e-03 [1.00]	1.02e-02 [1.00]	8.33e-03 [1.00]	1.75e-03 [1.03]

Table 2.9: [Test case 1.3] Relative L^2-errors of the *pressure* with nonconforming time grids. The corresponding convergence rates are shown in square brackets.

		Preconditioned GTP-Schur GTO-Schwarz			Preconditioned GTD-Schur Preconditioned GTF-Schur		
Δt	Δt_γ	Ω_1	Ω_2	γ	Ω_1	Ω_2	γ
T/4	T/16	8.51e-02	2.88e-01	1.97e-01	8.38e-02	2.86e-01	1.18e-01
T/8	T/32	4.54e-02 [0.91]	1.49e-01 [0.95]	9.83e-02 [1.00]	4.41e-02 [0.93]	1.47e-01 [0.96]	5.73e-02 [1.04]
T/16	T/64	2.34e-02 [0.96]	7.55e-02 [0.98]	4.93e-02 [0.99]	2.26e-02 [0.96]	7.36e-02 [0.99]	2.80e-02 [1.03]
T/32	T/128	1.18e-02 [0.99]	3.77e-02 [1.00]	2.46-02 [1.00]	1.13e-02 [1.00]	3.66e-02 [1.01]	1.37e-02 [1.03]

Table 2.10: [Test case 1.3] Relative L^2-errors of the *velocity* with nonconforming time grids. The corresponding convergence rates are shown in square brackets.

$\Delta t_1 = \Delta t_2$	T/4	T/8	T/16	T/32
Δt_γ	T/16	T/32	T/64	T/128
Preconditioned GTP-Schur	16	14	14	14
Preconditioned GTD-Schur	42	50	60	66
Preconditioned GTF-Schur	18	20	22	24
GTO-Schwarz	23	24	24	24

Table 2.11: [Test case 1.3] Numbers of subdomain solves when *nonconforming* time steps are used; the tolerance for GMRES is set to be 10^{-8}.

are presented in Table 2.9 and Table 2.10. Similar to Test case 1.1, we impose the same large time step in the subdomains and a smaller one in the fracture: $\Delta t_1 = \Delta t_2 = \Delta t = 4\Delta t_\gamma$. We consider the same groups of errors as in Test case 1.1. By comparing with Table 2.7, we can see that the fine time grids in the fracture do not affect the errors in the fracture for both pressure and velocity observed from Group 1, that is, we still obtain the same errors as when we

only have coarse time grids in the subdomains and in the fracture. On the contrary, such errors provided by Group 2 are smaller, and closer to the ones obtained when we apply the same fine time grids in the subdomains and the fracture. These behaviors are as expected as explained in Test case 1.1.

Finally, we present the number of subdomain solves for each method to reach the relative residual smaller than 10^{-8} to analyze their convergent behaviors. These numbers are shown in Table 2.11. It can be seen that we obtain nearly the same numbers as those in Table 2.8. Hence, as in Test case 1.1, these methods are applicable under nonconforming time discretizations. From what we have observed so far, similar to Test case 1.2, Test case 1.3 is more challenging than Test case 1.1, which can be seen in the increasing of the subdomain solves. However, the preconditioned GTF-Schur still shows its efficiency as it has relatively fast convergence speed and preserves the accuracy in time when we have different time steps in the fracture and in the subdomains.

Conclusion

In this chapter, three global-in-time DD methods, namely GTP-Schur, GTD-Schur, and GTF-Schur, have been developed for a reduced fracture model of compressible flow problems, in which different time steps can be used in the fracture and in the matrix. Efficient preconditioners have been derived for GTP-Schur and GTD-Schur to enhance the convergence of the iterative algorithms. This new preconditioner of GTP-Schur significantly improve the performance of the method compared to the existing preconditioners. Importantly, a new method, GTF-Schur, is proposed; this method is typical of the reduced fracture model and requires no preconditioner. Numerical experiments for 2D problems with different types of fractures and with two or more subdomains have been carried out to investigate and compare the performance of the proposed methods with GTO-Schwarz on conforming and nonconforming time grids. We discretize the models in space by using mixed finite elements with the lowest order Raviart-Thomas spaces on triangles and in time by applying first-order backward Euler method. The obtained results suggest that among the global-in-time DD methods presented in

this chapter, GTF-Schur is the most efficient method as it converges fast without the need of a preconditioner while still preserves the accuracy in time in the fracture when smaller time steps are used in the fracture and larger ones in the rock matrix. In the next chapters, we consider the reduced fracture model of the advection-diffusion problem and aim to derive local time stepping solvers for this model by coupling the above global-in-time DD methods with operator splitting.

Chapter 3

Local time-stepping methods for the reduced fracture model of transport problems with operator splitting

Contents

In this chapter, we construct three global-in-time DD methods, namely GTP-Schur, GTF-Schur, and GTO-Schwarz, in the context of operator splitting to solve numerically the reduced fracture model of the transport problems. The use of operator splitting allows separate treatment for the advection equation and the diffusion equation: the former is approximated with the explicit Euler method in time and with an upwind, cell-centered finite volume method in

space, while the latter is discretized with the implicit Euler method in time and with a mixed finite element method in space. This chapter consists of three main parts. In the first part, we introduce the reduced fracture model of the linear advection-diffusion equation and its fully discrete formulation using operator splitting. For the second part, we derive GTP-Schur, GTF-Schur, and GTO-Schwarz from the mono-domain solver by constructing appropriate transmission conditions for the advection part and combining them with those for the diffusion part. We also describe how to formulate these interface equations when nonconforming time grids are used via L^2-projection operators introduced in Chapter 2. In the last part, we present numerical results with different Péclet numbers and with different types of fracture to investigate and compare the performance of the proposed methods.

3.1. Operator splitting and discretization of reduced fracture models

3.1.1. Reduced fracture model of linear transport problems

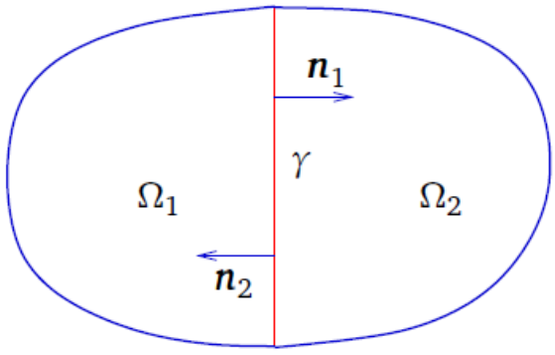

Figure 3.1: The domain Ω with the fracture-interface γ.

In this chapter, Ω is a bounded domain in $\mathbb{R}^d$ $(d = 2,\ \ 3)$ having Lipschitz boundary $\partial\Omega$ which is divided into two disjoint subdomains $\Omega_i,\ i = 1,\ 2$, by a fracture γ, which is a surface of dimension $(d-1)$ as depicted in Figure 3.1. The fracture is supposed to be a subdomain of Ω with higher permeability compared to that in the subdomains. Its thickness δ is supposed to be small compared to the size of the domain Ω, so it is considered to be an interface between the subdomains. We denote by $\boldsymbol{n}_i$ the unit outside normal to $\partial\Omega_i \cap \partial\Omega$, and by $\boldsymbol{n}_\gamma$ that to $\partial\gamma$.

We consider the following linear advection-diffusion equations written in mixed formulation

$$\begin{aligned} \phi\partial_t c + \text{div}\,(\boldsymbol{u}c + \boldsymbol{r}) &= q && \text{in } \Omega \times (0,T), \\ \boldsymbol{r} &= -\boldsymbol{K}\nabla c && \text{in } \Omega \times (0,T), \\ c &= 0 && \text{on } \partial\Omega \times (0,T), \\ c(\cdot,0) &= c_0 && \text{in } \Omega, \end{aligned} \tag{3.1}$$

where c is the concentration of a contaminant dissolved in a fluid, q is the source term, ϕ is the porosity, $\boldsymbol{u}$ is the Darcy velocity (assume to be given and time-independent), and $\boldsymbol{D}$ is a symmetric time-independent diffusion tensor.

For each $i = 1,\ 2,\ \gamma$, we denote by c_i the concentration of a contaminant dissolved in a fluid, $\boldsymbol{r_i}$ the transport velocity, i_i the porosity, q_i the source term, $\boldsymbol{u}_i$ the Darcy velocity, and $\boldsymbol{D}_i$ the symmetric time-independent diffusion tensor, in each subdomain and in the fracture, respectively. With such notation, by following the same steps introduced in Section 2.1, we obtain the reduced fracture model of (3.1) which consists of the following equations in the subdomains

$$\begin{aligned} \phi_i\partial_t c_i + \text{div}\,(\boldsymbol{u}_i c_i + \boldsymbol{r}_i) &= q_i && \text{in } \Omega_i \times (0,T), \\ \boldsymbol{r}_i &= -\boldsymbol{D}_i\nabla c_i && \text{in } \Omega_i \times (0,T), \\ c_i &= 0 && \text{on } (\partial\Omega_i \cap \partial\Omega) \times (0,T), \\ c_i &= c_\gamma && \text{on } \gamma \times (0,T), \\ c_i(\cdot,0) &= c_{0,i} && \text{in } \Omega_i, \end{aligned} \tag{3.2}$$

for $i = 1,\ 2$, and in the fracture

$$\begin{aligned} \phi_\gamma\partial_t c_\gamma + \text{div}_\tau\,(\boldsymbol{u}_\gamma c_\gamma + \boldsymbol{r}_\gamma) &= q_\gamma + \sum_{i=1}^{2}(\boldsymbol{r}_i\cdot\boldsymbol{n}_i + (\boldsymbol{u}_i\cdot\boldsymbol{n}_i)c_i)_{|\gamma} && \text{in } \gamma \times (0,T), \\ \boldsymbol{r}_\gamma &= -\boldsymbol{D}_\gamma\delta\nabla_\tau c_\gamma && \text{in } \gamma \times (0,T), \\ c_\gamma &= 0 && \text{on } \partial\gamma \times (0,T), \\ c_\gamma(\cdot,0) &= c_{0,\gamma} && \text{in } \gamma. \end{aligned} \tag{3.3}$$

In the next subsection, we use operator splitting to discretize the advection and the diffusion to obtain the fully discrete formulation for (3.2)-(3.3).

3.1.2. Operator splitting for the monolithic problem

We consider a first-order time splitting method to separate the advection and the diffusion in (3.2)-(3.3) and treat them with different spatial and temporal discretization. In time, the

advection is approximated by the forward Euler method and the diffusion by the backward Euler method. In space, we consider two locally mass-conserving approximation schemes: an upwind, cell-centered finite volume method for the advection equation, and a mixed finite element method for the diffusion equation. In the following, we present the fully discrete problem associated with these techniques. Note that operator splitting can be derived without considering the spatial discretization for the advection and diffusion problems.

For the discretization in time, we consider a uniform partition of $(0,\ T)$ into N sub-intervals $(t^n,\ t^{n+1})$ of length $\Delta t = t^{n+1} - t^n$, for $n = 0, \ldots, N-1$. This partition will be used for the diffusion step. For the advection step, we further divide each interval $(t^n,\ t^{n+1})$ (for $n = 0, \ldots, N-1$) into L sub-intervals $\{(t^{n,l},\ t^{n,l+1})\}_{l=0,\ldots,L-1}$ of length $\Delta t_a = \Delta t/L,\ \ L \geq 1$ with $t^{n,0} = t^n,\ \ t^{n,L} = t^{n+1}$ and $t^{n,l} = t^n + l\Delta t_a$ for $l = 1, \ldots, L-1$. This second partition allows our explicit scheme used on the advection equations to satisfy the CFL condition without imposing that condition on the diffusion equations.

For the discretization in space, we let $\mathcal{K}_{h,i}$ be a finite element partition of $\Omega_i\ (i = 1,\ 2)$ into d-simplicial elements (i.e. triangles for $d = 2$ and tetrahedra for $d = 3$) such that the two partitions match up at the interface γ. For simplicity, we only consider $d = 2$. We denote by $\mathcal{E}_{h,i}$ the set of all edges of elements of $\mathcal{K}_{h,i}$, and $\mathcal{G}_{h,i}$ the set of those lying on the interface γ. Since $\mathcal{K}_1$ and $\mathcal{K}_2$ coincide on γ, the spaces $\mathcal{G}_{h,1}$ and $\mathcal{G}_{h,2}$ are identical, thus we set $\mathcal{G}_h := \mathcal{G}_{h,1} = \mathcal{G}_{h,2}$. For an element K_i of $\mathcal{K}_{h,i}$ (respectively an edge E_i of K_i), denote by $\boldsymbol{n}_{K_i}$ (respectively $\boldsymbol{n}_{E,i}$) the unit, outward normal vector on ∂K_i (respectively ∂E_i). For $i = 1,\ 2$, we consider the lowest order Raviart-Thomas mixed finite element spaces $M_{h,i} \times \Sigma_{h,i} \subset L^2(\Omega_i) \times H(\mathrm{div}, \Omega_i)$:

$$M_{h,i} = \left\{\mu \in L^2(\Omega_i) :\ \mu_{|K_i} = \text{const},\ \ \forall K_i \in \mathcal{K}_{h,i}\right\},$$

$$\Sigma_{h,i} = \left\{\boldsymbol{v} \in H(\mathrm{div}, \Omega_i) :\ \boldsymbol{v}_{|K_i} = (b_{K,i} + a_{K,i}x,\ c_{K,i} + a_{K,i}y), (a_{K,i},\ b_{K,i},\ c_{K,i}) \in \mathbb{R}^3,\ \forall K_i \in \mathcal{K}_{h,i}\right\}.$$

Similarly for the fracture, let $\Lambda_h \times \Sigma_{h,\gamma} \subset L^2(\gamma) \times H(\mathrm{div}_\tau, \gamma)$ be the lowest order Raviart-Thomas spaces in one dimension:

$$\Lambda_h = \left\{\lambda \in L^2(\gamma) :\ \lambda_{|E} = \text{const},\ \forall E \in \mathcal{G}_h\right\},$$

$$\Sigma_{h,\gamma} = \left\{\boldsymbol{w} \in H(\mathrm{div}_\tau, \gamma) :\ \boldsymbol{w}_{|E} = az + b,\ (a,\ b) \in \mathbb{R}^2,\ \forall E \in \mathcal{G}_h\right\}.$$

As the advection equations are solved using an upwind scheme, we let

$$\mathcal{G}_{h,i}^{\text{in}} = \left\{E \in \mathcal{G}_h : \int_E \boldsymbol{u}_i \cdot \boldsymbol{n}_{K_i} < 0\right\}, \quad \mathcal{G}_{h,i}^{\text{out}} = \left\{E \in \mathcal{G}_h : \int_E \boldsymbol{u}_i \cdot \boldsymbol{n}_{K_i} > 0\right\},$$
$$\mathcal{G}_{h,i}^{\text{in}} = \left\{E \in \mathcal{G}_h : \int_E \boldsymbol{u}_i \cdot \boldsymbol{n}_{K_i} < 0\right\}, \quad \mathcal{G}_{h,i}^{\text{out}} = \left\{E \in \mathcal{G}_h : \int_E \boldsymbol{u}_i \cdot \boldsymbol{n}_{K_i} > 0\right\},$$

The sets $\mathcal{G}_{h,i}^{\text{in}}$ and $\mathcal{G}_{h,i}^{\text{out}}$, $i = 1, 2$ represent the inflow and outflow boundary edges on the interface for each subdomain. We remark that because of the presence of the fracture with strong heterogeneity property, the normal component of the Darcy velocity may not be continuous across the fracture-interface; therefore, $\mathcal{G}_{h,i}^{\text{in}}$ and $\mathcal{G}_{h,j}^{\text{out}}$ for $i = 1,\ 2,\ j = (3-i)$ are not the same. This is different from the case with artificial interfaces (resulted from nonoverlapping domain decomposition) where the flux is continuous across the interfaces (see, e.g., [66]). Next, we define the upwind values $\hat{c}_{h,i}^{n,l}$, for $n = 0, \ldots, N-1$, $l = 0, \ldots, L-1$, on each edge of the subdomain mesh, which depend on the normal component of the Darcy velocity $\boldsymbol{u}_i,\ i = 1,\ 2$. For $E \in \mathcal{E}_{h,i}$ and $E \not\subset \partial\Omega$, let $u_{K_i,E} := \dfrac{1}{|E|}\int_E \boldsymbol{u}_i \cdot \boldsymbol{n}_{K_i}$, where $K_i \in \mathcal{K}_{h,i}$ such that $E \subset \partial K_i$. If $E \in \mathcal{E}_{h,i}$ lying on the boundary $\partial\Omega$, let $u_{\Omega_i,E} := \dfrac{1}{|E|}\int_E \boldsymbol{u}_i \cdot \boldsymbol{n}_i$. The upwind values for the two-dimensional advection problems in the subdomains are defined using the upwind operators $\mathcal{U}_{h,i},\ i = 1,\ 2$:

$$\begin{aligned} \mathcal{U}_{h,i} : \ M_{h,i} \times \Lambda_i \ &\longrightarrow \mathcal{N}_{h,i} \\ \left(c_{h,i}^{n,l}, c_{h,\gamma}^{n,l}\right) \ &\mapsto \hat{c}_{h,i}^{n,l}, \end{aligned} \tag{3.4}$$

where

$$\left(\hat{c}_{h,i}^{n,l}\right)_{|E} = \begin{cases} 0, & \text{if } E \subset \partial\Omega_i \cap \Omega \text{ and } u_{\Omega_i,E} < 0, \\ \left(c_{h,i}^{n,l}\right)_{|K}, & \text{if } E \subset \Omega_i \text{ and } K \text{ is an element in } \mathcal{K}_{h,i}, \\ & \text{having } E \text{ as an edge and } u_{K_i,E} \geq 0, \\ \left(c_{h,\gamma}^{n,l}\right)_{|E}, & \text{if } E \subset \mathcal{G}_{h,i}^{\text{in}}. \end{cases} \tag{3.5}$$

Similarly for the one-dimensional advection equation in the fracture, the upwind values $\left(\hat{c}_{h,\gamma}^{n,l}\right)_{\substack{n=0,\ldots,N-1 \\ l=0,\ldots,L-1}}$ are defined at each endpoint P of the edge E in $\mathcal{G}_h$ and are given by $\hat{c}_{h,\gamma}^{n,l} := \mathcal{U}_{h,\gamma}\left(c_{h,\gamma}^{n,l}\right)$:

$$\left(\hat{c}_{h,\gamma}^{n,l}\right)_{|P} = \begin{cases} 0 & \text{if } P \in \partial\gamma \text{ and } u_{P,E} \leq 0, \\ \left(c_{h,\gamma}^{n,l}\right)_{|E} & \text{if } u_{P,E} > 0, \end{cases} \tag{3.6}$$

where $u_{P,E} = (\boldsymbol{u}_\gamma \cdot \boldsymbol{n}_E)_{|P}$. Finally, let $c_{h,i}^0$ be the L^2-projection of $c_{0,i}$ onto $M_{h,i}$ for $i = 1,\ 2$:

$$c_{h,i|K_i}^0 := \frac{1}{|K_i|}\int_{K_i} c_{0,i}, \quad \forall K_i \in \mathcal{K}_{h,i}, \tag{3.7}$$

and $c^0_{h,\gamma}$ be the L^2-projection of $c_{0,\gamma}$ onto Λ_h:

$$c^0_{h,\gamma|E} := \frac{1}{|E|}\int_E c_{0,\gamma}, \quad \forall E \in \mathcal{G}_h. \tag{3.8}$$

With the above notation, the fully discrete problem for (3.2)-(3.3) is defined as follows: for $n = 0, \ldots, N-1$,

1. set $c^{n,0}_{h,i} = c^n_{h,i},\ i = 1,\ 2$, and $c^{n,0}_{h,\gamma} = c^n_{h,\gamma}$ where $c^0_{h,i},\ c^0_{h,\gamma}$ are given by (3.7) and (3.8), respectively;

2. for $l = 0, \ldots, L-1$,

   (a) set $\hat{c}^{n,l}_{h,i}\ \ (i = 1,\ \ 2)$ and $\hat{c}^{n,l}_{h,\gamma}$ as in (3.5) and (3.6),

   (b) solve the advection equations in $\Omega_i\ (i = 1,\ 2)$ and on γ:

$$\int_{K_i} \phi_i \frac{c^{n,l+1}_{h,i} - c^{n,l}_{h,i}}{\Delta t_a} + \sum_{E \in \partial K_i} \left(\hat{c}^{n,l}_{h,i}\right)_{|E} |E| u_{K_i,E} \ = \ 0, \quad \forall K_i \in \mathcal{K}_{h,i}, \tag{3.9}$$

$$\int_E \phi_\gamma \frac{c^{n,l+1}_{h,\gamma} - c^{n,l}_{h,\gamma}}{\Delta t_a} + \sum_{P \in \partial E} \left(\hat{c}^{n,l}_{h,\gamma}\right)_{|P} u_{P,E} \ = \ \int_E \sum_{i=1}^{2} \hat{c}^{n,l}_{h,i} (\boldsymbol{u}_i \cdot \boldsymbol{n}_{i|\gamma}), \quad \forall E \in \mathcal{G}_h, \tag{3.10}$$

   with $c^{n,l}_{h,i}$ and $c^{n,l}_{h,\gamma}$ known to obtain $c^{n,l+1}_{h,i}$ and $c^{n,l+1}_{h,\gamma}$;

3. solve the coupled diffusion problem in $\Omega_i\ \ (i = 1,\ 2)$ and on γ with the initial conditions $c^{n,L}_{h,i}$ and $c^{n,L}_{h,\gamma}$:

$$\begin{aligned} &\int_{K_i} \phi_i \frac{c^{n+1}_{h,i} - c^{n,L}_{h,i}}{\Delta t} + \int_{K_i} \text{div}\, \boldsymbol{r}^{n+1}_{h,i} = \int_{K_i} q_i(t^{n+1}), \quad \forall K_i \in \mathcal{K}_{h,i}, \\ &\int_\Omega \boldsymbol{D}_i^{-1} \boldsymbol{r}^{n+1}_{h,i} \cdot \boldsymbol{v}_{h,i} - \int_\Omega c^{n+1}_{h,i} \text{div}\, \boldsymbol{v}_{h,i} = -\int_\gamma c^{n+1}_{h,\gamma} \left(\boldsymbol{v}_{h,i} \cdot \boldsymbol{n}_{i|\gamma}\right), \quad \forall \boldsymbol{v}_{h,i} \in \Sigma_{h,i}, \end{aligned} \tag{3.11}$$

$$\begin{aligned} &\int_E \phi_\gamma \frac{c^{n+1}_{h,\gamma} - c^{n,L}_{h,\gamma}}{\Delta t} + \int_E \text{div}_\tau \boldsymbol{r}^{n+1}_{h,\gamma} = \int_E \left(q_\gamma(t^{n+1}) + \sum_{i=1}^{2} \boldsymbol{r}^{n+1}_{h,i} \cdot \boldsymbol{n}_{i|\gamma}\right), \quad \forall E \in \mathcal{G}_h, \\ &\int_\gamma (\boldsymbol{D}_\gamma \delta)^{-1} \boldsymbol{r}^{n+1}_{h,\gamma} \cdot \boldsymbol{v}_{h,\gamma} - \int_\gamma c^{n+1}_{h,\gamma} \text{div}_\tau \boldsymbol{v}_{h,\gamma} = 0, \quad \forall \boldsymbol{v}_{h,\gamma} \in \Sigma_{h,\gamma}, \end{aligned} \tag{3.12}$$

   to obtain $c^{n+1}_{h,i}, \boldsymbol{r}^{n+1}_{h,i}, c^{n+1}_{h,\gamma},$ and $\boldsymbol{r}^{n+1}_{h,\gamma}$.

The fully discrete system (3.9)-(3.12) can be solved directly to obtain the approximate solution of the original problem (3.2)-(3.3). Alternatively, it can be reformulated as a global-in-time DD algorithm. We begin with decoupling (3.9)-(3.12) into the following local problems on each $\Omega_i,\ i = 1, 2$: for $n = 0, \ldots, N-1$,

1. set $c_{h,i}^{n,0} = c_{h,i}^{n}, \;\; i = 1,\; 2$, where $c_{h,i}^{0}$, are given by (3.7);

2. for $l = 0, \ldots, L-1$,

   (a) set $\hat{c}_{h,i}^{n,l} = \mathcal{U}_{h,i}\left(c_{h,i}^{n,l}, (c_{h,i}^{n,l})_{|\gamma}\right) \;\; (i = 1,\; 2)$,

   (b) solve the advection equation:

$$\int_{K_i} \phi_i \frac{c_{h,i}^{n,l+1} - c_{h,i}^{n,l}}{\Delta t_a} + \sum_{E \in \partial K_i} \left(\hat{c}_{h,i}^{n,l}\right)_{|E} |E| u_{K_i,E} \;\; = \;\; 0, \quad \forall K_i \in \mathcal{K}_{h,i}, \tag{3.13}$$

   with $c_{h,i}^{n,l}$ known to obtain $c_{h,i}^{n,l+1},\; i = 1, 2, ;$

3. solve the diffusion problem with the initial condition $c_{h,i}^{n,L}$:

$$\begin{aligned} &\int_{K_i} \phi_i \frac{c_{h,i}^{n+1} - c_{h,i}^{n,L}}{\Delta t} + \int_{K_i} \text{div}\, \boldsymbol{r}_{h,i}^{n+1} = \int_{K_i} q_i(t^{n+1}), \quad \forall K_i \in \mathcal{K}_{h,i}, \\ &\int_{\Omega} \boldsymbol{D}_i^{-1} \boldsymbol{r}_{h,i}^{n+1} \cdot \boldsymbol{v}_{h,i} - \int_{\Omega} c_{h,i}^{n+1} \text{div}\, \boldsymbol{v}_{h,i} = -\int_{\gamma} \left(c_{h,i}^{n+1}\right)_{|\gamma} \left(\boldsymbol{v}_{h,i} \cdot \boldsymbol{n}_{i|\gamma}\right), \quad \forall \boldsymbol{v}_{h,i} \in \Sigma_{h,i}, \end{aligned} \tag{3.14}$$

   to obtain $c_{h,i}^{n+1}, \boldsymbol{r}_{h,i}^{n+1},\; i = 1, 2.$

To recover the same solution as the monolithic system (3.9)-(3.12), the solution of the subdomain problems (3.13)-(3.14) is required to satisfy the following transmission conditions across $\gamma \times (0,\; T)$:

- for $n = 0, \ldots, N-1, \;\; l = 0, \ldots, L-1,$

$$\int_{E} c_{h,i}^{n,l} = \int_{E} c_{h,\gamma}^{n,l}, \quad \forall E \in \mathcal{G}_h, \;\; i = 1,\; 2, \tag{3.15}$$

$$\int_{E} \phi_\gamma \frac{c_{h,\gamma}^{n,l+1} - c_{h,\gamma}^{n,l}}{\Delta t_a} + \sum_{P \in \partial E} \left(\hat{c}_{h,\gamma}^{n,l}\right)_{|P} u_{P,E} = \int_{E} \sum_{i=1}^{2} \hat{c}_{h,i}^{n,l} (\boldsymbol{u}_i \cdot \boldsymbol{n}_{i|\gamma}), \quad \forall E \in \mathcal{G}_h, \tag{3.16}$$

- for $n = 0, \ldots, N-1,$

$$\int_{E} c_{h,i}^{n+1} = \int_{E} c_{h,\gamma}^{n+1}, \quad \forall E \in \mathcal{G}_h, \;\; i = 1,\; 2, \tag{3.17}$$

$$\begin{aligned} &\int_{E} \phi_\gamma \frac{c_{h,\gamma}^{n+1} - c_{h,\gamma}^{n,L}}{\Delta t} + \int_{E} \text{div}_\tau \boldsymbol{r}_{h,\gamma}^{n+1} \;\; = \int_{E} \left(q_\gamma\left(t^{n+1}\right) + \sum_{i=1}^{2} \boldsymbol{r}_{h,i}^{n+1} \cdot \boldsymbol{n}_{i|\gamma} \right), \quad \forall E \in \mathcal{G}_h, \\ &\int_{\gamma} \left(\boldsymbol{D}_\gamma \delta\right)^{-1} \boldsymbol{r}_{h,\gamma}^{n+1} \cdot \boldsymbol{v}_{h,\gamma} - \int_{\gamma} c_{h,\gamma}^{n+1} \text{div}_\tau \boldsymbol{v}_{h,\gamma} \;\; = 0, \quad \forall \boldsymbol{v}_{h,\gamma} \in \Sigma_{h,\gamma}. \end{aligned} \tag{3.18}$$

Due to operator splitting, we have separate transmission conditions for advection and diffusion. The transmission conditions (3.15) and (3.17) are the discrete counterparts of the pressure continuity across $\gamma \times (0,T)$ (the third equation of (3.2)), while the conditions (3.16) and (3.18) are the discretized versions of the tangential PDEs (3.3). Using these transmission conditions, we present in the next section three global-in-time DD methods: GTP-Schur, GTF-Schur, and GTO-Schwarz. Each method is formulated as a space-time interface problem on the fracture-interface, which is solved iteratively and globally in time. For the diffusion part, we use (3.17)-(3.18) and apply directly the formulations developed in Chapter 2 (for GTP-Schur and GTF-Schur) and [67] (for GTO-Schwarz) to write the respective interface equations. For the advection, the associated interface problem is derived using the transmission conditions (3.15)-(3.16).

3.2. Global-in-time DD methods with operator splitting

3.2.1. Global-in-time primal Schur (GTP-Schur) method

To derive the interface equation for the advection part, we introduce the advection concentration $\lambda_{h,a} = \left(\lambda_{h,a}^{n,l}\right)_{\substack{n=0,\dots,N-1 \\ l=0,\dots,L-1}} \in (\Lambda_h)^{N\times L}$ in the fracture and enforce (3.16) across the space-time fracture $\gamma \times (0,T)$. For the diffusion part, as in Section 2.2, we introduce the diffusion concentration $\lambda_h = \left(\lambda_{h,\gamma}^{n}\right)_{n=1,\dots,N} \in (\Lambda_h)^N$ in the fracture and use the tangential PDEs (3.18) as the interface equations. The two variables $\lambda_{h,a}$ and λ_h are the interface unknowns for the GTP-Schur method. Denote by

$$H^1_*(\Omega_i) := \left\{ v \in H^1(\Omega_i),\ \ v = 0 \text{ over } \partial\Omega_i \cap \partial\Omega \right\},\ \ i = 1,\ 2.$$

Next, we define the solution operators $\mathcal{D}_i,\ \ i = 1,\ \ 2$, for the advection step,

$$\begin{aligned} \mathcal{D}_i :\ \ (\Lambda_h)^{N\times L} \times (\Lambda_h)^N \times L^2(0,T;L^2(\Omega_i)) \times H^1_*(\Omega_i) \times H^1_0(\gamma) \ &\longrightarrow\ (\Lambda_h)^{N\times L} \\ (\lambda_{h,a},\ \lambda_h,\ q_i,\ c_{0,i},\ c_{0,\gamma}) \ &\mapsto\ \left(\hat{c}_{h,i}^{\Delta t,\Delta t_a}\right)_{|E},\quad \forall E \in \mathcal{G}_h, \end{aligned} \tag{3.19}$$

and the Dirichlet-to-Neumann operators $\mathcal{S}_i^{\text{DtN}},\ \ i = 1,\ \ 2$, for the diffusion step,

$$\begin{aligned}\mathcal{S}_i^{\mathrm{DtN}}: \quad (\Lambda_h)^{N\times L}\times(\Lambda_h)^N\times L^2(0,T;L^2(\Omega_i))\times H^1_*(\Omega_i)\times H^1_0(\gamma) \quad &\longrightarrow \quad (\Lambda_h)^N \\ (\lambda_{h,a},\ \lambda_h,\ q_i,\ c_{0,i},\ c_{0,\gamma}) \quad &\mapsto \quad \left(\boldsymbol{r}_{h,i}^{\Delta t}\cdot\boldsymbol{n}_i\right)_{|E}, \quad \forall E\in\mathcal{G}_h,\end{aligned} \tag{3.20}$$

where, for $i=1,2$,

$$\hat{c}_{h,i}^{\Delta t,\Delta t_a}=\left(\hat{c}_{h,i}^{n,l}\right)_{n=0,\dots,N-1,\,l=0,\dots,L-1}, \quad \text{and} \quad \left(c_{h,i}^{\Delta t},\ \boldsymbol{r}_{h,i}^{\Delta t}\right)=\left(c_{h,i}^{n},\ \boldsymbol{r}_{h,i}^{n}\right)_{n=1,\dots,N}, \tag{3.21}$$

are the solutions of the local problems (3.13)-(3.14) on each subdomain with Dirichlet boundary conditions on $\gamma\times(0,T)$: for $i=1,2$,

$$\begin{aligned}&\left(c_{h,i}^{n,l}\right)_{|\gamma}=\lambda_{h,a}^{n,l},\ \ n=0,1,\ \dots,\ N-1,\ l=0,\ \dots,\ L-1,\\ &\left(c_{h,i}^{n+1}\right)_{|\gamma}=\lambda_{h,\gamma}^{n+1},\ n=0,1,\ \dots,\ N-1.\end{aligned}$$

We note that the transmission conditions (3.15) and (3.17) are satisfied. By enforcing the remaining transmission conditions, i.e. (3.16) and (3.18), we obtain the interface problem for GTP-Schur, which consists of solving, for $n=0,\dots,N-1$,

- the advection equation: for $l=0,\dots,L-1$,

$$\int_E\phi_\gamma\frac{\lambda_{h,a}^{n,l+1}-\lambda_{h,a}^{n,l}}{\Delta t_a}+\sum_{P\in\partial E}\left(\hat{\lambda}_{h,a}^{n,l}\right)_{|P}u_{P,E}=\frac{1}{\Delta t_a}\int_{t^{n,l}}^{t^{n,l+1}}\int_E\sum_{i=1}^{2}\left(\boldsymbol{u}_i\cdot\boldsymbol{n}_{i|\gamma}\right)\mathcal{D}_i(\lambda_{h,a},\lambda_h,q_i,c_{0,i},c_{0,\gamma}),\quad\forall E\in\mathcal{G}_h, \tag{3.22}$$

- then the diffusion equation:

$$\int_E\phi_\gamma\frac{\lambda_{h,\gamma}^{n+1}-\lambda_{h,a}^{n,L}}{\Delta t}+\int_E\mathrm{div}_\tau\boldsymbol{r}_{h,\gamma}^{n+1}=\int_E q_\gamma(t^{n+1})+\frac{1}{\Delta t}\int_{t^n}^{t^{n+1}}\int_E\sum_{i=1}^{2}\mathcal{S}_i^{\mathrm{DtN}}\left(\lambda_{h,a},\lambda_h,q_i,c_{0,i},c_{0,\gamma}\right),\quad\forall E\in\mathcal{G}_h, \tag{3.23}$$

where $r_{h,\gamma}^{n+1}$ is computed by

$$\int_\gamma\left(\boldsymbol{D}_\gamma\delta\right)^{-1}\boldsymbol{r}_{h,\gamma}^{n+1}\cdot\boldsymbol{v}_{h,\gamma}-\int_\gamma\lambda_{h,\gamma}^{n+1}\mathrm{div}_\tau\boldsymbol{v}_{h,\gamma}=0,\quad\forall\boldsymbol{v}_{h,\gamma}\in\Sigma_{h,\gamma}. \tag{3.24}$$

As the equations are linear, we rewrite (3.22)-(3.23) equivalently as follows:

Find $(\lambda_{h,a},\ \lambda_h)\in(\Lambda_h)^{N\times L}\times(\Lambda_h)^N$ such that

$$S_{\mathrm{P}}\begin{pmatrix}\lambda_{h,a}\\ \lambda_h\end{pmatrix}=\chi_{\mathrm{P}}, \tag{3.25}$$

where

$$S_{\mathrm{P}}\begin{pmatrix}\lambda_{h,a}\\ \lambda_h\end{pmatrix}=\begin{pmatrix}\displaystyle\int_E\phi_\gamma\frac{\lambda_{h,a}^{n,l+1}-\lambda_{h,a}^{n,l}}{\Delta t_a}+\sum_{P\in\partial E}\left(\hat{\lambda}_{h,a}^{n,l}\right)_{|P}u_{P,E}-\frac{1}{\Delta t_a}\int_{t^{n,l}}^{t^{n,l+1}}\int_E\sum_{i=1}^{2}\left(\boldsymbol{u}_i\cdot\boldsymbol{n}_{i|\gamma}\right)\mathcal{D}_i(\lambda_{h,a},\lambda_h,0,0,0)\\ \displaystyle\int_E\phi_\gamma\frac{\lambda_{h,\gamma}^{n+1}-\lambda_{h,a}^{n,L}}{\Delta t}+\int_E\mathrm{div}_\tau\boldsymbol{r}_{h,\gamma}^{n+1}-\frac{1}{\Delta t}\int_{t^n}^{t^{n+1}}\int_E\sum_{i=1}^{2}\mathcal{S}_i^{\mathrm{DtN}}\left(\lambda_{h,a},\ \lambda_h,\ 0,\ 0,\ 0\right)\end{pmatrix}_{\substack{E\in\mathcal{G}_h\\ n=0,\dots,N-1\\ l=0,\dots,L-1}},$$

and

$$\chi_{\mathrm{P}}=\begin{pmatrix}\displaystyle\frac{1}{\Delta t_a}\int_{t^{n,l}}^{t^{n,l+1}}\int_E\sum_{i=1}^{2}\left(\boldsymbol{u}_i\cdot\boldsymbol{n}_{i|\gamma}\right)\mathcal{D}_i(0,\ 0,\ q_i,\ c_{0,i},\ c_{0,\gamma})\\ \displaystyle\int_E q_\gamma(t^{n+1})+\frac{1}{\Delta t}\int_{t^n}^{t^{n+1}}\int_E\sum_{i=1}^{2}\mathcal{S}_i^{\mathrm{DtN}}\left(0,\ 0,\ q_i,\ c_{0,i},\ c_{0,\gamma}\right)\end{pmatrix}_{\substack{E\in\mathcal{G}_h\\ n=0,\dots,N-1\\ l=0,\dots,L-1}}.$$

The interface problem (3.25) can be solved iteratively using a Krylov subspace method, e.g., GMRES. At each GMRES iteration, instead of computing explicitly the operator S_{P}, only the matrix-vector product $S_{\mathrm{P}}(\lambda_{h,a},\lambda_h)$ is needed. Hence, our proposed method is matrix-free. However, it has been shown numerically for the pure diffusion problem that the convergence of the GTP-Schur method is significantly slow [67, 70], and preconditioning is needed to enhance the speed of convergence. Obviously, using a preconditioner could increase the computational time as additional local problems need to be solved to construct the preconditioner. In the next section, we formulate the discrete space-time interface system for the GTF-Schur method, which does not require any preconditioners for fast convergence.

3.2.2. Global-in-time fracture-based Schur (GTF-Schur) method

Unlike GTP-Schur, here the interface variable for the advection represents the total normal advective flux and is denoted by $\psi_h=\left(\psi_h^{n,l}\right)_{\substack{n=0,\dots,N-1\\ l=0,\dots,L-1}}\in\left(\Lambda_h\right)^{N\times L}$, where

$$\int_E\psi_h^{n,l}\coloneqq\int_E\sum_{i=1}^{2}\left(\boldsymbol{u}_i\cdot\boldsymbol{n}_{i|\gamma}\right)\hat{c}_{h,i}^{n,l},\quad\forall n=0,\dots,N-1,\ \forall l=0,\ \dots,\ L-1,\ \forall E\in\mathcal{G}_h.\tag{3.26}$$

Equations (3.26) are also used to write the discrete space-time interface equations for the advection. This way, we obtain for the advection an interface operator which is close to the identity operator, thus, making the interface equations a well-conditioned system.

For the diffusion part, the interface equations will be the discrete counterpart of the ones derived in Section 2.4. One main advantage of this approach is that the interface operator for

the diffusion is also closed to the identity, hence, it does not need any preconditioners. We introduce the interface variable $\varphi_h = (\varphi_h^n)_{n=1,\dots,N} \in (\Lambda_h)^N$ representing the discrete total normal flux across $\gamma \times (0,T)$:

$$\int_E \varphi_h^n := \int_E \sum_{i=1}^{2} \boldsymbol{r}_{h,i}^n \cdot \boldsymbol{n}_{i|\gamma}, \quad \text{for } n = 1, \dots N, \quad E \in \mathcal{G}_h. \tag{3.27}$$

Next, we define the solution operators $\mathcal{H}_{\gamma,a}$ and $\mathcal{H}_\gamma$ as follows:

$$\begin{array}{rccc} \mathcal{H}_{\gamma,a}: & (\Lambda_h)^{N\times L} \times (\Lambda_h)^N \times L^2(0,T;L^2(\gamma)) \times H_0^1(\gamma) & \longrightarrow & (\Lambda_h)^{N\times L} \\ & (\psi_h,\ \varphi_h,\ q_\gamma,\ c_{0,\gamma}) & \mapsto & c_{h,\gamma}^{\Delta t,\Delta t_a}, \end{array}$$

$$\begin{array}{rccc} \mathcal{H}_{\gamma}: & (\Lambda_h)^{N\times L} \times (\Lambda_h)^N \times L^2(0,T;L^2(\gamma)) \times H_0^1(\gamma) & \longrightarrow & (\Lambda_h)^{N} \\ & (\psi_h,\ \varphi_h,\ q_\gamma,\ c_{0,\gamma}) & \mapsto & c_{h,\gamma}^{\Delta t}, \end{array}$$

where

$$c_{h,\gamma}^{\Delta t,\Delta t_a} = \left(c_{h,\gamma}^{n,l}\right)_{n=0,\dots,N-1,\ l=0,\dots,L-1}, \text{ and } \left(c_{h,\gamma}^{\Delta t},\ \boldsymbol{r}_{h,\gamma}^{\Delta t}\right) = \left(c_{h,\gamma}^{n},\ \boldsymbol{r}_{h,\gamma}^{n}\right)_{n=1,\dots,N}, \tag{3.28}$$

are the solutions of the following problem in the fracture: for $n = 0, \dots, N-1$,

1. set $c_{h,\gamma}^{n,0} = c_{h,\gamma}^n$, where $c_{h,\gamma}^0$ is given as in (3.8);
2. for $l = 0, \dots, L-1$,
   (a) compute the upwind value $\hat{c}_{h,\gamma}^{n,l} = \mathcal{U}_{h,\gamma}\left(c_{h,\gamma}^{n,l}\right)$ as in (3.6),
   (b) solve the advection problem in the fracture:

$$\int_E \phi_\gamma \frac{c_{h,\gamma}^{n,l+1} - c_{h,\gamma}^{n,l}}{\Delta t_a} + \sum_{P\in\partial E} \left(\hat{c}_{h,\gamma}^{n,l}\right)_{|P} u_{P,E} = \int_E \psi_h^{n,l}, \quad \forall E \in \mathcal{G}_h, \tag{3.29}$$

   with $c_{h,\gamma}^{n,l}$ known to obtain $c_{h,\gamma}^{n,l+1}$;
3. solve the diffusion equation on fracture with initial value $c_{h,\gamma}^{n,L}$:

$$\begin{array}{rcl} \displaystyle\int_E \phi_\gamma \frac{c_{h,\gamma}^{n+1} - c_{h,\gamma}^{n,L}}{\Delta t} + \int_E \operatorname{div} \boldsymbol{r}_{h,\gamma}^{n+1} &=& \displaystyle\int_E \varphi_h^{n+1}, \quad \forall E \in \mathcal{G}_h, \\ \displaystyle\int_\gamma \left(\boldsymbol{D}_\gamma \delta\right)^{-1} \boldsymbol{r}_{h,\gamma}^{n+1} \cdot \boldsymbol{v}_{h,\gamma} - \int_\gamma c_{h,\gamma}^{n+1} \operatorname{div}_\tau \boldsymbol{v}_{h,\gamma} &=& 0, \quad \forall \boldsymbol{v}_{h,\gamma} \in \Sigma_{h,\gamma}, \end{array} \tag{3.30}$$

to obtain $c_{h,\gamma}^{n+1}$ and $\boldsymbol{r}_{h,\gamma}^{n+1}$.

For the subdomain problems, we reuse the operators $\mathcal{D}_i$ and $\mathcal{S}_i^{\text{DtN}},\ i=1,\ 2$ as defined for the previous method (cf. (3.19) and (3.20)). The interface problem for GTF-Schur is obtained by enforcing (3.26) and (3.27):

$$\begin{aligned}
\int_{t^{n,l}}^{t^{n,l+1}}\int_E \psi_h &= \int_{t^{n,l}}^{t^{n,l+1}}\int_E \sum_{i=1}^{2}(\boldsymbol{u}_i\cdot\boldsymbol{n}_{i|\gamma})\mathcal{W}_i(\psi_h,\ \varphi_h,\ q_i,\ c_{0,i},\ q_\gamma,\ c_{0,\gamma}),\\
\int_{t^n}^{t^{n+1}}\int_E \varphi_h &= \int_{t^n}^{t^{n+1}}\int_E \sum_{i=1}^{2}\mathcal{V}_i(\psi_h,\ \varphi_h,\ q_i,\ c_{0,i},\ q_\gamma,\ c_{0,\gamma}),\\
&\qquad \forall n=0,\dots,N-1,\ \ \forall l=0,\dots,L-1,\quad \forall E\in\mathcal{G}_h,
\end{aligned} \tag{3.31}$$

where, for $i=1,2$,

$$\begin{aligned}
\mathcal{W}_i(\psi_h,\ \varphi_h,\ q_i,\ c_{0,i},\ q_\gamma,\ c_{0,\gamma}) &:= \mathcal{D}_i\left(\mathcal{H}_{\gamma,a}(\psi_h,\varphi_h,q_\gamma,c_{0,\gamma}),\mathcal{H}_\gamma(\psi_h,\varphi_h,q_\gamma,c_{0,\gamma}),q_i,c_{0,i},c_{0,\gamma}\right),\\
\mathcal{V}_i(\psi_h,\ \varphi_h,\ q_i,\ c_{0,i},\ q_\gamma,\ c_{0,\gamma}) &:= \mathcal{S}_i^{\text{DtN}}\left(\mathcal{H}_{\gamma,a}(\psi_h,\varphi_h,q_\gamma,c_{0,\gamma}),\mathcal{H}_\gamma(\psi_h,\varphi_h,q_\gamma,c_{0,\gamma}),q_i,c_{0,i},c_{0,\gamma}\right).
\end{aligned}$$

Problem (3.31) can be rewritten equivalently as follows:

Find $(\psi_h,\ \varphi_h)\in(\Lambda_h)^{N\times L}\times(\Lambda_h)^N$ such that

$$S_{\text{F}}\begin{pmatrix}\psi_h\\ \varphi_h\end{pmatrix} = \chi_{\text{F}}, \tag{3.32}$$

where

$$S_{\text{F}}\begin{pmatrix}\psi_h\\ \varphi_h\end{pmatrix} = \begin{pmatrix}\displaystyle\int_{t^{n,l}}^{t^{n,l+1}}\int_E \psi_h - \int_{t^{n,l}}^{t^{n,l+1}}\int_E \sum_{i=1}^{2}(\boldsymbol{u}_i\cdot\boldsymbol{n}_{i|\gamma})\mathcal{W}_i(\psi_h,\ \varphi_h,\ 0,\ 0,\ 0,\ 0)\\ \displaystyle\int_{t^n}^{t^{n+1}}\int_E \varphi_h - \int_{t^n}^{t^{n+1}}\int_E \sum_{i=1}^{2}\mathcal{V}_i(\psi_h,\ \varphi_h,\ 0,\ 0,\ 0,\ 0)\end{pmatrix}_{\substack{n=0,\dots,N-1\\ l=0,\dots,L-1\\ E\in\mathcal{G}_h}},$$

and

$$\chi_{\text{F}} = \begin{pmatrix}\displaystyle\int_{t^{n,l}}^{t^{n,l+1}}\int_E \sum_{i=1}^{2}(\boldsymbol{u}_i\cdot\boldsymbol{n}_{i|\gamma})\mathcal{W}_i(0,\ 0,\ q_i,\ c_{0,i},\ q_\gamma,\ c_{0,\gamma})\\ \displaystyle\int_{t^n}^{t^{n+1}}\int_E \sum_{i=1}^{2}\mathcal{V}_i(0,\ 0,\ q_i,\ c_{0,i},\ q_\gamma,\ c_{0,\gamma})\end{pmatrix}_{\substack{n=0,\dots,N-1\\ l=0,\dots,L-1\\ E\in\mathcal{G}_h}}.$$

3.2.3. Global-in-time optimized Schwarz (GTO-Schwarz) method

The interface equations for the diffusion part of the GTO-Schwarz method are based on the Ventcel-to-Robin transmission conditions as proposed in [67]. These generalized transmission conditions are derived by introducing $\left(c_{i,\gamma}^n\right)_{n=1,\ldots,N}$, $i = 1,\ 2$, with $c_{i,\gamma}^n$ representing the trace of $c_{h,i}^n$ on $\gamma \times (0,\ T)$. For each $c_{i,\gamma}^n$, we denote by $\boldsymbol{r}_{\gamma,i}^n$ the discrete tangential velocity associated with $c_{i,\gamma}^n$ through the second equation of (3.18):

$$\int_\gamma (\boldsymbol{D}_\gamma \delta)^{-1} \boldsymbol{r}_{\gamma,i}^n \cdot \boldsymbol{v}_{h,\gamma} - \int_\gamma c_{i,\gamma}^n \mathrm{div}_\tau \boldsymbol{v}_{h,\gamma} = 0, \quad \forall \boldsymbol{v}_{h,\gamma} \in \Sigma_{h,\gamma},\ \forall n = 1, \ldots, N. \tag{3.33}$$

Due to the continuity of the concentration across the discrete counterpart of $\gamma \times (0,\ T)$, we have, for $n = 1, \ldots, N$,

$$\boldsymbol{r}_{\gamma,1}^n = \boldsymbol{r}_{\gamma,2}^n = \boldsymbol{r}_{h,\gamma}^n.$$

Under sufficient regularity, the transmission conditions (3.17)-(3.18) can be replaced by the following Ventcel-to-Robin transmission conditions: for $n = 0, \ldots, N-1$

$$\begin{aligned}
-\int_E \boldsymbol{r}_{h,1}^{n+1} \cdot \boldsymbol{n}_{1|\gamma} + \alpha \int_E c_{1,\gamma}^{n+1} + \int_E \phi_\gamma \frac{c_{1,\gamma}^{n+1} - c_{1,\gamma}^{n,L}}{\Delta t} + \int_E \mathrm{div}_\tau \boldsymbol{r}_{\gamma,1}^{n+1} & \\
= \int_E q_\gamma\left(t^{n+1}\right) + \int_E \boldsymbol{r}_{h,2}^{n+1} \cdot \boldsymbol{n}_{2|\gamma} + \alpha \int_E c_{2,\gamma}^{n+1}, \quad \forall E \in \mathcal{G}_h, & \\
\int_\gamma (\boldsymbol{D}_\gamma \delta)^{-1} \boldsymbol{r}_{\gamma,1}^{n+1} \cdot \boldsymbol{v}_{h,\gamma} - \int_\gamma c_{1,\gamma}^{n+1} \mathrm{div}_\tau \boldsymbol{v}_{h,\gamma} = 0, \quad \forall \boldsymbol{v}_{h,\gamma} \in \Sigma_{h,\gamma}, &
\end{aligned} \tag{3.34}$$

$$\begin{aligned}
-\int_E \boldsymbol{r}_{h,2}^{n+1} \cdot \boldsymbol{n}_{2|\gamma} + \alpha \int_E c_{2,\gamma}^{n+1} + \int_E \phi_\gamma \frac{c_{2,\gamma}^{n+1} - c_{2,\gamma}^{n,L}}{\Delta t} + \int_E \mathrm{div}_\tau \boldsymbol{r}_{\gamma,2}^{n+1} & \\
= \int_E q_\gamma\left(t^{n+1}\right) + \int_E \boldsymbol{r}_{h,1}^{n+1} \cdot \boldsymbol{n}_{1|\gamma} + \alpha \int_E c_{1,\gamma}^{n+1}, \quad \forall E \in \mathcal{G}_h, & \\
\int_\gamma (\boldsymbol{D}_\gamma \delta)^{-1} \boldsymbol{r}_{\gamma,2}^{n+1} \cdot \boldsymbol{v}_{h,\gamma} - \int_\gamma c_{2,\gamma}^{n+1} \mathrm{div}_\tau \boldsymbol{v}_{h,\gamma} = 0, \quad \forall \boldsymbol{v}_{h,\gamma} \in \Sigma_{h,\gamma}, &
\end{aligned} \tag{3.35}$$

for some parameter $\alpha > 0$.

For the advection, we also introduce $\left(c_{i,\gamma}^{n,l}\right)_{\substack{n=0,\ldots,N-1 \\ l=0,\ldots,L}}$, $i = 1,\ 2$, which are the traces of the advection concentration on $\gamma \times (0, T)$. The interface equation associated with the advection is treated in the same way as for GTF-Schur. In particular, the interface unknown for the advection part is $\psi_h = \left(\psi_h^{n,l}\right)_{\substack{n=0,\ldots,N-1 \\ l=0,\ldots,L-1}} \in (\Lambda_h)^{N \times L}$ satistying equation (3.26).

The discrete space-time interface problem for the GTO-Schwarz method is then derived using the transmission conditions (3.26) and (3.34)-(3.35). To this end, we denote by $\theta_{h,i} = \left(\theta_{h,i}^n\right)_{n=1,\dots,N}$ in $(\Lambda_h)^N,\ i = 1,\ 2$, the space$-$time discrete Robin data transmitted from one sub-domain to the neighboring sub-domain at each diffusion time step:

$$\int_E \theta_{h,i}^n = \int_E \left(\boldsymbol{r}_{h,i}^n \cdot \boldsymbol{n}_{i|\gamma} + \alpha c_{i,\gamma}^n\right),\ \forall n = 1, \dots, N.$$

We next define the solution operators $\mathcal{R}_i$ and the Ventcel-to-Robin operators $\mathcal{S}_i^{\text{VtR}},\ (i = 1,\ 2)$:

$$\begin{gathered}
\mathcal{R}_i : (\Lambda_h)^{N\times L} \times (\Lambda_h)^N \times L^2(0,T;L^2(\Omega_i)) \times H_*^1(\Omega_i) \times L^2(0,T;L^2(\gamma)) \times H_0^1(\gamma) \longrightarrow (\Lambda_h)^{N\times L} \\
(\psi_h,\ \theta_{h,i},\ q_i,\ c_{0,i},\ q_\gamma,\ c_{0,\gamma}) \mapsto \left(\hat{c}_{h,i}^{\Delta t,\Delta t_a}\right)_{|E}, \quad \forall E \in \mathcal{G}_h, \\
\mathcal{S}_i^{\text{VtR}} : (\Lambda_h)^{N\times L} \times (\Lambda_h)^N \times L^2(0,T;L^2(\Omega_i)) \times H_*^1(\Omega_i) \times L^2(0,T;L^2(\gamma)) \times H_0^1(\gamma) \longrightarrow (\Lambda_h)^N \\
(\psi_h,\ \theta_{h,i},\ q_i,\ c_{0,i},\ q_\gamma,\ c_{0,\gamma}) \mapsto \left(\boldsymbol{r}_{h,i}^{\Delta t} \cdot \boldsymbol{n}_i + \alpha c_{i,\gamma}^{\Delta t}\right)_{|E}, \quad \forall E \in \mathcal{G}_h,
\end{gathered}$$

where $\left(\hat{c}_{h,i}^{\Delta t,\,\Delta t_a},\ c_{h,i}^{\Delta t},\ \boldsymbol{r}_{h,i}^{\Delta t}\right)$ and $\left(c_{i,\gamma}^{\Delta t},\ \boldsymbol{r}_{\gamma,i}^{\Delta t}\right)$ are given as in (3.21) and (3.28), respectively, and are computed by solving the following subdomain problem defined on $\Omega_i,\ i = 1,\ 2$: for $n = 0, \dots, N-1$,

1. set $c_{h,i}^{n,0} = c_{h,i}^n,\ \ c_{i,\gamma}^{n,0} = c_{i,\gamma}^n$, where $c_{h,i}^0,\ \ c_{i,\gamma}^0$ are given by (3.7) and (3.8), respectively;

2. for $l = 0, \dots, L-1$,

   (a) calculate the upwind values $\hat{c}_{h,i}^{n,l} = \mathcal{U}_{h,i}\left(c_{h,i}^{n,l},\ c_{i,\gamma}^{n,l}\right)$ and $\hat{c}_{h,\gamma}^{n,l} = \mathcal{U}_{h,\gamma}(c_{i,\gamma}^{n,l})$,

   (b) solve the advection equations in the subdomain and in the fracture:

$$\begin{aligned}
&\int_{K_i} \phi_i \frac{c_{h,i}^{n,l+1} - c_{h,i}^{n,l}}{\Delta t_a} + \sum_{E\in\partial K_i} \left(\hat{c}_{h,i}^{n,l}\right)_{|E} |E| u_{K_i,E} = 0, \quad \forall K_i \in \mathcal{K}_{h,i}, \\
&\int_E \phi_\gamma \frac{c_{i,\gamma}^{n,l+1} - c_{i,\gamma}^{n,l}}{\Delta t_a} + \sum_{P\in\partial E} \left(\hat{c}_{i,\gamma}^{n,l}\right)_{|P} u_{P,E} = \int_E \psi_h^{n,l}, \quad \forall E \in \mathcal{G}_h,
\end{aligned} \tag{3.36}$$

   with $c_{h,i}^{n,l},\ \ c_{i,\gamma}^{n,l}$ known to obtain $c_{h,i}^{n,l+1}$ and $c_{i,\gamma}^{n,l+1}$;

3. solve the coupled diffusion equation in the subdomain with initial conditions $(c_{h,i}^{n,L},\ c_{i,\gamma}^{n,L})$:

$$
\begin{aligned}
\int_{K_i} \phi_i \frac{c_{h,i}^{n+1} - c_{h,i}^{n,L}}{\Delta t} + \int_{K_i} \operatorname{div} \boldsymbol{r}_{h,i}^{n+1} &= \int_{K_i} q_i(t^{n+1}), \quad \forall K_i \in \mathcal{K}_{h,i}, \\
\int_\Omega \boldsymbol{D}_i^{-1} \boldsymbol{r}_{h,i}^{n+1} \cdot \boldsymbol{v}_i - \int_\Omega c_{h,i}^{n+1} \operatorname{div} \boldsymbol{v}_{h,i} + \int_\gamma c_{i,\gamma}^{n+1} \left(\boldsymbol{v}_{h,i} \cdot \boldsymbol{n}_{i|\gamma} \right) &= 0, \quad \forall \boldsymbol{v}_{h,i} \in \Sigma_{h,i}, \\
-\int_E \boldsymbol{r}_{h,i}^{n+1} \cdot \boldsymbol{n}_i + \alpha \int_E c_{i,\gamma}^{n+1} + \int_E \phi_\gamma \frac{c_{i,\gamma}^{n+1} - c_{i,\gamma}^{n,L}}{\Delta t} + \int_E \operatorname{div} \boldsymbol{r}_{\gamma,i}^{n+1} &= \int_E \left(\theta_{h,i}^{n+1} + q_\gamma \left(t^{n+1} \right) \right), \\
&\quad \forall E \in \mathcal{G}_h, \\
\int_\gamma \left(\boldsymbol{D}_\gamma \delta \right)^{-1} \boldsymbol{r}_{\gamma,i}^{n+1} \cdot \boldsymbol{v}_{h,\gamma} - \int_\gamma c_{i,\gamma}^{n+1} \operatorname{div} \boldsymbol{v}_{h,\gamma} &= 0, \quad \forall \boldsymbol{v}_{h,\gamma} \in \Sigma_{h,\gamma},
\end{aligned}
\tag{3.37}
$$

to obtain $c_{h,i}^{n+1}$, $\boldsymbol{r}_{h,i}^{n+1}$, $c_{i,\gamma}^{n+1}$, and $\boldsymbol{r}_{\gamma,i}^{n+1}$.

With these operators, the interface problem for the GTO-Schwarz method can be formulated as follows: find $(\psi_h,\ \theta_{h,1},\ \theta_{h,2}) \in (\Lambda_h)^{N \times L} \times (\Lambda_h)^N \times (\Lambda_h)^N$ such that

$$
\begin{aligned}
\int_{t^{n,l}}^{t^{n,l+1}} \int_E \psi_h &= \int_{t^{n,l}}^{t^{n,l+1}} \int_E \sum_{i=1}^{2} (\boldsymbol{u}_i \cdot \boldsymbol{n}_{i|\gamma}) \mathcal{R}_i(\psi_h,\ \theta_{h,i},\ q_i,\ c_{0,i},\ q_\gamma,\ c_{0,\gamma}), \\
\int_{t^n}^{t^{n+1}} \int_E \theta_{h,1} &= \int_E q_\gamma \left(t^{n+1} \right) + \int_{t^n}^{t^{n+1}} \mathcal{S}_2^{\mathrm{VtR}}(\psi_h,\ \theta_{h,2},\ q_2,\ c_{0,2},\ q_\gamma,\ c_{0,\gamma}), \\
\int_{t^n}^{t^{n+1}} \int_E \theta_{h,2} &= \int_E q_\gamma \left(t^{n+1} \right) + \int_{t^n}^{t^{n+1}} \mathcal{S}_1^{\mathrm{VtR}}(\psi_h,\ \theta_{h,1},\ q_1,\ c_{0,1},\ q_\gamma,\ c_{0,\gamma}), \\
&\quad \forall n = 0, \ldots, N-1, \quad \forall l = 0, \ldots, L-1, \quad \forall E \in \mathcal{G}_h.
\end{aligned}
\tag{3.38}
$$

Equivalently, (3.38) can be formulated in a more compact form:

find $(\psi_h,\ \theta_{h,1},\ \theta_{h,2}) \in (\Lambda_h)^{N \times L} \times (\Lambda_h)^N \times (\Lambda_h)^N$ such that

$$
S_{\mathrm{O}} \begin{pmatrix} \psi_h \\ \theta_{h,1} \\ \theta_{h,2} \end{pmatrix} = \chi_{\mathrm{O}},
\tag{3.39}
$$

where

$$
S_{\mathrm{O}} \begin{pmatrix} \psi_h \\ \theta_{h,1} \\ \theta_{h,2} \end{pmatrix} = \begin{pmatrix} \displaystyle\int_{t^{n,l}}^{t^{n,l+1}} \int_E \psi_h - \int_{t^{n,l}}^{t^{n,l+1}} \int_E \sum_{i=1}^{2} (\boldsymbol{u}_i \cdot \boldsymbol{n}_{i|\gamma}) \mathcal{R}_i(\psi_h,\ \theta_{h,i},\ 0,\ 0,\ 0,\ 0) \\ \displaystyle\int_{t^n}^{t^{n+1}} \int_E \theta_{h,1} - \int_{t^n}^{t^{n+1}} \mathcal{S}_2^{\mathrm{VtR}}(\psi_h,\ \theta_{h,2},\ 0,\ 0,\ 0,\ 0) \\ \displaystyle\int_{t^n}^{t^{n+1}} \int_E \theta_{h,2} - \int_{t^n}^{t^{n+1}} \mathcal{S}_1^{\mathrm{VtR}}(\psi_h,\ \theta_{h,1},\ 0,\ 0,\ 0,\ 0) \end{pmatrix}_{\substack{n=0,\ldots,N-1 \\ l=0,\ldots,L-1 \\ E \in \mathcal{G}_h}},
$$

and

$$\chi_{\mathrm{O}} = \begin{pmatrix} \displaystyle\int_{t^{n,l}}^{t^{n,l+1}} \int_E \sum_{i=1}^{2} (\boldsymbol{u}_i \cdot \boldsymbol{n}_{i|\gamma}) \mathcal{R}_i(0,\ 0,\ q_i,\ c_{0,i},\ q_\gamma,\ c_{0,\gamma}) \\ \displaystyle\int_E q_\gamma\left(t^{n+1}\right) + \int_{t^n}^{t^{n+1}} \mathcal{S}_2^{\mathrm{VtR}}(0,\ 0,\ q_2,\ c_{0,2},\ q_\gamma,\ c_{0,\gamma}) \\ \displaystyle\int_E q_\gamma\left(t^{n+1}\right) + \int_{t^n}^{t^{n+1}} \mathcal{S}_1^{\mathrm{VtR}}(0,\ 0,\ q_1,\ c_{0,1},\ q_\gamma,\ c_{0,\gamma}) \end{pmatrix}_{\substack{n=0,\dots,N-1 \\ l=0,\dots,L-1 \\ E\in\mathcal{G}_h}} .$$

Remark 3.1. *With operator splitting, we have formulated the interface equations for the GTO-Schwartz where the Ventcel-Robin parameter α only appears in the diffusion equations. Therefore, the optimized parameter can be calculated in the same way as in the pure diffusion problems (see [67]).*

The space-time interface system derived for each method is global-in-time, thus, one can impose different time steps in the fracture and in the subdomains. In the next section, we show how to formulate the interface problem for each method when nonconforming time grids are used.

3.3. Nonconforming discretization in time

In this section, we derive the discrete interface problems for the GTP-Schur, the GTF-Schur and the GTO-Schwarz methods with nonconforming time grids.

Let $\mathcal{T}_1,\ \mathcal{T}_2$, and $\mathcal{T}_\gamma$ be three different uniform partitions of the time interval $(0,\ T]$ into $N_1,\ N_2$ and N_γ sub-intervals $J_i^n = (t_i^{n-1},\ t_i^n],\ n = 1, \dots, N_i$, with length $\Delta t_i,\ $ for $i = 1,\ 2,\ \gamma$, respectively (see Figure 3.2). As the fracture is assumed to have much larger permeability than the surrounding domain, we choose Δt_γ such that $\Delta t_\gamma \ll \Delta t_i,\ i = 1,\ 2$. The sub-time step for the advection in each subdomain is defined by $\Delta t_i = L_i \Delta t_{i,a},\ i = 1,\ 2,\ \gamma$, and we denote by $\mathcal{T}_i^a,\ i = 1,\ ,2,\ \gamma$, the corresponding partition of $(0,\ T]$ into $N_i L_i$ sub-intervals for the advection. For $n = 1, \dots, N_i$, we let $J_i^{n,l} = (t_i^{n-1,l-1},\ t_i^{n-1,l}]$, $l = 1, \dots, L_i$, be the sub-intervals of J_i^n resulted from the partition $\mathcal{T}_i^a,\ i = 1,\ 2,\ \gamma$.

For $i = 1,\ 2,\ \gamma$, we denote by $P_0\left(\mathcal{T}_i,\ L^2(\gamma)\right)$ the space of functions which are piecewise constant in time on grid $\mathcal{T}_i$ with values in $L^2(\gamma)$:

$$P_0\left(\mathcal{T}_i,\ L^2(\gamma)\right) = \left\{\psi : (0,T) \to L^2(\gamma),\ \psi \ \text{ is constant on } J,\ \forall J \in \mathcal{T}_i\right\}.$$

In order to exchange data on the space-time interface between different time grids, we define, for $i,\ j = \{1,\ 2,\ \gamma\}$, the projection Π_{ji} from $P_0\left(\mathcal{T}_i,\ L^2(\gamma)\right)$ to $P_0\left(\mathcal{T}_j,\ L^2(\gamma)\right)$ as follows: for $\psi \in P_0\left(\mathcal{T}_i,\ L^2(\gamma)\right)$, $\Pi_{ji}\psi_{|J_j^n}$ is the average value of ψ on J_j^n, for $n = 1, \ldots, N_j$:

$$\Pi_{ji}\psi_{|J_j^n} = \frac{1}{|J_j^n|}\sum_{l=1}^{N_i}\int_{J_j^n \cap J_i^l} \psi. \tag{3.40}$$

Similarly, we define the average-value projection Π_{ji}^a from $P_0\left(\mathcal{T}_i^a,\ L^2(\gamma)\right)$ to $P_0\left(\mathcal{T}_j^a,\ L^2(\gamma)\right)$, for $i,\ j$ in $\{1,\ 2,\ \gamma\}$.

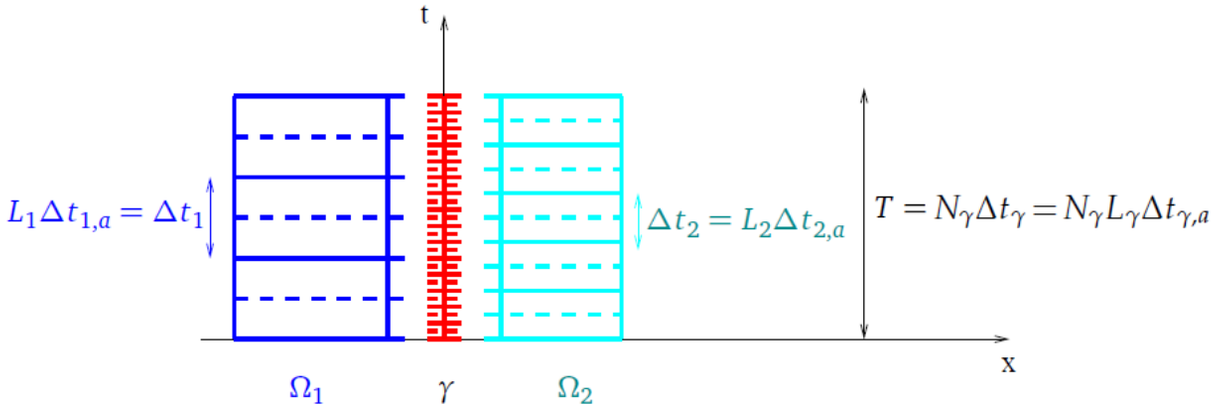

Figure 3.2: Nonconforming advection and diffusion time grids in the rock matrix and fracture.

To write the interface equations for the diffusion and the advection, we enforce the transmission conditions weakly over the nonconforming time grids. It can be done similarly as in the pure diffusion case which has been presented in Section 2.5 of Chapter 2.

3.3.1. GTP-Schur method

We choose $\lambda_{h,a}$ and λ_h to be piecewise constant in time on the advection and diffusion time grids imposed in the fracture, respectively. The interface system (3.22)-(3.23) is rewritten as:

$$\begin{aligned}
&\int_E \phi_\gamma \frac{\lambda_{h,a}^{n,l+1} - \lambda_{h,a}^{n,l}}{\Delta t_{\gamma,a}} + \sum_{P\in\partial E}\left(\hat{\lambda}_{h,a}^{n,l}\right)_{|P} u_{P,E} = \frac{1}{\Delta t_{\gamma,a}}\int_{t_\gamma^{n,l}}^{t_\gamma^{n,l+1}} \int_E \sum_{i=1}^{2}\left(\boldsymbol{u}_i \cdot \boldsymbol{n}_{i|\gamma}\right)\Pi_{\gamma i}^a \mathcal{F}_i(\Pi_{i\gamma}^a\lambda_{h,a}, \Pi_{i\gamma}\lambda_h, q_i, c_{0,i}),\\
&\int_E \phi_\gamma \frac{\lambda_{h,\gamma}^{n+1} - \lambda_{h,a}^{n,L}}{\Delta t_\gamma} + \int_E \mathrm{div}_\tau \boldsymbol{r}_{h,\gamma}^{n+1} = \int_E q_\gamma(t_\gamma^{n+1}) + \frac{1}{\Delta t_\gamma}\int_{t_\gamma^n}^{t_\gamma^{n+1}} \int_E \sum_{i=1}^{2}\Pi_{\gamma i}\mathcal{S}_i^{\mathrm{DtN}}\left(\Pi_{i\gamma}^a\lambda_{h,a}, \Pi_{i\gamma}\lambda_h, q_i, c_{0,i}\right),
\end{aligned} \tag{3.41}$$

where $r_{h,\gamma}^{n+1}$ is computed as:

$$\int_\gamma (\boldsymbol{D}_\gamma \delta)^{-1} \boldsymbol{r}_{h,\gamma}^{n+1} \cdot \boldsymbol{v}_{h,\gamma} - \int_\gamma \lambda_{h,\gamma}^{n+1} \mathrm{div}_\tau \boldsymbol{v}_{h,\gamma} = 0, \quad \forall \boldsymbol{v}_{h,\gamma} \in \Sigma_{h,\gamma}, \\ \forall n = 0, \ldots, N_\gamma - 1, \ \forall l = 0, \ldots, L_\gamma - 1, \quad \forall E \in \mathcal{G}_h. \tag{3.42}$$

3.3.2. GTF-Schur method

We choose $\varphi_h, \ \psi_h$ to be piecewise constant in time on the advection and diffusion time grids imposed in the fracture, respectively. The interface system (3.31) is then rewritten as:

$$\begin{aligned} \int_{t_\gamma^{n,l}}^{t_\gamma^{n,l+1}} \int_E \psi_h &= \int_{t_\gamma^{n,l}}^{t_\gamma^{n,l+1}} \int_E \sum_{i=1}^{2} (\boldsymbol{u}_i \cdot \boldsymbol{n}_{i|\gamma}) \Pi_{\gamma i}^a \mathcal{W}_i(\Pi_{i\gamma}^a \psi_h, \Pi_{i\gamma} \varphi_h, q_i, c_{0,i}, q_\gamma, c_{0,\gamma}), \\ \int_{t_\gamma^n}^{t_\gamma^{n+1}} \int_E \varphi_h &= \int_{t_\gamma^n}^{t_\gamma^{n+1}} \int_E \sum_{i=1}^{2} \Pi_{\gamma i} \mathcal{V}_i(\Pi_{i\gamma}^a \psi_h, \Pi_{i\gamma} \varphi_h, q_i, c_{0,i}, q_\gamma, c_{0,\gamma}), \\ & \forall n = 0, \ldots, N_\gamma - 1, \ \forall l = 0, \ldots, L_\gamma - 1, \quad \forall E \in \mathcal{G}_h. \end{aligned} \tag{3.43}$$

3.3.3. GTO-Schwar method

We choose φ_h to be piecewise constant in time on the advection time grid imposed in the fracture. For the Ventcel term $\theta_{h,i}, \ i = 1, \ 2$, we employ the same technique as in [67]. The interface system (3.38) is rewritten as:

$$\begin{aligned} \int_{t_\gamma^{n,l}}^{t_\gamma^{n,l+1}} \int_E \psi_h &= \int_{t_\gamma^{n,l}}^{t_\gamma^{n,l+1}} \int_E \sum_{i=1}^{2} (\boldsymbol{u}_i \cdot \boldsymbol{n}_{i|\gamma}) \Pi_{\gamma i}^a \mathcal{R}_i(\Pi_{i\gamma}^a \psi_h, \Pi_{i\gamma} \theta_{h,i}, q_i, c_{0,i}, q_\gamma, c_{0,\gamma}), \\ \int_{t_\gamma^n}^{t_\gamma^{n+1}} \int_E \theta_{h,1} &= \int_E q_\gamma \left(t^{n+1}\right) + \int_{t_\gamma^n}^{t_\gamma^{n+1}} \Pi_{\gamma i} \mathcal{S}_2^{\mathrm{VtR}}(\Pi_{i\gamma}^a \psi_h, \Pi_{i\gamma} \theta_{h,2}, q_2, c_{0,2}, q_\gamma, c_{0,\gamma}), \\ \int_{t_\gamma^n}^{t_\gamma^{n+1}} \int_E \theta_{h,2} &= \int_E q_\gamma \left(t^{n+1}\right) + \int_{t_\gamma^n}^{t_\gamma^{n+1}} \Pi_{\gamma i} \mathcal{S}_1^{\mathrm{VtR}}(\Pi_{i\gamma}^a \psi_h, \Pi_{i\gamma} \theta_{h,1}, q_1, c_{0,1}, q_\gamma, c_{0,\gamma}), \\ & \forall n = 0, \ldots, N_\gamma - 1, \ \forall l = 0, \ldots, L_\gamma - 1, \quad \forall E \in \mathcal{G}_h. \end{aligned} \tag{3.44}$$

3.4. Numerical results

Numerical results are presented in this section to illustrate and compare the convergence behavior and the errors in time of the three methods proposed in the previous sections: GTP-Schur, GTF-Schur, and GTO-Schwarz. Two test cases are considered: Test case 2.1 with non-immersed fracture and Test case 2.2 with partially immersed fracture where the diffusion

$\boldsymbol{D}_i = d_i\mathbf{I}$ is isotropic and constant in each subdomain and on the fracture, in which $\mathbf{I}$ is the 2D identity matrix. The velocity $\boldsymbol{u} = (\boldsymbol{u}_1, \boldsymbol{u}_2, \boldsymbol{u}_\gamma)$ presented in (3.2)-(3.3) is obtained by solving the steady-state flow problem on the subdomains

$$\begin{aligned}
\text{div}\, \boldsymbol{u}_i &= 0 && \text{in } \Omega_i \times (0,\ T), \\
\boldsymbol{u}_i &= -k_i \nabla p_i && \text{in } \Omega_i \times (0,\ T), \\
p_i &= g_i && \text{on } (\partial\Omega_i \cap \partial\Omega) \times (0,\ T), \quad i = 1, 2, \\
p_i &= p_\gamma && \text{on } \gamma \times (0,\ T), \\
p_i(\cdot, 0) &= p_{0,i} && \text{in } \Omega_i,
\end{aligned} \tag{3.45}$$

and in the fracture,

$$\begin{aligned}
\text{div}_\tau \boldsymbol{u}_\gamma &= \sum_{i=1}^{2} \boldsymbol{u}_i \cdot \boldsymbol{n}_{i|\gamma} && \text{in } \gamma \times (0, T), \\
\boldsymbol{u}_\gamma &= -k_\gamma \delta \nabla_\tau p_\gamma && \text{in } \gamma \times (0, T), \\
p_\gamma &= g_\gamma && \text{on } \partial\gamma \times (0, T), \\
p_\gamma(\cdot, 0) &= p_{0,\gamma} && \text{in } \gamma,
\end{aligned} \tag{3.46}$$

where, for $i = 1,\ 2,\ \gamma,\ q_i$ is the source term, p_i the pressure, $\boldsymbol{u}_i$ the Darcy velocity, and k_i the time-independent hydraulic conductivity in the subdomains and in the fracture, respectively. The global Péclect (Pe) numbers on each subdomain and on the fracture are defined as

$$\text{Pe}_i = \max_{K \in \mathcal{K}_{h,i}} \frac{H_i \max\limits_{(x,y)\in K} |\boldsymbol{u}_{i,K}(x,y)|}{d_i}, i = 1, 2, \quad \text{Pe}_\gamma = \max_{E \in \mathcal{E}_h^\gamma} \frac{H_\gamma \max\limits_{y \in E} |\boldsymbol{u}_{\gamma,E}(y)|}{d_\gamma}, \tag{3.47}$$

where $H_i, i = 1,\ 2,\ \gamma$ are the size of the subdomains Ω_i, respectively and $\boldsymbol{u}_{i,K}, i = 1,\ 2$ and $\boldsymbol{u}_{\gamma,E}$ are the restrictions of $\boldsymbol{u}_i$ and $\boldsymbol{u}_\gamma$ on the element K and the edge E, respectively. We also include in Table 3.1 the values of the Péclet numbers corresponding to the given parameters.

The discrete interface problem for each method is solved iteratively using GMRES with a random initial guess. The iterations are stopped when the relative residual error is less than 10^{-6} (Test case 2.1) or 10^{-8} (Test case 2.2). All computed errors are relative space-time errors in the space $L^2(0, T;\ \ L^2(\mathcal{O}))$-norm, where $\mathcal{O}$ is either Ω_1, Ω_2, or γ. For both test cases, the errors are computed using a reference solution on a fine time step $\Delta t_{\text{ref}} = T/512$ with $T = 2$. To compare the convergence speed of different iterative algorithms, we report the number of subdomain solves for each method to reach the same GMRES relative residual. Without preconditioning, the number of subdomain solves is the same as the number of GMRES iterations; however,

when a preconditioner is used (cf. Test case 2.2), one iteration of the preconditioned GTF-Schur method costs twice as much as one iteration of GTF-Schur with no preconditioner (in terms of number of subdomain solves). We fix the spatial mesh size $h = 1/50$ for Test case 2.1 and $h = /80$ for Test case 2.2, while varying the time step size to verify the accuracy in time.

3.4.1. Test case 2.1: non-immersed fracture

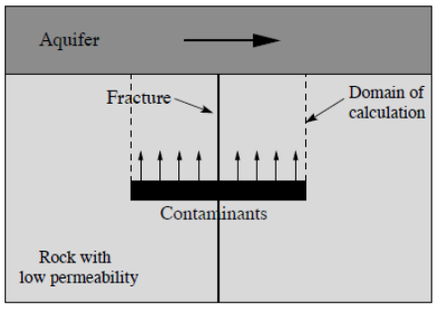

Figure 3.3: A contaminant storage crossed by a fracture.

We consider an adapted version of the test case used in [5]. A contaminant repository, located in a rock with low permeability, is leaking (Figure 3.3). The repository is crossed by a fracture and transported mostly upward. The rock is covered by an aquifer and the contaminant is assumed to be moved away instantly at the top boundary of the domain calculation so the boundary condition there is a vanishing concentration. The actual physical parameters are given in Table 3.1.

Parameters	*Subdomains*	*Fracture*
Hydraulic conductivity k_i	3.15×10^{-8}	10^{-7}
Molecular diffusion d_i	10^{-5}	3.15×10^{-4}
Porosity ϕ_i	0.05	0.1
Subdomains dimensions	10×10	-
Fracture width	-	1
Péclet number Pe_i	6.77e-02	3.00e-04

Table 3.1: Physical parameters for the experiment shown in Figure 3.3.

Boundary conditions are as follows. For the velocity, we assume that there is no horizontal flow on the lateral sides of the domain while a pressure drop constant in time is given between the top and bottom boundaries. At the top, the pressure is constant in space while at the bottom it is increasing slightly from the fracture toward the lateral sides. For the concentration, it is given, constant, at the top and bottom boundaries, vanishing at the top. On the lateral sides, we assume that there is no exchange with the outside.

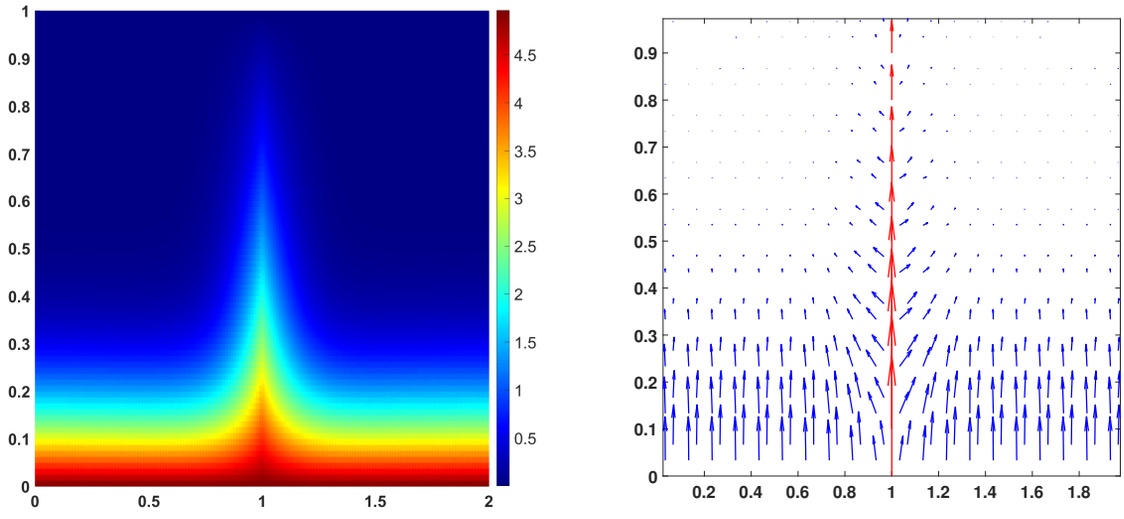

Figure 3.4: [Test case 2.1] Concentration field (left) and velocity field (right).

We show in Figure 3.4 the snapshots of the concentration and the velocity fields at the final time $T = 4$. The blue and red arrows represent the flows in the subdomains and in the fracture, respectively. Their lengths are proportional to the magnitude of the velocities. The concentration is moved upward by the velocity and the one near the fracture is quickly transported. There is an interaction between the velocity field in the fracture and in the subdomains as some of them flow out of the fracture and some flow into it (near the top of the fracture). Since $\mathrm{k}_f \gg \mathrm{k}_i,\ i = 1,\ 2$, the velocity is much larger in the fracture than in the surrounding porous media.

We first consider the case with *conforming* temporal discretization and illustrate the performance of the following methods: GTP-Schur, GTF-Schur, and GTO-Schwarz. We vary the time step sizes $\Delta t_i = \Delta t$ for $i = 1,\ 2,\ \gamma$. We begin with verifying the errors in time of these methods.

The sub-time step L is fixed and is equal to 2. Table 3.2 shows the L^2-errors for the pressure and velocity computed once GMRES converges. As all methods produce nearly the same approximate solutions, only one table is presented. Moreover, the numbers shown in the square brackets confirm the first-order convergence in time for both concentration and velocity.

We next investigate the convergence speed of these methods when different Péclet numbers are used via the relative residuals versus the number of subdomain solves shown in Figure 3.5. Since the GTP-Schur method converges very slowly, we only show the curves after 50 iterations for figure purpose. Three sets of Péclet (Pe) numbers are chosen based on the values

of the hydraulic conductivity. The final time T is set to be $T = 0.05$. We impose the same time step $\Delta t = T/N$ in the fracture and in the subdomains where $N = 16$. To satisfy the CFL condition for the upwind scheme used to solve the advection equation, a sub-time step L will be chosen corresponding to each value of the Pe number. The parameters for these three cases are shown in Table 3.3.

	Errors for concentration			Errors for velocity		
Δt	Ω_1	Ω_2	γ	Ω_1	Ω_2	γ
T/4	4.87e-02	4.87e-02	3.86e-02	8.79e-02	8.79e-02	6.13e-02
T/8	2.48e-02 [0.97]	2.48e-02 [0.97]	1.93e-02 [1.00]	4.36e-02 [1.01]	4.36e-02 [1.01]	2.96e-02 [1.05]
T/16	1.23e-02 [1.01]	1.23e-02 [1.01]	9.52e-03 [1.02]	2.15e-02 [1.02]	2.15e-02 [1.02]	1.44e-02 [1.04]
T/32	6.00e-03 [1.04]	6.00e-03 [1.04]	4.61e-03 [1.05]	1.04e-02 [1.05]	1.04e-02 [1.05]	6.91e-03 [1.06]

Table 3.2: [Test case 2.1] Relative L^2-errors of the concentration and velocity with *conforming* time grid. The corresponding convergence rates are shown in square brackets.

Parameters					
k_i		Ω_1	$1e$-06	$1e$-05	$2.3e$-05
		Ω_2	$1e$-06	$1e$-05	$2.3e$-05
		Ω_f	$7e$-03	$7e$-02	$1.4e$-01
Pe_i		Ω_1	≈ 0.37	≈ 3.8	≈ 8.4
		Ω_2	≈ 0.37	≈ 3.8	≈ 8.4
		Ω_f	≈ 4.4	≈ 44	≈ 89
Final time T			0.05	0.05	0.05
Number of time steps N	Nonconforming	Ω_1	8	8	8
		Ω_2	8	8	8
		Ω_f	16	16	16
	Conforming		16	16	16
Number of sub-time step L			4	8	16

Table 3.3: [Test case 2.1] Parameters for different cases.

From Figure 3.5, we see that, for all cases, the GTP-Schur method has the slowest convergence speed compared to the other methods. Only the GTF-Schur method has nearly the same convergence rate as the GTO-Schwarz method. This shows the efficiency of this method as it does not need any preconditioners to achieve such fast convergence. Finally, GTF-Schur

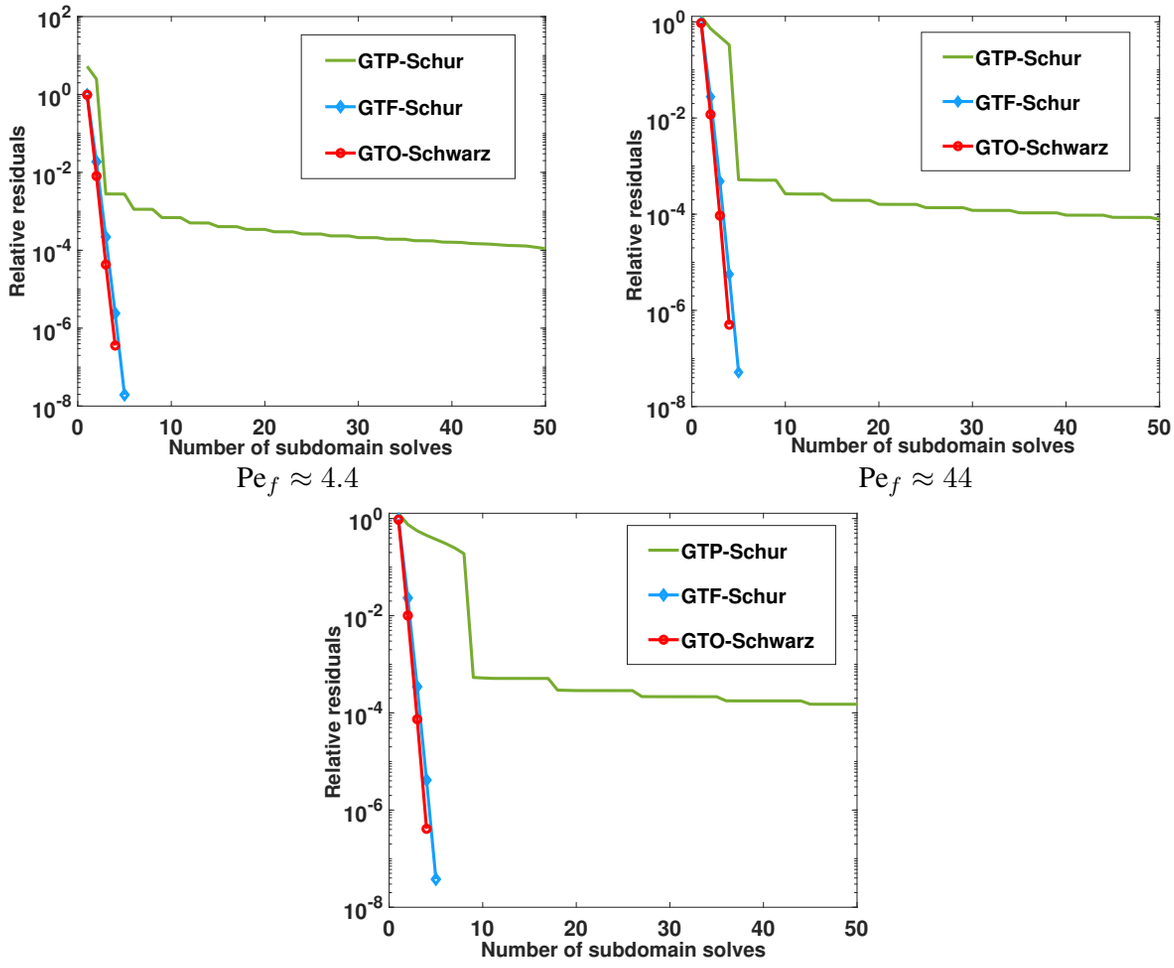

$\mathrm{Pe}_f \approx 4.4$ $\mathrm{Pe}_f \approx 44$

$\mathrm{Pe}_f \approx 89$

Figure 3.5: [Test case 2.1] Relative residual versus number of subdomain solves obtained from each method with different Péclet numbers with *conforming* time grid.

and GTO-Schwarz are insensitive to the effect of the advection, as their curves do not change shapes when we increase the Péclet numbers.

Next, we examine the above three methods in the case of *nonconforming* time grids. Similar to the *conforming* case, we first analyze the errors in time obtained from these methods when the stopping criteria of GMRES are reached. Since we have the same diffusion coefficients in the subdomains which are smaller than that in the fracture, we impose the same large time step in the subdomains and a smaller one in the fracture: $\Delta t_1 = \Delta t_2 = 2\Delta t_\gamma$. The relative errors of the concentration and velocity are shown in Table 3.4 and 3.5, respectively. From the numbers in the square brackets, we see that these methods still preserved the first-order convergence in time. However, due to the nonconforming time projections, the errors obtained from these methods are different. By comparing with Table 3.2, the errors in the fracture by

GTP-Schur and GTF-Schur are close to those with *fine* time steps imposed on the whole domain, while for GTO-Schwarz, these errors are close to the ones with uniform *coarse* time steps instead. We have these error differences because, for GTF-Schur and GTP-Schur, the local problems in the fracture are solved independently of those on the subdomains, while for the GTO-Schwarz, these problems are coupled through the Ventcel boundary condition. Such behavior is expected and has been observed in the pure diffusion case as what has been shown in the previous chapter, which highlights one of the main benefits of GTF-Schur.

		GTO-Schwarz			GTF-Schur GTP-Schur		
Δt_i	Δt_γ	Ω_1	Ω_2	γ	Ω_1	Ω_2	γ
T/4	T/8	4.87e-02	4.87e-02	3.84e-02	4.87e-02	4.87e-02	1.74e-02
T/8	T/16	2.47e-02 [0.97]	2.47e-02 [0.97]	1.92e-02 [0.99]	2.47e-02 [0.97]	2.47e-02 [0.97]	8.59e-03 [1.00]
T/16	T/32	1.23e-02 [1.01]	1.23e-02 [1.01]	9.46e-03 [1.02]	1.23e-02 [1.01]	1.23-02 [1.01]	4.16e-03 [1.02]
T/32	T/64	5.99e-03 [1.04]	5.99e-03 [1.04]	4.58e-03 [1.05]	5.96e-03 [1.04]	5.96e-03 [1.04]	1.93e-03 [1.05]

Table 3.4: [Test case 2.1] Relative L^2-errors of the *concentration* with nonconforming time grid. The corresponding convergence rates are shown in square brackets.

		GTO-Schwarz			GTF-Schur GTP-Schur		
Δt_i	Δt_γ	Ω_1	Ω_2	γ	Ω_1	Ω_2	γ
T/4	T/8	8.79e-02	8.79e-02	6.11e-02	8.79e-02	8.79e-02	2.99e-02
T/8	T/16	4.36e-02 [1.01]	4.36e-02 [1.01]	2.96e-02 [1.05]	4.35e-02 [1.01]	4.35e-02 [1.01]	1.45e-02 [1.05]
T/16	T/32	2.15e-02 [1.02]	2.15e-02 [1.02]	1.44e-02 [1.04]	2.13e-02 [1.02]	2.13-02 [1.02]	6.93e-03 [1.04]
T/32	T/64	1.04e-02 [1.05]	1.04e-02 [1.05]	6.90e-03 [1.06]	1.03e-02 [1.03]	1.03e-02 [1.03]	3.22e-03 [1.06]

Table 3.5: [Test case 2.1] Relative L^2-errors of the *velocity* with nonconforming time grid. The corresponding convergence rates are shown in square brackets.

We conclude this subsection by showing in Figure 3.6 the residual curves versus the number of subdomain solves. For the nonconforming case, we use a large time step in the subdomains and a smaller one in the fracture: $\Delta t_1 = \Delta t_2 = \Delta t = T/N$, $\Delta t_f = T/N_f$ where $N = 8$ and $N_f = 16$ (see Table 3.3). The sub-time step L for each value of the Péclet number is

chosen to be the same as in the conforming case. The GTF-Schur and the GTO-Schwarz methods still have nearly the same fast convergence, while the GTP-Schur method has the slowest convergence speed. Moreover, like the conforming case, these methods are not affected by the advection as they maintain their convergence rate regardless of the values of the Péclect numbers. In summary, for Test case 2.1, we see that GTF-Schur is the most effective method since it achieves a remarkably fast convergence without the need of a preconditioner as well as preserves the accuracy in time when nonconforming time grids are used.

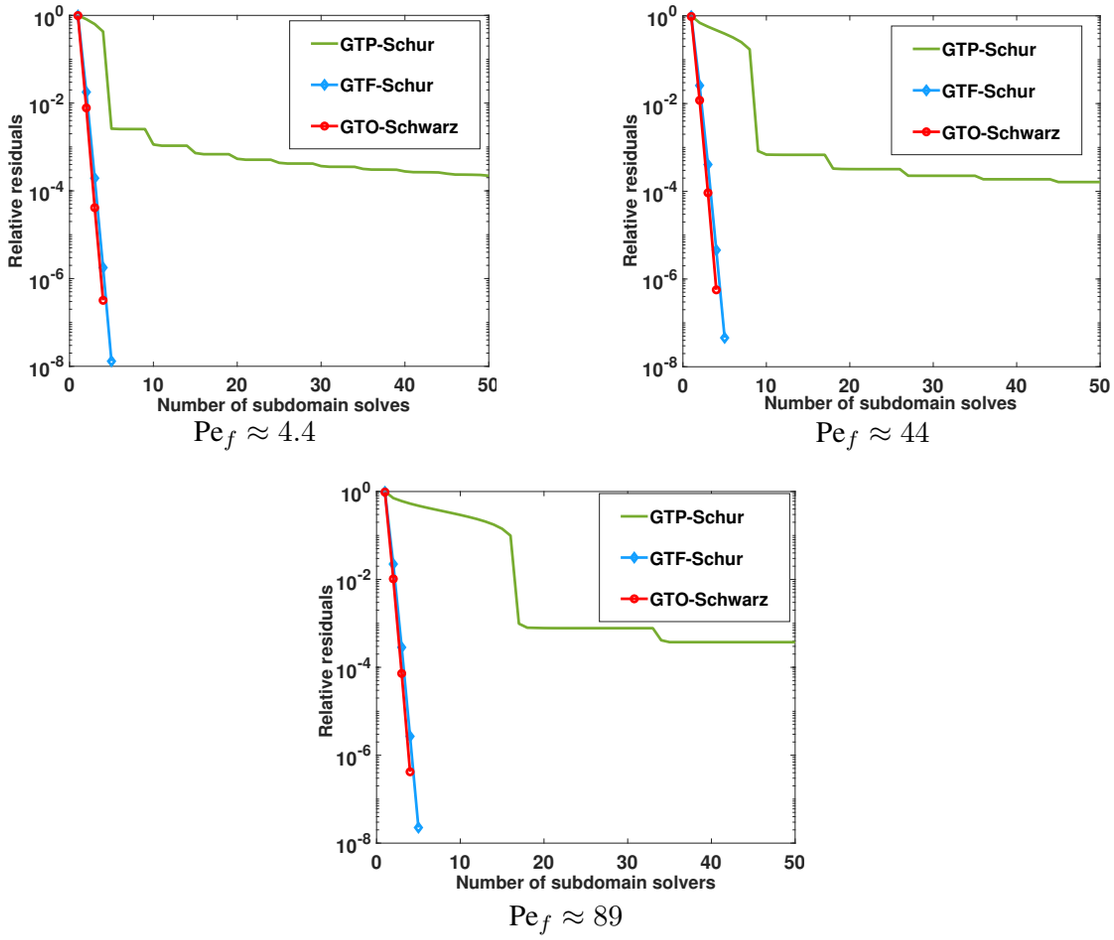

Figure 3.6: [Test case 2.1] Relative residual versus number of subdomain solves obtained from each method with different Péclet numbers with *nonconforming* time grid.

3.4.2. Test case 2.2: immersed fracture

In this section, we aim to study numerically the performance of the GTF-Schur and the GTO-Schwarz methods using Test case 2.2, which is the case where the porous media contains a partially immersed fracture. In this case, we consider the same geometry, boundary conditions, and parameters as in Test case 2.1, except now only one tip of the fracture is attached to the

external boundary, while the other tip is submerged inside the rock matrix. Consequently, a no-flow boundary condition is considered at the immersed tip.

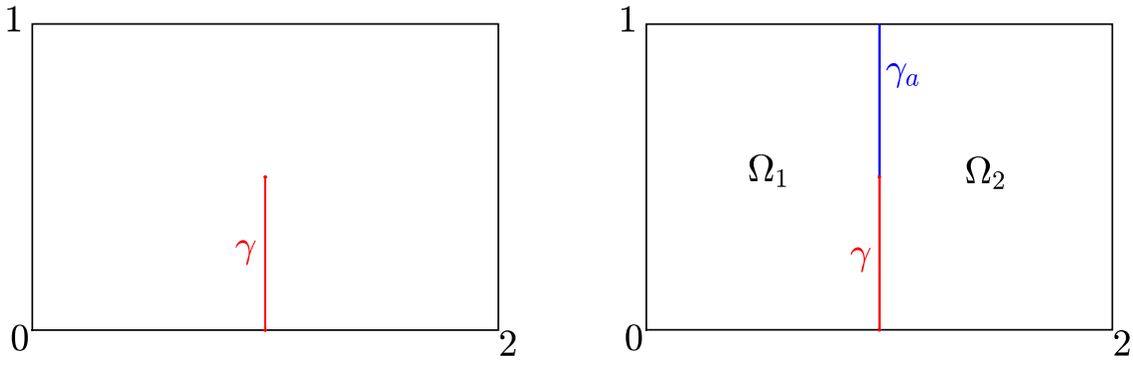

Figure 3.7: [Test case 2.2] (Left) Geometry of the rock matrix with immersed fracture γ. (Right) An artificial interface γ_a is introduced to decompose the domain into two disjoint subdomains.

To solve Test case 2.2 using global-in-time DD methods, we first introduce an additional interface γ_a so that, together with the partially immersed fracture γ, they form a single fracture Γ separating the original domain into two disjoint subdomains (as depicted in Figure 3.7). Due to operator splitting, each interface system on $\Gamma \times (0, T)$ consists of equations imposing the transmission conditions across γ and γ_a for both diffusion and advection. Similar to the non-immersed case, the interface equations for the diffusion on $\gamma \times (0, T)$ and $\gamma_a \times (0, T)$ are derived using the techniques developed in Chapter 2. For the advection part, the interface equations on $\gamma \times (0, T)$ will be the same as derived for the non-immersed fracture case (the first equations of (3.31) for GTF-Schur and of (3.38) for GTO-Schwarz). For the space-time artificial interface $\gamma_a \times (0, T)$, we employ the technique developed in [66] for the case with a normal fracture. Since we need to precondition the interface system for the diffusion of the GTF-Schur method as in Chapter 2, we call this method preconditioner GTF-Schur. We shall carry out in this section several numerical experiments to demonstrate and compare the performance of preconditioner GTF-Schur with GTO-Schwarz.

We first show in Figure 3.8 the snapshots of the concentration and the velocity fields at the final time $T = 4$. As the boundary conditions on the external boundary edges of the rock matrix are the same as in Test case 2.1, similar behaviors for the concentration and the velocity fields are observed. However, the length of the red arrows representing the magnitude of the fracture velocity decreases as the flow travels toward the immersed tip since a no-flow boundary

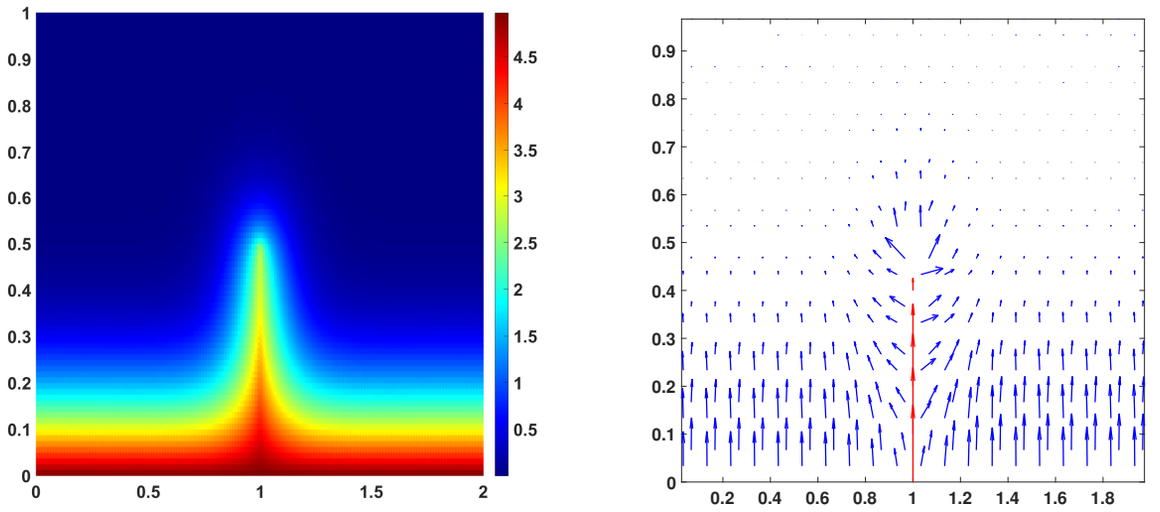

Figure 3.8: [Test case 2.2] Concentration field (left) and velocity field (right).

condition is imposed there. Moreover, at the immersed tip, the subdomain velocities tend to flow into the subdomains instead of converging at the endpoint of the fracture.

We next present the numerical results obtained from these methods when *conforming* time grids are imposed. We show in Table 3.6 the relative L^2-errors computed from all methods for concentration and velocity. Like Test case 2.1, only one table is needed to be shown as both methods return nearly the same approximate solutions. Moreover, first-order convergence in time is still observed for both concentration and velocity. Next, we report in Table 3.7 the number of subdomain solves needed to achieve the required tolerance. Unlike Test case 2.1, GTF-Schur converges more slowly than GTO-Schwarz, but its convergence speed is still relatively fast. This behavior has been observed for the pure diffusion problems in the previous chapter due to the complexity of the problem which requires us to apply a preconditioner to enhance the performance of GTF-Schur.

	Errors for concentration			Errors for velocity		
Δt	Ω_1	Ω_2	γ	Ω_1	Ω_2	γ
T/4	4.69e-02	4.69e-02	4.28e-02	8.60e-02	8.60e-02	6.55e-02
T/8	2.38e-02 [0.98]	2.38e-02 [0.98]	2.19e-02 [0.97]	4.27e-02 [1.01]	4.27e-02 [1.01]	3.25-02 [1.01]
T/16	1.18e-02 [1.01]	1.18e-02 [1.01]	1.11e-02 [0.98]	2.12e-02 [1.01]	2.12e-02 [1.01]	1.62e-02 [1.00]
T/32	5.64e-03 [1.07]	5.64e-03 [1.07]	5.49e-03 [1.02]	1.08e-02 [0.97]	1.08e-02 [0.97]	8.00e-03 [1.02]

Table 3.6: [Test case 2.2] Relative L^2-errors of the concentration and velocity with *conforming* time grid. The corresponding convergence rates are shown in square brackets.

Methods	Δt	T/4	T/8	T/16	T/32
Preconditioned GTF-Schur		16	16	18	18
GTO-Schwarz		13	13	13	13

Table 3.7: [Test case 2.2] Numbers of subdomain solves when *conforming* time grid is used; the tolerance for GMRES is set to be 10^{-8}.

		GTO-Schwarz			Preconditioned GTF-Schur		
Δt	Δt_γ	Ω_1	Ω_2	γ	Ω_1	Ω_2	γ
T/4	T/8	4.69e-02	4.69e-02	4.29e-02	4.72-02	4.72e-02	1.79e-02
T/8	T/16	2.38e-02 [0.98]	2.38e-02 [0.98]	2.20e-02 [0.96]	2.38e-02 [0.99]	2.38e-02 [0.99]	9.14e-03 [0.97]
T/16	T/32	1.18e-02 [1.01]	1.18e-02 [1.01]	1.11e-02 [0.99]	1.18e-02 [1.01]	1.18e-02 [1.01]	4.57e-03 [1.00]
T/32	T/64	5.64e-03 [1.07]	5.64e-03 [1.07]	5.50-03 [1.01]	5.63e-03 [1.07]	5.63e-03 [1.07]	2.23e-03 [1.04]

Table 3.8: [Test case 2.2] Relative L^2-errors of the *concentration* with nonconforming time grid. The corresponding convergence rates are shown in square brackets.

		GTO-Schwarz			Preconditioned GTF-Schur		
Δt	Δt_γ	Ω_1	Ω_2	γ	Ω_1	Ω_2	γ
T/4	T/8	8.61e-02	8.61e-02	6.56e-02	8.57e-02	8.57e-02	2.97e-02
T/8	T/16	4.28e-02 [1.01]	4.28e-02 [1.01]	3.25e-02 [1.01]	4.24e-02 [1.02]	4.24e-02 [1.02]	1.46e-02 [1.02]
T/16	T/32	2.12e-02 [1.01]	2.12e-02 [1.01]	1.62e-02 [1.00]	2.09e-02 [1.02]	2.09e-02 [1.02]	7.15e-03 [1.03]
T/32	T/64	1.08e-02 [0.97]	1.08e-02 [0.97]	8.01e-03 [1.02]	1.07e-02 [0.97]	1.07e-02 [0.97]	3.46e-03 [1.05]

Table 3.9: [Test case 2.2] Relative L^2-errors of the *velocity* with nonconforming time grid. The corresponding convergence rates are shown in square brackets.

	$\Delta t_1 = \Delta t_2$	T/4	T/8	T/16	T/32
	Δt_γ	T/8	T/16	T/32	T/64
Preconditioned GTF-Schur		16	16	18	18
GTO-Schwarz		13	13	13	14

Table 3.10: [Test case 2.2] Numbers of subdomain solves when *nonconforming* time grid is used; the tolerance for GMRES is set to be 10^{-8}.

Finally, we consider the case with *nonconforming* time grids and investigate the numerical performance of these methods. We impose the same large time step in the subdomains and a

smaller one in the fracture as in Test case 2.1: $\Delta t_1 = \Delta t_2 = \Delta t = 2\Delta t_\gamma$. We begin with presenting the relative errors in time for concentration and velocity in Table 3.8 and Table 3.9. Like Test case 2.1, the GTF-Schur method gives better accuracy in the fracture than the GTO-Schwarz method as the errors in the fracture obtained from GTF-Schur are close to the values we receive when we impose the same fine time grid in the subdomains and in the fracture.

We conclude this subsection by showing in Table 3.10 the number of subdomain solves for each method obtained when we reach the stopping criterion of GMRES. We can see that these numbers are nearly the same as those shown in Table 3.7, which implies these methods are still applicable when nonconforming time grids are imposed. From what we have observed so far, Test case 2.2 is more challenging than Test case 2.1, which can be seen from the increasing of number of subdomain solves of both methods. However, GTF-Schur still shows its efficiency as this method has a relatively fast convergence speed without requiring any precondition as well as preserves the accuracy in time when different time steps are used in the subdomains and in the fracture.

Conclusion

In this chapter, three global-in-time DD methods, namely GTP-Schur, GTF-Schur, and GTO-Schwarz, have been studied for the linear transport equation in a fractured porous medium. These methods are coupled with operator splitting so that not only local time stepping can be used in the fracture and in the matrix, but also different time steps can be imposed for the advection and the diffusion. Numerical experiments with different Péclet numbers and different types of fracture have been carried out to demonstrate the performance of the proposed methods with conforming and nonconforming time grids. Our results show that the GTF-Schur and GTO-Schwarz methods outperform the GTP-Schur method in terms of subdomain solves needed to reach the same stopping criterion (by a factor of more than 5 in our test cases). Moreover, GTF-Schur and GTO-Schwarz can handle mildly advection-dominant problems very well; they converge fast without requiring any preconditioners for such problems. Among these two methods, only GTF-Schur preserves the accuracy in time when fine time steps are used in the fracture and coarse ones in the rock matrix. More precisely, the errors in the fracture of GTF-Schur in

such a situation are close to the errors obtained from the case when a conforming fine time step is imposed on the whole domain. From the above observations, we conclude that GTF-Schur is the most efficient method. In the next chapter, we aim to tackle the case when the advection is strongly dominated. For this purpose, we construct a more efficient upwind local time stepping methods by utilizing the idea of mixed hybrid finite element methods. Rigorous error estimates for the proposed methods will also be presented.

Chapter 4

Monolithic and local time-stepping decoupled algorithms for transport problems in fractured porous media

Contents

In the previous chapter, we have derived local time-stepping methods for the reduced fracture model of the linear advection-diffusion equations by coupling global-in-time DD methods with operator splitting. In this chapter, we employ mixed hybrid finite elements to derive global-in-time DD methods to tackle the same problems with the aim of handling the case when the advection is strongly dominated. This chapter consists of three main parts. In the first part, a fully discrete formulation of the reduced fracture model is derived by using the hybridization process of the mixed hybrid finite elements which leads to a monolithic upwind algorithm.

Well-posedness as well as error estimates for the scheme are also proved. In the second part, we construct from the monolithic scheme two upwind local time stepping methods, namely GTF-Schur and GTO-Schwarz, by coupling global-in-time DD with mixed hybrid finite elements. A space-time interface system is formulated for each method and is solved iteratively. The convergence analysis for GTO-Schwarz with conforming time steps on the fracture and on the subdomains will be presented. Finally, in the last part, we carry out numerical experiments to verify numerically our theoretical parts and to investigate and compare the performance of our proposed methods.

4.1. Upwind-mixed hybrid finite element method for the reduced fracture model

4.1.1. Reduced fracture model of the linear transport problem

Let $T > 0$ be some fixed time. We consider Ω to have the same setting as in Chapter 2, that is, Ω is a bounded domain in $\mathbb{R}^2$ with Lipschitz boundary $\partial\Omega$ which is separated into two non-overlapping subdomains $\Omega_i,\ i = 1, 2$, by a fracture Ω_f of thickness δ as depicted in Figure 2.1. For simplicity, we assume further that Ω_f can be expressed as

$$\Omega_f = \left\{ \boldsymbol{x} \in \Omega : \boldsymbol{x} = \boldsymbol{x}_\gamma + s\boldsymbol{n},\ \text{where } \boldsymbol{x}_\gamma \in \gamma \text{ and } s \in \left(-\frac{\delta}{2}, \frac{\delta}{2}\right) \right\},$$

where γ is the intersection between a line and Ω and that Ω_f has higher permeability than that of Ω_i.

We consider the linear advection-diffusion problem written in mixed formulation as follows:

$$\begin{aligned} \phi\partial_t c + \operatorname{div} \boldsymbol{\varphi} &= q && \text{in } \Omega \times (0,T), \\ \boldsymbol{\varphi} &= \boldsymbol{u}c - \boldsymbol{D}\nabla c && \text{in } \Omega \times (0,T), \\ c &= 0 && \text{on } \partial\Omega \times (0,T), \\ c(\cdot,0) &= c_0 && \text{in } \Omega, \end{aligned} \tag{4.1}$$

where c is the concentration of a contaminant dissolved in a fluid, q is the source term, ϕ is the porosity, $\boldsymbol{u}$ is the Darcy velocity (assume to be given and time-independent), and $\boldsymbol{D}$ is a symmetric time-independent diffusion tensor.

Denote by $\boldsymbol{n}_i$, ∇_τ and div_τ the unit, outward-pointing, normal vector field on $\partial\Omega_i$, tangential gradient and tangential divergence, respectively, and let $\phi_\gamma := \delta\phi_f$ and $\boldsymbol{D}_\gamma := \delta\boldsymbol{D}_{f,\tau}$, where $\boldsymbol{D}_{f,\tau}$ is the tangential component of $\boldsymbol{D}_f$. Note that we have $\boldsymbol{n} = \boldsymbol{n}_1 = -\boldsymbol{n}_2$. By follow a similar approach described in Chapter 2, we obtained the following reduced model for (4.1) which consists of equations in the subdomains,

$$\begin{aligned}
\phi_i \partial_t c_i + \text{div}\, \boldsymbol{\varphi}_i &= q_i && \text{in } \Omega_i \times (0,T), \\
\boldsymbol{\varphi}_i &= \boldsymbol{u}_i c_i - \boldsymbol{D}_i \nabla c_i && \text{in } \Omega_i \times (0,T), \\
c_i &= 0 && \text{on } (\partial\Omega_i \cap \partial\Omega) \times (0,T), \\
c_i &= c_\gamma && \text{on } \gamma \times (0,T), \\
c_i(\cdot,0) &= c_{0,i} && \text{in } \Omega_i,
\end{aligned} \tag{4.2}$$

for $i = 1, 2$, coupled with the following equation in the one-dimensional fracture,

$$\begin{aligned}
\phi_\gamma \partial_t c_\gamma + \text{div}_\tau \boldsymbol{\varphi}_\gamma &= q_\gamma + \sum_{i=1}^{2} \boldsymbol{\varphi}_i \cdot \boldsymbol{n}_{i|\gamma} && \text{in } \gamma \times (0,T), \\
\boldsymbol{\varphi}_\gamma &= \boldsymbol{u}_\gamma c_\gamma - \boldsymbol{D}_\gamma \nabla_\tau c_\gamma && \text{in } \gamma \times (0,T), \\
c_\gamma &= 0 && \text{on } \partial\gamma \times (0,T), \\
c_\gamma(\cdot,0) &= c_{0,\gamma} && \text{in } \gamma.
\end{aligned} \tag{4.3}$$

Throughout this chapter, we assume that:

(A1) The coefficient matrices $\boldsymbol{D}_i^{-1}, i = 1,2$ and $\boldsymbol{D}_\gamma^{-1}$ are symmetric and uniformly positive definite. Furthermore, there exists two pairs of positive numbers $(D^-,\ D^+)$ and $\left(D_\gamma^-,\ D_\gamma^+\right)$ such that

$$\begin{aligned}
&D^-|\eta|^2 \le \eta^T \boldsymbol{D}_i^{-1}(x)\,\eta \le D^+|\eta|^2, \ \text{ for a.e. } x \in \Omega_i,\ \forall \eta \in R^2,\ i = 1,2, \\
&D_\gamma^-|\varsigma|^2 \le \varsigma^T \boldsymbol{D}_\gamma^{-1}(s)\,\varsigma \le D_\gamma^+|\varsigma|^2, \ \text{ for a.e. } s \in \gamma,\ \forall \varsigma \in R.
\end{aligned}$$

(A2) There exists two positive numbers ϕ^- and ϕ^+ such that

$$\phi^- \le \phi_i(x) \le \phi^+, \text{ for a.e. } x \in \Omega_i,\ i = 1,2, \text{ and } \phi^- \le \phi_\gamma(s) \le \phi^+, \text{ for a.e. } s \in \gamma.$$

(A3) Let $J = (0,T)$ and $H^1_*(\Omega_i) = \{g \in H^1(\Omega_i) :\ g = 0 \text{ on } \partial\Omega_i \cap \partial\Omega\}$, the following regularity conditions hold: $\boldsymbol{u}_i \in C\left(\bar{J}; \left(W^{1,\infty}(\Omega_i)\right)^2\right)$, $q_i \in C\left(J, L^2(\Omega_i)\right)$ and $c_{0,i} \in H^1_*(\Omega_i)$, for $i = 1,\ 2$, and $\boldsymbol{u}_\gamma \in C\left(\bar{J}; \left(W^{1,\infty}(\gamma)\right)^2\right)$, $q_\gamma \in C\left(J, L^2(\gamma)\right)$ and $c_{0,\gamma} \in H^1_0(\gamma)$.

We utilize the following notation to derive the weak formulations of (4.2)-(4.3). For any measurable subset $\mathcal{O}$ of $\mathbb{R}^2$, let $(\cdot,\cdot)_{\mathcal{O}}$ and $\|\cdot\|_{0,\mathcal{O}}$ denote the inner product and norm on $L^2(\mathcal{O})$ or $(L^2(\mathcal{O}))^2$, respectively, and let $\|\cdot\|_{k,\mathcal{O}}$ stand for the norm on $H^k(\mathcal{O}) := W^{k,2}(\mathcal{O})$ ($H^k(\mathcal{O})$ concides with $L^2(\mathcal{O})$ when $k=0$). Let $H(\mathrm{div},\mathcal{O})$ denote the space of functions in $(L^2(\mathcal{O}))^2$ having the divergence in $L^2(\mathcal{O})$. We next define the following Hilbert spaces:

$$
\begin{aligned}
&M = \{\mu = (\mu_1,\mu_2,\mu_\gamma) \in L^2(\Omega_1)\times L^2(\Omega_2)\times L^2(\gamma)\},\\
&\boldsymbol{\Sigma} = \Big\{\boldsymbol{v} = (\boldsymbol{v}_1,\boldsymbol{v}_2,\boldsymbol{v}_\gamma) \in (L^2(\Omega_1))^2\times(L^2(\Omega_2))^2\times L^2(\gamma) : \mathrm{div}\,\boldsymbol{v}_i \in L^2(\Omega_i),\ i=1,2,\\
&\qquad\qquad \text{and } \mathrm{div}_\tau \boldsymbol{v}_\gamma - \sum_{n=1}^{2}(\boldsymbol{v}_i\cdot\boldsymbol{n}_i)_{|\gamma} \in L^2(\gamma)\Big\}.
\end{aligned}
$$

Finally, we introduce the following bilinear forms $a(\cdot,\cdot)$, $b(\cdot,\cdot)$, $r_\phi(\cdot,\cdot)$, $d_{\boldsymbol{u}}(\cdot,\cdot)$ and $e(\cdot,\cdot)$ on $\boldsymbol{\Sigma}\times\boldsymbol{\Sigma}$, $\boldsymbol{\Sigma}\times M$, $M\times M$, $M\times\boldsymbol{\Sigma}$ and $M\times\boldsymbol{\Sigma}$, respectively,

$$
\begin{aligned}
&a(\boldsymbol{w},\boldsymbol{v}) = \sum_{i=1}^{2}\left(\boldsymbol{D}_i^{-1}\boldsymbol{w}_i,\boldsymbol{v}_i\right)_{\Omega_i} + \left(\boldsymbol{D}_\gamma^{-1}\boldsymbol{w}_\gamma,\boldsymbol{v}_\gamma\right)_\gamma, \quad b(\boldsymbol{w},\mu) = \sum_{i=1}^{2}(\mathrm{div}\,\boldsymbol{w}_i,\mu_i)_{\Omega_i} + (\mathrm{div}_\tau\,\boldsymbol{w}_\gamma,\mu_\gamma)_\gamma,\\
&r_\phi(\eta,\mu) = \sum_{i=1}^{2}(\phi_i\eta_i,\mu_i)_{\Omega_i} + (\phi_\gamma\eta_\gamma,\mu_\gamma)_\gamma, \quad d_{\boldsymbol{u}}(\mu,\boldsymbol{w}) = \sum_{i=1}^{2}\left(\boldsymbol{D}_i^{-1}\boldsymbol{u}_i\mu_i,\boldsymbol{w}_i\right)_{\Omega_i} + \left(\boldsymbol{D}_\gamma^{-1}\boldsymbol{u}_\gamma\mu_\gamma,\boldsymbol{w}_\gamma\right)_\gamma,\\
&e(\boldsymbol{w},\mu) = \sum_{i=1}^{2}\left\langle\boldsymbol{w}_i\cdot\boldsymbol{n}_{i|\gamma},\mu_\gamma\right\rangle_\gamma,
\end{aligned}
\tag{4.4}
$$

and the linear form L_q on M: $L_q(\mu) = \sum_{i=1}^{2}(q_i,\mu_i)_{\Omega_i} + (q_\gamma,\mu_\gamma)_\gamma$. With these spaces and forms, the weak form of (4.2)-(4.3) can be written as follows:

Find $c=(c_1,c_2,c_\gamma)\in H^1(0,T;M)$ and $\boldsymbol{\varphi}=(\boldsymbol{\varphi}_1,\boldsymbol{\varphi}_2,\boldsymbol{\varphi}_\gamma)\in L^2(0,T;\boldsymbol{\Sigma})$ such that

$$
\begin{aligned}
a(\boldsymbol{\varphi},\boldsymbol{v}) - b(\boldsymbol{v},c) + e(\boldsymbol{v},c) - d_{\boldsymbol{u}}(c,\boldsymbol{v}) &= 0 \qquad \forall \boldsymbol{v}\in\boldsymbol{\Sigma},\\
r_\phi(\partial_t c,\mu) + b(\boldsymbol{\varphi},\mu) - e(\boldsymbol{\varphi},\mu) &= L_q(\mu) \quad \forall \mu\in M,
\end{aligned}
\tag{4.5}
$$

together with the initial conditions:

$$
c_i(\cdot,0) = c_{0,i},\ \text{in } \Omega_i,\ i=1,2, \quad \text{and} \quad c_\gamma(\cdot,0) = c_{0,\gamma},\ \text{in } \gamma. \tag{4.6}
$$

For error analysis purpose, we shall assume that the solution $(\boldsymbol{\varphi},c)$ of (4.5)-(4.6) satisfies the following regularity condition:

(A4) $(\boldsymbol{\varphi},c)\in C\left(\bar{J},\boldsymbol{\mathcal{H}}^1\right)\times\left(H^1(J;\mathcal{H}^1)\cap H^2(J;M)\cap C(J,\mathcal{H}^1)\right)$, where $\mathcal{H}^k := H^k(\Omega_1)\times H^k(\Omega_2)\times H^k(\gamma)$ and $\boldsymbol{\mathcal{H}}^k := (H^k(\Omega_1))^2\times(H^k(\Omega_2))^2\times H^k(\gamma)$, $k=0,1$.

4.1.2. Upwind-mixed hybrid finite element method for the monolithic problem

We now derive the fully discrete upwind-mixed hybrid finite element algorithm to find a numerical solution to (4.5)-(4.6). We begin with discretizing the equations in (4.5) in space based on the lowest-order Raviart-Thomas mixed finite element method. For simplicity, assume Ω is a rectangular domain. Let $\mathcal{K}_{h,i},\ i=1,2$ be a finite element partition of each Ω_i into rectangles such that they match on γ and their union $\mathcal{K}_h = \cup_{i=1}^{2}\mathcal{K}_{h,i}$ forms a finite element partition of Ω. Note that the analysis presented below also holds for triangular meshes that satisfy assumptions (M1) - (M6) in [26] and match on the interface.

For $i=1,2$, let $\mathcal{E}_{h,i}^{I}$ be the set of all interior edges and $\mathcal{E}_{h,i}^{D}$ be the set of edges of the external boundary $\partial\Omega_i \cap \partial\Omega$. Moreover, we denote by $\mathcal{E}_h^{\gamma}$ the set of edges of elements in $\mathcal{K}_{h,1}$ or $\mathcal{K}_{h,2}$ that lie on γ. We then denote by $\mathcal{E}_{h,i}$ the set of all edges of elements in $\mathcal{K}_{h,i}$:

$$\mathcal{E}_{h,i} = \mathcal{E}_{h,i}^{I} \cup \mathcal{E}_{h,i}^{D} \cup \mathcal{E}_h^{\gamma},\ i=1,2.$$

We also denote by $\mathcal{P}_h^{\gamma}$ the set of endpoints P of all interface edges $E \in \mathcal{E}_h^{\gamma}$. For any $K \in \mathcal{K}_{h,i},\ i=1,2$, let $\boldsymbol{n}_K$ denote the unit, normal, outward-pointing vector field on the boundary ∂K; for each edge E on ∂K, let $\boldsymbol{n}_E$ denote the unit normal vector of E, outward to K and let $\boldsymbol{n}_{\partial E}$ be the unit tangential vector field of E at the two endpoints of E, outward to E. Let $h_K = \text{diam}(K), h_E = |E|$, $h_i = \max\limits_{K\in\mathcal{K}_{h,i}} h_K, i=1,2$, $h_\gamma = \max\limits_{E\in\mathcal{E}_h^{\gamma}} h_E$, and $h = \max\{h_1, h_2, h_\gamma\}$. With the given notation, the lowest-order Raviart-Thomas mixed finite element spaces on Ω_i are defined as follows:

$$M_{h,i} := \left\{\mu_i \in L^2(\Omega_i) : \mu_{i|K} = \text{constant}, \forall K \in \mathcal{K}_{h,i}\right\},$$
$$\boldsymbol{\Sigma}_{h,i} := \left\{\boldsymbol{v}_{h,i} \in H(\text{div},\, \Omega_i) : \boldsymbol{v}_{h,i|K} \in \boldsymbol{\Sigma}_K, \forall K \in \mathcal{K}_{h,i}\right\}, i=1,2,$$

where $\boldsymbol{\Sigma}_K := \left\{\boldsymbol{w} : K \to \mathbb{R}^2,\ \boldsymbol{w}(x,y) = (a_K + b_K x, a_K^{'} + b_K^{'} y), (a_K, b_K, a_K^{'}, b_K^{'}) \in \mathbb{R}^4\right\}$ is the local Raviart –Thomas space of lowest order on $K \in \mathcal{K}_{h,i}$. Similarly, for the discretization on γ, we have the following mixed finite element spaces:

$$M_{h,\gamma} := \left\{\mu_\gamma \in L^2(\gamma) : \mu_{\gamma|E} = \text{ constant on } E,\ \forall E \in \mathcal{E}_h^{\gamma}\right\},$$
$$\boldsymbol{\Sigma}_{h,\gamma} := \left\{\boldsymbol{v}_\gamma \in H(\text{div}_\tau,\, \gamma) : \boldsymbol{v}_{\gamma|E} \in \boldsymbol{\Sigma}_{\gamma,E}, \forall E \in \mathcal{E}_h^{\gamma}\right\},$$

where $\mathbf{\Sigma}_{\gamma,E} := \{\boldsymbol{v}_\gamma : E \to \mathbb{R},\ \boldsymbol{v}_\gamma(s) = a_E + b_E s,\ (a_E, b_E) \in \mathbb{R}^2\}$, for $E \in \mathcal{E}_h^\gamma$.

Instead of using these classical mixed finite element spaces, in this work we apply a hybridization technique to obtain an equivalent hybrid formulation, namely the mixed hybrid finite element method [105, 23]. For this approach, the continuity constraint of the normal fluxes across inter-element boundaries is relaxed and is imposed by virtue of an additional equation involving Lagrange multipliers. The finite element spaces related to the mixed hybrid finite element scheme are defined as

$$
\begin{aligned}
&\widetilde{\mathbf{\Sigma}}_{h,i} := \left\{\boldsymbol{v}_i \in (L^2(\Omega_i))^2 : \boldsymbol{v}_{i|K} \in \mathbf{\Sigma}_K, \forall K \in \mathcal{K}_{h,i}\right\}, i = 1, 2,\\
&\widetilde{\mathbf{\Sigma}}_{h,\gamma} := \left\{\boldsymbol{v}_\gamma \in L^2(\gamma) : \boldsymbol{v}_{\gamma|E} \in \mathbf{\Sigma}_{\gamma,E}, \forall E \in \mathcal{E}_h^\gamma\right\},\\
&\Theta_{h,i} := \left\{\eta \in L^2(\mathcal{E}_{h,i}) : \eta_{|E} = \text{ constant on } E,\ \forall E \in \mathcal{E}_{h,i}^I \cup \mathcal{E}_h^\gamma \text{ and } \eta_{|E} = 0,\ \forall E \in \mathcal{E}_{h,i}^D\right\}, i = 1,\ 2,\\
&\Theta_{h,\gamma} := \left\{\varsigma : \mathcal{P}_h^\gamma \to \mathbb{R},\ \varsigma(P) = 0 \text{ if } P \in \partial\gamma\right\},
\end{aligned}
$$

where the last two spaces are for the Lagrange multipliers of the two-dimensional problems on the subdomains and the one-dimensional equations on the fracture, respectively. Next, we introduce several products of these finite element spaces:

$$
\begin{aligned}
&M_h = M_{h,1} \times M_{h,2} \times M_{h,\gamma}, \quad &&\mathbf{\Sigma}_h = \mathbf{\Sigma}_{h,1} \times \mathbf{\Sigma}_{h,2} \times \mathbf{\Sigma}_{h,\gamma},\\
&\widetilde{\mathbf{\Sigma}}_h = \widetilde{\mathbf{\Sigma}}_{h,1} \times \widetilde{\mathbf{\Sigma}}_{h,2} \times \widetilde{\mathbf{\Sigma}}_{h,\gamma}, &&\Theta_h = \Theta_{h,1} \times \Theta_{h,2} \times \Theta_{h,\gamma}.
\end{aligned}
\tag{4.7}
$$

For $i = 1, 2$, and any $c_{h,i}(t) \in M_{h,i}$, we have the unique representation:

$$
c_{h,i}(t, x, y) = \sum_{K \in \mathcal{K}_{h,i}} c_{i,K}(t)\chi_K(x, y),
$$

where χ_K is the characteristic function of element $K \in \mathcal{K}_{h,i}$ and $c_{i,K}$ represents the average of $c_{h,i}$ on K. Similarly, for the Lagrange multipliers $\theta_{h,i} \in \Theta_{h,i}$ of $c_{h,i}$, it can be represented uniquely as

$$
\theta_{h,i}(t, x, y) = \sum_{E \in \mathcal{E}_{h,i}} \theta_{i,E}(t)\chi_E(x, y),
$$

where χ_E is the characteristic function of edge $E \in \mathcal{E}_{h,i}$ and $\theta_{i,E}$ is the average value of $\theta_{h,i}$ on E. The velocity $\boldsymbol{\varphi}_{h,i}(t) \in \widetilde{\mathbf{\Sigma}}_{h,i}$ is defined locally as

$$
\boldsymbol{\varphi}_{h,i}(t, x, y)_{|K} = \sum_{E \subset \partial K} \varphi_{i,KE}(t)\boldsymbol{w}_{i,KE}(x, y),\ \forall K \in \mathcal{K}_{h,i},
$$

where $\varphi_{i,KE}$ is the normal flux leaving $K \in \mathcal{K}_{h,i}$ through the edge E and $\{\boldsymbol{w}_{i,KE}\}_{E \subset \partial K}$ are the basis functions of the local Raviart-Thomas space $\mathbf{\Sigma}_K$ satisfying

$$\int_{E'} \boldsymbol{w}_{i,KE} \cdot \boldsymbol{n}_K = \delta_{E,E'},\ \forall E' \subset \partial K.$$

Similarly, for any $c_{h,\gamma}(t) \in M_{h,\gamma}$ and $\boldsymbol{\varphi}_{h,\gamma}(t) \in \widetilde{\boldsymbol{\Sigma}}_{h,\gamma}$, we have the following unique expressions

$$c_{h,\gamma}(t,y) = \sum_{E \in \mathcal{E}_h^\gamma} c_{\gamma,E}(t)\chi_E(y), \quad \text{and } \boldsymbol{\varphi}_{h,\gamma}(t,y)_{|E} = \sum_{P \in \partial E} \varphi_{\gamma,EP}(t)\boldsymbol{w}_{\gamma,EP}(y),\ \forall E \in \mathcal{E}_h^\gamma,$$

where $\{\boldsymbol{w}_{\gamma,EP}\}_{P\in\partial E}$ are the local basis functions of $\boldsymbol{\Sigma}_{\gamma,E}$. We also denote by $\boldsymbol{u}_h = (\boldsymbol{u}_{h,1}, \boldsymbol{u}_{h,2}, \boldsymbol{u}_{h,\gamma})$ the projections of $\boldsymbol{u} = (\boldsymbol{u}_1, \boldsymbol{u}_2, \boldsymbol{u}_\gamma)$ on $\boldsymbol{\Sigma}_{h,1} \times \boldsymbol{\Sigma}_{h,2} \times \boldsymbol{\Sigma}_{h,\gamma}$:

$$\boldsymbol{u}_{h,i}(x,y) := \sum_{K \in \mathcal{K}_{h,i}} \sum_{E \subset \partial K} u_{i,KE}\boldsymbol{w}_{i,KE}(x,y), \quad \boldsymbol{u}_{h,\gamma}(y) := \sum_{E \in \mathcal{E}_h^\gamma} \sum_{P \in \partial E} u_{\gamma,EP}\boldsymbol{w}_{\gamma,EP}(y), \tag{4.8}$$

where $u_{i,KE} = \frac{1}{|E|}\int_E \boldsymbol{u}_i \cdot \boldsymbol{n}_K$ and $u_{\gamma,EP} = (\boldsymbol{u}_\gamma \cdot \boldsymbol{n}_{\partial E})_{|P}$.

The classical mixed finite element scheme for the problem (4.5)-(4.6) is given by:

Find $(c_h(t), \boldsymbol{\varphi}_h(t)) \in M_h \times \boldsymbol{\Sigma}_h$ for a.e. $t \in (0,T)$ such that

$$\begin{array}{lcll} a(\boldsymbol{\varphi}_h, \boldsymbol{v}_h) - b(\boldsymbol{v}_h, c_h) + e(\boldsymbol{v}_h, c_h) - d_{\boldsymbol{u}_h}(c_h, \boldsymbol{v}_h) & = & 0 & \forall \boldsymbol{v}_h \in \boldsymbol{\Sigma}_h, \\ r_\phi(\partial_t c_h, \mu_h) + b(\boldsymbol{\varphi}_h, \mu_h) - e(\boldsymbol{\varphi}_h, \mu_h) & = & L_q(\mu_h) & \forall \mu_h \in M_h, \end{array} \tag{4.9}$$

with the initial condition

$$(c_h(0), \mu_h) = (c_0, \mu_h),\ \forall \mu_h \in M_h, \tag{4.10}$$

where $c_h = (c_{h,1}, c_{h,2}, c_{h,\gamma})$, $c_0 = (c_{0,1}, c_{0,2}, c_{0,\gamma})$ and $\boldsymbol{\varphi}_h = (\boldsymbol{\varphi}_{h,1}, \boldsymbol{\varphi}_{h,2}, \boldsymbol{\varphi}_{h,\gamma})$.

It is well-known that if we employ the basis functions of M_h and $\boldsymbol{\Sigma}_h$ in the system (4.9), the resulting linear algebra system is in general indefinite [102, 26, 110]. Moreover, it is not guaranteed that the scheme works for strongly advection-dominated problems [102]. To overcome these difficulties, we apply a hybridization process to replace $\boldsymbol{\Sigma}_h$ by $\widetilde{\boldsymbol{\Sigma}}_h$, thus, the continuity conditions of the normal components of the flux variables across element interfaces are no longer required. These conditions are later imposed by introducing the Lagrange multipliers from the space Θ_h to ensure the equivalence of both algorithms. Towards this end, we define, in addition to the forms in (4.4), the following mapping on $\Theta_h \times \widetilde{\boldsymbol{\Sigma}}_h$:

$$l(\eta_h, \boldsymbol{v}_h) = \sum_{i=1}^{2} \sum_{K \in \mathcal{K}_{h,i}} \sum_{\substack{E \subset \partial K \\ E \in \mathcal{E}_{h,i} \setminus \mathcal{E}_h^\gamma}} \langle \eta_{h,i}, \boldsymbol{v}_{h,i} \cdot \boldsymbol{n}_K \rangle_E + \sum_{E \in \mathcal{E}_h^\gamma} \langle \eta_{h,\gamma},\ \boldsymbol{v}_{h,\gamma} \cdot \boldsymbol{n}_{\partial E} \rangle_{\partial E}, \tag{4.11}$$

where $\eta_h = (\eta_{h,1}, \eta_{h,2}, \eta_{h,\gamma}) \in \Theta_h$ and $\boldsymbol{v}_h = (\boldsymbol{v}_{h,1}, \boldsymbol{v}_{h,2}, \boldsymbol{v}_{h,\gamma}) \in \widetilde{\boldsymbol{\Sigma}}_h$. To take into account the interface as part of the subdomain boundary, we define the space

$$\Theta_{h,i}^0 := \left\{ \eta \in \Theta_{h,i} : \eta_{|E} = 0,\ \forall E \in \mathcal{E}_h^\gamma \right\},\ i = 1, 2,$$

and denote by Θ_h^0 the product space $\Theta_{h,1}^0 \times \Theta_{h,2}^0 \times \Theta_{h,\gamma}$. Altogether, the semi-discrete mixed hybrid formulation associated with (4.9) is written as follows:

Find $(c_h(t), \boldsymbol{\varphi}_h(t), \theta_h(t)) \in M_h \times \widetilde{\boldsymbol{\Sigma}}_h \times \Theta_h$ for a.e. $t \in (0, T)$ such that

$$\begin{aligned}
&a(\boldsymbol{\varphi}_h, \boldsymbol{v}_h) - b(\boldsymbol{v}_h, c_h) + e(\boldsymbol{v}_h, c_h) - d_{\boldsymbol{u}_h}(c_h, \boldsymbol{v}_h) + l(\theta_h, \boldsymbol{v}_h) = 0, \\
&r_\phi(\partial_t c_h, \mu_h) + b(\boldsymbol{\varphi}_h, \mu_h) - e(\boldsymbol{\varphi}_h, \mu_h) = L(q, \mu_h), \qquad \forall (\mu_h, \boldsymbol{v}_h, \eta_h) \in M_h \times \widetilde{\boldsymbol{\Sigma}}_h \times \Theta_h^0, \\
&l(\eta_h, \boldsymbol{\varphi}_h) = 0,
\end{aligned} \tag{4.12}$$

with the initial conditions (4.10), where $\theta_h = (\theta_{h,1}, \theta_{h,2}, \theta_{h,\gamma})$.

For advection-diffusion equations, the Lagrange multipliers can also be used to discretize the advective terms via upwind operators, which leads to an upwind-mixed hybrid scheme [102, 26] that can handle strongly advection-dominated problems. Specifically, we define an approximation of the advective flux $d_{\boldsymbol{u}_h}(\cdot, \cdot)$ as follows: for $\mu_h = (\mu_{h,1}, \mu_{h,2}, \mu_{h,\gamma}) \in M_h$, $\eta_h = (\eta_{h,1}, \eta_{h,2}, \eta_{h,\gamma}) \in \Theta_h$ and $\boldsymbol{v}_h = (\boldsymbol{v}_{h,1}, \boldsymbol{v}_{h,2}, \boldsymbol{v}_{h,\gamma}) \in \widetilde{\boldsymbol{\Sigma}}_h$,

$$\begin{aligned}
\widetilde{d}_{\boldsymbol{u}_h}((\mu_h, \eta_h), \boldsymbol{v}_h) \ = \sum_{i=1}^{2} \sum_{K \in \mathcal{K}_{h,i}} \Bigg(& \sum_{\substack{E \subset \partial K \\ E \in \mathcal{E}_{h,i} \backslash \mathcal{E}_h^\gamma}} u_{i,KE} \mathcal{U}_{i,KE}(\mu_{i,K}, \eta_{i,E}) (\boldsymbol{D}_i^{-1} \boldsymbol{w}_{i,KE}, \boldsymbol{v}_{h,i})_K \\
& + \sum_{\substack{E \subset \partial K \\ E \in \mathcal{E}_h^\gamma}} u_{i,KE} \mathcal{U}_{i,KE}^\gamma(\mu_{i,K}, \mu_{\gamma,E}) (\boldsymbol{D}_i^{-1} \boldsymbol{w}_{i,KE}, \boldsymbol{v}_{h,i})_K \Bigg) \\
& + \sum_{E \in \mathcal{E}_h^\gamma} \sum_{P \in \partial E} u_{\gamma,EP} \mathcal{U}_{\gamma,EP}(\mu_{\gamma,E}, \eta_{\gamma,P}) (\boldsymbol{D}_\gamma^{-1} \boldsymbol{w}_{\gamma,EP}, \boldsymbol{v}_{h,\gamma})_\gamma,
\end{aligned} \tag{4.13}$$

where, for any $K \in \mathcal{K}_{h,i}$ and $E \subset \partial K$:

i) if $E \in \mathcal{E}_{h,i} \backslash \mathcal{E}_h^\gamma$, the upwind value $\mathcal{U}_{i,KE}$ is computed by

$$\mathcal{U}_{i,KE}(\mu_{i,K}, \eta_{i,E}) = \begin{cases} \mu_{i,K}, & \text{if } u_{i,KE} \geq 0, \\ 2\eta_{i,E} - \mu_{i,K}, & \text{if } E \in \mathcal{E}_{h,i}^I \text{ and } u_{i,KE} < 0, \\ 0, & \text{if } E \in \mathcal{E}_{h,i}^D \text{ and } u_{i,KE} < 0, \end{cases} \quad i = 1, 2, \tag{4.14}$$

ii) if $E \in \mathcal{E}_h^\gamma$, the upwind value $\mathcal{U}_{i,KE}^\gamma$ is computed by

$$\mathcal{U}^{\gamma}_{i,KE}(\mu_{i,K},\mu_{\gamma,E})=\begin{cases}\mu_{i,K}, & \text{if } u_{i,KE}\geq 0,\\ \mu_{\gamma,E}, & \text{if } u_{i,KE}<0,\end{cases}\quad i=1,2, \tag{4.15}$$

while for any $E\in\mathcal{E}_h^{\gamma}$ and $P\in\partial E$, the upwind value $\mathcal{U}_{\gamma,EP}$ is given by

$$\mathcal{U}_{\gamma,EP}(\mu_{\gamma,E},\eta_{\gamma,P})=\begin{cases}\mu_{\gamma,E}, & \text{if } u_{\gamma,EP}\geq 0,\\ 2\eta_{\gamma,P}-\mu_{\gamma,E}, & \text{if } P\notin\partial\gamma \text{ and } u_{\gamma,EP}<0,\\ 0, & \text{if } P\in\partial\gamma \text{ and } u_{\gamma,EP}<0.\end{cases} \tag{4.16}$$

By replacing $d_{\boldsymbol{u}_h}(\cdot,\cdot)$ in (4.12) with the new operator defined by (4.13), we obtain the following semi-discrete upwind-mixed hybrid scheme:

Find $(c_h(t),\boldsymbol{\varphi}_h(t),\theta_h(t))\in M_h\times\widetilde{\boldsymbol{\Sigma}}_h\times\Theta_h$ for a.e. $t\in(0,T)$ such that

$$\begin{aligned}&a(\boldsymbol{\varphi}_h,\boldsymbol{v}_h)-b(\boldsymbol{v}_h,c_h)+e(\boldsymbol{v}_h,c_h)-\widetilde{d}_{\boldsymbol{u}_h}((c_h,\theta_h),\boldsymbol{v}_h)+l(\theta_h,\boldsymbol{v}_h)=0,\\ &r_\phi(\partial_t c_h,\mu_h)+b(\boldsymbol{\varphi}_h,\mu_h)-e(\boldsymbol{\varphi}_h,\mu_h)=L_q(\mu_h), \qquad \forall(\mu_h,\boldsymbol{v}_h,\eta_h)\in M_h\times\widetilde{\boldsymbol{\Sigma}}_h\times\Theta_h^0.\\ &l(\eta_h,\boldsymbol{\varphi}_h)=0,\end{aligned} \tag{4.17}$$

Finally, we discretize (4.17) in time by the backward Euler scheme and obtain the fully discrete upwind-mixed hybrid finite element method. We define the time step size $\Delta t=T/N$ and the discrete times $t_n=n\Delta t, n=1,\ldots,N$, where N is a positive integer. The time derivatives are approximated by the backward difference quotient

$$\bar{\partial}c^n=\frac{c^n-c^{n-1}}{\Delta t}, n=1,\ldots,N,$$

where the superscript n indicates the evaluation of a function at the discrete time $t=t^n$. The fully-discrete version of (4.17) reads as follows:

For $n=1,\ldots,N$, find $(c_h^n,\boldsymbol{\varphi}_h^n,\theta_h^n)\in M_h\times\widetilde{\boldsymbol{\Sigma}}_h\times\Theta_h$ satisfying

$$\begin{aligned}&a(\boldsymbol{\varphi}_h^n,\boldsymbol{v}_h)-b(\boldsymbol{v}_h,c_h^n)+e(\boldsymbol{v}_h,c_h^n)-\widetilde{d}_{\boldsymbol{u}_h}((c_h^n,\theta_h^n),\boldsymbol{v}_h)+l(\theta_h^n,\boldsymbol{v}_h)=0,\\ &r_\phi(\bar{\partial}c_h^n,\mu_h)+b(\boldsymbol{\varphi}_h^n,\mu_h)-e(\boldsymbol{\varphi}_h^n,\mu_h)=L_{q^n}(\mu_h), \qquad \forall(\mu_h,\boldsymbol{v}_h,\eta_h)\in M_h\times\widetilde{\boldsymbol{\Sigma}}_h\times\Theta_h^0,\\ &l(\eta_h,\boldsymbol{\varphi}_h^n)=0,\end{aligned} \tag{4.18}$$

where the initial conditions $(c_{h,1}^0,c_{h,2}^0,c_{h,\gamma}^0)$ are given by

$$c_{h,i|K_i}^0:=\frac{1}{|K_i|}\int_{K_i}c_{0,i},\ \ \forall K_i\in\mathcal{K}_{h,i},i=1,2,\ \text{ and }\ c_{h,\gamma|E}^0:=\frac{1}{|E|}\int_E c_{0,\gamma},\ \ \forall E\in\mathcal{G}_h. \tag{4.19}$$

That means $c_{h,i}^0$ is the L^2-projection of $c_{0,i}$ onto $M_{h,i}$, for $i = 1, 2$, and $c_{h,\gamma}^0$ is the L^2-projection of $c_{0,\gamma}$ onto $M_{h,\gamma}$.

In the next section, we establish the existence, uniqueness and derive a priori error estimates for the solution of the upwind-mixed hybrid scheme (4.18).

4.2. Analysis of the upwind-mixed hybrid finite element method

For analysis purpose, we make use of the Raviart-Thomas projection operators $\Pi_{h,i} \times P_{h,i} : (H^1(\Omega_i))^2 \times L^2(\Omega_i) \to \boldsymbol{\Sigma}_{h,i} \times M_{h,i}, i = 1, 2$, and $\Pi_{h,\gamma} \times P_{h,\gamma} : H^1(\gamma) \times L^2(\gamma) \to \boldsymbol{\Sigma}_{h,\gamma} \times M_{h,\gamma}$. The following properties hold for these operators [41, 103]:

(P1) $P_{h,1}, P_{h,2}$ and $P_{h,\gamma}$ are the L^2-orthogonal projections onto $M_{h,1}$, $M_{h,2}$ and $M_{h,\gamma}$, respectively.

(P2) For any $(\boldsymbol{v}_1, \boldsymbol{v}_2, \boldsymbol{v}_\gamma) \in (H^1(\Omega_1))^2 \times (H^1(\Omega_2))^2 \times H^1(\gamma)$ and $(\mu_1, \mu_2, \mu_\gamma) \in L^2(\Omega_1) \times L^2(\Omega_2) \times L^2(\gamma)$,

$$\begin{aligned} &(\mathrm{div}(\boldsymbol{v}_i - \Pi_{h,i}\boldsymbol{v}_i), w_{h,i})_{\Omega_i} = 0, \ \forall\, w_{h,i} \in M_{h,i}, \quad (\mathrm{div}_\tau(\boldsymbol{v}_\gamma - \Pi_{h,\gamma}\boldsymbol{v}_\gamma), w_{h,\gamma})_\gamma = 0, \ \forall\, w_{h,\gamma} \in M_{h,\gamma}, \\ &(\mathrm{div}\ \boldsymbol{v}_{h,i}, P_{h,i}\mu_i - \mu_i)_{\Omega_i} = 0, \ \forall\, \boldsymbol{v}_{h,i} \in \boldsymbol{\Sigma}_{h,i}, \quad (\mathrm{div}_\tau \boldsymbol{v}_{h,\gamma}, P_{h,\gamma}\mu_\gamma - \mu_\gamma)_\gamma = 0, \ \forall\, \boldsymbol{v}_{h,\gamma} \in \boldsymbol{\Sigma}_{h,\gamma}. \end{aligned} \tag{4.20}$$

(P3) The following approximation properties hold:

$$\begin{aligned} &\|\boldsymbol{v}_i - \Pi_{h,i}\boldsymbol{v}_i\|_{0,\Omega_i} \le Ch\,\|\boldsymbol{v}_i\|_{1,\Omega_i}, \ \forall \boldsymbol{v}_i \in (H^1(\Omega_i))^2, \ \ \|\boldsymbol{v}_\gamma - \Pi_{h,\gamma}\boldsymbol{v}_\gamma\|_{0,\gamma} \le Ch\,\|\boldsymbol{v}_\gamma\|_{1,\gamma}, \ \forall \boldsymbol{v}_i \in H^1(\gamma), \\ &\|\mu_i - P_{h,i}\mu_i\|_{0,\Omega_i} \le Ch\,\|\mu_i\|_{1,\Omega_i}, \ \forall \mu_i \in L^2(\Omega_i), \ \ \|\mu_\gamma - P_{h,\gamma}\mu_\gamma\|_{0,\gamma} \le Ch\,\|\mu_\gamma\|_{1,\gamma}, \ \forall \mu_\gamma \in L^2(\gamma). \end{aligned} \tag{4.21}$$

(P4) For sufficiently smooth $\boldsymbol{v}_i \in (H^1(\Omega_i))^2$, we also have [41]

$$\|(\boldsymbol{v}_i - \Pi_{h,i}\boldsymbol{v}_i)\cdot \boldsymbol{n}_i\|_{0,\gamma} \le Ch\,\|\boldsymbol{v}_i \cdot \boldsymbol{n}_i\|_{1,\gamma}, i = 1, 2. \tag{4.22}$$

Finally, we define the following norms for any function g in $\mathcal{H}^k$ or $\boldsymbol{\mathcal{H}}^k$: $\|g\|_k^2 := \|g_1\|_{k,\Omega_1}^2 + \|g_2\|_{k,\Omega_2}^2 + \|g_\gamma\|_{k,\gamma}^2, \ k = 0, 1.$

4.2.1. Well-posedness analysis

Theorem 4.1. *For every $n \in \{1, \ldots, N\}$ and sufficiently small Δt and h, problem* (4.18) *has a unique solution.*

Proof. Since problem (4.18) is linear, it suffices to show its uniqueness. For this purpose, we consider the corresponding homogeneous system:

$$\begin{aligned}
&a(\boldsymbol{\varphi}_h^n, \boldsymbol{v}_h) - b(\boldsymbol{v}_h, c_h^n) - \widetilde{d}_{\boldsymbol{u}_h}((c_h^n, \theta_h^n), \boldsymbol{v}_h) + e(\boldsymbol{v}_h, c_h^n) + l(\theta_h^n, \boldsymbol{v}_h) = 0 \\
&r_\phi(\bar{\partial} c_h^n, \mu_h) + b(\boldsymbol{\varphi}_h^n, \mu_h) - e(\boldsymbol{\varphi}_h^n, \mu_h) = 0, \qquad (\mu_h, \boldsymbol{v}_h, \eta_h) \in M_h \times \widetilde{\boldsymbol{\Sigma}}_h \times \Theta_h^0, \\
&l(\eta_h, \boldsymbol{\varphi}_h^n) = 0,
\end{aligned} \tag{4.23}$$

for $n = 1, 2, \ldots, N$, given that the initial condition $\left(c_h^{n-1}, \boldsymbol{\varphi}_h^{n-1}, \theta_h^{n-1}\right)$ is zero. We show that the only solution $(c_h^n,\ \boldsymbol{\varphi}_h^n, \theta_h^n)$ to (4.23) is zero. Let $\mu_h = c_h^n$, $\boldsymbol{v}_h = \Delta t \boldsymbol{\varphi}_h^n$ and $\eta_h = (\eta_{h,1}, \eta_{h,2}, \eta_{h,\gamma})$ in (4.23) where, for $i = 1, 2$,

$$(\eta_{h,i})_{|E} = \begin{cases} -\Delta t \theta_{i,E}^n, & \text{on } E \in \mathcal{E}_{h,i}^I \\ 0, & \text{otherwise,} \end{cases}, \quad (\eta_{h,\gamma})_{|P} = \begin{cases} -\Delta t \theta_{\gamma,P}^n, & \text{at interior point } P, \\ 0, & \text{otherwise ,} \end{cases}$$

and adding the resulting equations, we obtain

$$r_\phi(c_h^n, c_h^n) + \Delta t a(\boldsymbol{\varphi}_h^n, \boldsymbol{\varphi}_h^n) = \Delta t \widetilde{d}_{\boldsymbol{u}_h}((c_h^n, \theta_h^n), \boldsymbol{\varphi}_h^n). \tag{4.24}$$

We next provide an estimate for the error $\|\theta_h^n\|_{0,E}$ on each edge $E \in \mathcal{E}_{h,i}$, $i = 1, 2$ by utilizing the technique in [12]. Fix $i \in \{1, 2\}$, for $K \in \mathcal{K}_{h,i}$, $E \subset \partial K$, let τ_E denote the unique element of $\widetilde{\boldsymbol{\Sigma}}_{h,i}$ with supp$(\tau_E) \subseteq K$ and

$$\tau_E \cdot \boldsymbol{n}_{E'} = \begin{cases} \theta_{i,E}^n, & \text{on } E = E', \\ 0, & \text{otherwise.} \end{cases}$$

Then, it follows from a scaling argument [12] that

$$h_K \|\tau_E\|_{1,K} + \|\tau_E\|_{0,K} \leq C h_K^{1/2} \left\|\theta_{h,i}^n\right\|_{0,E}. \tag{4.25}$$

By using $\boldsymbol{v}_h = (v_{h,1}, v_{h,2}, 0)$ where $v_{h,i} = \tau_E$, $v_{h,j} = 0,\ j = 3 - i$ as a test function in the first equation of (4.23), utilizing (4.25) and the weighted Cauchy-Schwarz inequality, we obtain

$$\|\theta_{h,i}\|_{0,E} \leq C \left(h_K^{1/2} \left\|\boldsymbol{\varphi}_{h,i}^n\right\|_{0,K} + h_K^{-1/2} \left\|c_{h,i}^n\right\|_{0,K} + h_K \sum_{E' \in \mathcal{E}(K)} \|\theta_{h,i}\|_{0,E'} \right). \tag{4.26}$$

Summing this estimate over all edges of K and pushing back the last term for h sufficiently small yields

$$\|\theta_{h,i}\|_{0,E} \leq C\left(h_K^{1/2}\left\|\boldsymbol{\varphi}_{h,i}^n\right\|_{0,K} + h_K^{-1/2}\left\|c_{h,i}^n\right\|_{0,K}\right). \tag{4.27}$$

Similarly, for the Lagrange multipliers on the fracture, we have

$$\left|(\theta_{h,\gamma})_{|P}\right| \leq C\left(h_E^{1/2}\left\|\boldsymbol{\varphi}_{h,\gamma}^n\right\|_{0,E} + h_E^{-1/2}\left\|c_{h,\gamma}^n\right\|_{0,E}\right). \tag{4.28}$$

By using (4.27) and Young's inequality, we have, for $i = 1, 2$,

$$\begin{aligned}
&\Delta t \sum_{K\in\mathcal{K}_{h,i}}\left(\sum_{\substack{E\subset\partial K\\ E\in\mathcal{E}_{h,i}\setminus\mathcal{E}_h^\gamma}} u_{i,KE}\mathcal{U}_{i,KE}(c_{i,K}^n,\theta_{i,K}^n)(\boldsymbol{D}_i^{-1}\boldsymbol{w}_{i,KE},\boldsymbol{\varphi}_{h,i}^n)_K + \sum_{\substack{E\subset\partial K\\ E\in\mathcal{E}_h^\gamma}} u_{i,KE}\mathcal{U}_{i,KE}^\gamma(c_{i,K}^n,c_{\gamma,E}^n)(\boldsymbol{D}_i^{-1}\boldsymbol{w}_{i,KE},\boldsymbol{\varphi}_{h,i}^n)_K\right)\\
&\leq C_i\Delta t\sum_{K\in\mathcal{K}_{h,i}}\left\|c_{h,i}^n\right\|_{0,K}\left\|\boldsymbol{\varphi}_{h,i}^n\right\|_{0,K} + C_i\Delta t\sum_{K\in\mathcal{K}_{h,i}}\sum_{\substack{E\subset\partial K\\ E\in\mathcal{E}_h^\gamma}}\left\|c_{h,\gamma}^n\right\|_{0,E}\left\|\boldsymbol{\varphi}_{h,i}^n\right\|_{0,K} + C_i\Delta t\sum_{K\in\mathcal{K}_{h,i}} h_K\left\|\boldsymbol{\varphi}_{h,i}^n\right\|_{0,K}^2\\
&\leq C_i\epsilon\left\|c_{h,i}^n\right\|_{0,\Omega_i}^2 + C_i\epsilon\left\|c_{h,\gamma}^n\right\|_{0,\gamma}^2 + C_i\frac{\Delta t^2}{4\epsilon}\left\|\boldsymbol{\varphi}_{h,i}^n\right\|_{0,\Omega_i}^2 + C_i\Delta t h_i\left\|\boldsymbol{\varphi}_{h,i}^n\right\|_{0,\Omega_i}^2.
\end{aligned} \tag{4.29}$$

Similarly, from (4.28) and Young's inequality, we have

$$\begin{aligned}
&\Delta t\sum_{E\in\mathcal{E}_h^\gamma}\sum_{P\in\partial E} u_{\gamma,EP}\mathcal{U}_{\gamma,EP}(c_{\gamma,E}^n,\theta_{\gamma,P}^n)(\boldsymbol{D}_\gamma^{-1}\boldsymbol{w}_{\gamma,EP},\boldsymbol{\varphi}_{h,\gamma}^n)_\gamma\\
&\qquad\leq C_\gamma\epsilon\left\|c_{h,\gamma}^n\right\|_{0,\gamma}^2 + C_\gamma\frac{\Delta t^2}{4\epsilon}\left\|\boldsymbol{\varphi}_{h,\gamma}^n\right\|_{0,\gamma}^2 + C_\gamma\Delta t h_\gamma\left\|\boldsymbol{\varphi}_{h,\gamma}^n\right\|_{0,\gamma}^2.
\end{aligned} \tag{4.30}$$

Altogether, we combine (4.24), (4.29), and (4.30) to find

$$r_\phi(c_h^n,c_h^n) + \Delta t a(\boldsymbol{\varphi}_h^n,\boldsymbol{\varphi}_h^n) \leq C\epsilon\left\|c_h^n\right\|_0^2 + \left(\frac{C\left(\Delta t\right)^2}{4\epsilon} + C\Delta t h\right)\left\|\boldsymbol{\varphi}_h^n\right\|_0^2, \tag{4.31}$$

where $C = \max\{C_1, C_2, C_\gamma\}$. To give a lower bound for the left-hand side of (4.31), we use the assumptions (A1) - (A2) to find

$$r_\phi(c_h^n,c_h^n) \geq \phi^-\left\|c_h^n\right\|_0^2, \quad a(\boldsymbol{\varphi}_h^n,\boldsymbol{\varphi}_h^n) \geq D_{\min}^-\left\|\boldsymbol{\varphi}_h^n\right\|_0^2, \tag{4.32}$$

where $D_{\min}^- = \min\{D^-,\ D_\gamma^-\}$. By substituting (4.32) into (4.31),we have

$$\phi^-\left\|c_h^n\right\|_0^2 + D_{\min}^-\Delta t\left\|\boldsymbol{\varphi}_h^n\right\|_0^2 \leq C\epsilon\left\|c_h^n\right\|_0^2 + \left(\frac{C\left(\Delta t\right)^2}{4\epsilon} + C\Delta t h\right)\left\|\boldsymbol{\varphi}_h^n\right\|_0^2. \tag{4.33}$$

By taking Δt, h and ϵ in (4.33) sufficiently small such that $\phi^- - C\epsilon > 0,\ \ D_{\min}^- - Ch - C\frac{\Delta t}{4\epsilon} > 0$, we have $c_h^n,\ \boldsymbol{\varphi}_h^n$ vanish. Then θ_h^n vanishes according to (4.27)-(4.28). □

4.2.2. A priori error estimates

We first state some preliminary lemmas: Lemma 4.1 is a direct consequence of the Bochner's inequality [37, Theorem 8, Appendix E.5], Lemma 4.2 is a discrete version of integration by parts, Lemma 4.3 demonstrates the discrete Gronwall's inequality, and Lemma 4.4 is a generalization of [26, Lemma 4.2] to the reduced fracture model of transport problems. We remark that the key result needed for our proof of error estimates is Lemma 4.4 which is used to control the advective terms. The proof of Lemma 4.4 relies on [12, Lemma 2.1] and can be found in Appendix A.

Lemma 4.1. *Let X be any Banach space with norm $\|\cdot\|_X$ and let $f : [0,T] \to X$ be a measurable mapping such that the mapping $t \mapsto \|f(t)\|_X$ is also measurable. Then, we have*

$$\left\| \int_0^T f(s)ds \right\|_X \leq \int_0^T \|f(s)\|_X \, ds. \tag{4.34}$$

Lemma 4.2. *[26, Lemma 4.3] Let $(a_n)_{n\in\mathbb{N}_0}$ and $(b_n)_{n\in\mathbb{N}_0}$ be real sequences. Then, for any $m \in \mathbb{N}_0$,*

$$\sum_{n=1}^{m}(a_n - a_{n-1})b_n = a_m b_m - a_0 b_0 - \sum_{n=1}^{m} a_{n-1}(b_n - b_{n-1}).$$

Lemma 4.3. *[100] Let $\tau > 0, B \geq 0$, and let $a_m, b_m, c_m, d_m, m \geq 0$, be non-negative sequences such that $a_0 \leq B$ and*

$$a_m + \tau \sum_{l=1}^{m} b_l \leq \tau \sum_{l=1}^{m-1} d_l a_l + \tau \sum_{l=1}^{m} c_l + B, \ m \geq 1.$$

Then

$$a_m + \tau \sum_{l=1}^{m} b_l \leq exp\left(\tau \sum_{l=1}^{m-1} d_l\right)\left(\tau \sum_{l=1}^{m} c_l + B\right), \ m \geq 1.$$

Lemma 4.4. *Assume that the solution $(c, \boldsymbol{\varphi})$ of* (4.5)-(4.6) *satisfies* $(A4)$. *Let $(c_h^n, \boldsymbol{\varphi}_h^n, \theta_h^n) \in M_h \times \widetilde{\boldsymbol{\Sigma}}_h \times \Theta_h$ be the solution of* (4.18). *Then, for h sufficiently small, there exists a constant $C > 0$, independent of n and h, such that*

$$\sum_{i=1}^{2}\sum_{K\in\mathcal{K}_{h,i}}\left(\sum_{\substack{E\subset\partial K\\ E\in\mathcal{E}_{h,i}\setminus\mathcal{E}_h^\gamma}}|E|^2(\theta_{i,E}^n-c_{i,K}^n)^2+\sum_{\substack{E\subset\partial K\\ E\in\mathcal{E}_h^\gamma}}|E|^2(c_{\gamma,E}^n-c_{i,K}^n)^2\right)+\sum_{E\in\mathcal{E}_h^\gamma}\sum_{P\in\partial E}(\theta_{\gamma,P}^n-c_{\gamma,E}^n)^2$$
$$\leq C\left(\|c^n-c_h^n\|_0^2+\|\boldsymbol{\varphi}^n-\boldsymbol{\varphi}_h^n\|_0^2+h^2\|\boldsymbol{u}c^n-\boldsymbol{u}_hc_h^n\|_0^2+h^2\|c^n\|_1^2\right). \tag{4.35}$$

We now state the first-order convergence in both space and time of the upwind-mixed hybrid algorithm (4.18). Unlike [26], here the reduced fracture model consists of an extra term representing the total normal flux across the fracture which may cause the loss in spatial accuracy if it is not treated carefully. In the following analysis, we eliminate that total normal flux term in the formulation by employing the orthogonality property of the L^2-projection $P_{h,\gamma}$ since with conforming spatial discretization, the traces on the fracture of the discrete normal fluxes belong to $M_{h,\gamma}$, the same space as the scalar variable in the fracture.

Theorem 4.2. *Assume that Δt and h are sufficiently small and the solution of problem* (4.5)-(4.6) *satisfies (A4). Let $(c_h^n,\boldsymbol{\varphi}_h^n,\theta_h^n)$ be the solution of problem* (4.18)*, then there exists a constant $C>0$ independent of Δt and h, such that*

$$\begin{aligned}&\max_{n=1,\dots,N}\|c(t^n)-c_h^n\|_0^2+\Delta t\sum_{n=1}^{N}\|\boldsymbol{\varphi}(t^n)-\boldsymbol{\varphi}_h^n\|_0^2\\&\quad\leq C\left(\|\partial_{tt}c\|_{L^2(0,T;\mathcal{H}^0)}^2\Delta t^2+\|c\|_{L^\infty(0,T;\mathcal{H}^0)}^2h^2+\|c\|_{L^\infty(0,T;\mathcal{H}^1)}^2h^2+\|\partial_tc\|_{L^2(0,T;\mathcal{H}^1)}^2h^2\right.\\&\qquad\left.+\|\boldsymbol{\varphi}\|_{L^\infty(0,T;\boldsymbol{\mathcal{H}}^1)}^2h^2+\sum_{i=1}^{2}\|\boldsymbol{\varphi}_i\cdot\boldsymbol{n}_i\|_{L^\infty(0,T;H^1(\gamma))}^2h^2\right).\end{aligned} \tag{4.36}$$

Proof. We first take $v_h\in\boldsymbol{\Sigma}_h$ in (4.18) and use the continuity of concentration across the interface to obtain

$$\begin{aligned}&a(\boldsymbol{\varphi}_h^n,\boldsymbol{v}_h)-b(\boldsymbol{v}_h,c_h^n)+e(\boldsymbol{v}_h,c_h^n)-\widetilde{d}_{\boldsymbol{u}_h}((c_h^n,\theta_h^n),\boldsymbol{v}_h)=0,\\&r_\phi(\bar{\partial}c_h^n,\mu_h)+b(\boldsymbol{\varphi}_h^n,\mu_h)-e(\boldsymbol{\varphi}_h^n,\mu_h)=L_{q^n}(\mu_h),\end{aligned}\qquad\forall(\mu_h,\boldsymbol{v}_h)\in M_h\times\boldsymbol{\Sigma}_h. \tag{4.37}$$

In (4.5), we take $t=t^n$ and $\boldsymbol{v}=\boldsymbol{v}_h\in\boldsymbol{\Sigma}_h$ and substract (4.37) from the resulting equations to have the following error equations

$$\begin{aligned}&a(\boldsymbol{\varphi}^n-\boldsymbol{\varphi}_h^n,\boldsymbol{v}_h)-b(\boldsymbol{v}_h,c^n-c_h^n)+e(\boldsymbol{v}_h,c^n-c_h^n)-d_{\boldsymbol{u}}(c^n,\boldsymbol{v}_h)+\widetilde{d}_{\boldsymbol{u}_h}((c_h^n,\theta_h^n),\boldsymbol{v}_h)=0,\\&r_\phi(\partial_tc^n-\bar{\partial}c_h^n,\mu_h)+b(\boldsymbol{\varphi}^n-\boldsymbol{\varphi}_h^n,\mu_h)-e(\boldsymbol{\varphi}^n-\boldsymbol{\varphi}_h^n,\mu_h)=0,\end{aligned}\qquad\forall(\mu_h,\boldsymbol{v}_h)\in M_h\times\boldsymbol{\Sigma}_h. \tag{4.38}$$

Let $\boldsymbol{v}_h=\Pi_h\boldsymbol{\varphi}^n-\boldsymbol{\varphi}_h^n$, $\mu_h=P_hc^n-c_h^n$ in (4.38), where $\Pi_h\boldsymbol{\varphi}=(\Pi_{h,1}\boldsymbol{\varphi}_1,\Pi_{h,2}\boldsymbol{\varphi}_2,\Pi_{h,\gamma}\boldsymbol{\varphi}_\gamma)$ and $P_hc=(P_{h,1}c_1,P_{h,2}c_2,P_{h,\gamma}c_\gamma)$, we have

$$
\begin{aligned}
&a(\boldsymbol{\varphi}^n-\boldsymbol{\varphi}_h^n,\Pi_h\boldsymbol{\varphi}^n-\boldsymbol{\varphi}_h^n)-b(\Pi_h\boldsymbol{\varphi}^n-\boldsymbol{\varphi}_h^n,c^n-c_h^n)+e(\Pi_h\boldsymbol{\varphi}^n-\boldsymbol{\varphi}_h^n,c^n-c_h^n)\\
&\qquad\qquad -d_{\boldsymbol{u}}(c^n,\Pi_h\boldsymbol{\varphi}^n-\boldsymbol{\varphi}_h^n)+\widetilde{d}_{\boldsymbol{u}_h}((c_h^n,\theta_h^n),\Pi_h\boldsymbol{\varphi}^n-\boldsymbol{\varphi}_h^n)=0,\\
&r_\phi(\partial_t c^n-\bar{\partial}c_h^n,P_hc^n-c_h^n)+b(\boldsymbol{\varphi}^n-\boldsymbol{\varphi}_h^n,P_hc^n-c_h^n)-e(\boldsymbol{\varphi}^n-\boldsymbol{\varphi}_h^n,P_hc^n-c_h^n)=0.
\end{aligned}
\tag{4.39}
$$

By adding both equations in (4.39) and using property (4.20) of the Raviart-Thomas projection operators, we find that

$$
\begin{aligned}
&a(\boldsymbol{\varphi}^n-\boldsymbol{\varphi}_h^n,\Pi_h\boldsymbol{\varphi}^n-\boldsymbol{\varphi}_h^n)+r_\phi(\partial_t c^n-\bar{\partial}c_h^n,P_hc^n-c_h^n)\\
&=d_{\boldsymbol{u}}(c^n,\Pi_h\boldsymbol{\varphi}^n-\boldsymbol{\varphi}_h^n)-\widetilde{d}_{\boldsymbol{u}_h}((c_h^n,\theta_h^n),\Pi_h\boldsymbol{\varphi}^n-\boldsymbol{\varphi}_h^n)-e(\Pi_h\boldsymbol{\varphi}^n-\boldsymbol{\varphi}_h^n,P_hc^n-c^n)\\
&\quad+e(\boldsymbol{\varphi}^n-\Pi_h\boldsymbol{\varphi}^n,P_hc^n-c_h^n).
\end{aligned}
\tag{4.40}
$$

Equivalently, (4.40) can be rewritten as

$$
\begin{aligned}
&a(\boldsymbol{\varphi}^n-\boldsymbol{\varphi}_h^n,\boldsymbol{\varphi}^n-\boldsymbol{\varphi}_h^n)+r_\phi(\bar{\partial}(c^n-c_h^n),c^n-c_h^n)\\
&=-a(\boldsymbol{\varphi}^n-\boldsymbol{\varphi}_h^n,\Pi_h\boldsymbol{\varphi}^n-\boldsymbol{\varphi}^n)-r_\phi(\partial_t c^n-\bar{\partial}c^n,P_hc^n-c^n)-r_\phi(\partial_t c^n-\bar{\partial}c^n,c^n-c_h^n)\\
&\quad-r_\phi(\bar{\partial}(c^n-c_h^n),P_hc^n-c^n)+d_{\boldsymbol{u}}(c^n,\Pi_h\boldsymbol{\varphi}^n-\boldsymbol{\varphi}_h^n)-d_{\boldsymbol{u}_h}(c_h^n,\Pi_h\boldsymbol{\varphi}^n-\boldsymbol{\varphi}_h^n)+d_{\boldsymbol{u}_h}(c_h^n,\Pi_h\boldsymbol{\varphi}^n-\boldsymbol{\varphi}_h^n)\\
&\quad-\widetilde{d}_{\boldsymbol{u}_h}((c_h^n,\theta_h^n),\Pi_h\boldsymbol{\varphi}^n-\boldsymbol{\varphi}_h^n)+e(\Pi_h\boldsymbol{\varphi}^n-\boldsymbol{\varphi}_h^n,P_hc^n-c^n)+e(\boldsymbol{\varphi}^n-\Pi_h\boldsymbol{\varphi}^n,P_hc^n-c_h^n).
\end{aligned}
\tag{4.41}
$$

Fix any $1\le m\le N$, by summing both sides of (4.41) from $n=1,\dots,m$, and multiplying by $2\Delta t$, we have

$$
2\Delta t\sum_{n=1}^{m}a(\boldsymbol{\varphi}^n-\boldsymbol{\varphi}_h^n,\boldsymbol{\varphi}^n-\boldsymbol{\varphi}_h^n)+2\Delta t\sum_{n=1}^{m}c_\phi(\bar{\partial}(c^n-c_h^n),c^n-c_h^n)=T_1+T_2+...T_7,
\tag{4.42}
$$

where

$$
\begin{aligned}
&T_1=-2\Delta t\sum_{n=1}^{m}a(\boldsymbol{\varphi}^n-\boldsymbol{\varphi}_h^n,\Pi_h\boldsymbol{\varphi}^n-\boldsymbol{\varphi}^n),\quad T_2=-2\Delta t\sum_{n=1}^{m}r_\phi(\partial_t c^n-\bar{\partial}c^n,P_hc^n-c^n),\\
&T_3=-2\Delta t\sum_{n=1}^{m}r_\phi(\partial_t c^n-\bar{\partial}c^n,c^n-c_h^n),\quad T_4=-2\Delta t\sum_{n=1}^{m}r_\phi(\bar{\partial}(c^n-c_h^n),P_hc^n-c^n),\\
&T_5=2\Delta t\sum_{n=1}^{m}d_{\boldsymbol{u}}(c^n,\Pi_h\boldsymbol{\varphi}^n-\boldsymbol{\varphi}_h^n)-2\Delta t\sum_{n=1}^{m}d_{\boldsymbol{u}_h}(c_h^n,\Pi_h\boldsymbol{\varphi}^n-\boldsymbol{\varphi}_h^n),\\
&T_6=2\Delta t\sum_{n=1}^{m}d_{\boldsymbol{u}_h}(c_h^n,\Pi_h\boldsymbol{\varphi}^n-\boldsymbol{\varphi}_h^n)-2\Delta t\sum_{n=1}^{m}\widetilde{d}_{\boldsymbol{u}_h}((c_h^n,\theta_h^n),\Pi_h\boldsymbol{\varphi}^n-\boldsymbol{\varphi}_h^n),\\
&T_7=2\Delta t\sum_{n=1}^{m}e(\Pi_h\boldsymbol{\varphi}^n-\boldsymbol{\varphi}_h^n,P_hc^n-c^n)+2\Delta t\sum_{n=1}^{m}e(\boldsymbol{\varphi}^n-\Pi_h\boldsymbol{\varphi}^n,P_hc^n-c_h^n).
\end{aligned}
$$

Our next step is to give an upper bound for each term $T_i, 1\le i\le 7$. By using the Cauchy-Schwarz inequality and Young's inequality, we first obtain

$$
\begin{aligned}
|T_1| &\le 2\Delta t \sum_{i=1}^{2}\sum_{n=1}^{m}\left|\left(\boldsymbol{D}_i^{-1}(\boldsymbol{\varphi}_i^n-\boldsymbol{\varphi}_{h,i}^n),\Pi_{h,i}\boldsymbol{\varphi}_i^n-\boldsymbol{\varphi}_i^n\right)_{\Omega_i}\right| + 2\Delta t\sum_{n=1}^{m}\left|\left(\boldsymbol{D}_\gamma^{-1}(\boldsymbol{\varphi}_\gamma^n-\boldsymbol{\varphi}_{h,\gamma}^n),\Pi_{h,\gamma}\boldsymbol{\varphi}_\gamma^n-\boldsymbol{\varphi}_\gamma^n\right)_{\gamma}\right| \\
&\le 2\Delta t\sum_{i=1}^{2}\sum_{n=1}^{m}\left\|\boldsymbol{D}_i^{-1}\left(\boldsymbol{\varphi}_i^n-\boldsymbol{\varphi}_{h,i}^n\right)\right\|_{0,\Omega_i}\left\|\Pi_{h,i}\boldsymbol{\varphi}_i^n-\boldsymbol{\varphi}_i^n\right\|_{0,\Omega_i} + 2\Delta t\sum_{n=1}^{m}\left\|\boldsymbol{D}_\gamma^{-1}\left(\boldsymbol{\varphi}_\gamma^n-\boldsymbol{\varphi}_{h,\gamma}^n\right)\right\|_{0,\gamma}\left\|\Pi_{h,\gamma}\boldsymbol{\varphi}_\gamma^n-\boldsymbol{\varphi}_\gamma^n\right\|_{0,\gamma} \\
&\le D^+\Delta t\varepsilon\sum_{n=1}^{m}\left\|\boldsymbol{\varphi}_i^n-\boldsymbol{\varphi}_{h,i}^n\right\|_{0,\Omega_i}^2 + \frac{D^+\Delta t}{\varepsilon}\sum_{n=1}^{m}\left\|\Pi_{h,i}\boldsymbol{\varphi}_i^n-\boldsymbol{\varphi}_i^n\right\|_{0,\Omega_i}^2 + D_\gamma^+\Delta t\varepsilon\sum_{n=1}^{m}\left\|\boldsymbol{\varphi}_\gamma^n-\boldsymbol{\varphi}_{h,\gamma}^n\right\|_{0,\gamma}^2 \\
&\quad + \frac{D_\gamma^+\Delta t}{\varepsilon}\sum_{n=1}^{m}\left\|\Pi_{h,\gamma}\boldsymbol{\varphi}_\gamma^n-\boldsymbol{\varphi}_\gamma^n\right\|_{0,\gamma}^2 \\
&\le C_1\Delta t\varepsilon\sum_{n=1}^{m}\left\|\boldsymbol{\varphi}^n-\boldsymbol{\varphi}_h^n\right\|_0 + \frac{C_1\Delta t}{\varepsilon}\sum_{n=1}^{m}\left\|\Pi_h\boldsymbol{\varphi}^n-\boldsymbol{\varphi}^n\right\|_0^2.
\end{aligned}
\tag{4.43}
$$

where $C_1=\max\{D^+,\ D_\gamma^+\}$. It follows from the Cauchy-Schwarz inequality, Bochner's inequality (4.34) and the regularity of c that

$$
\begin{aligned}
|T_2| &\le \Delta t\sum_{n=1}^{m}\left\|\partial_t c^n-\frac{c^n-c^{n-1}}{\Delta t}\right\|_0^2 + \Delta t\sum_{n=1}^{m}\left\|P_hc^n-c^n\right\|_0^2 \\
&\le \sum_{n=1}^{m}\frac{1}{\Delta t}\left\|\Delta t\partial_t c^n-c^n-c^{n-1}\right\|_0^2 + \Delta t\sum_{n=1}^{m}\left\|P_hc^n-c^n\right\|_0^2 \\
&\le \sum_{n=1}^{m}\frac{1}{\Delta t}\left\|\int_{t^{n-1}}^{t^n}\int_s^{t^n}\partial_{tt}c(\eta)d\eta ds\right\|_0^2 + \Delta t\sum_{n=1}^{m}\left\|P_hc^n-c^n\right\|_0^2 \\
&\le (\Delta t)^2\sum_{n=1}^{m}\int_{t^{n-1}}^{t^n}\left\|\partial_{tt}c(\eta)\right\|_0^2 d\eta + \Delta t\sum_{n=1}^{m}\left\|P_hc^n-c^n\right\|_0^2 \\
&\le \left\|\partial_{tt}c\right\|_{L^2(0,T;\mathcal{H}^0)}^2(\Delta t)^2 + \Delta t\sum_{n=1}^{m}\left\|P_hc^n-c^n\right\|_0^2.
\end{aligned}
\tag{4.44}
$$

Similarly, we obtain the following upper bound for T_3:

$$
|T_3| \le \Delta t\sum_{n=1}^{m}\left\|\partial_t c^n-\frac{c^n-c^{n-1}}{\Delta t}\right\|_0^2 + \Delta t\sum_{n=1}^{m}\left\|c^n-c^n\right\|_0^2 \le \left\|\partial_{tt}c\right\|_{L^2(0,T;\mathcal{H}^0)}^2(\Delta t)^2 + \Delta t\sum_{n=1}^{m}\left\|c^n-c_h^n\right\|_0^2.
\tag{4.45}
$$

To obtain an upper bound for the term T_4, we first use Lemma 4.3 and get

$$
\begin{aligned}
T_4 &= 2\sum_{n=1}^{m}c_\phi\left((c^n-c_h^n)-(c^{n-1}-c_h^{n-1}),P_hc^n-c^n\right) \\
&= 2c_\phi\left(c^m-c_h^m,P_hc^m-c^m\right) - 2c_\phi\left(c^0-c_h^0,P_hc^0-c^0\right) - 2\sum_{n=1}^{m}c_\phi\left(c^{n-1}-c_h^{n-1},(P_h-I)(c^n-c^{n-1})\right).
\end{aligned}
\tag{4.46}
$$

We then apply the Cauchy-Schwarz inequality, Bochner's inequality (4.34) and the regularity of c on the right-hand side of (4.46):

$$
\begin{aligned}
|T_4| &\le \varepsilon\left\|c^m-c_h^m\right\|_0^2 + \frac{1}{\varepsilon}\|P_hc^m-c^m\|_0^2 + C_4\left\|P_hc^0-c^0\right\|_0^2 + \Delta t\sum_{n=1}^{m-1}\left\|c^n-c_h^n\right\|_0^2 \\
&\quad + \frac{1}{\Delta t}\sum_{n=1}^{m}\left\|(P_h-I)(c^n-c^{n-1})\right\|_0^2 \\
&\le \varepsilon\left\|c^m-c_h^m\right\|_0^2 + \frac{h^2}{\varepsilon}\|c^m\|_1^2 + \Delta t\sum_{n=1}^{m-1}\left\|c^n-c_h^n\right\|_0^2 + C_4\left\|c^0\right\|_1^2h^2 + \left\|\partial_t c\right\|_{L^2(0,T;\mathcal{H}^1)}^2h^2.
\end{aligned}
\tag{4.47}
$$

For T_5, we decompose it into three subterms $T_{5,1}, T_{5,2}$ and $T_{5,\gamma}$, where

$$T_{5,i} = 2\Delta t \sum_{n=1}^{m} \left(\boldsymbol{D}_i^{-1}(\boldsymbol{u}_{h,i}c_{h,i}^n - \boldsymbol{u}_i c_i^n), \Pi_{h,i}\boldsymbol{\varphi}_i^n - \boldsymbol{\varphi}_i^n \right)_{\Omega_i} + 2\Delta t \sum_{n=1}^{m} \left(\boldsymbol{D}_i^{-1}(\boldsymbol{u}_{h,i}c_{h,i}^n - \boldsymbol{u}_i c_i^n), \boldsymbol{\varphi}_i^n - \boldsymbol{\varphi}_{h,i}^n \right)_{\Omega_i}, \ i = 1, 2,$$
$$T_{5,\gamma} = 2\Delta t \sum_{n=1}^{m} \left(\boldsymbol{D}_\gamma^{-1}(\boldsymbol{u}_{h,\gamma}c_{h,\gamma}^n - \boldsymbol{u}_\gamma c_\gamma^n), \ \Pi_{h,\gamma}\boldsymbol{\varphi}_\gamma^n - \boldsymbol{\varphi}_\gamma^n \right)_{\gamma} + 2\Delta t \sum_{n=1}^{m} \left(\boldsymbol{D}_\gamma^{-1}(\boldsymbol{u}_{h,\gamma}c_{h,\gamma}^n - \boldsymbol{u}_\gamma c_\gamma^n), \ \boldsymbol{\varphi}_\gamma^n - \boldsymbol{\varphi}_{h,\gamma}^n \right)_{\gamma}.$$

By using the Cauchy-Schwarz inequality, Young's inequality and the $L^\infty-$approximation properties of $\Pi_{h,i}, i = 1, 2$ [36], we have

$$\begin{aligned}
2\Delta t \sum_{n=1}^{m} \left| \left(\boldsymbol{D}_i^{-1}(\boldsymbol{u}_{h,i}c_{h,i}^n - \boldsymbol{u}_i c_i^n), \Pi_{h,i}\boldsymbol{\varphi}_i^n - \boldsymbol{\varphi}_i^n \right)_{\Omega_i} \right| &\leq 2\Delta t \sum_{n=1}^{m} \left\| \boldsymbol{D}_i^{-1}(\boldsymbol{u}_{h,i}c_{h,i}^n - \boldsymbol{u}_i c_i^n) \right\|_{0,\Omega_i} \|\Pi_{h,i}\boldsymbol{\varphi}_i^n - \boldsymbol{\varphi}_i^n\|_{0,\Omega_i} \\
&\leq 2\Delta t \sum_{n=1}^{m} \left(\left\| \boldsymbol{D}_i^{-1}\boldsymbol{u}_{h,i}(c_{h,i}^n - c_i^n) \right\|_{0,\Omega_i} \|\Pi_{h,i}\boldsymbol{\varphi}_i^n - \boldsymbol{\varphi}_i^n\|_{0,\Omega_i} + \left\| \boldsymbol{D}_i^{-1}(\boldsymbol{u}_{h,i} - \boldsymbol{u}_i)c_i^n \right\|_{0,\Omega_i} \|\Pi_{h,i}\boldsymbol{\varphi}_i^n - \boldsymbol{\varphi}_i^n\|_{0,\Omega_i} \right) \\
&\leq C_5\Delta t \sum_{n=1}^{m} \left\| c_{h,i}^n - c_i^n \right\|_{0,\Omega_i}^2 + C_5\Delta t h^2 \sum_{n=1}^{m} \|c_i^n\|_{0,\Omega_i}^2 + C_5\Delta t \sum_{n=1}^{m} \|\Pi_{h,i}\boldsymbol{\varphi}_i^n - \boldsymbol{\varphi}_i^n\|_{0,\Omega_i}^2 .
\end{aligned} \tag{4.48}$$

Similarly,

$$\begin{aligned}
&2\Delta t \sum_{n=1}^{m} \left| \left(\boldsymbol{D}_\gamma^{-1}(\boldsymbol{u}_{h,\gamma}c_{h,\gamma}^n - \boldsymbol{u}_\gamma c_\gamma^n), \ \Pi_{h,\gamma}\boldsymbol{\varphi}_\gamma^n - \boldsymbol{\varphi}_\gamma^n \right)_{\gamma} \right| \\
&\quad \leq C_5\Delta t \sum_{n=1}^{m} \left\| c_{h,\gamma}^n - c_\gamma^n \right\|_{0,\gamma}^2 + C_5\Delta t h^2 \sum_{n=1}^{m} \left\| c_\gamma^n \right\|_{0,\gamma}^2 + C_5\Delta t \sum_{n=1}^{m} \left\| \Pi_{h,\gamma}\boldsymbol{\varphi}_\gamma^n - \boldsymbol{\varphi}_\gamma^n \right\|_{0,\gamma}^2 .
\end{aligned} \tag{4.49}$$

By repeating the steps in (4.48) and (4.49) for the second terms of $T_{5,i}, \ i = 1, 2, \gamma$, we obtain the following upper bound for the term T_5:

$$\begin{aligned}
|T_5| \leq\ & C_5\Delta t \sum_{n=1}^{m} \|c^n - c_h^n\|_0^2 + C_5\Delta t h^2 \sum_{n=1}^{m} \|c^n\|_0^2 + C_5\Delta t \sum_{n=1}^{m} \|\Pi_h\boldsymbol{\varphi}^n - \boldsymbol{\varphi}^n\|_0^2 \\
&+ \frac{C_5\Delta t}{\varepsilon} \sum_{n=1}^{m} \|c^n - c_h^n\|_0^2 + \frac{C_5\Delta t h^2}{\varepsilon} \sum_{n=1}^{m} \|c^n\|_0^2 + C_5\varepsilon\Delta t \sum_{n=1}^{m} \|\boldsymbol{\varphi}^n - \boldsymbol{\varphi}_h^n\|_0^2 .
\end{aligned} \tag{4.50}$$

To handle T_6, we first perform the decomposition $T_6 = T_{6,1} + T_{6,2} + T_{6,\gamma}$, where

$$\begin{aligned}
T_{6,i} = 2\Delta t \sum_{n=1}^{m} \sum_{K \in \mathcal{K}_{h,i}} \Bigg(& \sum_{\substack{E \subset \partial K \\ E \in \mathcal{E}_{h,i} \backslash \mathcal{E}_h^\gamma}} u_{i,KE} \left(\mathcal{U}_{i,KE}(c_{i,K}^n, \theta_{i,E}^n) - c_{i,K}^n \right) \left(\boldsymbol{D}_i^{-1}\boldsymbol{w}_{i,KE}, \ \Pi_{h,i}\boldsymbol{\varphi}_i^n - \boldsymbol{\varphi}_{h,i}^n \right)_K \\
& + \sum_{\substack{E \subset \partial K \\ E \in \mathcal{E}_h^\gamma}} u_{i,KE} \left(\mathcal{U}_{i,KE}^\gamma(c_{i,K}^n, c_{\gamma,E}^n) - c_{i,K}^n \right) \left(\boldsymbol{D}_i^{-1}\boldsymbol{w}_{i,KE}, \ \Pi_{h,i}\boldsymbol{\varphi}_i^n - \boldsymbol{\varphi}_{h,i}^n \right)_K \Bigg), \ i = 1, 2, \\
T_{6,\gamma} = 2\Delta t \sum_{n=1}^{m} \sum_{E \in \mathcal{E}_h^\gamma} \sum_{P \in \partial E} & u_{\gamma,EP} \left(\mathcal{U}_{\gamma,EP}(c_{\gamma,E}^n, \theta_{\gamma,P}^n) - c_{\gamma,E}^n \right) \left(\boldsymbol{D}_\gamma^{-1}\boldsymbol{w}_{\gamma,EP}, \ \Pi_{h,\gamma}\boldsymbol{\varphi}_\gamma^n - \boldsymbol{\varphi}_{h,\gamma}^n \right)_{\gamma} .
\end{aligned}$$

Applying the Cauchy-Schwarz inequality, Young's inequality, and Lemma 4.4 yields

$$
\begin{aligned}
|T_6| \leq & \frac{C_6\Delta t}{\varepsilon}\sum_{n=1}^{m}\sum_{i=1}^{2}\sum_{K\in\mathcal{K}_{h,i}}\left(\sum_{\substack{E\subset\partial K\\ E\in\mathcal{E}_{h,i}\setminus\mathcal{E}_h^\gamma}}|E|^2(\theta_{i,E}^n-c_{i,K}^n)^2+\sum_{\substack{E\subset\partial K\\ E\in\mathcal{E}_h^\gamma}}|E|^2(c_{\gamma,E}^n-c_{i,K}^n)^2\right)\\
&+C_6\Delta t\varepsilon\sum_{n=1}^{m}\sum_{i=1}^{2}\left\|\Pi_{h,i}\boldsymbol{\varphi}_i^n-\boldsymbol{\varphi}_{h,i}^n\right\|_{0,\Omega_i}^2+\frac{C_6\Delta t}{\varepsilon}\sum_{n=1}^{m}\sum_{E\in\mathcal{E}_h^\gamma}\sum_{P\in\partial E}(\theta_{\gamma,P}^n-c_{\gamma,E}^n)^2\\
&+C_6\Delta t\varepsilon\sum_{n=1}^{m}\left\|\Pi_{h,\gamma}\boldsymbol{\varphi}_\gamma^n-\boldsymbol{\varphi}_{h,\gamma}^n\right\|_{0,\gamma}^2\\
\leq & \frac{C_6h^2\Delta t}{\varepsilon}\sum_{n=1}^{m}\|c^n\|_1^2+\frac{C_6h^4\Delta t}{\varepsilon}\sum_{n=1}^{m}\|c^n\|_0^2+C_6\varepsilon\Delta t\sum_{n=1}^{m}\|\Pi_h\boldsymbol{\varphi}^n-\boldsymbol{\varphi}^n\|_0^2\\
&+\frac{C_6\Delta t}{\varepsilon}\left(1+h^2\right)\sum_{n=1}^{m}\|c^n-c_h^n\|_0^2+C_6\left(\frac{h^2}{\varepsilon}+\varepsilon\right)\Delta t\sum_{n=1}^{m}\|\boldsymbol{\varphi}^n-\boldsymbol{\varphi}_h^n\|_0^2.
\end{aligned}
\tag{4.51}
$$

By collecting the estimates (4.43)-(4.51) and plugging them in the right-hand side of (4.42), then using the L^2-approximation properties (4.21), we deduce that

$$
\begin{aligned}
&2\Delta t\sum_{n=1}^{m}a(\boldsymbol{\varphi}^n-\boldsymbol{\varphi}_h^n,\boldsymbol{\varphi}^n-\boldsymbol{\varphi}_h^n)+2\Delta t\sum_{n=1}^{m}c_\phi(\bar\partial(c^n-c_h^n),c^n-c_h^n)\\
&\leq\left(C_1\varepsilon+C_5\varepsilon+C_6\left(\frac{h^2}{\varepsilon}+\varepsilon\right)\right)\Delta t\sum_{n=1}^{m}\|\boldsymbol{\varphi}^n-\boldsymbol{\varphi}_h^n\|_0^2+\varepsilon\|c^m-c_h^m\|_0^2\\
&\quad+\left(2+C_5+\frac{C_5}{\varepsilon}+\frac{C_6}{\varepsilon}\left(1+h^2\right)\right)\Delta t\sum_{n=1}^{m}\|c^n-c_h^n\|+\frac{h^2}{\varepsilon}\|c^m\|_1^2+C_4h^2\left\|c^0\right\|_1^2\\
&\quad+\left(C_5+\frac{C_5}{\varepsilon}+\frac{C_6h^2}{\varepsilon}\right)h^2\Delta t\sum_{n=1}^{m}\|c^n\|_0^2+\left(\frac{C_1}{\varepsilon}+C_5+C_6\varepsilon\right)h^2\Delta t\sum_{n=1}^{m}\|\boldsymbol{\varphi}^n\|_1^2\\
&\quad+\left(\frac{C_6}{\varepsilon}+1\right)h^2\Delta t\sum_{n=1}^{m}\|c^n\|_1^2+\|\partial_t c\|_{L^2(0,T;\mathcal{H}^1)}^2h^2+\|\partial_{tt}c\|_{L^2(0,T;\mathcal{H}^0)}^2(\Delta t)^2+|T_7|.
\end{aligned}
\tag{4.52}
$$

For the left-hand side of (4.52), by using assumptions $(\mathrm{A1})-(\mathrm{A2})$ and Lemma 4.2, we have

$$
\begin{aligned}
&2\Delta t\sum_{n=1}^{m}a(\boldsymbol{\varphi}^n-\boldsymbol{\varphi}_h^n,\boldsymbol{\varphi}^n-\boldsymbol{\varphi}_h^n)+2\Delta t\sum_{n=1}^{m}c_\phi(\bar\partial(c^n-c_h^n),c^n-c_h^n)\\
&\qquad\geq 2D_{\min}^-\Delta t\sum_{n=1}^{m}\|\boldsymbol{\varphi}^n-\boldsymbol{\varphi}_h^n\|_0^2+\phi^-\|c^m-c_h^m\|_0^2-\phi^+\left\|c^0-c_h^0\right\|_0^2.
\end{aligned}
\tag{4.53}
$$

From (4.52)-(4.53) and (4.21), it is implied that

$$
\begin{aligned}
&2D_{\min}^-\Delta t\sum_{n=1}^{m}\|\boldsymbol{\varphi}^n-\boldsymbol{\varphi}_h^n\|_0^2+\phi^-\|c^m-c_h^m\|_0^2\\
&\leq\left(C_1\varepsilon+C_5\varepsilon+C_6\left(\frac{h^2}{\varepsilon}+\varepsilon\right)\right)\Delta t\sum_{n=1}^{m}\|\boldsymbol{\varphi}^n-\boldsymbol{\varphi}_h^n\|_0^2+\varepsilon\|c^m-c_h^m\|_0^2\\
&\quad+\left(2+C_5+\frac{C_5}{\varepsilon}+\frac{C_6}{\varepsilon}\left(1+h^2\right)\right)\Delta t\sum_{n=1}^{m}\|c^n-c_h^n\|_0^2+\frac{h^2}{\varepsilon}\|c^m\|_1^2+(C_4+\phi^+)h^2\left\|c^0\right\|_1^2\\
&\quad+\left(C_5+\frac{C_5}{\varepsilon}+\frac{C_6h^2}{\varepsilon}\right)h^2\Delta t\sum_{n=1}^{m}\|c^n\|_0^2+\left(\frac{C_1}{\varepsilon}+C_5+C_6\varepsilon\right)h^2\Delta t\sum_{n=1}^{m}\|\boldsymbol{\varphi}^n\|_1^2\\
&\quad+\left(\frac{C_6}{\varepsilon_6}+1\right)h^2\Delta t\sum_{n=1}^{m}\|c^n\|_1^2+\|\partial_t c\|_{L^2(0,T;\mathcal{H}^1)}^2h^2+\|\partial_{tt}c\|_{L^2(0,T;\mathcal{H}^0)}^2(\Delta t)^2+|T_7|.
\end{aligned}
\tag{4.54}
$$

For the last term T_7, we recall that

$$\begin{aligned} T_7 = 2\Delta t \sum_{n=1}^{m}\sum_{i=1}^{2} \left(\left(\Pi_{h,i}\boldsymbol{\varphi}_i^n - \boldsymbol{\varphi}_{h,i}^n\right)\cdot \boldsymbol{n}_{i|\gamma}, P_{h,\gamma}c_\gamma^n - c_\gamma^n \right)_\gamma \\ -2\Delta t \sum_{n=1}^{m}\sum_{i=1}^{2} \left(\left(\Pi_{h,i}\boldsymbol{\varphi}_i^n - \boldsymbol{\varphi}_i^n\right)\cdot \boldsymbol{n}_{i|\gamma}, P_{h,\gamma}c_\gamma^n - c_{h,\gamma}^n \right)_\gamma . \end{aligned} \tag{4.55}$$

It follows from [23, Proposition 3.2] that for any local lowest-order Raviart-Thomas mixed finite element space $\boldsymbol{\Sigma}_K$ in which K is a triangle, the traces on ∂K of the normal component of any function in $\boldsymbol{\Sigma}_K$ are constant. This result also holds true when K is a rectangle [23]. Therefore, for any $K \in \mathcal{K}_{h,i}, i = 1,2$, we have $\boldsymbol{\varphi}_{h,i}^n \cdot \boldsymbol{n}_{i|E}$ is constant for any $E \subset \partial K$. Moreover, since the spatial mesh grids on the two subdomains are conforming and match up on the fracture γ, we have $\boldsymbol{\varphi}_{h,i}^n \cdot \boldsymbol{n}_{i|E}$ is also constant for any $E \in \mathcal{E}_h^\gamma$. In other words, we have $\boldsymbol{\varphi}_{h,i}^n \cdot \boldsymbol{n}_{i|\gamma} \in M_{h,\gamma}$ for $i = 1,2$. Similarly, we have $\Pi_{h,i}\boldsymbol{\varphi}_i^n \cdot \boldsymbol{n}_{i|\gamma} \in M_{h,\gamma}$ for $i = 1,2$. Therefore, the first term in (4.55) vanishes due to the orthogonality property of the L^2-projection operator $P_{h,\gamma}$. By using the approximation property (4.22) and Young's inequality, we have

$$\begin{aligned} |T_7| &\le \sum_{i=1}^{2}\Delta t \sum_{n=1}^{m}\left(\frac{1}{\varepsilon}\left\|(\Pi_{h,i}\boldsymbol{\varphi}_i^n - \boldsymbol{\varphi}_i^n)\cdot\boldsymbol{n}_{i|\gamma}\right\|_{0,\gamma}^2 + \varepsilon \left\|P_{h,\gamma}c_\gamma^n - c_{h,\gamma}^n\right\|_{0,\gamma}^2 \right) \\ &\le \frac{C_7 h^2}{\varepsilon}\sum_{i=1}^{2}\sum_{n=1}^{m}\left\|\boldsymbol{\varphi}_i^n\cdot\boldsymbol{n}_{i|\gamma}\right\|_{1,\gamma}^2 + \Delta t\varepsilon\sum_{n=1}^{m}\left\|P_{h,\gamma}c_\gamma^n - c_\gamma^n\right\|_{0,\gamma}^2 + \Delta t\varepsilon\sum_{n=1}^{m}\left\|c_\gamma^n - c_{h,\gamma}^n\right\|_{0,\gamma}^2 \\ &\le \frac{C_7 h^2}{\varepsilon}\sum_{i=1}^{2}\sum_{n=1}^{m}\left\|\boldsymbol{\varphi}_i^n\cdot\boldsymbol{n}_{i|\gamma}\right\|_{1,\gamma}^2 + C_7\varepsilon h^2\sum_{n=1}^{m}\|c_h^n\|_{1,\gamma}^2 + \Delta t\varepsilon\sum_{n=1}^{m}\left\|c_\gamma^n - c_{h,\gamma}^n\right\|_{0,\gamma}^2. \end{aligned} \tag{4.56}$$

It follows from (4.54) and (4.56) that

$$\begin{aligned} &2D_{\min}^- \Delta t\sum_{n=1}^{m}\|\boldsymbol{\varphi}^n - \boldsymbol{\varphi}_h^n\|_0^2 + \phi^-\|c^m - c_h^m\|_0^2 \\ &\le \left(C_1\varepsilon + C_5\varepsilon + C_6\left(\frac{h^2}{\varepsilon}+\varepsilon\right)\right)\Delta t\sum_{n=1}^{m}\|\boldsymbol{\varphi}^n - \boldsymbol{\varphi}_h^n\|_0^2 + \varepsilon\|c^m - c_h^m\|_0^2 + \frac{h^2}{\varepsilon}\|c^m\|_1^2 \\ &\quad +(C_4+\phi^+)h^2\left\|c^0\right\|_1^2 + \left(2 + C_5 + \frac{C_5}{\varepsilon} + \frac{C_6}{\varepsilon}\left(1+h^2\right)\right)\Delta t\sum_{n=1}^{m}\|c^n - c_h^n\|_0^2 \\ &\quad + \left(C_5 + \frac{C_5}{\varepsilon} + \frac{C_6 h^2}{\varepsilon}\right)h^2\Delta t\sum_{n=1}^{m}\|c^n\|_0^2 + \left(\frac{C_1}{\varepsilon} + C_5 + C_6\varepsilon\right)h^2\Delta t\sum_{n=1}^{m}\|\boldsymbol{\varphi}^n\|_1^2 \\ &\quad + \left(\frac{C_6}{\varepsilon} + 1 + C_7\varepsilon\right)h^2\Delta t\sum_{n=1}^{m}\|c^n\|_1^2 + \|\partial_t c\|_{L^2(0,T;\mathcal{H}^1)}^2 h^2 \\ &\quad + \|\partial_{tt}c\|_{L^2(0,T;\mathcal{H}^0)}^2 (\Delta t)^2 + \frac{C_7 h^2\Delta t}{\varepsilon}\sum_{i=1}^{2}\sum_{n=1}^{m}\left\|\boldsymbol{\varphi}_i^n\cdot\boldsymbol{n}_{i|\gamma}\right\|_{1,\gamma}^2 . \end{aligned} \tag{4.57}$$

In (4.57), we fix ε small enough such that $\phi^- - \varepsilon > 0, \;\; 2 - (C_1 + C_5 + C_6)\varepsilon > 0$, then choose Δt and h sufficiently small to find

$$
\begin{aligned}
&\Delta t \sum_{n=1}^{m} \|\boldsymbol{\varphi}^n - \boldsymbol{\varphi}_h^n\|_0^2 + \|c^m - c_h^m\|_0^2 \\
&\leq C\Delta t \sum_{n=1}^{m-1} \|c^n - c_h^n\|_0^2 + Ch^2\Delta t \sum_{n=1}^{m} \|c^n\|_0^2 + Ch^2\Delta t \sum_{n=1}^{m} \|\boldsymbol{\varphi}^n\|_1^2 + Ch^2\Delta t \sum_{n=1}^{m} \|c^n\|_1^2 + Ch^2 \|c^m\|_1^2 \\
&+Ch^2 \left\|c^0\right\|_1^2 + Ch^2\Delta t \sum_{i=1}^{2}\sum_{n=1}^{m} \left\|\boldsymbol{\varphi}_i^n \cdot \boldsymbol{n}_{i|\gamma}\right\|_{1,\gamma}^2 + \|\partial_t c\|_{L^2(0,T;\mathcal{H}^1)}^2 h^2 + \|\partial_{tt} c\|_{L^2(0,T;\mathcal{H}^0)}^2 (\Delta t)^2 \\
&\leq C\Delta t \sum_{n=1}^{m-1} \|c^n - c_h^n\|_0^2 + C\left(\|c\|_{L^\infty(0,T;\mathcal{H}^0)}^2 h^2 + \|\boldsymbol{\varphi}\|_{L^\infty(0,T;\boldsymbol{\mathcal{H}}^1)}^2 h^2 + \|c\|_{L^\infty(0,T;\mathcal{H}^1)}^2 h^2\right. \\
&\left. + \sum_{i=1}^{2} \left\|\boldsymbol{\varphi}_i \cdot \boldsymbol{n}_{i|\gamma}\right\|_{L^\infty(0,T;H^1(\gamma))h^2}^2 + \|\partial_t c\|_{L^2(0,T;\mathcal{H}^1)}^2 h^2 + \|\partial_{tt} c\|_{L^2(0,T;\mathcal{H}^0)}^2 (\Delta t)^2\right).
\end{aligned}
\tag{4.58}
$$

Let B be the term in the bracket in the last inequality of (4.58). By applying Lemma 4.3 in (4.58) with $a_m = \|c^m - c_h^m\|_0^2$, $b_m = \|\boldsymbol{\varphi}^m - \boldsymbol{\varphi}_h^m\|_0^2$, $c_m = 0$, $d_m = 1$, we obtain

$$
\|c^m - c_h^m\|_0^2 + \Delta t \sum_{n=1}^{m} \|\boldsymbol{\varphi}^n - \boldsymbol{\varphi}_h^n\|_0^2 \leq \exp\left(\Delta t(m-1)\right) B \leq \exp\left(\Delta t N\right) B \leq \exp(T) B \leq CB.
\tag{4.59}
$$

Since (4.59) holds for any $1 \leq m \leq N$, we obtain (4.36). □

Remark 4.3. *The proof of Theorem 4.2 relies on Lemma 4.4 to bound the advection terms* $T_{6,i},\ i = 1, 2, \gamma$, *which involve the upwind operators and Lagrange multipliers arising from the hybridization. For simplicity of presentation, we have considered only the lowest order Raviart-Thomas* RT_0 *space on rectangular grids. The results are also valid for any two-dimensional* RT_k *spaces of arbitrary order* k *by invoking [12, Lemma 2.1] if* k *is even (cf.* (A.4)- (A.7) *in Appendix A) or using the arguments* $(3.25) - (3.32)$ *in [23, pp. 189-190] if* k *is odd. Extension to other mixed finite element spaces such as* BDM_k *and* $BDFM_k$ *[23] can be obtained by using the results in [22, 24, 25] which are analogous to [12, Lemma 2.1] and valid for both two- and three-dimensional cases.*

The upwind-mixed scheme (4.18) can be solved directly to find an approximate solution to (4.5)-(4.6). However, as $\boldsymbol{D}_f \gg \boldsymbol{D}_i, i = 1, 2$, it would be more efficient to have a smaller time step on the fracture than on the subdomains. In the next section, we use global-in-time non-overlapping DD [68, 68, 67, 66, 65, 70, 72] to decouple (4.18) and enforce local time-stepping.

4.3. Fully-discrete, global-in-time nonoverlapping domain decomposition methods

We first decompose (4.18) into local problems on the subdomains:

For $i=1,2$, and for $n=1,\ldots,N$, find $(c_{h,i}^n,\boldsymbol{\varphi}_{h,i}^n,\theta_{h,i}^n)\in M_{h,i}\times\widetilde{\boldsymbol{\Sigma}}_{h,i}\times\Theta_{h,i}$ such that

$$
\begin{aligned}
\Big(\boldsymbol{D}_i^{-1}\boldsymbol{\varphi}_{h,i}^n,\boldsymbol{v}_{h,i}\Big)_{\Omega_i}-\Big(\text{div }\boldsymbol{v}_{h,i},c_{h,i}^n\Big)_{\Omega_i}-\sum_{K\in\mathcal{K}_{h,i}}\Bigg(\sum_{\substack{E\subset\partial K\\ E\in\mathcal{E}_{h,i}\setminus\mathcal{E}_h^\gamma}}u_{i,KE}\mathcal{U}_{i,KE}(c_{i,K}^n,\theta_{i,E}^n)(\boldsymbol{D}_i^{-1}\boldsymbol{w}_{i,KE},\boldsymbol{v}_{h,i})_K\\
+\sum_{\substack{E\subset\partial K\\ E\in\mathcal{E}_h^\gamma}}u_{i,KE}\mathcal{U}_{i,KE}^\gamma(c_{i,K}^n,(c_{h,i}^n)_{|E})(\boldsymbol{D}_i^{-1}\boldsymbol{w}_{i,KE},\boldsymbol{v}_{h,i})_K\Bigg)+\Big\langle\boldsymbol{v}_{h,i}\cdot\boldsymbol{n}_{i|\gamma},(c_{h,i}^n)_{|\gamma}\Big\rangle_\gamma\\
+\sum_{K\in\mathcal{K}_{h,i}}\sum_{\substack{E\subset\partial K\\ E\in\mathcal{E}_{h,i}\setminus\mathcal{E}_h^\gamma}}\Big\langle\theta_{h,i}^n,\boldsymbol{v}_{h,i}\cdot\boldsymbol{n}_K\Big\rangle_E=0,\quad\forall\boldsymbol{v}_{h,i}\in\widetilde{\boldsymbol{\Sigma}}_{h,i},\\
\Big(\phi_i\bar{\partial}c_{h,i}^n,\mu_{h,i}\Big)_{\Omega_i}+\Big(\text{div }\boldsymbol{\varphi}_{h,i}^n,\mu_{h,i}\Big)_{\Omega_i}=(q_i^n,\mu_{h,i})_{\Omega_i},\quad\forall\mu_{h,i}\in M_{h,i},\\
\sum_{K\in\mathcal{K}_{h,i}}\sum_{\substack{E\subset\partial K\\ E\in\mathcal{E}_{h,i}\setminus\mathcal{E}_h^\gamma}}\Big\langle\eta_{h,i},\boldsymbol{\varphi}_{h,i}^n\cdot\boldsymbol{n}_K\Big\rangle_E=0,\ \forall\eta_{h,i}\in\Theta_{h,i}^0,
\end{aligned}
\tag{4.60}
$$

where the initial data $c_{h,i}^0$ is given by (4.19). Moreover, to recover the solution of (4.18), the solutions of (4.60) are required to satisfy the following transmission conditions across the space-time interface $\gamma\times(0,T)$: for $n=1,\ldots,N$,

$$
\int_E c_{h,i}^n=\int_E c_{h,\gamma}^n,\ \forall E\in\mathcal{E}_h^\gamma,
\tag{4.61}
$$

$$
\begin{aligned}
\Big(\boldsymbol{D}_\gamma^{-1}\boldsymbol{\varphi}_{h,\gamma}^n,\boldsymbol{v}_{h,\gamma}\Big)_\gamma-\Big(\text{div}_\tau\boldsymbol{v}_{h,\gamma},c_{h,\gamma}^n\Big)_\gamma-\sum_{E\in\mathcal{E}_h^\gamma}\sum_{P\in\partial E}u_{\gamma,EP}\mathcal{U}_{\gamma,EP}(c_{\gamma,E}^n,\theta_{\gamma,P}^n)(\boldsymbol{D}_\gamma^{-1}\boldsymbol{w}_{\gamma,EP},\boldsymbol{v}_{h,\gamma})_\gamma\\
+\sum_{E\in\mathcal{E}_h^\gamma}\Big\langle\theta_{h,\gamma}^n,\ \boldsymbol{v}_{h,\gamma}\cdot\boldsymbol{n}_{\partial E}\Big\rangle_{\partial E}=0,\quad\forall\boldsymbol{v}_{h,\gamma}\in\widetilde{\boldsymbol{\Sigma}}_{h,\gamma},\\
\Big(\phi_\gamma\bar{\partial}c_{h,\gamma}^n,\mu_{h,\gamma}\Big)_\gamma+\Big(\text{div}_\tau\boldsymbol{\varphi}_{h,\gamma}^n,\mu_{h,\gamma}\Big)_\gamma=\big(q_\gamma^n,\mu_{h,\gamma}\big)_\gamma+\sum_{i=1}^2\Big\langle\boldsymbol{\varphi}_{h,i}^n\cdot\boldsymbol{n}_{i|\gamma},\mu_{h,\gamma}\Big\rangle_\gamma,\ \forall\mu_{h,\gamma}\in M_{h,\gamma},\\
\sum_{E\in\mathcal{E}_h^\gamma}\Big\langle\eta_{h,\gamma},\ \boldsymbol{\varphi}_{h,\gamma}^n\cdot\boldsymbol{n}_{\partial E}\Big\rangle_{\partial E}=0,\quad\forall\eta_{h,\gamma}\in\Theta_{h,\gamma}.
\end{aligned}
\tag{4.62}
$$

Based on these transmission conditions, we develop two global-in-time DD methods: GTF-Schur and GTO-Schwarz. The former is derived using directly the equations (4.61)-(4.62), while the latter is constructed based on more general transmission conditions, namely Ventcel-to-Robin transmission conditions which will be derived in Subsection 4.3.2. For each method, a fully discrete interface system is formulated on the space-time fracture $\gamma\times(0,T)$ and is solved iteratively. Throughout this section for any mixed finite element space $\mathcal{O}_h$ defined in the previous section, we write $\varsigma_h:=(\varsigma_h^n)_{n=1}^N\in(\mathcal{O}_h)^N$.

4.3.1. Global-in-time fracture-based Schur method

The idea of GTF-Schur is to construct an interface operator which is close to the identity operator by making use of the presence of the fracture. In particular, the contribution of the traces on γ of the discrete normal fluxes from both subdomains is considered as the interface unknown, and is denoted by $\psi_{h,\gamma} = \left(\psi_{h,\gamma}^n\right)_{n=1}^N \in (M_{h,\gamma})^N$, where

$$\int_E \psi_{h,\gamma}^n := \int_E \sum_{i=1}^2 \boldsymbol{\varphi}_{h,i}^n \cdot \boldsymbol{n}_{i|\gamma}, \quad \text{for } n = 1, \dots N, \quad E \in \mathcal{E}^\gamma. \tag{4.63}$$

We also use (4.63) to write the discrete space-time interface system for GTF-Schur. For the pure diffusion problems, this approach has been shown to work effectively without the need of any preconditioner [70, 72]. To formulate the interface problem for GTF-Schur, we first introduce the solution operator $\mathcal{R}_\gamma$:

$$\begin{aligned} \mathcal{R}_\gamma : (M_{h,\gamma})^N \times L^2(0,T;L^2(\gamma)) \times H_0^1(\gamma) \quad &\longrightarrow \quad (M_{h,\gamma})^N \\ (\psi_{h,\gamma},\ q_\gamma,\ c_{0,\gamma}) \qquad\qquad\qquad\quad &\mapsto \quad c_{h,\gamma}, \end{aligned}$$

where $(c_{h,\gamma}, \boldsymbol{\varphi}_{h,\gamma}, \theta_{h,\gamma}) \in (M_{h,\gamma})^N \times \left(\widetilde{\boldsymbol{\Sigma}}_{h,\gamma}\right)^N \times (\Theta_{h,\gamma})^N$ is the solution to the following time-dependent problem on the fracture:

For $n = 1, \dots, N$, find $(c_{h,\gamma}^n, \boldsymbol{\varphi}_{h,\gamma}^n, \theta_{h,\gamma}^n) \in M_{h,\gamma} \times \widetilde{\boldsymbol{\Sigma}}_{h,\gamma} \times \Theta_{h,\gamma}$ such that

$$\begin{aligned} &\left(\boldsymbol{D}_\gamma^{-1}\boldsymbol{\varphi}_{h,\gamma}^n, \boldsymbol{v}_{h,\gamma}\right)_\gamma - \left(\mathrm{div}_\tau \boldsymbol{v}_{h,\gamma}, c_{h,\gamma}^n\right)_\gamma - \sum_{E\in\mathcal{E}_h^\gamma}\sum_{P\in\partial E} u_{\gamma,EP}\mathcal{U}_{\gamma,EP}(c_{\gamma,E}^n, \theta_{\gamma,P}^n)(\boldsymbol{D}_\gamma^{-1}\boldsymbol{w}_{\gamma,EP}, \boldsymbol{v}_{h,\gamma})_\gamma \\ &\qquad + \sum_{E\in\mathcal{E}_h^\gamma} \left\langle \theta_{h,\gamma}^n,\ \boldsymbol{v}_{h,\gamma}\cdot\boldsymbol{n}_{\partial E}\right\rangle_{\partial E} = 0,\ \forall \boldsymbol{v}_{h,\gamma} \in \widetilde{\boldsymbol{\Sigma}}_{h,\gamma}, \\ &\left(\phi_\gamma \bar{\partial} c_{h,\gamma}^n, \mu_{h,\gamma}\right)_\gamma + \left(\mathrm{div}_\tau \boldsymbol{\varphi}_{h,\gamma}^n, \mu_{h,\gamma}\right)_\gamma = \left(q_\gamma^n, \mu_{h,\gamma}\right)_\gamma + \left(\psi_{h,\gamma}^n, \mu_{h,\gamma}\right)_\gamma,\ \forall \mu_{h,\gamma} \in M_{h,\gamma}, \\ &\sum_{E\in\mathcal{E}_h^\gamma} \left\langle \eta_{h,\gamma},\ \boldsymbol{\varphi}_{h,\gamma}^n\cdot\boldsymbol{n}_{\partial E}\right\rangle_{\partial E} = 0,\ \forall \eta_{h,\gamma} \in \Theta_{h,\gamma}, \end{aligned} \tag{4.64}$$

where the initial data $c_{h,\gamma}^0$ is given by (4.19). To compute the right-hand side of (4.63), we define the space-time Dirichlet-to-Neumann operators $\mathcal{S}_i^{\mathrm{DtN}},\ i = 1, 2$:

$$\begin{aligned} \mathcal{S}_i^{\mathrm{DtN}} : \quad (M_{h,\gamma})^N \times L^2(0,T;L^2(\Omega_i)) \times H_*^1(\Omega_i) \quad &\longrightarrow \quad (M_{h,\gamma})^N \\ (\lambda_{h,\gamma},\ q_i,\ c_{0,i}) \qquad\qquad\qquad\quad &\mapsto \quad \left(\boldsymbol{\varphi}_{h,i}\cdot\boldsymbol{n}_i\right)_{|\gamma}, \end{aligned} \tag{4.65}$$

where $(c_{h,i}, \boldsymbol{\varphi}_{h,i}, \theta_{h,i}) \in (M_{h,i})^N \times \left(\widetilde{\boldsymbol{\Sigma}}_{h,i}\right)^N \times (\Theta_{h,i})^N$ is the solution of the local problem (4.60) with Dirichlet boundary conditions

$$(c_{h,i}^n)_{|\gamma} = \lambda_{h,\gamma}^n, \quad \text{for } n = 1, 2, \ldots, N. \tag{4.66}$$

Altogether, the fully-discrete interface problem for GTF-Schur is obtained by enforcing (4.63):

Find $\psi_{h,\gamma} \in (M_{h,\gamma})^N$ such that

$$\int_{t^{n-1}}^{t^n} \int_E \psi_{h,\gamma}\, d\gamma dt = \int_{t^{n-1}}^{t^n} \int_E \sum_{i=1}^{2} \mathcal{S}_i^{\text{DtN}}(\mathcal{R}_\gamma(\psi_{h,\gamma}, q_\gamma, c_{0,\gamma}), q_i, c_{0,i})\, d\gamma dt, \;\; \forall n = 1, \ldots, N, \; \forall E \in \mathcal{E}_h^\gamma,$$

or, equivalently, find $\psi_{h,\gamma} \in (M_{h,\gamma})^N$ such that

$$\mathcal{S}_{\text{F}} \psi_{h,\gamma} = \chi_{\text{F}}, \tag{4.67}$$

where

$$\mathcal{S}_{\text{F}} \psi_{h,\gamma} = \left(\int_{t^{n-1}}^{t^n} \int_E \psi_{h,\gamma}\, d\gamma dt - \int_{t^{n-1}}^{t^n} \int_E \sum_{i=1}^{2} \mathcal{S}_i^{\text{DtN}}(\mathcal{R}_\gamma(\psi_{h,\gamma}, 0, 0), 0, 0)\, d\gamma dt \right)_{n=1,\ldots,N,\; E \in \mathcal{E}_h^\gamma},$$

and

$$\chi_{\text{F}} = \left(\int_{t^{n-1}}^{t^n} \int_E \sum_{i=1}^{2} \mathcal{S}_i^{\text{DtN}}(\mathcal{R}_\gamma(0, q_\gamma, c_{0,\gamma}), q_i, c_{0,i})\, d\gamma dt \right)_{n=1,\ldots,N,\; E \in \mathcal{E}_h^\gamma}.$$

The interface problem (4.67) is then solved iteratively by using GMRES without applying any preconditioner.

4.3.2. Global-in-time Optimized Schwarz method

To derive the interface problem for GTO-Schwarz, we first transform the transmission conditions (4.61)-(4.62) into more general ones, namely Ventcel-to-Robin transmission conditions. For each $i = 1, 2$, let $c_{i,\gamma} = (c_{i,\gamma,E})_{E \in \mathcal{E}_h^\gamma} \in M_{h,\gamma}$ be the trace of $c_{h,i}$ on γ and $\theta_{i,\gamma} = (\theta_{i,\gamma,P})_{P \in \mathcal{P}_h^\gamma} \in \Theta_{h,\gamma}$ the Lagrange multipliers of $c_{i,\gamma}$ at the endpoints of each edge $E \in \mathcal{E}_h^\gamma$. We denote by $\boldsymbol{\varphi}_{\gamma,i}$ the tangential velocity associated with $c_{i,\gamma}$ through the second equation of (4.18). Due to the continuity of the concentration across the discrete counterpart of $\gamma \times (0, T)$, we have:

$$\boldsymbol{\varphi}_{\gamma,1}^n = \boldsymbol{\varphi}_{\gamma,2}^n = \boldsymbol{\varphi}_{h,\gamma}^n, \quad \text{for } n = 1, \ldots, N.$$

Under sufficient regularity, the transmission conditions (4.61)-(4.62) can be replaced by the following Ventcel-to-Robin transmission conditions: for $i = 1, 2$, $j = 3 - i$, and for $n = 1, \ldots, N$,

$$
\begin{aligned}
&\left(\boldsymbol{D}_\gamma^{-1}\boldsymbol{\varphi}_{\gamma,i}^n, \boldsymbol{v}_{h,\gamma}\right)_\gamma - \left(\mathrm{div}_\tau \boldsymbol{v}_{h,\gamma}, c_{i,\gamma}^n\right)_\gamma - \sum_{E\in\mathcal{E}_h^\gamma}\sum_{P\in\partial E} u_{\gamma,EP}\mathcal{U}_{\gamma,EP}(c_{\gamma,E}^n, \theta_{i,\gamma,P}^n)(\boldsymbol{D}_\gamma^{-1}\boldsymbol{w}_{\gamma,EP}, \boldsymbol{v}_{h,\gamma})_\gamma \\
&\qquad + \sum_{E\in\mathcal{E}_h^\gamma}\left\langle \theta_{i,\gamma}^n,\ \boldsymbol{v}_{h,\gamma}\cdot\boldsymbol{n}_{\partial E}\right\rangle_{\partial E} = 0,\ \forall \boldsymbol{v}_{h,\gamma} \in \widetilde{\boldsymbol{\Sigma}}_{h,\gamma}, \\
&\left(-\boldsymbol{\varphi}_{h,i}^n\cdot\boldsymbol{n}_{i|\gamma} + \alpha c_{i,\gamma}^n, \mu_{h,\gamma}\right)_\gamma + (\phi_\gamma \bar{\partial} c_{i,\gamma}^n, \mu_{h,\gamma})_\gamma + (\mathrm{div}_\tau \boldsymbol{\varphi}_{\gamma,i}^n, \mu_{h,\gamma})_\gamma \\
&\qquad = (q_\gamma, \mu_{h,\gamma})_\gamma + \left(\boldsymbol{\varphi}_{h,j}^n\cdot\boldsymbol{n}_{j|\gamma} + \alpha c_{j,\gamma}^n, \mu_{h,\gamma}\right)_\gamma,\ \forall \mu_{h,\gamma} \in M_{h,\gamma}, \\
&\sum_{E\in\mathcal{E}_h^\gamma}\left\langle \eta_{h,\gamma},\ \boldsymbol{\varphi}_{\gamma,i}^n\cdot\boldsymbol{n}_{\partial E}\right\rangle_{\partial E} = 0,\ \forall \eta_{h,\gamma} \in \Theta_{h,\gamma},
\end{aligned}
\tag{4.68}
$$

where $\alpha > 0$. We denote by $\zeta_{h,i} = \left(\zeta_{h,i}^n\right)_{n=1}^N \in \left(M_{h,\gamma}\right)^N$, $i = 1, 2$, the space-time discrete Robin data transmitted from one sub-domain to the neighboring sub-domain at each time step:

$$
\int_E \zeta_{h,i}^n = \int_E \left(\boldsymbol{\varphi}_{h,j}^n\cdot\boldsymbol{n}_{j|\gamma} + \alpha c_{j,\gamma}^n\right),\ \forall n = 1, \ldots, N,\ j = 3 - i. \tag{4.69}
$$

We then define the Ventcel-Robin operators S_i^{VtR}, for $i = 1, 2$:

$$
\begin{aligned}
\mathcal{S}_i^{\mathrm{VtR}} : \left(M_{h,\gamma}\right)^N \times L^2(0,T;L^2(\Omega_i)) \times H_*^1(\Omega_i) \times H_0^1(\gamma) &\longrightarrow \left(M_{h,\gamma}\right)^N \\
(\varsigma_h,\ q_i,\ c_{0,i},\ c_{0,\gamma}) &\mapsto \boldsymbol{\varphi}_{h,i}\cdot\boldsymbol{n}_{i|\gamma} + \alpha c_{i,\gamma},
\end{aligned}
$$

where $(c_{h,i}, \boldsymbol{\varphi}_{h,i}, \theta_{h,i}, c_{i,\gamma}, \varphi_{\gamma,i}, \theta_{i,\gamma}) \in \left(M_{h,i}\right)^N \times \left(\widetilde{\boldsymbol{\Sigma}}_{h,i}\right)^N \times \left(\Theta_{h,i}\right)^N \times \left(M_{h,\gamma}\right)^N \times \left(\widetilde{\boldsymbol{\Sigma}}_{h,\gamma}\right)^N \times \left(\Theta_{h,\gamma}\right)^N$ is the solution to the time-dependent subdomain problem with Ventcel boundary conditions (4.68)-(4.69) on Ω_i:

For $n = 1, \ldots, N$, find $(c_{h,i}^n, \boldsymbol{\varphi}_{h,i}^n, \theta_{h,i}^n, c_{i,\gamma}^n, \varphi_{\gamma,i}^n, \theta_{i,\gamma}^n)$ such that

$$
\begin{aligned}
&\left(\boldsymbol{D}_i^{-1}\boldsymbol{\varphi}_{h,i}^n, \boldsymbol{v}_{h,i}\right)_{\Omega_i} + \left(\boldsymbol{D}_\gamma^{-1}\boldsymbol{\varphi}_{\gamma,i}^n, \boldsymbol{v}_{h,\gamma}\right)_\gamma - \left(\mathrm{div}\ \boldsymbol{v}_{h,i}, c_{h,i}^n\right)_{\Omega_i} - \left(\mathrm{div}_\tau \boldsymbol{v}_{h,\gamma}, c_{i,\gamma}^n\right)_\gamma \\
&- \sum_{K\in\mathcal{K}_{h,i}}\left(\sum_{\substack{E\subset\partial K \\ E\in\mathcal{E}_{h,i}\setminus\mathcal{E}_h^\gamma}} u_{i,KE}\mathcal{U}_{i,KE}(c_{i,K}^n, \theta_{i,E}^n)(\boldsymbol{D}_i^{-1}\boldsymbol{w}_{i,KE}, \boldsymbol{v}_{h,i})_K + \sum_{\substack{E\subset\partial K \\ E\in\mathcal{E}_h^\gamma}} u_{i,KE}\mathcal{U}_{i,KE}^\gamma(c_{i,K}^n, c_{i,\gamma,E}^n)(\boldsymbol{D}_i^{-1}\boldsymbol{w}_{i,KE}, \boldsymbol{v}_{h,i})_K\right) \\
&\quad - \sum_{E\in\mathcal{E}_h^\gamma}\sum_{P\in\partial E} u_{\gamma,EP}\mathcal{U}_{\gamma,EP}(c_{\gamma,E}^n, \theta_{i,\gamma,P}^n)(\boldsymbol{D}_\gamma^{-1}\boldsymbol{w}_{\gamma,EP}, \boldsymbol{v}_{h,\gamma})_\gamma + \left\langle \boldsymbol{v}_{h,i}\cdot\boldsymbol{n}_{i|\gamma}, c_{i,\gamma}^n\right\rangle_\gamma \\
&\qquad + \sum_{K\in\mathcal{K}_{h,i}}\sum_{\substack{E\subset\partial K \\ E\in\mathcal{E}_{h,i}\setminus\mathcal{E}_h^\gamma}}\left\langle \theta_{h,i}^n, \boldsymbol{v}_{h,i}\cdot\boldsymbol{n}_K\right\rangle_E + \sum_{E\in\mathcal{E}_h^\gamma}\left\langle \theta_{i,\gamma}^n,\ \boldsymbol{v}_{h,\gamma}\cdot\boldsymbol{n}_{\partial E}\right\rangle_{\partial E} = 0,\ \forall (\boldsymbol{v}_{h,i}, \boldsymbol{v}_{h,\gamma}) \in \widetilde{\boldsymbol{\Sigma}}_{h,i} \times \widetilde{\boldsymbol{\Sigma}}_{h,\gamma}, \\
&\left(-\boldsymbol{\varphi}_{h,i}^n\cdot\boldsymbol{n}_{i|\gamma} + \alpha c_{i,\gamma}^n, \mu_{h,\gamma}\right)_\gamma + (\phi_i \bar{\partial} c_{h,i}^n, \mu_{h,i})_{\Omega_i} + (\phi_\gamma \bar{\partial} c_{i,\gamma}^n, \mu_{h,\gamma})_\gamma + (\mathrm{div}\ \boldsymbol{\varphi}_{h,i}^n, \mu_{h,i})_{\Omega_i} + (\mathrm{div}_\tau \boldsymbol{\varphi}_{\gamma,i}^n, \mu_{h,\gamma})_\gamma \\
&\qquad = (q_i^n, \mu_i)_{\Omega_i} + (q_\gamma^n, \mu_{h,\gamma})_\gamma + (\varsigma_h^n, \mu_{h,\gamma})_\gamma,\ \forall (\mu_{h,i}, \mu_{h,\gamma}) \in M_{h,i} \times M_{h,\gamma}, \\
&\sum_{K\in\mathcal{K}_{h,i}}\sum_{\substack{E\subset\partial K \\ E\in\mathcal{E}_{h,i}\setminus\mathcal{E}_h^\gamma}}\left\langle \eta_{h,i}, \boldsymbol{\varphi}_{h,i}^n\cdot\boldsymbol{n}_K\right\rangle_E + \sum_{E\in\mathcal{E}_h^\gamma}\left\langle \eta_{h,\gamma},\ \boldsymbol{\varphi}_{\gamma,i}^n\cdot\boldsymbol{n}_{\partial E}\right\rangle_{\partial E} = 0,\ \forall (\eta_{h,i}, \eta_{h,\gamma}) \in \Theta_{h,i}^0 \times \Theta_{h,\gamma},
\end{aligned}
\tag{4.70}
$$

where the initial data $c_{h,i}^0$ and $c_{i,\gamma}^0$ are given by (4.19). The fully-discrete interface problem for the GTO-Schwarz method may be written as:

Find $(\zeta_{h,1}, \zeta_{h,2}) \in (M_{h,\gamma})^{2N}$ such that

$$\begin{aligned}
\int_{t^{n-1}}^{t^n}\int_E \zeta_{h,1}\ d\gamma dt &= \int_{t^{n-1}}^{t^n}\int_E \mathcal{S}_2^{\text{VtR}}(\zeta_{h,2}, q_2, c_{0,2}, c_{0,\gamma})\ d\gamma dt,\\
\int_{t^{n-1}}^{t^n}\int_E \zeta_{h,2} d\gamma dt &= \int_{t^{n-1}}^{t^n}\int_E \mathcal{S}_1^{\text{VtR}}(\zeta_{h,1}, q_1, c_{0,1}, c_{0,\gamma})\ d\gamma dt,
\end{aligned} \qquad \forall n = 1, \ldots, N,\ \ \forall E \in \mathcal{E}_h^\gamma,$$

or, in a more compact form,

$$\mathcal{S}_{\text{O}} \begin{pmatrix} \zeta_{h,1} \\ \zeta_{h,2} \end{pmatrix} = \chi_{\text{O}}, \tag{4.71}$$

where

$$\mathcal{S}_{\text{O}} \begin{pmatrix} \zeta_{h,1} \\ \zeta_{h,2} \end{pmatrix} = \begin{pmatrix} \displaystyle\int_{t^{n-1}}^{t^n}\int_E \zeta_{h,1}\ d\gamma dt - \int_{t^{n-1}}^{t^n}\int_E \mathcal{S}_2^{\text{VtR}}(\zeta_{h,2}, 0, 0, 0)\ d\gamma dt \\ \displaystyle\int_{t^{n-1}}^{t^n}\int_E \zeta_{h,2} d\gamma dt - \int_{t^{n-1}}^{t^n}\int_E \mathcal{S}_1^{\text{VtR}}(\zeta_{h,1}, 0, 0, 0)\ d\gamma dt \end{pmatrix}_{n=1,\ldots,N,\ E\in\mathcal{E}_h^\gamma},$$

and

$$\chi_{\text{O}} = \begin{pmatrix} \displaystyle\int_{t^{n-1}}^{t^n}\int_E \mathcal{S}_2^{\text{VtR}}(0, q_2, c_{0,2}, c_{0,\gamma})\ d\gamma dt \\ \displaystyle\int_{t^{n-1}}^{t^n}\int_E \mathcal{S}_1^{\text{VtR}}(0, q_1, c_{0,1}, c_{0,\gamma})\ d\gamma dt \end{pmatrix}_{n=1,\ldots,N,\ E\in\mathcal{E}_h^\gamma}.$$

The interface problem (4.71) can be solved iteratively using either Jacobi iterations or GMRES. Performing Jacobi iterations leads to the following Optimized Schwarz waveform relaxation (OSWR) algorithm: at the kth iteration, solve in parallel the following time-dependent subdomain problems on $\Omega_i \times (0,T),\ i = 1, 2$: for $n = 1, \ldots, N$,

$$\begin{aligned}
&\left(\boldsymbol{D}_i^{-1}\boldsymbol{\varphi}_{h,i}^{k,n}, \boldsymbol{v}_{h,i}\right)_{\Omega_i} + \left(\boldsymbol{D}_\gamma^{-1}\boldsymbol{\varphi}_{\gamma,i}^{k,n}, \boldsymbol{v}_{h,\gamma}\right)_\gamma - \left(\text{div}\ \boldsymbol{v}_{h,i}, c_{h,i}^{k,n}\right)_{\Omega_i} - \left(\text{div}_\tau \boldsymbol{v}_{h,\gamma}, c_{i,\gamma}^{k,n}\right)_\gamma \\
&- \sum_{K\in\mathcal{K}_{h,i}} \left(\sum_{\substack{E\subset\partial K \\ E\in\mathcal{E}_{h,i}\setminus\mathcal{E}_h^\gamma}} u_{i,KE}\mathcal{U}_{i,KE}(c_{i,K}^{k,n}, \theta_{i,E}^{k,n})(\boldsymbol{D}_i^{-1}\boldsymbol{w}_{i,KE}, \boldsymbol{v}_{h,i})_K + \sum_{\substack{E\subset\partial K \\ E\in\mathcal{E}_h^\gamma}} u_{i,KE}\mathcal{U}_{i,KE}^\gamma(c_{i,K}^{k,n}, c_{i,\gamma,E}^{k,n})(\boldsymbol{D}_i^{-1}\boldsymbol{w}_{i,KE}, \boldsymbol{v}_{h,i})_K \right) \\
&- \sum_{E\in\mathcal{E}_h^\gamma}\sum_{P\in\partial E} u_{\gamma,EP}\mathcal{U}_{\gamma,EP}(c_{\gamma,E}^{k,n}, \theta_{i,\gamma,P}^{k,n})(\boldsymbol{D}_\gamma^{-1}\boldsymbol{w}_{\gamma,EP}, \boldsymbol{v}_{h,\gamma})_\gamma + \left\langle \boldsymbol{v}_{h,i}\cdot\boldsymbol{n}_{i|\gamma}, c_{i,\gamma}^{k,n}\right\rangle_\gamma \\
&\left(-\boldsymbol{\varphi}_{h,i}^{k,n}\cdot\boldsymbol{n}_{i|\gamma} + \alpha c_{i,\gamma}^{k,n}, \mu_{h,\gamma}\right)_\gamma + (\phi_i\bar{\partial}c_{h,i}^{k,n}, \mu_{h,i})_{\Omega_i} + (\phi_\gamma\bar{\partial}c_{i,\gamma}^{k,n}, \mu_{h,\gamma})_\gamma + (\text{div}\ \boldsymbol{\varphi}_{h,i}^{k,n}, \mu_{h,i})_{\Omega_i} + (\text{div}_\tau\boldsymbol{\varphi}_{\gamma,i}^{k,n}, \mu_{h,\gamma})_\gamma \\
&\qquad = (q_i^n, \mu_i)_{\Omega_i} + (q_\gamma^n, \mu_{h,\gamma})_\gamma + \left(\boldsymbol{\varphi}_{h,j}^{k-1,n}\cdot\boldsymbol{n}_{j|\gamma} + \alpha c_{j,\gamma}^{k-1,n}, \mu_{h,\gamma}\right)_\gamma,\ \forall(\mu_{h,i}, \mu_{h,\gamma}) \in M_{h,i}\times M_{h,\gamma}, \\
&\sum_{K\in\mathcal{K}_{h,i}}\sum_{\substack{E\subset\partial K \\ E\in_{h,i}\setminus\mathcal{E}_h^\gamma}} \left\langle \eta_{h,i}, \boldsymbol{\varphi}_{h,i}^{k,n}\cdot\boldsymbol{n}_K\right\rangle_E + \sum_{E\in\mathcal{E}_h^\gamma}\left\langle \eta_{h,\gamma},\ \boldsymbol{\varphi}_{\gamma,i}^{k,n}\cdot\boldsymbol{n}_{\partial E}\right\rangle_{\partial E} = 0,\ \forall(\eta_{h,i}, \eta_{h,\gamma}) \in \Theta_{h,i}^0\times\Theta_{h,\gamma},
\end{aligned} \tag{4.72}$$

with given initial guesses $g_{i,j}(t) := \boldsymbol{\varphi}^0_{h,i} \cdot \boldsymbol{n}_i + \alpha\theta^0_{i,\gamma} \in M_{h,\gamma}$, for $i = 1, 2,\ j = (3-i)$, to start the first iterate. We next show that for the OSWR iterative algorithm (4.72) converges. The following lemma is needed in our proof.

Lemma 4.5. *[11, Lemma 4.1] For $i = 1, 2$, there exists a constant $\bar{C}$ independent of h_i such that:*

$$\|\boldsymbol{v} \cdot \boldsymbol{n}\|_{0,\partial\Omega_i} \leq \bar{C} h_i^{-1/2} \|\boldsymbol{v}\|_{0,\Omega_i}, \quad \textit{for any } \boldsymbol{v} \in \boldsymbol{\Sigma}_{h,i}.$$

Theorem 4.4. *For any sufficiently small but fixed Δt and h such that $\Delta t/\bar{h} < (\phi^- D^-_{min})/(16\bar{C})$ where $\bar{h} = \min\{h_1, h_2\}$ and $\bar{C}$ is provided in Lemma 4.5, Algorithm* (4.72)*, initialized by $(g_{i,j}), i = 1, 2,\ j = (3-i)$, defines a unique sequence of iterates*

$$(c^k_{h,i}, \boldsymbol{\varphi}^k_{h,i}, \theta^k_{h,i}, c^k_{i,\gamma}, \boldsymbol{\varphi}^k_{\gamma,i}, \theta^k_{i,\gamma}) \in (M_{h,i})^N \times (\widetilde{\boldsymbol{\Sigma}}_{h,i})^N \times (\Theta_{h,i})^N \times (M_{h,\gamma})^N \times (\widetilde{\boldsymbol{\Sigma}}_{h,\gamma})^N \times (\Theta_{h,\gamma})^N,$$

that converges, as $k \to \infty$, to the solution of the problem

$$\begin{aligned}
&\left(\boldsymbol{D}_i^{-1}\boldsymbol{\varphi}^n_{h,i}, \boldsymbol{v}_{h,i}\right)_{\Omega_i} + \left(\boldsymbol{D}_\gamma^{-1}\boldsymbol{\varphi}^n_{\gamma,i}, \boldsymbol{v}_{h,\gamma}\right)_\gamma - \left(\text{div}\, \boldsymbol{v}_{h,i}, c^n_{h,i}\right)_{\Omega_i} - \left(\text{div}_\tau \boldsymbol{v}_{h,\gamma}, c^n_{i,\gamma}\right)_\gamma \\
&- \sum_{K\in\mathcal{K}_{h,i}} \left(\sum_{\substack{E\subset\partial K \\ E\in\mathcal{E}_{h,i}\setminus\mathcal{E}^\gamma_h}} u_{i,KE}\mathcal{U}_{i,KE}(c^n_{i,K}, \theta^n_{i,E})(\boldsymbol{D}_i^{-1}\boldsymbol{w}_{i,KE}, \boldsymbol{v}_{h,i})_K + \sum_{\substack{E\subset\partial K \\ E\in\mathcal{E}^\gamma_h}} u_{i,KE}\mathcal{U}^\gamma_{i,KE}(c^n_{i,K}, c^n_{i,\gamma,E})(\boldsymbol{D}_i^{-1}\boldsymbol{w}_{i,KE}, \boldsymbol{v}_{h,i})_K \right) \\
&- \sum_{E\in\mathcal{E}^\gamma_h} \sum_{P\in\partial E} u_{\gamma,EP}\mathcal{U}_{\gamma,EP}(c^n_{\gamma,E}, \theta^n_{i,\gamma,P})(\boldsymbol{D}_\gamma^{-1}\boldsymbol{w}_{\gamma,EP}, \boldsymbol{v}_{h,\gamma})_\gamma + \left\langle \boldsymbol{v}_{h,i}\cdot\boldsymbol{n}_{i|\gamma}, c^n_{i,\gamma}\right\rangle_\gamma \\
&+ \sum_{K\in\mathcal{K}_{h,i}} \sum_{\substack{E\subset\partial K \\ E\in\mathcal{E}_{h,i}\setminus\mathcal{E}^\gamma_h}} \left\langle \theta^n_{h,i}, \boldsymbol{v}_{h,i}\cdot\boldsymbol{n}_K\right\rangle_E + \sum_{E\in\mathcal{E}^\gamma_h} \left\langle \theta^n_{i,\gamma},\ \boldsymbol{v}_{h,\gamma}\cdot\boldsymbol{n}_{\partial E}\right\rangle_{\partial E} = 0,\ \forall (\boldsymbol{v}_{h,i}, \boldsymbol{v}_{h,\gamma}) \in \widetilde{\boldsymbol{\Sigma}}_{h,i} \times \widetilde{\boldsymbol{\Sigma}}_{h,\gamma}, \\
&\left(-\boldsymbol{\varphi}^n_{h,i}\cdot\boldsymbol{n}_{i|\gamma} + \alpha c^n_{i,\gamma}, \mu_{h,\gamma}\right)_\gamma + (\phi_i\bar{\partial}c^n_{h,i}, \mu_{h,i})_{\Omega_i} + (\phi_\gamma\bar{\partial}c^n_{i,\gamma}, \mu_{h,\gamma})_\gamma + (\text{div}\,\boldsymbol{\varphi}^n_{h,i}, \mu_{h,i})_{\Omega_i} + (\text{div}_\tau\boldsymbol{\varphi}^n_{\gamma,i}, \mu_{h,\gamma})_\gamma \\
&\qquad = (q^n_i, \mu_i)_{\Omega_i} + (q^n_\gamma, \mu_{h,\gamma})_\gamma + \left(\boldsymbol{\varphi}^n_{h,j}\cdot\boldsymbol{n}_{j|\gamma} + \alpha c^n_{j,\gamma}, \mu_{h,\gamma}\right)_\gamma,\ \forall (\mu_{h,i}, \mu_{h,\gamma}) \in M_{h,i} \times M_{h,\gamma}, \\
&\sum_{K\in\mathcal{K}_{h,i}} \sum_{\substack{E\subset\partial K \\ E\in\mathcal{E}_{h,i}\setminus\mathcal{E}^\gamma_h}} \left\langle \eta_{h,i}, \boldsymbol{\varphi}^n_{h,i}\cdot\boldsymbol{n}_K\right\rangle_E + \sum_{E\in\mathcal{E}^\gamma_h} \left\langle \eta_{h,\gamma},\ \boldsymbol{\varphi}^n_{\gamma,i}\cdot\boldsymbol{n}_{\partial E}\right\rangle_{\partial E} = 0,\ \forall (\eta_{h,i}, \eta_{h,\gamma}) \in \Theta^0_{h,i} \times \Theta_{h,\gamma}.
\end{aligned} \tag{4.73}$$

Proof. As the equations are linear, we take $q_i = 0,\ q_\gamma = 0$ and $c_{0,i} = 0,\ c_{0,\gamma} = 0$, and prove the sequence of iterates converges to zero. Fix i, for any $n = 1, \ldots, N$, let $(\eta_{h,i}, \eta_{h,\gamma})$ in $\Theta_{h,i} \times \Theta_{h,\gamma}$ be such that

$$(\eta_{h,i})_{|E} = \begin{cases} \theta^{k,n}_{i,E},\ \text{on } E \in \mathcal{E}^I_{h,i}, \\ 0 \text{ otherwise}, \end{cases}, \quad (\eta_{h,\gamma})_{|P} = \begin{cases} \theta^{k,n}_{i,\gamma,P},\ \text{on } P \notin \partial\gamma, \\ 0 \text{ otherwise} \end{cases}. \tag{4.74}$$

We then substitute $(\boldsymbol{v}_{h,i}, \boldsymbol{v}_{h,\gamma}) = \left(\boldsymbol{\varphi}^{k,n}_{h,i}, \boldsymbol{\varphi}^{k,n}_{\gamma,i}\right)$, $(\mu_{h,i}, \mu_{h,\gamma}) = \left(c^{k,n}_{h,i}, c^{k,n}_{i,\gamma}\right)$ and $(\eta_{h,i}, \eta_{h,\gamma})$ defined by (4.74) into the first two equations of (4.72) and add the resulting equations to obtain

$$\left(\boldsymbol{D}_i^{-1}\boldsymbol{\varphi}_{h,i}^{k,n},\boldsymbol{\varphi}_{h,i}^{k,n}\right)_{\Omega_i}+\left(\boldsymbol{D}_\gamma^{-1}\boldsymbol{\varphi}_{\gamma,i}^{k,n},\boldsymbol{\varphi}_{\gamma,i}^{k,n}\right)_{\gamma}+\alpha\left\|c_{i,\gamma}^{k,n}\right\|_{0,\gamma}^2+\left(\phi_i\bar{\partial}c_{h,i}^{k,n},c_{h,i}^{k,n}\right)_{\Omega_i}+\left(\phi_\gamma\bar{\partial}c_{i,\gamma}^{k,n},c_{i,\gamma}^{k,n}\right)_{\gamma}$$
$$=\sum_{K\in\mathcal{K}_{h,i}}\left(\sum_{\substack{E\subset\partial K\\E\in\mathcal{E}_{h,i}\setminus\mathcal{E}_h^\gamma}}u_{i,KE}\mathcal{U}_{i,KE}(c_{i,K}^{k,n},\theta_{i,E}^{k,n})(\boldsymbol{D}_i^{-1}\boldsymbol{w}_{i,KE},\boldsymbol{\varphi}_{h,i}^{k,n})_K+\sum_{\substack{E\subset\partial K\\E\in\mathcal{E}_h^\gamma}}u_{i,KE}\mathcal{U}_{i,KE}^{\gamma}(c_{i,K}^{k,n},c_{i,\gamma,E}^{k,n})(\boldsymbol{D}_i^{-1}\boldsymbol{w}_{i,KE},\boldsymbol{\varphi}_{h,i}^{k,n})_K\right)$$
$$+\sum_{E\in\mathcal{E}_h^\gamma}\sum_{P\in\partial E}u_{\gamma,EP}\mathcal{U}_{\gamma,EP}(c_{\gamma,E}^{k,n},\theta_{i,\gamma,P}^{k,n})(\boldsymbol{D}_\gamma^{-1}\boldsymbol{w}_{\gamma,EP},\boldsymbol{\varphi}_{\gamma,i}^{k,n})_\gamma+\left(\boldsymbol{\varphi}_{h,j}^{k-1,n}\cdot\boldsymbol{n}_{j|\gamma}+\alpha c_{j,\gamma}^{k-1,n},c_{i,\gamma}^{k,n}\right)_{\gamma}. \tag{4.75}$$

By summing (4.75) from $n=1,\ldots,N$ and then multiplying both sides of the resulting equation by $2\Delta t$, we have

$$2\Delta t\sum_{n=1}^{N}\left(\boldsymbol{D}_i^{-1}\boldsymbol{\varphi}_{h,i}^{k,n},\boldsymbol{\varphi}_{h,i}^{k,n}\right)_{\Omega_i}+2\Delta t\sum_{n=1}^{N}\left(\boldsymbol{D}_\gamma^{-1}\boldsymbol{\varphi}_{\gamma,i}^{k,n},\boldsymbol{\varphi}_{\gamma,i}^{k,n}\right)_{\gamma}+2\alpha\Delta t\sum_{n=1}^{N}\left\|c_{i,\gamma}^{k,n}\right\|_{0,\gamma}^2+2\Delta t\sum_{n=1}^{N}\left(\phi_i\bar{\partial}c_{h,i}^{k,n},c_{h,i}^{k,n}\right)_{\Omega_i}$$
$$+2\Delta t\sum_{n=1}^{N}\left(\phi_\gamma\bar{\partial}c_{i,\gamma}^{k,n},c_{i,\gamma}^{k,n}\right)_{\gamma}=2\Delta t\sum_{n=1}^{N}\sum_{K\in\mathcal{K}_{h,i}}\left(\sum_{\substack{E\subset\partial K\\E\in\mathcal{E}_{h,i}\setminus\mathcal{E}_h^\gamma}}u_{i,KE}\mathcal{U}_{i,KE}(c_{i,K}^{k,n},\theta_{i,E}^{k,n})(\boldsymbol{D}_i^{-1}\boldsymbol{w}_{i,KE},\boldsymbol{\varphi}_{h,i}^{k,n})_K\right.$$
$$\left.+\sum_{\substack{E\subset\partial K\\E\in\mathcal{E}_h^\gamma}}u_{i,KE}\mathcal{U}_{i,KE}^{\gamma}(c_{i,K}^{k,n},c_{i,\gamma,E}^{k,n})(\boldsymbol{D}_i^{-1}\boldsymbol{w}_{i,KE},\boldsymbol{\varphi}_{h,i}^{k,n})_K\right)$$
$$+2\Delta t\sum_{n=1}^{N}\sum_{E\in\mathcal{E}_h^\gamma}\sum_{P\in\partial E}u_{\gamma,EP}\mathcal{U}_{\gamma,EP}(c_{\gamma,E}^{k,n},\theta_{i,\gamma,P}^{k,n})(\boldsymbol{D}_\gamma^{-1}\boldsymbol{w}_{\gamma,EP},\boldsymbol{\varphi}_{\gamma,i}^{k,n})_\gamma$$
$$+2\Delta t\sum_{n=1}^{N}\left(\boldsymbol{\varphi}_{h,j}^{k-1,n}\cdot\boldsymbol{n}_{j|\gamma}+\alpha c_{j,\gamma}^{k-1,n},c_{i,\gamma}^{k,n}\right)_{\gamma}. \tag{4.76}$$

By proceeding in the same manner as in (4.29), (4.30) and (4.32), we obtain from (4.76) that

$$\phi^-\left\|c_{h,i}^{k,N}\right\|_{0,\Omega_i}^2+2\Delta tD_{\min}^-\sum_{n=1}^{N}\left\|\boldsymbol{\varphi}_{h,i}^{k,n}\right\|_{0,\Omega_i}^2+\phi^-\left\|c_{i,\gamma}^{k,N}\right\|_{0,\gamma}^2+2\Delta tD_{\min}^-\sum_{n=1}^{N}\left\|\boldsymbol{\varphi}_{\gamma,i}^{k,n}\right\|_{0,\gamma}^2+2\alpha\Delta t\sum_{n=1}^{N}\left\|c_{i,\gamma}^{k,n}\right\|_{0,\gamma}^2$$
$$\le\frac{C\Delta t}{\varepsilon}\sum_{n=1}^{N}\left\|c_{h,i}^{k,n}\right\|_{0,\Omega_i}^2+\frac{C\Delta t\varepsilon}{4}\sum_{n=1}^{N}\left\|\boldsymbol{\varphi}_{h,i}^{k,n}\right\|_{0,\Omega_i}^2+C\Delta th\sum_{n=1}^{N}\left\|\boldsymbol{\varphi}_{h,i}^{k,n}\right\|_{0,\Omega_i}^2+\frac{C\Delta t}{\varepsilon}\sum_{n=1}^{N}\left\|c_{i,\gamma}^{k,n}\right\|_{0,\gamma}^2$$
$$+\frac{C\Delta t\varepsilon}{4}\sum_{n=1}^{N}\left\|\boldsymbol{\varphi}_{\gamma,i}^{k,n}\right\|_{0,\gamma}^2+C\Delta th\sum_{n=1}^{N}\left\|\boldsymbol{\varphi}_{\gamma,i}^{k,n}\right\|_{0,\gamma}^2+2\Delta t\sum_{n=1}^{N}\left(\boldsymbol{\varphi}_{h,j}^{k-1,n}\cdot\boldsymbol{n}_{j|\gamma}+\alpha c_{j,\gamma}^{k-1,n},c_{i,\gamma}^{k,n}\right)_{\gamma}. \tag{4.77}$$

We choose ε small enough such that $2D_{\min}^- - \dfrac{C\varepsilon}{4} > D_{\min}^-$, and then Δt, and h small enough such that

$$\phi^- - \frac{C\Delta t}{\varepsilon} > \frac{\phi^-}{2}, \quad D_{\min}^- - Ch > \frac{D_{\min}^-}{2}. \tag{4.78}$$

From (4.77) and (4.78), we find

$$\frac{\phi^-}{2}\left\|c_{h,i}^{k,N}\right\|_{0,\Omega_i}^2+\frac{D_{\min}^-}{2}\Delta t\sum_{n=1}^{N}\left\|\boldsymbol{\varphi}_{h,i}^{k,n}\right\|_{0,\Omega_i}^2+\frac{\phi^-}{2}\left\|c_{i,\gamma}^{k,N}\right\|_{0,\gamma}^2+\frac{D_{\min}^-}{2}\Delta t\sum_{n=1}^{N}\left\|\boldsymbol{\varphi}_{\gamma,i}^{k,n}\right\|_{0,\gamma}^2+2\alpha\Delta t\sum_{n=1}^{N}\left\|c_{i,\gamma}^{k,n}\right\|_{0,\gamma}^2$$
$$\le\frac{C\Delta t}{\varepsilon}\sum_{n=1}^{N-1}\left\|c_{h,i}^{k,n}\right\|_{0,\Omega_i}^2+\frac{C\Delta t}{\varepsilon}\sum_{n=1}^{N-1}\left\|\theta_{i,\gamma}^{k,n}\right\|_{0,\gamma}^2+2\Delta t\sum_{n=1}^{N}\left(\boldsymbol{\varphi}_{h,j}^{k-1,n}\cdot\boldsymbol{n}_{j|\gamma}+\alpha c_{j,\gamma}^{k-1,n},c_{i,\gamma}^{k,n}\right)_{\gamma}. \tag{4.79}$$

By summing over the iterates k from 1 to K in (4.79), we obtain,

$$\frac{\phi^-}{2}\sum_{k=1}^{K}\left\|c_{h,i}^{k,N}\right\|_{0,\Omega_i}^2+\frac{D_{\min}^-}{2}\Delta t\sum_{n=1}^{N}\left(\sum_{k=1}^{K}\left\|\boldsymbol{\varphi}_{h,i}^{k,n}\right\|_{0,\Omega_i}^2\right)+\frac{\phi^-}{2}\sum_{k=1}^{K}\left\|c_{i,\gamma}^{k,N}\right\|_{0,\gamma}^2+\frac{D_{\min}^-}{2}\Delta t\sum_{n=1}^{N}\left(\sum_{k=1}^{K}\left\|\boldsymbol{\varphi}_{\gamma,i}^{k,n}\right\|_{0,\gamma}^2\right)$$
$$+2\alpha\Delta t\sum_{n=1}^{N}\left(\sum_{k=1}^{K}\left\|c_{i,\gamma}^{k,n}\right\|_{0,\gamma}^2\right)\leq\frac{C\Delta t}{\varepsilon}\sum_{n=1}^{N-1}\left(\sum_{k=1}^{K}\left\|c_{h,i}^{k,n}\right\|_{0,\Omega_i}^2\right)+\frac{C\Delta t}{\varepsilon}\sum_{n=1}^{N-1}\left(\sum_{k=1}^{K}\left\|c_{i,\gamma}^{k,n}\right\|_{0,\gamma}^2\right)+$$
$$2\Delta t\sum_{n=1}^{N}\sum_{k=1}^{K-1}\left(\boldsymbol{\varphi}_{h,j}^{k,n}\cdot\boldsymbol{n}_{j|\gamma}+\alpha c_{j,\gamma}^{k,n},c_{i,\gamma}^{k+1,n}\right)_\gamma+2\Delta t\sum_{n=1}^{N}\left(\boldsymbol{\varphi}_{h,j}^{0,n}\cdot\boldsymbol{n}_{j|\gamma}+\alpha c_{j,\gamma}^{0,n},c_{i,\gamma}^{1,n}\right)_\gamma. \tag{4.80}$$

By applying the weighted Cauchy-Schwarz inequality and Lemma 4.5, we obtain, for $i=1,2$, $j=3-i$:

$$\begin{aligned}2\Delta t\sum_{n=1}^{N}\left(\boldsymbol{\varphi}_{h,j}^{k-1,n}\cdot\boldsymbol{n}_{j|\gamma},c_{i,\gamma}^{k,n}\right)_\gamma&\leq 2\Delta t\sum_{n=1}^{N}\left\|\boldsymbol{\varphi}_{h,j}^{k-1,n}\cdot\boldsymbol{n}_{j|\gamma}\right\|_{0,\gamma}\left\|c_{i,\gamma}^{k,n}\right\|_{0,\gamma}\\&\leq\Delta t\sum_{n=1}^{N}\left(\rho h_i\left\|\boldsymbol{\varphi}_{h,j}^{k-1,n}\cdot\boldsymbol{n}_{j|\gamma}\right\|_{0,\gamma}^2+\frac{1}{\rho h_i}\left\|c_{i,\gamma}^{k,n}\right\|_{0,\gamma}^2\right)\\&\leq\Delta t\sum_{n=1}^{N}\left(\bar{C}\rho\left\|\boldsymbol{\varphi}_{h,j}^{k-1,n}\right\|_{0,\Omega_j}^2+\frac{1}{\rho\bar{h}}\left\|c_{i,\gamma}^{k,n}\right\|_{0,\gamma}^2\right).\end{aligned}$$

Using this and the weighted Cauchy-Schwarz inequality on the last two terms on the right-hand side of (4.80) yields

$$\frac{\phi^-}{2}\sum_{k=1}^{K}\left\|c_{h,i}^{k,N}\right\|_{0,\Omega_i}^2+\frac{D_{\min}^-\Delta t}{2}\sum_{n=1}^{N}\left(\sum_{k=1}^{K}\left\|\boldsymbol{\varphi}_{h,i}^{k,n}\right\|_{0,\Omega_i}^2\right)+\frac{\phi^-}{2}\sum_{k=1}^{K}\left\|c_{i,\gamma}^{k,N}\right\|_{0,\gamma}^2+\frac{D_{\min}^-\Delta t}{2}\sum_{n=1}^{N}\left(\sum_{k=1}^{K}\left\|\boldsymbol{\varphi}_{\gamma,i}^{k,n}\right\|_{0,\gamma}^2\right)$$
$$+2\alpha\Delta t\sum_{n=1}^{N}\left(\sum_{k=1}^{K}\left\|c_{i,\gamma}^{k,n}\right\|_{0,\gamma}^2\right)\leq\frac{C\Delta t}{\varepsilon}\sum_{n=1}^{N-1}\left(\sum_{k=1}^{K}\left\|c_{h,i}^{k,n}\right\|_{0,\Omega_i}^2\right)+\frac{C\Delta t}{\varepsilon}\sum_{n=1}^{N-1}\left(\sum_{k=1}^{K}\left\|c_{i,\gamma}^{k,n}\right\|_{0,\gamma}^2\right)$$
$$+\alpha\Delta t\sum_{n=1}^{N}\left(\sum_{k=1}^{K-1}\left\|c_{j,\gamma}^{k,n}\right\|_{0,\gamma}^2\right)+\alpha\Delta t\sum_{n=1}^{N}\left(\sum_{k=1}^{K-1}\left\|c_{i,\gamma}^{k+1,n}\right\|_{0,\gamma}^2\right)+\bar{C}\rho\Delta t\sum_{n=1}^{N}\left(\sum_{k=1}^{K-1}\left\|\boldsymbol{\varphi}_{h,j}^{k,n}\right\|_{0,\Omega_j}^2\right)$$
$$+\frac{\Delta t}{\rho\bar{h}}\sum_{n=1}^{N}\left(\sum_{k=1}^{K-1}\left\|c_{i,\gamma}^{k+1,n}\right\|_{0,\gamma}^2\right)+\frac{\Delta t}{\alpha}\sum_{n=1}^{N}\left\|\boldsymbol{\varphi}_{h,j}^{0,n}\cdot\boldsymbol{n}_{j|\gamma}+\alpha c_{j,\gamma}^{0,n}\right\|_{0,\gamma}^2+\alpha\Delta t\sum_{n=1}^{N}\left\|c_{i,\gamma}^{1,n}\right\|_{0,\gamma}^2.$$

We then fix $\rho=\dfrac{D_{\min}^-}{4\bar{C}}$ and use the assumption $\dfrac{\Delta t}{\bar{h}}<\dfrac{\phi^-D_{\min}^-}{16\bar{C}}$ to deduce that

$$\frac{\phi^-}{4}\sum_{k=1}^{K}\left\|c_{h,i}^{k,N}\right\|_{0,\Omega_i}^2+\frac{D_{\min}^-\Delta t}{2}\sum_{n=1}^{N}\left(\sum_{k=1}^{K}\left\|\boldsymbol{\varphi}_{h,i}^{k,n}\right\|_{0,\Omega_i}^2\right)+\frac{\phi^-}{4}\sum_{k=1}^{K}\left\|c_{i,\gamma}^{k,N}\right\|_{0,\gamma}^2+\frac{D_{\min}^-\Delta t}{2}\sum_{n=1}^{N}\left(\sum_{k=1}^{K}\left\|\boldsymbol{\varphi}_{\gamma,i}^{k,n}\right\|_{0,\gamma}^2\right)$$
$$+\alpha\Delta t\sum_{n=1}^{N}\left(\sum_{k=1}^{K}\left\|c_{i,\gamma}^{k,n}\right\|_{0,\gamma}^2\right)\leq\frac{C\Delta t}{\varepsilon}\sum_{n=1}^{N-1}\left(\sum_{k=1}^{K}\left\|c_{h,i}^{k,n}\right\|_{0,\Omega_i}^2\right)+\left(\frac{C\Delta t}{\varepsilon}+\frac{4\Delta t\bar{C}}{D_{\min}^-\bar{h}}\right)\sum_{n=1}^{N-1}\left(\sum_{k=1}^{K}\left\|c_{i,\gamma}^{k,n}\right\|_{0,\gamma}^2\right)$$
$$+\alpha\Delta t\sum_{n=1}^{N}\left(\sum_{k=1}^{K-1}\left\|c_{j,\gamma}^{k,n}\right\|_{0,\gamma}^2\right)+\frac{D_{\min}^-\Delta t}{4}\sum_{n=1}^{N}\left(\sum_{k=1}^{K-1}\left\|\boldsymbol{\varphi}_{h,j}^{k,n}\right\|_{0,\Omega_j}^2\right)$$
$$+\frac{\Delta t}{\alpha}\sum_{n=1}^{N}\left\|\boldsymbol{\varphi}_{h,j}^{0,n}\cdot\boldsymbol{n}_{j|\gamma}+\alpha c_{j,\gamma}^{0,n}\right\|_{0,\gamma}^2. \tag{4.81}$$

By summing over the index i for i from 1 to 2, we obtain from (4.81),

$$\frac{\phi^-}{4}\left(\sum_{k=1}^{K}\sum_{i=1}^{2}\left\|c_{h,i}^{k,N}\right\|_{0,\Omega_i}^2+\sum_{k=1}^{K}\sum_{i=1}^{2}\left\|c_{i,\gamma}^{k,N}\right\|_{0,\gamma}^2\right)+\frac{D_{\min}^-\Delta t}{2}\sum_{n=1}^{N}\left(\sum_{k=1}^{K}\sum_{i=1}^{2}\left\|\boldsymbol{\varphi}_{h,i}^{k,n}\right\|_{0,\Omega_i}^2\right)+\frac{D_{\min}^-\Delta t}{2}\sum_{n=1}^{N}\left(\sum_{k=1}^{K}\sum_{i=1}^{2}\left\|\boldsymbol{\varphi}_{\gamma,i}^{k,n}\right\|_{0,\gamma}^2\right)$$
$$+\alpha\Delta t\sum_{n=1}^{N}\left(\sum_{i=1}^{2}\left\|c_{i,\gamma}^{K,n}\right\|_{0,\gamma}^2\right)\leq\frac{C\Delta t}{\varepsilon}\sum_{n=1}^{N-1}\left(\sum_{k=1}^{K}\sum_{i=1}^{2}\left\|c_{h,i}^{k,n}\right\|_{0,\Omega_i}^2\right)+\left(\frac{C\Delta t}{\varepsilon}+\frac{4\Delta t\bar{C}}{D_{\min}^-\bar{h}}\right)\sum_{n=1}^{N-1}\left(\sum_{k=1}^{K}\sum_{i=1}^{2}\left\|c_{i,\gamma}^{k,n}\right\|_{0,\gamma}^2\right)$$
$$+\frac{D_{\min}^-}{4}\Delta t\sum_{n=1}^{N}\left(\sum_{k=1}^{K-1}\sum_{i=1}^{2}\left\|\boldsymbol{\varphi}_{h,i}^{k,n}\right\|_{0,\Omega_i}^2\right)+\frac{\Delta t}{\alpha}\sum_{n=1}^{N}\left(\sum_{i=1}^{2}\left\|\boldsymbol{\varphi}_{h,i}^{0,n}\cdot\boldsymbol{n}_{i|\gamma}+\alpha c_{i,\gamma}^{0,n}\right\|_{0,\gamma}^2\right).$$

Consequently, we have

$$\frac{\phi^-}{4}\left(\sum_{k=1}^{K}\sum_{i=1}^{2}\left\|c_{h,i}^{k,N}\right\|_{0,\Omega_i}^2+\sum_{k=1}^{K}\sum_{i=1}^{2}\left\|c_{i,\gamma}^{k,N}\right\|_{0,\gamma}^2\right)+\frac{D_{\min}^-\Delta t}{4}\sum_{n=1}^{N}\left(\sum_{k=1}^{K}\sum_{i=1}^{2}\left\|\boldsymbol{\varphi}_{h,i}^{k,n}\right\|_{0,\Omega_i}^2+\sum_{k=1}^{K}\sum_{i=1}^{2}\left\|\boldsymbol{\varphi}_{\gamma,i}^{k,n}\right\|_{0,\gamma}^2\right)$$
$$+\alpha\Delta t\sum_{n=1}^{N}\left(\sum_{i=1}^{2}\left\|c_{i,\gamma}^{K,n}\right\|_{0,\gamma}^2\right)\leq\frac{C\Delta t}{\varepsilon}\sum_{n=1}^{N-1}\left(\sum_{k=1}^{K}\sum_{i=1}^{2}\left\|c_{h,i}^{k,n}\right\|_{0,\Omega_i}^2\right)+\left(\frac{C}{\varepsilon}+\frac{4\bar{C}}{D_{\min}^-\bar{h}}\right)\Delta t\sum_{n=1}^{N-1}\left(\sum_{k=1}^{K}\sum_{i=1}^{2}\left\|c_{i,\gamma}^{k,n}\right\|_{0,\gamma}^2\right)$$
$$+\frac{\Delta t}{\alpha}\sum_{n=1}^{N}\left(\sum_{i=1}^{2}\left\|\boldsymbol{\varphi}_{h,i}^{0,n}\cdot\boldsymbol{n}_{i|\gamma}+\alpha c_{i,\gamma}^{0,n}\right\|_{0,\gamma}^2\right).\tag{4.82}$$

Denote the positive numbers

$$R_{\phi,\boldsymbol{D},\alpha}=\min\left\{\frac{\phi^-}{4},\frac{D_{\min}^-}{4},\alpha\right\},\quad L_h=\frac{\max\left\{\dfrac{C}{\varepsilon},C+\dfrac{4\bar{C}}{D_{\min}^-\bar{h}}\right\}}{R_{\phi,\boldsymbol{D},\alpha}},$$

and the sequences

$$a_n=\sum_{k=1}^{K}\sum_{i=1}^{2}\left\|c_{h,i}^{k,n}\right\|_{0,\Omega_i}^2+\sum_{k=1}^{K}\sum_{i=1}^{2}\left\|c_{i,\gamma}^{k,n}\right\|_{0,\gamma}^2,\qquad b_n=\sum_{k=1}^{K}\sum_{i=1}^{2}\left\|\boldsymbol{\varphi}_{h,i}^{k,n}\right\|_{0,\Omega_i}^2+\sum_{k=1}^{K}\sum_{i=1}^{2}\left\|\boldsymbol{\varphi}_{\gamma,i}^{k,n}\right\|_{0,\gamma}^2,$$
$$c_n=\frac{1}{\alpha R_{\phi,\boldsymbol{D},\alpha}}\sum_{i=1}^{2}\left\|\boldsymbol{\varphi}_{h,i}^{0,n}\cdot\boldsymbol{n}_{i|\gamma}+\alpha c_{i,\gamma}^{0,n}\right\|_{0,\gamma}^2.$$

We obtain from (4.82) the following inequality

$$a_N+\Delta t\sum_{n=1}^{N}b_n\leq\Delta t\sum_{n=1}^{N-1}L_ha_n+\Delta t\sum_{n=1}^{N}c_n.\tag{4.83}$$

By using Lemma 4.3 in (4.83) with $\tau=\Delta t$, $B=0$, and $d_l=L_h$, we obtain, (using $n\Delta t\leq N\Delta t=T$ for any n)

$$a_N+\Delta t\sum_{n=1}^{N}b_n\leq\exp\left(\Delta t(N-1)L_h\right)\left(\Delta t\sum_{n=1}^{N}c_n\right)\leq\exp\left(L_hT\right)\left(\frac{1}{\alpha}\int_0^{t_N}\sum_{i=1}^{2}\|g_{i,j}\|_{0,\Omega_i}^2\right).\tag{4.84}$$

From (4.84), we deduce that a_N and b_n are bounded since the right-hand side of (4.84) does not depend on k. Hence, $\left\|c_{h,i}^{k,n}\right\|_{0,\Omega_i}$, $\left\|\boldsymbol{\varphi}_{h,i}^{k,n}\right\|_{0,\Omega_i}$ $\left\|c_{i,\gamma}^{k,N}\right\|_{0,\gamma}$, and $\left\|\boldsymbol{\varphi}_{\gamma,i}^{k,n}\right\|_{0,\gamma}$ converge to 0 as $k\to\infty$, for $i=1,2$ and for $n=1,\ldots,N$. Note that (4.84) can be established for any $1\leq n\leq N$, hence, we have $\left\|c_{h,i}^{k,n}\right\|_{0,\Omega_i}$, $\left\|c_{i,\gamma}^{k,n}\right\|_{0,\gamma}$ converge to 0 as $k\to\infty$ for any $1\leq n\leq N$.

To show the well-posedness of (4.72) for $i = 1, 2$, it suffices to show uniqueness which can be obtained by repeating similar steps as above. □

Remark 4.5. *In our convergence analysis, we assumed some relation between Δt and h to handle the traces on the fracture of the normal fluxes $\boldsymbol{\varphi}_{h,i}^n \cdot \boldsymbol{n}_{i|\gamma}, i = 1, 2$ from both subdomains. However, such an assumption is not needed when one has Robin-Robin or Ventcel-Ventcel transmission conditions since for these cases, the boundary terms from both sides of the fracture can be manipulated in such a way that they cancel each other (e.g., [64, 58]). Thus, it is possible to show the convergence of the OSWR algorithm with nonconforming temporal discretization in the absence of the fracture. For the reduced fracture model, this remains an open question.*

The space-time interface system derived for each method is global-in-time, thus one can impose different time steps on the fracture and on the subdomains. In the next section, we show how to formulate the interface problem for each method with nonconforming discretization in time.

4.4. Nonconforming discretization in time

Let $\mathcal{T}_1, \mathcal{T}_2$, and $\mathcal{T}_\gamma$ be different partitions of the time interval $(0, T]$ into subintervals $J_m^i = \left(t_{m-1}^i, t_m^i\right]$ for $m = 1, \ldots, N_i$, and $i = 1, 2, \gamma$, respectively (see Figure 4.1). For simplicity, we consider uniform partitions and denote by $\Delta t_i,\ i = 1, 2, \gamma$, the corresponding time steps such that $\Delta t_\gamma \ll \Delta t_i,\ i = 1, 2$ (note that the fracture is assumed to have much larger permeability than the surrounding rock matrix).

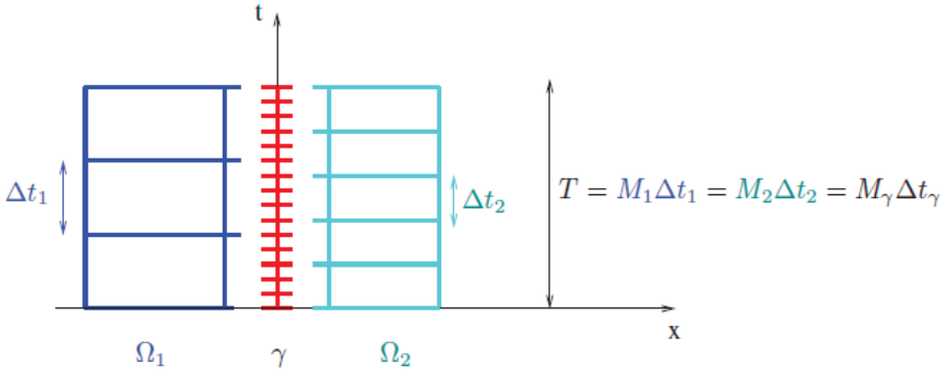

Figure 4.1: Nonconforming time grids in the rock matrix and in the fracture.

We denote by $P_0\left(\mathcal{T}_i,\ \mathcal{W}\right)$ the space of functions which are piecewise constant in time on grid $\mathcal{T}_i$ with values in $\mathcal{W}$: $P_0\left(\mathcal{T}_i,\ \mathcal{W}\right) = \{\psi : (0, T) \to \mathcal{W}, \psi \text{ is constant on } J,\ \forall J \in \mathcal{T}_i\}$.

In order to exchange data on the space-time interface between different time grids $\mathcal{T}_i$ and $\mathcal{T}_j$ (for i, j in $\{1, 2, \gamma\}$), we use the L^2 projection Π_{ji} from $P_0(\mathcal{T}_i,\ \mathcal{W})$ to $P_0(\mathcal{T}_j,\ \mathcal{W})$: for $\psi \in P_0(\mathcal{T}_i,\ \mathcal{W})$, $\Pi_{ji}\psi_{|J_m^j}$ is the average value of ψ on J_m^j, for $m = 1, \ldots, N_j$.

To write the interface equations for GTF-Schur and GTO-Schwarz with nonconconforming time grids, we enforce the transmission conditions weakly over the fracture time subintervals, which has been done in Section 2.5 and Section 3.3.

4.4.1. GTF-Schur method

We choose $\psi_{h,\gamma} = \left(\psi_{h,\gamma}^n\right)_{n=1}^{N_\gamma} \in P_0(\mathcal{T}_\gamma, M_{h,\gamma})$ to be piecewise constant in time on the time grid imposed on the fracture. The interface system (4.67) is then rewritten as:

$$\int_{t_\gamma^{n-1}}^{t_\gamma^n}\int_E \psi_{h,\gamma}\, d\gamma dt = \int_{t_\gamma^{n-1}}^{t_\gamma^n}\int_E \sum_{i=1}^{2} \Pi_{\gamma i}\mathcal{S}_i^{\text{DtN}}(\Pi_{i\gamma}\mathcal{R}_\gamma(\psi_{h,\gamma}, q_\gamma, c_{0,\gamma}), q_i, c_{0,i})\, d\gamma dt, \quad \forall n = 1, \ldots, N_\gamma, \forall E \in \mathcal{E}_h^\gamma. \tag{4.85}$$

4.4.2. GTO-Schwarz method

The two interface unknowns represent the Ventcel term on each subdomain, thus, we let $\zeta_{h,i} = \left(\zeta_{h,i}^n\right)_{n=1}^{N_\gamma} \in P_0(\mathcal{T}_\gamma, M_{h,\gamma}), i = 1, 2$. The interface problem (4.71) of GTO-Schwarz is rewritten as:

$$\begin{aligned}
&\int_{t_\gamma^{n-1}}^{t_\gamma^n}\int_E \zeta_{h,1}\, d\gamma dt = \int_{t_\gamma^{n-1}}^{t_\gamma^n}\int_E \Pi_{\gamma 2} S_2^{\text{VtR}}(\Pi_{2\gamma}\zeta_{h,2}, q_2, c_{0,2}, c_{0,\gamma})\, d\gamma dt,\\
&\int_{t_\gamma^{n-1}}^{t_\gamma^n}\int_E \zeta_{h,2} d\gamma dt = \int_{t_\gamma^{n-1}}^{t_\gamma^n}\int_E \Pi_{\gamma 1} S_1^{\text{VtR}}(\Pi_{1\gamma}\zeta_{h,1}, q_1, c_{0,1}, c_{0,\gamma})\, d\gamma dt,
\end{aligned} \quad \forall n = 1, \ldots, N_\gamma,\ \ \forall E \in \mathcal{E}_h^\gamma. \tag{4.86}$$

4.5. Numerical results

We reconsinder Test case 2.1 presented in Section 3.4, and aim to demonstrate the performance of the DD methods in this chapter when the advection is dominated. Recall that the diffusion $\boldsymbol{D}_i = d_i\mathbf{I}$ is isotropic and constant in each subdomain and on the fracture, where $\mathbf{I}$ is the 2D identity matrix and the velocity $\boldsymbol{u} = (\boldsymbol{u}_1, \boldsymbol{u}_2, \boldsymbol{u}_\gamma)$ presented in (4.2)-(4.3) is obtained by solving the steady-state flow problem on the subdomains

$$
\begin{aligned}
\operatorname{div} \boldsymbol{u}_i &= 0 && \text{in } \Omega_i \times (0,\ T), \\
\boldsymbol{u}_i &= -k_i \nabla p_i && \text{in } \Omega_i \times (0,\ T), \\
p_i &= g_i && \text{on } (\partial\Omega_i \cap \partial\Omega) \times (0,\ T), \quad i = 1, 2, \\
p_i &= p_\gamma && \text{on } \gamma \times (0,\ T), \\
p_i(\cdot, 0) &= p_{0,i} && \text{in } \Omega_i,
\end{aligned}
\tag{4.87}
$$

and in the fracture,

$$
\begin{aligned}
\operatorname{div}_\tau \boldsymbol{u}_\gamma &= \sum_{i=1}^{2} \boldsymbol{u}_i \cdot \boldsymbol{n}_{i|\gamma} && \text{in } \gamma \times (0, T), \\
\boldsymbol{u}_\gamma &= -k_\gamma \delta \nabla_\tau p_\gamma && \text{in } \gamma \times (0, T), \\
p_\gamma &= g_\gamma && \text{on } \partial\gamma \times (0, T), \\
p_\gamma(\cdot, 0) &= p_{0,\gamma} && \text{in } \gamma,
\end{aligned}
\tag{4.88}
$$

where, for $i = 1, 2, \gamma$, q_i is the source term, p_i the pressure, $\boldsymbol{u}_i$ the Darcy velocity, and k_i the time-independent hydraulic conductivity in the subdomains and in the fracture, respectively. All parameters are the same as in Table 3.1.

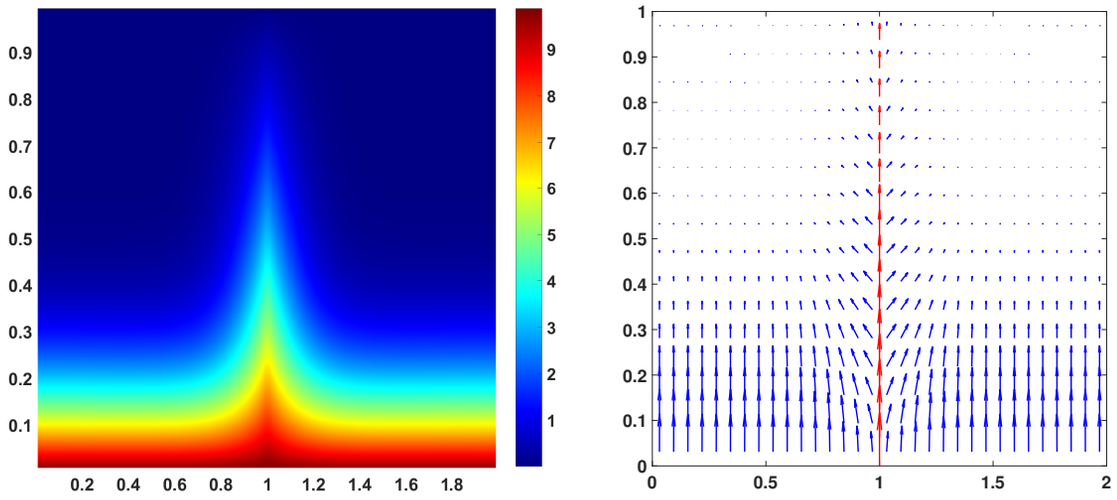

Figure 4.2: Snapshots of the concentration c (left) and the flux field $\boldsymbol{\varphi}$ (right) at $T = 4$.

		Errors for concentration			Errors for velocity		
h	Δt	Ω_1	Ω_2	γ	Ω_1	Ω_2	γ
1/8	T/4	8.15e-01	8.15e-01	4.74e-01	2.39e-01	2.39e-01	1.59e-03
1/16	T/8	4.07e-01 [1.00]	4.07e-01 [1.00]	2.38e-01 [0.99]	1.12e-01 [1.09]	1.12e-01 [1.09]	7.90e-04 [1.01]
1/32	T/16	2.04e-01 [0.99]	2.04e-01 [0.99]	1.18e-01 [1.01]	5.16e-02 [1.12]	5.16e-02 [1.12]	3.90e-04 [1.02]
1/64	T/32	1.01e-01 [1.01]	1.01e-01 [1.01]	5.72e-02 [1.04]	2.20e-02 [1.23]	2.20e-02 [1.23]	1.91e-04 [1.03]

Table 4.1: Converge in both space and time for the monolithic upwind-mixed hybrid scheme with *conforming* time steps. The corresponding convergence rates are shown in square brackets.

We first show in Figure 4.2 the snapshots of the concentration c and the flux field $\boldsymbol{\varphi}$ at the final time $T = 4$. We see that we obtain similar figures as in Figure 3.4 for the case with operator splitting. We fix $T = 1$ and verify numerically the optimal first-order error estimates (cf. Theorem 4.2) of the monolithic scheme (4.18). Table 4.1 reports the errors in the $L^2(0,T;\mathcal{O})$-norm (where $\mathcal{O}$ is either Ω_1, Ω_2, or γ) of the concentration and velocity with decreasing uniform spatial and time step sizes. These errors are computed by comparing with a reference solution on a fine mesh $h_{\text{ref}} = 1/256$ and fine time step $\Delta t_{\text{ref}} = T/512$. First-order convergence is observed in the subdomains as well as on the fracture for both the concentration and velocity.

Next we consider global-in-time DD methods to enforce nonconforming temporal discretizations. We examine the accuracy in time of both GTF-Schur and GTO-Schwarz where smaller time step sizes are used on the fracture and larger ones in the subdomains. The space-time L^2 errors of the concentration and velocity are computed using the reference solution obtained from (4.18) on a fine time grid $dt_{\text{ref}} = T/512$ with $T = 1$. We report the errors for both methods in Tables 4.2 and 4.3; the corresponding convergence rates are shown in the square brackets. We first notice that the two DD methods preserve the first-order convergence in time in nonconforming time grids. By checking the columns corresponding to γ in Tables 4.2 and 4.3, we find that the errors on the fracture by GTF-Schur are approximately half the values of those by GTO-Schwarz (note that $\Delta t_f = \Delta t_i/2$). This behavior has also been observed in previous chapters, only GTF-Schur preserves the accuracy in time with nonconforming temporal discretization.

		GTO-Schwarz			GTF-Schur		
Δt_i	Δt_γ	Ω_1	Ω_2	γ	Ω_1	Ω_2	γ
T/4	T/8	1.14e-01	1.14e-01	1.47e-01	1.14e-01	1.14e-01	6.42e-02
T/8	T/16	5.80e-02 [0.97]	5.80e-02 [0.97]	7.31e-02 [1.01]	5.78e-02 [0.98]	5.78e-02 [0.98]	3.16e-02 [1.02]
T/16	T/32	2.90e-02 [1.00]	2.90e-02 [1.00]	3.60e-02 [1.02]	2.88e-02 [1.01]	2.88e-02 [1.01]	1.52e-02 [1.06]
T/32	T/64	1.41e-02 [1.04]	1.41e-02 [1.04]	1.74e-02 [1.05]	1.40e-02 [1.04]	1.40e-02 [1.04]	7.02e-03 [1.11]

Table 4.2: Converge in time of the *concentration* with nonconforming time grids. The corresponding convergence rates are shown in square brackets.

		GTO-Schwarz			GTF-Schur		
Δt_i	Δt_γ	Ω_1	Ω_2	γ	Ω_1	Ω_2	γ
T/4	T/8	6.14e-04	6.14e-04	7.27e-04	6.14e-04	6.14e-04	3.58e-04
T/8	T/16	3.06e-04 [1.00]	3.06e-04 [1.00]	3.49e-04 [1.06]	3.04e-04 [1.01]	3.04e-04 [1.01]	1.71e-04 [1.07]
T/16	T/32	1.51e-04 [1.02]	1.51e-04 [1.02]	1.69e-04 [1.05]	1.50e-04 [1.02]	1.50e-04 [1.02]	8.15e-05 [1.07]
T/32	T/64	7.29e-05 [1.05]	7.29e-05 [1.05]	8.08e-05 [1.06]	7.24e-05 [1.05]	7.24e-05 [1.05]	3.77e-05 [1.11]

Table 4.3: Convergence in time of the *velocity* with nonconforming time grids. The corresponding convergence rates are shown in square brackets.

Parameters					
k_i	Ω_1	$6.5e-06$	$6.5e-05$	$1.4e-04$	$2.4e-03$
	Ω_2	$6.5e-06$	$6.5e-05$	$1.4e-04$	$2.4e-03$
	Ω_f	$4.4e-02$	$4.4e-01$	$9e-01$	$9e-00$
Pe_i	Ω_1	≈ 0.45	≈ 4.45	≈ 9.6	≈ 165
	Ω_2	≈ 0.45	≈ 4.45	≈ 9.6	≈ 165
	Ω_f	≈ 4.4	≈ 44	≈ 91	≈ 907

Table 4.4: Parameters for different cases.

We now increase Péclet numbers and investigate the convergence of both DD methods with either conforming or nonconforming time grids. We vary the values of the hydraulic conductivity $k_i,\ i = 1, 2, \gamma$, while keeping other physical parameters as in Table 3.1. Four sets of Péclet numbers corresponding to different choices of k_i are shown in Table 4.4. Again, the final time is $T = 1$. We first consider the uniform time step $\Delta t = T/N$ in the fracture and in the subdomains, where $N = 32$. The convergence speed of GTF-Schur and GTO-Schwarz are illustrated via the relative residuals versus the number of subdomain solves as shown in Figure 4.3. We observe that both GTF-Schur and GTO-Schwarz exhibit nearly the same fast convergence speed. In addition, similarly to the results shown in Section 2.6 and Section 3.4, they converge quickly without the need for preconditioners, which highlights the efficiency of both methods. Moreover, GTF-Schur and GTO-Schwarz are insensitive to the effect of the advection, which can be observed from the consistency of their convergence curves as the Péclet number increases. Such robustness with respect to the Péclet number is obtained due to the construction of the interface problem for GTF-Schur and the optimized parameters for GTO-Schwarz; the use of upwind operators does not affect this behavior of the proposed DD

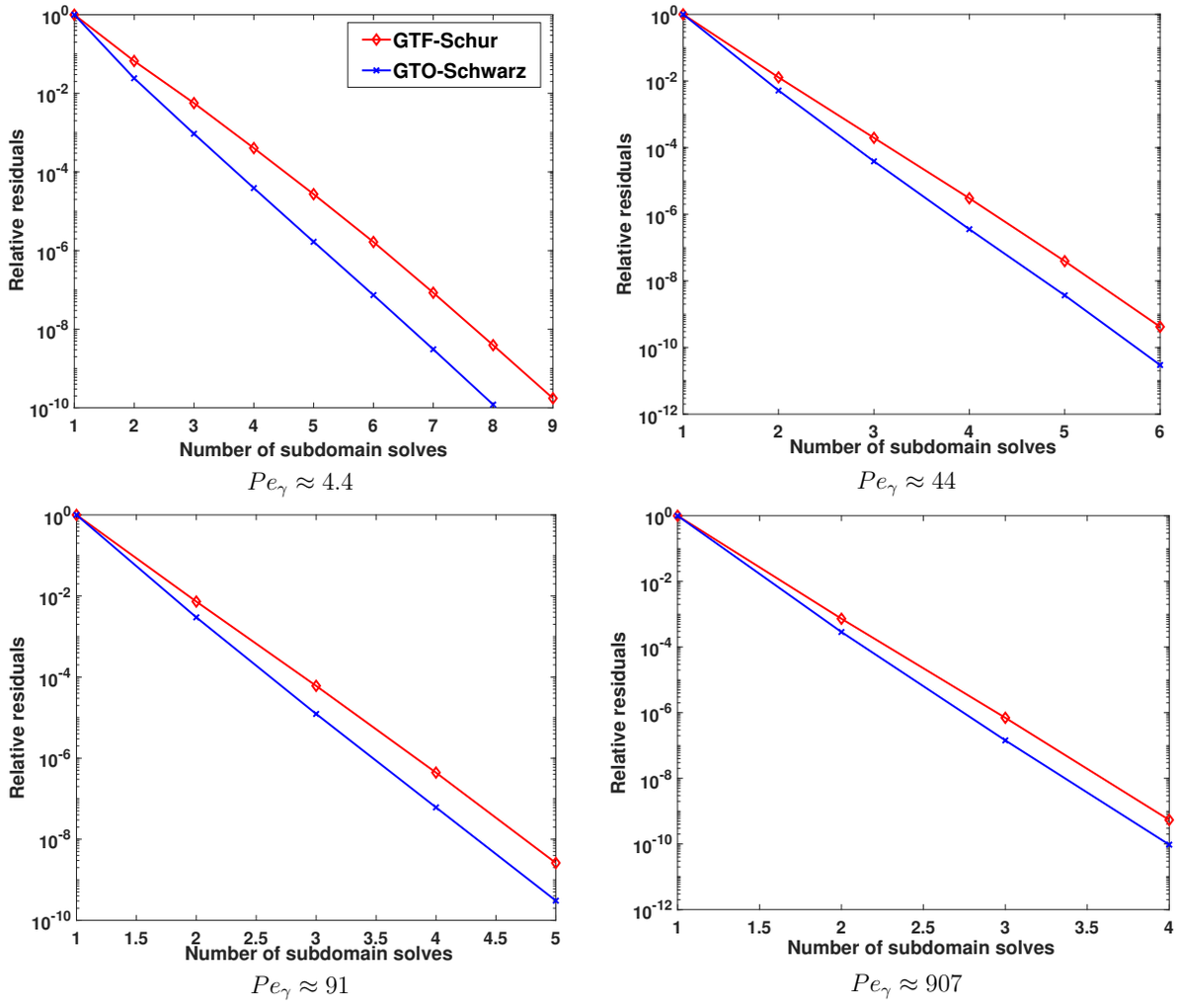

Figure 4.3: Relative residuals of GTF-Schur and GTO-Schwarz with different Peclét numbers and *conforming time grid.*

methods. We remark that in Chapter 3 when operator splitting is used, the convergence of GTF-Schur and GTO-Schwarz is also independent of the Péclet number. However, unlike the methods presented in Chapter 3, here no CFL conditions are imposed on the time step size.

Finally we consider *nonconforming* time grids on the subdomains and on the fracture. Since we have the same diffusion coefficients in the subdomains, which are smaller than that in the fracture, we impose the same large time step in the subdomains and a smaller one in the fracture: $\Delta t_1 = \Delta t_2 = 2\Delta t_\gamma$. For this experiment, we fix $\Delta t_1 = \Delta t_2 = \Delta t = T/N$, $\Delta t_f = T/N_f$ where $N = 32$ and $N_f = 64$ (see Table 4.4). Figure 4.4 shows the residual curves versus the number of subdomain solves with increasing Peclét numbers. From these curves, we deduce that the GTF-Schur and the GTO-Schwarz methods preserve their fast convergence speed and remain unaffected by the magnitudes of the advection when nonconforming temporal discretization is employed.

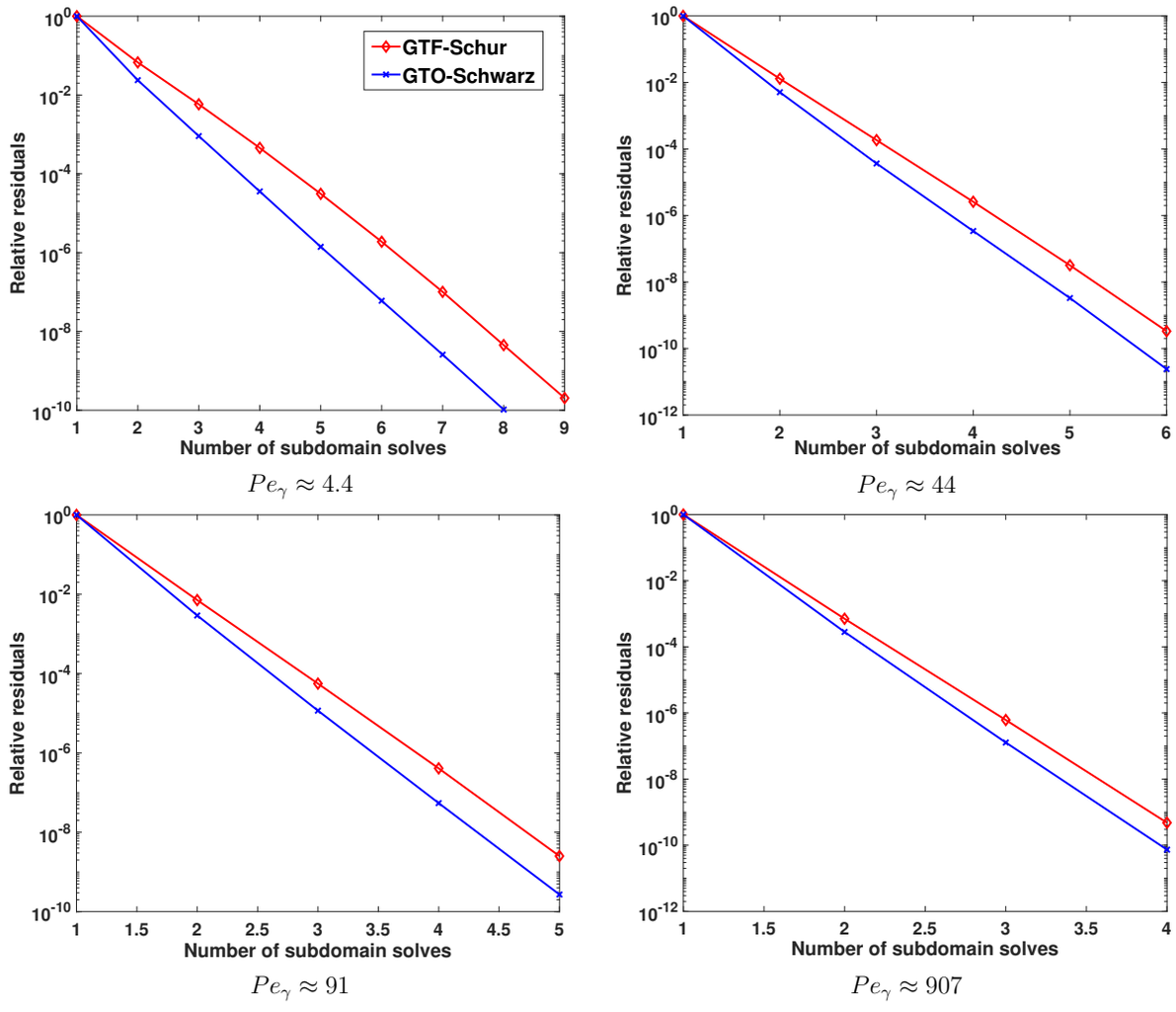

Figure 4.4: Relative residuals of GTF-Schur and GTO-Schwarz with different Peclét numbers and *nonconforming time grid*.

Conclusion

In this chapter, we have investigated new monolithic and decoupled numerical methods for the reduced fracture model of the linear advection-diffusion equation in a fractured porous medium. The Euler-implicit upwind-mixed hybrid finite element algorithm was first introduced to discretize the coupled system in space and time, in which a mixed finite element method with a hybridization technique is considered and Lagrange multipliers are used for the discretization of the advection terms. We proved the existence and uniqueness of the discrete solution, as well as optimal first-order convergence in both temporal and spatial errors of the monolithic solver. To accommodate different time steps on the fracture and on the subdomains, we then proposed two non-overlapping global-in-time DD methods, namely GTF-Schur and GTO-Schwarz in the context of mixed hybrid finite elements. The convergence of GTO-Schwarz with conforming

temporal discretization was also proved. Several numerical experiments were conducted to verify the accuracy of the monolithic solver and to compare the performance of the two DD methods with different Péclet numbers and with both conforming and nonconforming temporal discretizations. The results demonstrate that both GTF-Schur and GTO-Schwarz are capable of handling strongly advection-dominated problems as they maintain the same fast convergence speed regardless of the values of the Péclet numbers. Importantly, they achieved such fast convergence without applying any preconditioners. Moreover, the methods are fully implicit and have no CFL constraints on the time step size. Finally, GTF-Schur provided better accuracy in time on the fracture than GTO-Schwarz with nonconforming temporal discretization as the errors on the fracture obtained from GTF-Schur in such case were smaller than those of GTO-Schwarz. Thus, we conclude that among the two DD methods, GTF-Schur is the most efficient method in terms of accuracy and convergence speed. Future work includes extending the error estimates (4.36) to the case with both nonconforming temporal and spatial discretizations, proving the convergence of GTO-Schwarz with nonconforming discretization in time, and developing local time-stepping algorithms for multiphysics problems in fractured porous media.

Appendix A. Proof of Lemma 4.4

We now present the proof of Lemma 4.4. The proof follows a similar idea as in [26, Lemma 4.2]. For$i = 1, 2$, let $\boldsymbol{v}_h = (\boldsymbol{v}_{h,1}, \boldsymbol{v}_{h,2}, 0) \in \widetilde{\boldsymbol{\Sigma}}_h$ be such that $\boldsymbol{v}_{h,j} = 0$ if $j \neq i$. By taking $\boldsymbol{v}_h$ as a test function in the first equation of (4.18), we obtain

$$\begin{aligned}
&\left(\boldsymbol{D}_i^{-1}\boldsymbol{\varphi}_{h,i}^n, \boldsymbol{v}_{h,i}\right)_{\Omega_i} - \left(\operatorname{div} \boldsymbol{v}_{h,i}, c_{h,i}^n\right)_{\Omega_i} + \left\langle \boldsymbol{v}_{h,i}\cdot\boldsymbol{n}_{i|\gamma}, c_{h,\gamma}^n\right\rangle_\gamma + \sum_{K\in\mathcal{K}_{h,i}} \sum_{\substack{E\subset\partial K\\ E\in\mathcal{E}_{h,i}\setminus\mathcal{E}_h^\gamma}} \left\langle \theta_{h,i}^n, \boldsymbol{v}_{h,i}\cdot\boldsymbol{n}_K\right\rangle_E \\
&- \sum_{K\in\mathcal{K}_{h,i}} \left(\sum_{\substack{E\subset\partial K\\ E\in\mathcal{E}_{h,i}\setminus\mathcal{E}_h^\gamma}} u_{i,KE}\mathcal{U}_{i,KE}(c_{i,K}^n, \theta_{i,E}^n)(\boldsymbol{D}_i^{-1}\boldsymbol{w}_{i,KE}, \boldsymbol{v}_{h,i})_K - \sum_{\substack{E\subset\partial K\\ E\in\mathcal{E}_h^\gamma}} u_{i,KE}\mathcal{U}_{i,KE}^\gamma(c_{i,K}^n, c_{\gamma,E}^n)(\boldsymbol{D}_i^{-1}\boldsymbol{w}_{i,KE}, \boldsymbol{v}_{h,i})_K \right) \\
&\qquad = 0,\ \forall \boldsymbol{v}_{h,i} \in \widetilde{\boldsymbol{\Sigma}}_{h,i}.
\end{aligned} \tag{A.1}$$

For any $K \in \mathcal{K}_{h,i}$, we divide K into two triangles T_1^K and T_2^K by drawing a diagonal E^K:

$$K = T_1^K \cup T_2^K \cup E^K, \;\; T_1^K \cap T_2^K = \emptyset, \;\; \partial T_1^K \cap \partial T_2^K = E^K.$$

Let $\mathcal{T}_{h,i} = \left\{T_1^K, T_2^K\right\}_{K\in\mathcal{K}_{h,i}}$ be a partition of Ω_i into triangles, and let $\tilde{\mathcal{E}}_{h,i} = \mathcal{E}_{h,i} \cup \left\{E^K\right\}_{K\in\mathcal{K}_{h,i}}$. Moreover, let $\mathcal{Q}_{h,i}^0$ be the L^2-projection from $L^2\left(\tilde{\mathcal{E}}_{h,i}\right)$ onto $\mathcal{P}^0\left(\tilde{\mathcal{E}}_{h,i}\right)$ where $\mathcal{P}^0\left(\tilde{\mathcal{E}}_{h,i}\right)$ is the space of piecewise constant functions on $\tilde{\mathcal{E}}_{h,i}$. We then denote a new element $\xi_{h,i}^n \in \mathcal{P}^0\left(\tilde{\mathcal{E}}_{h,i}\right)$ as follows

$$\xi_{h,i|E}^n = \xi_{i,E}^n := \begin{cases} \theta_{i,E}^n, \;\; \text{if } E \in \mathcal{E}_{h,i}, \\ c_{\gamma,E}^n, \;\; \text{if } E \in \mathcal{E}_h^\gamma, \\ \mathcal{Q}_{h,i}^0 c_{i|E}^n, \;\; \text{if } E \in \left\{E^K\right\}_{K\in\mathcal{K}_{h,i}}. \end{cases} \tag{A.2}$$

We begin with providing the following estimate:

$$\begin{aligned} &\sum_{K\in\mathcal{K}_{h,i}} \sum_{\substack{E\subset\partial K \\ E\in\mathcal{E}_{h,i}}} |E|^2 (\xi_{i,E}^n - c_{i,K}^n)^2 \\ &\qquad \le C\left(\left\|c_i^n - c_{h,i}^n\right\|_{0,\Omega_i}^2 + \left\|\boldsymbol{\varphi}_i^n - \boldsymbol{\varphi}_{h,i}^n\right\|_{0,\Omega_i}^2 + h^2\left\|\boldsymbol{u}_i {c^n}_i - \boldsymbol{u}_{h,i} c_{h,i}^n\right\|_{0,\Omega_i}^2 + h^2\left\|c_i^n\right\|_{1,\Omega_i}^2\right). \end{aligned} \tag{A.3}$$

By [12, Lemma 2.1], there exists unique elements $\tilde{c}_{h,i}^n, \hat{c}_{h,i}^n$ in the space $\mathcal{P}_1^{\mathrm{CR}}\left(\mathcal{T}_{h,i}\right)$ of linear Crouzeix–Raviart elements [31] by means of

$$\mathcal{Q}_{h,i}^0 \tilde{c}_{h,i}^n = \xi_{h,i}^n, \qquad \mathcal{Q}_{h,i}^0 \hat{c}_i^n = \mathcal{Q}_{h,i}^0 c_{h,i}^n. \tag{A.4}$$

Then, by standard arguments, it follows that

$$\left\|\hat{c}_{h,i}^n - c_i^n\right\|_{0,\Omega_i} \le Ch\left\|c_i^n\right\|_{1,\Omega_i}. \tag{A.5}$$

From (A.4), we have $\mathcal{Q}_{h,i}^0(\tilde{c}_{h,i}^n - \hat{c}_{h,i}^n) = \xi_{h,i}^n - \mathcal{Q}_{h,i}^0 c_i^n$. Thus, it follows from [12, Lemma 2.1] and the definition of $\xi_{h,i}^n$ on $E \in \left\{E^K\right\}_{K\in\mathcal{K}_{h,i}}$ that for any $K \in \mathcal{K}_{h,i}$,

$$\begin{aligned} \left\|\tilde{c}_{h,i}^n - \hat{c}_{h,i}^n\right\|_{0,K} &\le \left\|\tilde{c}_{h,i}^n - \hat{c}_{h,i}^n\right\|_{0,H_1^K} + \left\|\tilde{c}_{h,i}^n - \hat{c}_{h,i}^n\right\|_{0,H_2^K} \\ &\le Ch_K^{1/2} \sum_{\substack{E\subset\partial H_1^K \\ E\in\tilde{\mathcal{E}}_{h,i}}} \left\|\xi_{h,i}^n - \mathcal{Q}_{h,i}^0 c_i^n\right\|_{0,E} + Ch_K^{1/2} \sum_{\substack{E\subset\partial H_2^K \\ E\in\tilde{\mathcal{E}}_{h,i}}} \left\|\xi_{h,i}^n - \mathcal{Q}_{h,i}^0 c_i^n\right\|_{0,E} \\ &\le Ch_K^{1/2} \sum_{\substack{E\subset\partial K \\ E\in\mathcal{E}_{h,i}}} \left\|\xi_{h,i}^n - \mathcal{Q}_{h,i}^0 c_i^n\right\|_{0,E}. \end{aligned} \tag{A.6}$$

By combining (A.5)- (A.6) with the triangle inequality and Cauchy-Schwarz inequality, we find

$$\left\|\tilde{c}_{h,i}^n - c_{h,i}^n\right\|_{0,\Omega_i}^2 \leq 3\left\|\tilde{c}_{h,i}^n - \hat{c}_h^n\right\|_{0,\Omega_i}^2 + 3\left\|\hat{c}_{h,i}^n - c_i^n\right\|_{0,\Omega_i}^2 + 3\left\|c_i^n - c_{h,i}^n\right\|_{0,\Omega_i}^2$$
$$\leq C\left(h\sum_{K\in\mathcal{K}_{h,i}}\sum_{\substack{E\subset\partial K\\ E\in\mathcal{E}_{h,i}}}\left\|\xi_{h,i}^n - \mathcal{Q}_{h,i}^0 c_i^n\right\|_{0,E}^2 + \left\|c_i^n - c_{h,i}^n\right\|_{0,\Omega_i}^2 + h^2\left\|c_i^n\right\|_{0,\Omega_i}^2\right). \tag{A.7}$$

We now use that for any piecewise linear polynomial $p_h \in \mathcal{P}_1(\mathcal{T}_{h,i})$, the following estimate holds [23, p. 112]:

$$\|p_h\|_{L^1(\partial H_j^K)} \leq C\|p_h\|_{0,H_j^K},\ j = 1, 2. \tag{A.8}$$

By applying (A.8) and the definition of $\tilde{c}_{h,i}^n$, we obtain

$$|E|(\xi_{i,E}^n - c_{i,K}^n) = \left\langle \tilde{c}_{h,i}^n - c_{i,K}^n, 1\right\rangle_E \leq C\left\|\tilde{c}_{h,i}^n - c_{i,K}^n\right\|_{L^1(\partial H_1^K)} \leq C\left\|\tilde{c}_{h,i}^n - c_{i,K}^n\right\|_{0,H_1^K} \leq \left\|\tilde{c}_{h,i}^n - c_{h,i}^n\right\|_{0,K}. \tag{A.9}$$

It follows from (A.7) and (A.9) that

$$\sum_{K\in\mathcal{K}_{h,i}}\sum_{\substack{E\subset\partial K\\ E\in\mathcal{E}_{h,i}}}|E|^2(\xi_{i,E}^n - c_{i,K}^n)^2 \leq 3\left\|\tilde{c}_{h,i}^n - c_{h,i}^n\right\|_{0,\Omega_i}^2$$
$$\leq C\left(h\sum_{K\in\mathcal{K}_{h,i}}\sum_{\substack{E\subset\partial K\\ E\in\mathcal{E}_{h,i}}}\left\|\xi_{h,i}^n - \mathcal{Q}_{h,i}^0 c_i^n\right\|_{0,E}^2 + \left\|c_i^n - c_{h,i}^n\right\|_{0,\Omega_i}^2 + h^2\left\|c_i^n\right\|_{0,\Omega_i}^2\right). \tag{A.10}$$

Finally, we show that

$$\left\|\xi_{h,i}^n - \mathcal{Q}_{h,i}^0 c_i^n\right\|_{0,E} \leq C\left(h_K^{1/2}\left\|\boldsymbol{\varphi}_i^n - \boldsymbol{\varphi}_{h,i}^n\right\|_{0,K} + h_K^{1/2}\sum_{E'\subset\partial K}|E'||\xi_{i,E'}^n - c_{i,K}^n|\right.$$
$$\left. + h_K^{1/2}\left\|\boldsymbol{u}_i c_i^n - \boldsymbol{u}_{h,i} c_{h,i}^n\right\|_{0,K} + h_K^{-1/2}\left\|c_i^n - c_{h,i}^n\right\|_{0,K}\right), \tag{A.11}$$
$$\forall\ K\in\mathcal{K}_{h,i}, \forall\ E\in\mathcal{E}_{h,i}, E\subset\partial K.$$

For any $K\in\mathcal{K}_{h,i}$ and $E\subset\partial K, E\in\mathcal{E}_{h,i}$, it follows from [12] that there exist a unique element $\boldsymbol{\tau}_{i,E}\in\widetilde{\boldsymbol{\Sigma}}_{h,i}$ such that $\text{supp}(\boldsymbol{\tau})_{i,E}\subseteq K$ and

$$\boldsymbol{\tau}_{i,E}\cdot\boldsymbol{n}_E = \begin{cases} \xi_{h,i}^n - \mathcal{Q}_{h,i}^0 c_i^n, & \text{on } E,\\ 0, & \text{on } \partial K\backslash E.\end{cases}$$

It follows from a scaling argument [12] that

$$h_K\left\|\boldsymbol{\tau}_{i,E}\right\|_{1,K} + \left\|\boldsymbol{\tau}_{i,E}\right\|_{0,K} \leq Ch_K^{1/2}\left\|\xi_{h,i}^n - \mathcal{Q}_{h,i}^0 c_i^n\right\|_{0,E}. \tag{A.12}$$

By using $\boldsymbol{v}_{h,i} = \boldsymbol{\tau}_{i,E}$ in the first equation of (A.1), we obtain

$$\left(\boldsymbol{D}_i^{-1}\boldsymbol{\varphi}_{h,i}^n, \boldsymbol{\tau}_{i,E}\right)_{\Omega_i} - \left(\operatorname{div} \boldsymbol{\tau}_{i,E}, c_{h,i}^n\right)_{\Omega_i} - \sum_{\substack{E'\subset\partial K \\ E'\in\mathcal{E}_{h,i}\setminus\mathcal{E}_h^\gamma}} u_{i,KE'}\mathcal{U}_{i,KE'}(c_{i,K}^n, \theta_{i,E'}^n)\left(\boldsymbol{D}_i^{-1}\boldsymbol{w}_{i,KE'}, \boldsymbol{\tau}_{i,E}\right)_K$$
$$\sum_{\substack{E'\subset\partial K \\ E'\in\mathcal{E}_h^\gamma}} u_{i,KE'}\mathcal{U}_{i,KE'}^\gamma(c_{i,K}^n, c_{\gamma,E'}^n)(\boldsymbol{D}_i^{-1}\boldsymbol{w}_{i,KE'}, \boldsymbol{\tau}_{i,E})_K = -\left\langle \xi_{h,i}^n, \xi_{h,i}^n - \mathcal{Q}_{h,i}^0 c_i^n\right\rangle_E. \tag{A.13}$$

From the relation $q_i^n = \boldsymbol{u}_i c_i^n - \boldsymbol{D}_i\nabla c_i^n$, by apply Green's formula, we obtain

$$\left(\boldsymbol{D}_i^{-1}\boldsymbol{\varphi}_i^n, \boldsymbol{\tau}_{i,E}\right)_{\Omega_i} - \left(\operatorname{div} \boldsymbol{\tau}_{i,E}, c_i^n\right)_{\Omega_i} - \left(\boldsymbol{D}_i^{-1}\boldsymbol{u}_i c_i^n, \boldsymbol{\tau}_{i,E}\right)_{\Omega_i} = -\left\langle c_i^n, \xi_{h,i}^n - \mathcal{Q}_{h,i}^0 c_i^n\right\rangle_E. \tag{A.14}$$

By subtracting (A.13) from (A.14) and using the definition of $\mathcal{Q}_{h,i}^0$, we find

$$\begin{aligned}
\left\|\xi_{h,i}^n - \mathcal{Q}_{h,i}^0 c_i^n\right\|_{0,E}^2 &= \left\langle \xi_{h,i}^n - c_i^n, \xi_{h,i}^n - \mathcal{Q}_{h,i}^0 c_i^n\right\rangle_E \\
&= \left(\boldsymbol{D}_i^{-1}(\boldsymbol{\varphi}_i^n - \boldsymbol{\varphi}_{h,i}^n), \boldsymbol{\tau}_{i,E}\right)_{\Omega_i} - \left(\operatorname{div} \boldsymbol{\tau}_{i,E}, c_i^n - c_{h,i}^n\right)_{\Omega_i} - \left(\boldsymbol{D}_i^{-1}\boldsymbol{u}_i(c_i^n - c_{h,i}^n), \boldsymbol{\tau}_{i,E}\right)_{\Omega_i} \\
&- \sum_{\substack{E'\subset\partial K \\ E'\in\mathcal{E}_{h,i}\setminus\mathcal{E}_h^\gamma}} u_{i,KE'}\left(\mathcal{U}_{i,KE'}(c_{i,K}^n, \theta_{i,E'}^n) - c_{i,K}^n\right)\left(\boldsymbol{D}_i^{-1}\boldsymbol{w}_{i,KE'}, \boldsymbol{\tau}_{i,E}\right)_K \\
&- \sum_{\substack{E'\subset\partial K \\ E'\in\mathcal{E}_h^\gamma}} u_{i,KE'}\left(\mathcal{U}_{i,KE'}^\gamma(c_{i,K}^n, c_{\gamma,E'}^n) - c_{i,K}^n\right)\left(\boldsymbol{D}_i^{-1}\boldsymbol{w}_{i,KE'}, \boldsymbol{\tau}_{i,E}\right)_K.
\end{aligned} \tag{A.15}$$

By applying the Cauchy-Schwarz inequality, we obtain from (A.15) that

$$\begin{aligned}
\left\|\xi_{h,i}^n - \mathcal{Q}_{h,i}^0 c^n\right\|_{0,E}^2 \le C\Bigg(&\left\|\boldsymbol{\varphi}_i^n - \boldsymbol{\varphi}_{h,i}^n\right\|_{0,K}\left\|\boldsymbol{\tau}_{i,E}\right\|_{0,K} + \left\|c_i^n - c_{h,i}^n\right\|_{0,K}\left\|\boldsymbol{\tau}_{i,E}\right\|_{1,K} \\
&+ \sum_{E'\subset\partial K}|E'||\xi_{i,E'}^n - c_{i,K}^n|\left\|\boldsymbol{\tau}_{i,E}\right\|_{0,K} + \left\|\boldsymbol{D}_i^{-1}\boldsymbol{u}_i(c_i^n - c_{h,i}^n)\right\|_{0,K}\left\|\boldsymbol{\tau}_{i,E}\right\|_{0,K}\Bigg), \\
&\forall\, K\in\mathcal{K}_{h,i}, \forall\, E\in\mathcal{E}_{h,i}, E\subset\partial K.
\end{aligned} \tag{A.16}$$

We then obtain (A.11) by combining (A.16) with (A.12) and applying the Cauchy-Schwarz inequality. By combining (A.10) with (A.11), we obtain

$$\begin{aligned}
\sum_{K\in\mathcal{K}_{h,i}}\sum_{E\subset\partial K}|E|^2(\xi_{i,E}^n - c_{i,K}^n)^2 \le C\Bigg(&h^2\left\|\boldsymbol{\varphi}_i^n - \boldsymbol{\varphi}_{h,i}^n\right\|_{0,\Omega_i}^2 + h^2\sum_{K\in\mathcal{K}_{h,i}}\sum_{E'\subset\partial K}|E'|^2\left(\xi_{i,E'}^n - c_{i,K}^n\right)^2 \\
&+h^2\left\|\boldsymbol{u}_i c_i^n - \boldsymbol{u}_{h,i}c_{h,i}^n\right\|_{0,\Omega_i}^2 + \left\|c_i^n - c_{h,i}^n\right\|_{0,\Omega_i}^2 + h^2\left\|c_i^n\right\|_{0,\Omega_i}^2\Bigg).
\end{aligned} \tag{A.17}$$

By choosing h small enough and pushing back the second term on the right-hand side of (A.17), we obtain (A.3).

For the advection term on the fracture, since we can derive analogous result to Lemma 4.2 for the 1-dimensional case, we can follow the steps in [26] and arrive at

$$\sum_{E\in\mathcal{E}_h^\gamma}\sum_{P\in\partial E}(\theta_{\gamma,P}^n - c_{\gamma,E}^n)^2 \leq C\left(h^2\left\|\boldsymbol{\varphi}_\gamma^n - \boldsymbol{\varphi}_{h,\gamma}^n\right\|_{0,\Omega_i}^2 + h^2\left\|\boldsymbol{u}_\gamma c_\gamma^n - \boldsymbol{u}_{h,\gamma}c_{h,\gamma}^n\right\|_{0,\gamma}^2 + \left\|c_\gamma^n - c_{h,\gamma}^n\right\|_{0,\gamma}^2 + h^2\left\|c_\gamma^n\right\|_{0,\gamma}^2\right). \tag{A.18}$$

(4.35) then follows from the combination of (A.3) and (A.18). □

Chapter 5

Conclusion and Future Work

In this thesis, we have developed two types of global-in-time DD methods for the reduced fracture models of flow and transport problems written in mixed formulations in porous media containing a fracture. The first type is called a Schur-type method, which is based on the Steklov-Poincaré operator, and the second type belongs to the class of the OSWR method with Ventcel-Robin transmission conditions. For all problems considered, each method is derived by formulating a space-time system on the fracture-interface between the subdomains, and is solved iteratively by utilizing matrix-free method, such as GMRES iteration. Since we are concerned with the use of different time steps on the fracture and on the subdomains, we have formulated the interface problem with nonconforming time grids in which the transmission conditions are enforced by using L^2-projections in time. Numerical results also show that all methods are applicable when different time steps are imposed on the fracture and on the subdomains as they preserve their behaviors and efficiency in such situation.

All methods are studied numerically and are compared to each other to illustrate their performance in different cases. Regarding the pure diffusion equation, the new preconditioner of GTP-Schur significantly improves the convergence of the method but does not give better accuracy in time on the fracture with nonconforming time grids. In most cases, we observe that GTF-Schur is the most efficient method as it converges as fast as GTO-Schwarz without applying any preconditioner as well as preserves the accuracy in time on the fracture when nonconforming time grids are imposed.

When coupling with operator splitting to treat the advection-diffusion equation, both GTF-Schur and GTO-Schwarz can handling efficiently the cases when the advection is mildly dominated as they are insensitive to the values of Péclet numbers and give similar fast convergence as in the case with only diffusion term. In terms of accuracy in time, similar to the pure diffusion case, GTF-Schur is the only method that gives the expected errors in time on the fracture when smaller time steps are imposed there and larger ones on the subdomains. However, when

the advection is strongly dominated, smaller time steps are needed to imposed for the advection step, which increases the computation time for both methods.

To deal with the case when the advection is strongly dominated, we derive both methods in the context of mixed hybrid finite elements, in which the hybridization process is utilized to constructed efficient upwind operator. Numerical results show that with this approach, both methods can treat the case when the Péclet is high very well. This approach also allows us to derive rigorous error analysis to gain better understanding of the performance of the proposed methods.

Regarding our future work, we aim to derive the error estimates (4.36) for the monolithic upwind-mixed scheme as well as the convergence of the GTO-Schwarz method when coupling with mixed hybrid finite elements in a more general setting as our current proofs still require the conforming assumption on both temporal and spatial discretization. We also aim to construct fast, efficient and accurate global-in-time DD methods for more complicated problems, such as multiphysics model where the physical processes in the fracture and in the subdomains are different. Moreover, there has been an increasing attempt of combining machine learning (ML) with domain decomposition methods (DDMs) for the solution of partial differential equations. Despite lacking of theoretical frameworks for explaining the effectiveness of multi-layer neural networks, its success in practices keeps attracting a great deal of interest. There are two possible directions in which we can utilize the advancement of machine learning to improve my global-in-time DD solvers. First of all, one can use ML techniques within the DDMs in order to improve the convergence properties or the computational efficiency [61]. Secondly, deep neural networks (DNNs) can be used to derive a mesh-free subdomain solvers which does not require any spatial discretization [80, 81]. We aim to combine ML with global-in-time DD to enhance the performance of the existing methods and reduce their computational costs for the case when the geometry of the domain is very complex. One more interesting direction is to perform more numerical simulation in 3D problems for modeling more realistic environmental phenomena.

References

[1] V. I. Agoshkov. “Poincaré-Steklov’s operators and domain decomposition methods in finite-dimensional spaces”. In: *First International Symposium on Domain Decomposition Methods for Partial Differential Equations*. Philadelphia, PA: SIAM, 1988, pp. 73–112.

[2] E. Ahmed, A. Fumagalli, and A. Budiša. “A multiscale flux basis for mortar mixed discretizations of reduced Darcy-Forchheimer fracture models”. In: *Comput. Methods Appl. Mech. Engrg.* 354 (2019), pp. 16–36.

[3] E. Ahmed, A. Fumagalli, A. Budiša, E. Keilegavlen, J. M. Nordbotten, and F. A. Radu. “Robust linear domain decomposition schemes for reduced nonlinear fracture flow models”. In: *SIAM J. Numer. Anal.* 59 (1) (2019), pp. 583–612.

[4] C. Alboin, J. Jaffré, J. E. Roberts, and C. Serres. “Domain decomposition for flow in fractured porous media”. In: *Domain Decomposition Methods in Science and Engineering* (1999). Ed. by C. H. Lai, P. E. Bjørstad, M. Cross, and O. B. Widlund, pp. 365–373.

[5] C. Alboin, J. Jaffré, J. E. Roberts, and C. Serres. “Modeling fractures as interfaces for flow and transport in porous media”. In: *Fluid flow and transport in porous media: mathematical and numerical treatment, vol.* 295 *of Contemp. Math., Amer. Math. Soc.* Providence, RI, 2001.

[6] I. Ambartsumyan, E. Khattatov, T. Nguyen, and I. Yotov. “Flow and transport in fractured poroelastic media”. In: *GEM-Int. J. Geomath.* 10 (11) (2019).

[7] L. Amir, M. Kern, V. Martin, and J. E. Roberts. “Décompositionn de domaine pour un milieu poreux fractureé: Un moéle en 3D avec fractures qui s’intersectent”. In: *Arima* 5 (2006), pp. 11–25.

[8] L. Amir, Michel Kern, Zoubida Mghazli, and Jean E. Roberts. “Intersecting fractures in porous media: mathematical and numerical analysis”. In: *Applicable Analysis* 102 (2021), pp. 1312 –1334.

[9] P. Angot, F. Boyer, and F. Hubert. “Asymptotic and numerical modelling of flows in fractured porous media”. In: *Math. Model. Numer. Anal.* 43 ((5)) (2009), pp. 239–275.

[10] T. Arbogast, S. Bryant, C. Dawson, F. Saaf, C.Wang, and M. Wheeler. “Computational methods for multiphase flow and reactive transport problems arising in subsurface contaminant remediation”. In: *J. Comput. Appl. Math.* 74 (1996), pp. 19–32.

[11] T. Arbogast, L. C. Cowsar, M. F. Wheeler, and I. Yotov. “Mixed finite element methods on nonmatching multiblock grids”. In: *SIAM J. Numer. Anal.* 37 (2000), pp. 1295–1315.

[12] D. N. Arnold and F. Brezzi. “Mixed and nonconforming finite element methods: implementation, postprocessing and error estimates”. In: *R.A.I.R.O Modél. Math. Anal. Numér* 19 (1985), pp. 7–32.

[13] A. Arrarás, F. J. Gaspar, L. Portero, and C. Rodrigo. “Mixed-dimensional geometric multigrid methods for single-phase flow in fractured porous media”. In: *SIAM J. Sci. Comput.* 41 (5) (2019), pp. 1082–1114.

[14] D. Bennequin, M. J. Gander, and L. Halpern. “A homographic best approximation problem with application to optimized Schwarz waveform relaxation”. In: *Math. Comput.* 78 (265) (2009), pp. 185–223.

[15] S. Berrone, S. Pieraccini, and S. Scialò. “Flow simulations in porous media with immersed intersecting fractures”. In: *J. Comput. Phys.* 345 (2017), pp. 768–791.

[16] P. E. Bjøstad, J. Brækhus, and A. Hvidsten. “Parallel substructuring algorithms in structural analysis, direct and iterative methods”. In: *Fourth International Symposium on Domain Decomposition Methods for Partial Differential Equations (Moscow 1990)*. Philadelphia, PA: SIAM, 1991, pp. 321–340.

[17] E. Blayo, L. Debreu, and F. Lemarié. “Toward an Optimized Global-in-Time Schwarz Algorithm for Diffusion Equations with Discontinuous and Spatially Variable Coefficients, Part 1: The Constant Coefficients Case”. In: *Electronic Transactions on Numerical Analysis* 40 (2013), pp. 148–169.

[18] F. Blayo, L. Halpern, and C. Japhet. “Optimized Schwarz waveform relaxation algorithms with nonconforming time discretization for coupling convection-diffusion problems with discontinuous coefficients”. In: *Domain decomposition methods in science and engineering XVI, vol. 55 of Lect. Notes Comput. Sci. Eng.* Berlin: Springer, 2007, pp. 267–274.

[19] W. M. Boon, J. M. Nordbotten, and I. Yotov. “Robust Discretization of Flow in Fractured Porous Media”. In: *SIAM J. Numer. Anal.* 56 (4) (2018), pp. 2203–2233.

[20] J.-F. Bourgat, R. Glowinski, P. Le Tallec, and M. Vidrascu. “Variational formulation and algorithm for trace operator in domain decomposition calculations”. In: *Domain decomposition methods (Los Angeles, CA, 1988)*. Philadelphia, PA: SIAM, 1989, pp. 3–16.

[21] F. Brezzi. “On the existence, uniqueness and approximation of saddle-point problems arising from lagrangian multiplers”. In: *RAIRO Anal. Numér.* 8 (1974), pp. 129–151.

[22] F. Brezzi, J. Douglas, and L. D. Marini. “Two families of mixed finite elements for second order elliptic problems”. In: *Numerische Mathematik* 47 (1985), pp. 217–235.

[23] F. Brezzi and M. Fortin. “Mixed and Hybrid Finite Element Methods”. In: *Springer Series in Computational Mathematics*. Vol. 15. 2011.

[24] F. Brezzi, J. Douglas, M. Fortin, and L. D. Marini. “Efficient rectangular mixed finite elements in two and three space variables”. In: *Math. Model. Numer. Anal.* 21 (1987), pp. 581–604.

[25] F. Brezzi, J. Douglas, R. G. Durán, and M. Fortin. “Mixed finite elements for second order elliptic problems in three variables”. In: *Numerische Mathematik* 51 (1987), pp. 237–250.

[26] F. Brunner, F. A. Radu, and P. Knabner. “Analysis of an upwind-mixed hybrid finite element method for transport problems”. In: *SIAM J. Numer. Anal.* 52 (2014), pp. 83–102.

[27] F. Brunner, F. A. Radu, M. Bause, and P. Knabner. “Optimal order convergence of a modified BDM1 mixed finite element scheme for reactive transport in porous media”. In: *Adv. Water Resources* 35 (2012), pp. 163–171.

[28] A. Chertock and A. Kurganov. “On splitting-based numerical methods for convection-diffusion equations”. In: *Quad. Mat.* 24 (2009), pp. 303–343.

[29] P. G. Ciarlet and P. A. Raviart. “A mixed finite element method for biharmonic equation”. In: *Mathematical aspects of finite elements in partial differential equations*. Ed. by C. de Boor. New York: Academic Press, 1974, pp. 125–145.

[30] L. C. Cowsar, J. Mandel, and M. F. Wheeler. “Balancing domain decomposition for mixed finite elements”. In: *Math. Comp.* 64 (1995), pp. 989–1015.

[31] M. Crouzeix and P. A. Raviart. “Conforming and nonconforming finite element methods for solving the stationary Stokes equations I”. In: *R.A.I.R.O* 7 (1973).

[32] C. D’Angelo and A. Scotti. “A mixed finite element method for Darcy flow in fractured porous media with non-matching grids”. In: *Math. Model. Anal.* 46 (2) (2012), pp. 465–489.

[33] C. N. Dawson. “Analysis of an upwind-mixed finite element method for nonlinear contaminant transport equations”. In: *SIAM J. Numer. Anal.* 35 (1998), pp. 1709–1724.

[34] C. N. Dawson and V. Aizinger. “Upwind mixed methods for transport equations”. In: *Computational Geosciences* 3 (1999), pp. 93–110.

[35] M. Dryja. “Substructuring methods for parabolic problems”. In: *Fourth International Symposium on Domain Decomposition Methods for Partial Differential Equations (Moscow, 1990)*. Philadelphia, PA: SIAM, 1991, pp. 264–271.

[36] R. G. Durán. “Error analysis in L^p, $1 \leq p \leq \infty$, for mixed finite element methods for linear and quasi-linear elliptic problems”. In: *R.A.I.R.O Modél. Math. Anal. Numér.* 22 (1988), 371–387.

[37] L. C. Evans. *Partial differential equations*. Providence, RI: American Mathematical Society, 1998.

[38] E. Flauraud, F. Natf, I. Faille, and R. Masson. “Domain decomposition for an symptotic geological fault modeling”. In: *Comptes Rendus Mécanique* 331 (12) (2003), pp. 849–855.

[39] N. Frih, J. E. Roberts, and A. Saada. “Modeling fractures as interfaces: A model for Forchheimer fractures”. In: *Comput. Geosci.* 12 (2008), pp. 91–104.

[40] N. Frih, J. E. Roberts, and A. Saâda. “Un modèle Darcy-Forchheimer pour un écoulement dans un milieu poreux fracturé”. In: *ARIMA* 5 (2006), pp. 129–143.

[41] N. Frih, V. Martin, J. E. Roberts, and A. Saâda. “Modeling fractures as interfaces with nonmatching grids”. In: *Comput. Geosci.* 16 (2) (2012), 1043–1060.

[42] M. J. Gander, L. Halpern, and M. Kern. “A Schwarz waveform relaxation method for advection- diffusion-reaction problems with continuous coefficients and non-matching grids”. In: *Domain decomposition methods in science and engineering XVI, vol.* 55 *of Lect. Notes Comput. Sci. Eng.* Berlin: Springer, 2007, pp. 283–290.

[43] M. J. Gander, L. Halpern, and F. Nataf. “Optimal convergence for overlapping and non-overlapping Schwarz waveform relaxation”. In: *Proceedings of the* 11*th International Conference on Domain Decomposition Methods*. Ed. by C-H. Lai, P. Bjørstad, M. Cross, and O. Widlund. 1999.

[44] M. J. Gander and Laurence Halpern. “Optimized Schwarz waveform relaxation methods for advection reaction diffusion problems”. In: *SIAM J. Numer. Anal.* 45 (2) (2007), pp. 666–697.

[45] M. J. Gander, J. Hennicker, and R. Masson. “Modeling and analysis of the coupling in discrete fracture matrix models”. In: *SIAM J. Numer. Anal.* 59 (2021), pp. 195–218.

[46] M. J. Gander and C. Japhet. “Algorithm 932: PANG: Software for nonmatching grid projections in 2D and 3D with linear complexity”. In: *ACM Trans. Math. Softw.* 40 (2013), 6:1–6:25.

[47] M. J. Gander, F. Kwok, and B.C. Mandal. “Dirichlet-Neumann and Neumann-Neumann waveform relaxation algorithms for parabolic problems”. In: *Electron, Trans. Numer. Anal.* 45 (2016), pp. 424–456.

[48] M. J. Gander, F. Kwok, and B.C. Mandal. “Dirichlet–Neumann waveform relaxation methods for parabolic and hyperbolic problems in multiple subdomains”. In: *BIT Numerical Mathematics* 61 (2020), pp. 173–207.

[49] M. J. Gander, C. Japhet, Y. Maday, and F. Nataf. “A new cement to glue nonconforming grids with Robin interface conditions: the finite element case. Domain decomposition methods in science and engineering”. In: *Lect. Notes Comput. Sci. Eng.* 40 (2007), pp. 259–366.

[50] B. Ganis, M. E. Mear, A. Sakhaee-Pour, M. F. Wheeler, and T. Wick. “Modeling fluid injection in fractures with a reservoir simulator coupled to a boundary element method”. In: *Comput. Geosci.* 18 (2014), pp. 613–624.

[51] B. Ganis, V. Girault, M. Mear, G. Singh, and M. F. Wheeler. “Modeling fractures in a poro-elastic meidum”. In: *Oil Gas Sci. Technol.* 69 (2014), pp. 515–528.

[52] L. Gastaldi. “A domain decomposition for the transport equation”. In: *Domain decomposition methods in science and engineering (Como, 1992) vol. 157 of Contemp. Math., Amer. Math. Soc.* Providence, RI, 1994, pp. 97–102.

[53] V. Girault, M. F. Wheeler, B. Ganis, and M. E. Mear. “A lubrication fracture model in a poro-elastic medium”. In: *Math. Models Methods Appl. Sci.* 25 (2015), pp. 587–645.

[54] R. Glowinski and M. F. Wheeler. “Domain decomposition and mixed finite element methods for elliptic problems”. In: *First International Symposium on Domain Decomposition Methods for Partial Differential Equations*. Philadelphia, PA: SIAM, 1988, pp. 144–172.

[55] S. Gross, M. A. Olshanskii, and A. Reusken. “A trace finite element method for a class of coupled bulk-interface transport problems”. In: *ESAIM: Math. Model Numer. Anal* 49 (5) (2015), pp. 1303–1330.

[56] L. Halpern, C. Japhet, and P. Omnes. “Nonconforming in time domain decomposition methods for porous method applications”. In: *Proceedings of the* 5*th European Conference on Computational Fluid Dynamics*. Lisbon, Portugal, 2010.

[57] L. Halpern, C. Japhet, and J. Szeftel. “Discontinuous Galerkin and nonconforming in time optimized Schwarz waveform relaxation”. In: *Domain decomposition methods in science and engineering XIX, vol. 78 of Lect. Notes Comput. Sci. Eng.* Heidelberg: Springer, 2011, pp. 133–140.

[58] L. Halpern, C. Japhet, and J. Szeftel. “Optimized Schwarz waveform relaxation and discontinuous Galerkin time stepping for heterogeneous problems”. In: *SIAM J. Numer. Anal.* 50 (5) (2012), pp. 2588–2611.

[59] Eskil Hansen and Emil Engström. *Linearly convergent nonoverlapping domain decomposition methods for quasilinear parabolic equations*. English. WorkingPaper. arXiv.org, 2023. DOI: 10.48550/arXiv.2308.15314.

[60] F. Hecht, Z. Mghazli, I. Naji, and J. E. Roberts. “A residual a posteriori error estimators for a model for flow in porous media with fractures”. In: *J. Sci. Comput.* 79 (2019), pp. 935–968.

[61] A. Heinlein, A. Klawonn, M. Lanser, and J. Weber. “Machine learning in adaptive domain decomposition methods - Predicting the geometric location of constraints”. In: *SIAM J. Sci. Comput.* 41 (2019), pp. 3887–3912.

[62] K. Hellan. “Analysis of elastic plates in flexure by a simplified finite element method”. In: *Acta Polytechnica Scandinavia, Civil Engineering Series* 46 (1967), pp. 1–19.

[63] L. R. Herrmann. “Finite element bending analysis for plates”. In: *J. Eng. Mech. Div. ASCE* 93 (1967), pp. 13–26.

[64] T.T.P. Hoang. “Fully implicit local time-stepping methods for advection-diffusion problems in mixed formulations”. In: *Comput. Math. with Appl.* 118 (2022).

[65] T.T.P. Hoang and H. K. Lee. “A global-in-time domain decomposition method for the coupled nonlinear Stokes and Darcy flows”. In: *Journal of Scientific Computing* 87 (1) (2021), pp. 1–22.

[66] T.T.P. Hoang, C. Japhet, M. Kern, and J. E. Roberts. “Space-time domain decomposition for advection-diffusion problems in mixed formulations”. In: *Math. Comput. Simul.* 137 (2017), pp. 366–389.

[67] T.T.P. Hoang, C. Japhet, M. Kern, and J. E. Roberts. “Space-time domain decomposition for reduced fracture models in mixed formulation”. In: *SIAM J. Numer. Anal.* 54 (1) (2016), pp. 288–316.

[68] T.T.P. Hoang, J. Jaffré, C. Japhet, M. Kern, and J. E. Roberts. “Space-time domain decomposition methods for diffusion problems in mixed formulations”. In: *SIAM J. Numer. Anal.* 51 (6) (2013), pp. 3532–3559.

[69] W. Hundsdorfer and J. Verwer. *Numerical solution of time-dependent advection-diffusion-reaction equations*. Berlin: Springer, 2003.

[70] P. T. Huynh, T. T. P. Hoang, and Yanzhao Cao. “Fast and accuracy-preserving domain decomposition methods for reduced fracture models with nonconforming time grids”. In: *Journal of Scientific Computing* 96 (2023), pp. 1–26.

[71] P. T. Huynh, T.T.P. Hoang, and Yanzhao Cao. “Monolithic and local time-stepping decoupled algorithms for transport problems in fractured porous media”. In: *IMA Journal of Numerical Analysis* (2024).

[72] P. T. Huynh, T.T.P. Hoang, and Yanzhao Cao. “Operator splitting and local time-stepping methods for transport problems in fractured porous media”. In: *Commun. Comput. Phys.* 34 (5) (2023), pp. 1215–1246.

[73] C. Japhet. “Méthode de décomposition de domaine et conditions aux limites artificielles en mécanique des fluides: méthode optimisée d’Ordre 2”. PhD Thesis. University of Paris XIII, 1998.

[74] C. Japhet. “Optimized Krylov-Ventcell method. Application to convection-diffusion problems”. In: *Domain decomposition methods in science and engineering IX*. Ed. by U. Bjørstad, M. Espedal, D.E. Keyes, and John Wiley & Sons Ltd. 1998, pp. 382–389.

[75] C. Japhet and Y. Maday. “Mortar methods with optimized transmission conditions for advection-diffusion problems”. In: *Domain decomposition methods in science and engineering XXII, vol.* 115 *of Lect. Notes Comput. Sci. Eng.* Ed. by T. Dickopf, M. Gander, L. Halpern, R. Krause, and L. Pavarino. 2016.

[76] C. Japhet, Y. Maday, and F. Nataf. “A new interface cement equilibrated mortar method with Ventcel conditions”. In: *Domain decomposition methods in science and engineering XXI, vol.* 98 *of Lect. Notes Comput. Sci. Eng.* Ed. by J. Erhel, M. Gander, L. Halpern, G. Pichot, T. Sassi, and O. Widlund. Springer, 2014.

[77] C. Johnson. “On the convergence of a mixed finite element for plate bending problems”. In: *Numer. Math.* 21 (1973), pp. 43–62.

[78] F. Kwok. “Neumann-Neumann waveform relaxation for the time-dependent heat equation”. In: *Domain Decomposition Methods in Science and Engineering XXI*. Ed. by J. Erhel, J. M. Gander, L. Halpern, G. Pichot, T. Sassi, and O. Widlund. Springer-Verlag, 2014, pp. 189–198.

[79] M. Lesinigo, C. D’Angelo, and A. Quarteroni. “A multiscale Darcy-Brinkman model for fluid flow in fractured porous media”. In: *Numer. Math.* 117 (2011), pp. 717–752.

[80] K. Li, T. Tang, T. Wu, and Q. Liao. “D3M: A deep domain decomposition method for partial differential equations”. In: *IEEE Access* 8 (2019), pp. 5283–5294.

[81] W. Li, X. Xiang, and Y. Xu. “Deep domain decomposition method: Elliptic problems”. In: *Proc. Mach. Learn. Res.* 107 (2020), pp. 269–286.

[82] J. Liesen and Z. Strakoš. *Krylov Subspace Methods: Principle and Analysis*. Oxford, UK: Oxford University Press, 2013.

[83] F. List, K. Kumar, I. S. Pop, and F. A. Radu. “Rigorous upscaling of unsaturated flow in fractured porous media”. In: *SIAM J. Math. Anal.* 52 (1) (2020), pp. 239–276.

[84] B. C. Mandal. “A time-dependent Dirichlet-Neumann method for the heat equation”. In: *Domain Decomposition Methods in Science and Engineering XXI*. Ed. by J. Erhel, J. M. Gander, Laurence Halpern, Pichot, Géraldine, Sassi, Taoufik, and O. Widlund. Springer-Verlag, 2014, pp. 467–475.

[85] J. Mandel. “Balancing domain decomposition”. In: *Comm. Numer. Methods Engrg* 9 (1993), pp. 233–241.

[86] J. Mandel and M. Brezina. “Balancing domain decomposition for problems with large jumps in coefficients”. In: *Math. Comput.* 65 (1996), pp. 1387–1401.

[87] V. Martin. “A optimized Schwarz waveform relaxation method for the unsteady convection diffusion equation in two dimensions”. In: *Appl. Numer. Math.* 52 (2005), pp. 401–428.

[88] V. Martin, J. Jaffré, and J. E. Roberts. “Modeling fractures and barriers as interfaces for flow in porous media”. In: *SIAM J. Sci. Comput.* 26 (2005), pp. 1667–1691.

[89] T. P. Mathew. “Domain decomposition and iterative refinement methods for mixed finite element discretizations of elliptic problems”. PhD Thesis. New York University, 1989.

[90] A. Mazzia, L. Bergamaschi, and M. Putti. “A Time-splitting technique for the advection-dispersion equation in groundwater”. In: *J. Comput. Phys.* 157 (2000), pp. 181–198.

[91] A. Mazzia, L. Bergamaschi, C.N. Dawson, and M. Putti. “Godunov mixed methods on triangular grids for advection–dispersion equations”. In: *Comput. Geosci.* 6 (2002), pp. 123–139.

[92] Z. Mghazli and I. Naji. “Guaranteed *a posteriori* error estimates for a fractured porous medium”. In: *Math. Comput. Simulation* 164 (2019), pp. 163–179.

[93] F. A. Morales and R. E. Showalter. “Interface approximation of Darcy flow in a narrow channel”. In: *Math. Methods Appl. Sci.* 35 (2012), pp. 182–195.

[94] F. A. Morales and R. E. Showalter. “The narrow fracture approximation by channeled flow”. In: *J. Math. Anal. Appl.* 365 (1) (2010), pp. 320–331.

[95] F. Nataf and F. Rogier. “Factorization of the convection-diffusion operator and the Schwarz algorithm”. In: *Math. Models Methods Appl. Sci.* 5 (1995), pp. 67–93.

[96] J. C. Nédélec. “Mixed finite elements in $\mathbf{R}^3$”. In: *Numer. Math.* 35 (1980), pp. 315–341.

[97] J. T. Oden and J. N. Reddy. “On mixed finite element approximations”. In: *SIAM J. Numer. Anal.* 13 (1976), pp. 392–404.

[98] J. E. Pasciak. “Domain decomposition preconditioners for elliptic problems in two and three dimensions: first approach”. In: *First International Symposium on Domain Decomposition Methods for Partial Differential Equations (Paris, 1987)*. Philadelphia, PA, 1988, pp. 62–72.

[99] A. M. Quarteroni and A. Valli. *Domain Decomposition Method for Partial Differential Equations*. Oxford, New York: Clarendon Press, 1999.

[100] A. M. Quarteroni and A. Valli. *Numerical Approximation of Partial Differential Equations*. Berlin, Heidelberg: Springer, 2008.

[101] A. M. Quarteroni and A. Valli. “Theory and application of Steklov-Poincaré operators for boundary value problems: the heterogeneous operator case”. In: *Fourth International Symposium on Domain Decomposition Methods for Partial Differential Equations*. SIAM, Philadelphia, PA, 1991, pp. 58–81.

[102] F. A. Radu, N. Suciu, J. Hoffmann, A. Vogel, O. Kolditz, C. H. Park, and S. Attinger. “Accuracy of numerical simulations of contaminant transport in heterogeneous aquifers: A comparative study”. In: *Adv. Water Resources* 34 (2011), pp. 47–61.

[103] P. A. Raviart and J. Thomas. “A mixed finite element method for 2nd order elliptic problems”. In: *Mathematical Aspects of the Finite Element Method, Lecture Notes in Math. 606*. New York: Springer, 1977.

[104] J. N. Reddy and J. T. Oden. “Mathematical theory of mixed finite element approximations”. In: *Q. Appl. Math.* 33 (1975), pp. 255–280.

[105] J. E. Roberts and J. M. Thomas. “Mixed and hybrid methods”. In: *Handbook of Numerical Analysis* 2 (1991), pp. 523–639.

[106] Y.-H. De Roeck and P. Le Tallec. “Analysis and test of a local domain-decomposition preconditioner”. In: *Fourth International Symposium on Domain Decomposition Methods for Partial Differential Equations (Moscow, 1990)*. Philadelphia, PA: SIAM, 1991, pp. 112–128.

[107] N. Schwenck, B. Flemisch, R. Helmig, and B. I. Wohlmuth. “Dimensionally reduced flow models in fractured porous media: crossings and boundaries”. In: *Comput. Geosci.* 19 (6) (2015), pp. 1219–1230.

[108] P. Siegel, R. Mosé, P. Ackerer, and J. Jaffré. “Solution of the advection-diffusion equation using a combination of discontinuous and mixed finite elements”. In: *Internat. J. Numer. Methods Fluids* 24 (1997), pp. 595–613.

[109] B. Fraeijs De Veubeke. “Displacement and equilibrium models in the finite element method”. In: *Stress Analysis*. Ed. by O. C. Zienkiewica and G. S. Holister. New York: Wiley, 1965, pp. 145–197.

[110] M. Vohralík. “A posteriori error estimates for lowest-order mixed finite element discretizations of convection-diffusion-reaction equations”. In: *SIAM J. Numer. Anal.* 45 (2007), pp. 1570–1599.

[111] M. F. Wheeler and C. N. Dawson. “An operator-splitting method for advection-diffusion-reaction problems”. In: *The Mathematics of Finite Elements and Applications VI*. Academic Press, 1988.

[112] O. B. Widlund. “Iterative substructuring methods: algorithms and theory for elliptic problems in the plane”. In: *First International Symposium on Domain Decomposition Methods for Partial Differential Equations (Paris, 1987)*. Philadelphia, PA: SIAM, 1988, pp. 113–128.